

JOURNAL OF RESEARCH OF THE U.S. GEOLOGICAL SURVEY

NOVEMBER-DECEMBER 1974
VOLUME 2, NUMBER 6

*Scientific notes and summaries
of investigations in geology,
hydrology, and related fields*



U.S. DEPARTMENT OF THE INTERIOR



UNITED STATES DEPARTMENT OF THE INTERIOR

ROGERS C. B. MORTON, Secretary

GEOLOGICAL SURVEY

V. E. McKelvey, Director

For sale by the Superintendent of Documents, U.S. Government Printing Office, Washington, DC 20402. Order by SD Catalog No. JRGS. Annual subscription rate \$15.50 (plus \$3.75 for foreign mailing). Single copy \$2.75. Make checks or money orders payable to the Superintendent of Documents.

Send all subscription inquiries and address changes to the Superintendent of Documents at the above address.

Purchase orders should not be sent to the U.S. Geological Survey library.

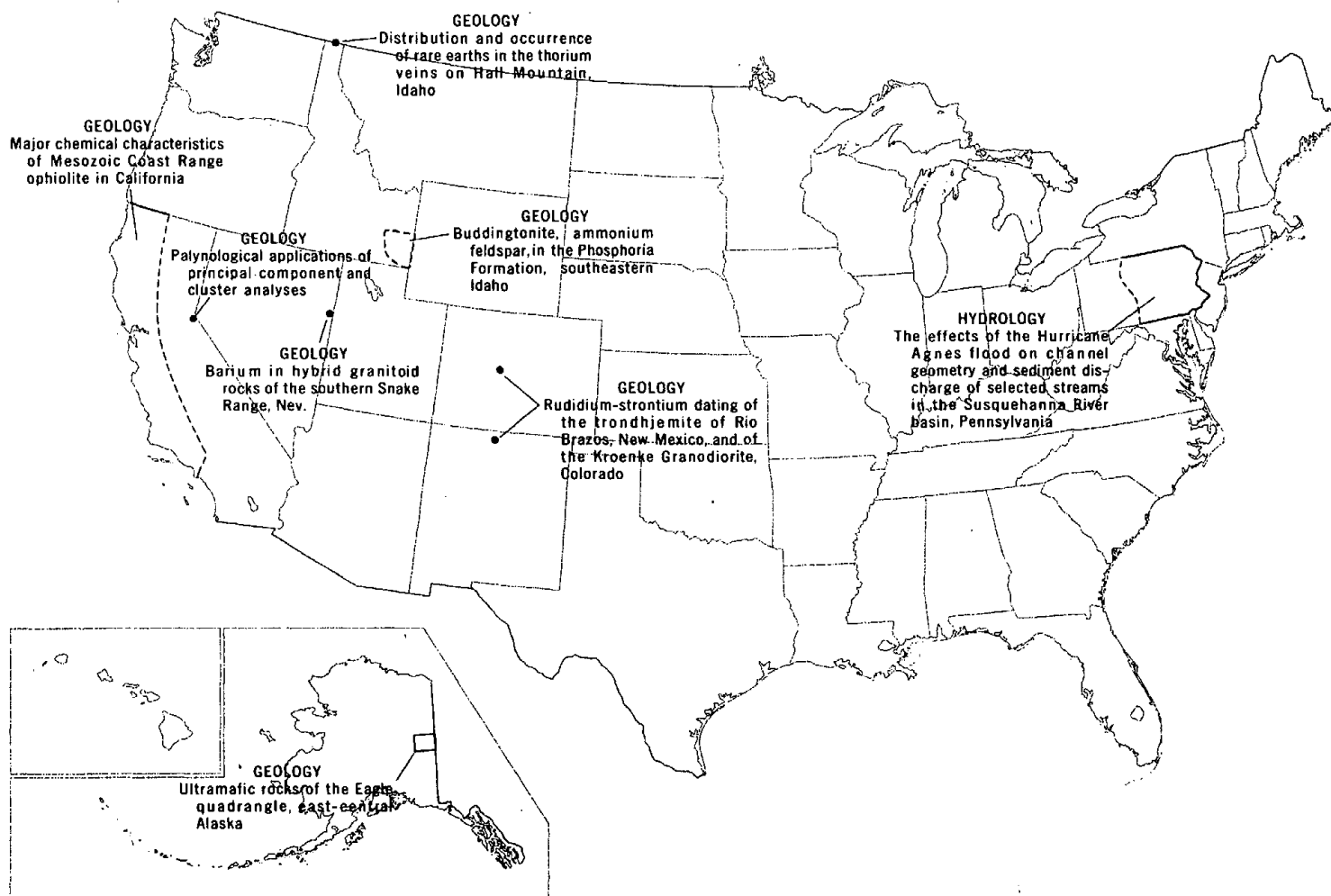
Library of Congress Catalog-card No. 72-600241.

The Journal of Research is published every 2 months by the U.S. Geological Survey. It contains papers by members of the Geological Survey and their professional colleagues on geologic, hydrologic, topographic, and other scientific and technical subjects.

Correspondence and inquiries concerning the Journal (other than subscription inquiries and address changes) should be directed to the Journal of Research, Publications Division, U.S. Geological Survey, National Center 321, Reston, VA 22092.

Papers for the Journal should be submitted through regular Division publication channels.

The Secretary of the Interior has determined that the publication of this periodical is necessary in the transaction of the public business required by law of this Department. Use of funds for printing this periodical has been approved by the Director of the Office of Management and Budget through February 11, 1975.



GEOGRAPHIC INDEX TO ARTICLES

See "Contents" for articles concerning areas outside the United States and articles without geographic orientation.

JOURNAL OF RESEARCH

of the
U.S. Geological Survey

Vol. 2 No. 6

Nov.-Dec. 1974

CONTENTS

Abbreviations	II
---------------------	----

GEOLOGIC STUDIES

Major chemical characteristics of Mesozoic Coast Range ophiolite in California	<i>E. H. Bailey and M. C. Blake, Jr.</i>	637
Ultramafic rocks of the Eagle quadrangle, east-central Alaska	<i>H. L. Foster and T. E. C. Keith</i>	657
Barium in hybrid granitoid rocks of the southern Snake Range, Nev.	<i>D. E. Lee and W. P. Doering</i>	671
Distribution and occurrence of rare earths in the thorium veins on Hall Mountain, Idaho	<i>M. H. Staatz, V. E. Shaw, and J. S. Wahlberg</i>	677
Origin of spongy cherts	<i>B. M. Madsen</i>	685
Analyses and economic potential of monazite in Liberia	<i>Sam Rosenblum</i>	689
Buddingtonite, ammonium feldspar, in the Phosphoria Formation, southeastern Idaho	<i>R. A. Gulbrandsen</i>	693
Optical and X-ray crystallographic investigations of strontioegnorites	<i>R. P. Christian, C. D. Eberlein, and J. A. Konnert</i>	699
Spectrophotometric determination of vanadium in rutile and in mafic igneous rocks	<i>John Marinenko and Leung Mei</i>	701
Rubidium-strontium dating of the trondhemite of Rio Brazos, New Mexico and of the Kroenke Granodiorite, Colorado	<i>Fred Barker, Z. E. Peterman, W. T. Henderson, and R. E. Hildreth</i>	705
Continental depositor of Antarctic tillite indicated by carbon and oxygen isotopes	<i>D. L. Schmidt and Irving Friedman</i>	711
Redescription of the Early Cambrian <i>Helenia bella</i> Walcott, an appendage of <i>Hyalolithes</i>	<i>E. L. Yochelson</i>	717
Evidence for the presence of a heart in Paleozoic ostracodes inconclusive	<i>I. C. Sohn</i>	723
Palynological applications of principal component and cluster analyses	<i>D. P. Adam</i>	727
Flashing flow in hot-water geothermal wells	<i>Manuel Nathenson</i>	743

HYDROLOGIC STUDIES

The effects of the Hurricane Agnes flood on channel geometry and sediment discharge of selected streams in the Susquehanna River basin, Pennsylvania	<i>J. R. Ritter</i>	753
--	---------------------	-----

TOPOGRAPHIC STUDIES

Unique cartographic characteristics of ERTS	<i>A. P. Colvocoresses</i>	763
---	----------------------------	-----

ANNUAL INDEX TO VOLUME 2

Subject	765
Author	770

Recent publications of the U.S. Geological Survey	Inside of back cover
---	----------------------

ABBREVIATIONS

A	ampere	l	liter
Å	angstrom	lb	pound
abs	absolute	lm	lumen
ADP	ammonium dihydrogen phosphate	ln	logarithm (natural)
atm	atmosphere	log	logarithm (common)
BOD	biochemical oxygen demand	M	molarity; molar (concentration)
Btu	British thermal unit	m	meter
b.y.	billion years	m ²	square meter
°C	degree Celsius	m ³	cubic meter
cal	calorie	m	molality; molal (concentration)
C.I.	color index	MA	megampere
CIPW	Cross, Iddings, Pirsson, and Washington	mA	milliampere
cm	centimeter	mg	milligram
cm ³	cubic centimeter	Mgal	million gallons
concd	concentrated	mGal	milligal
D	darcy	mi	mile
d	day	mi ²	square mile
DDD	dichloro-diphenyl- dichloro-ethane	mi ³	cubic mile
DDE	dichloro-diphenyl- dichloro-ethylene	min	minute
DDT	dichloro-diphenyl- trichloro-ethane	ml	milliliter
diam	diameter	mm	millimeter
DSDP	Deep Sea Drilling Project	mmol	millimole
Eh	oxidation-reduction potential	mo	month
emf	electromotive force	mol	mole
emu	electromagnetic unit	mol. wt	molecular weight
ERTS	Earth Resources Technology Satellite	mV	millivolt
eu	entropy unit	m.y.	million years
eV	electronvolt	μg	microgram
F.D.&C.	Food, Drug, and Cosmetic [dye]	μm	micrometer
ft	foot	μmho	micromho
ft ²	square foot	N	normality
ft ³	cubic foot	nA	nanoampere
g	gram	NASA	National Aeronautics and Space Administration
g	gravitational acceleration	nm	nanometer
γ	activity coefficient	OD	outside diameter
gal	gallon	P	poise
h	hour	PCB	polychlorinated biphenyls
ID	inside diameter	PDB	Peedee belemnite
IDOE	International Decade of Ocean Exploration	pH	measure of hydrogen ion activity
in.	inch	ppm	part per million
J	joule	‰	part per thousand
K	kelvin	rad	radian
keV	kiloelectronvolt	rms	root mean square
kg	kilogram	s	second
kHz	kilohertz	σ	population standard deviation
km	kilometer	SMOW	standard mean ocean water
km ²	square kilometer	v	volt
km ³	cubic kilometer	v/v	volume per volume
kV	kilovolt	W	watt
		w/w	weight per weight
		wt	weight
		yd ³	cubic yard
		yr	year

MAJOR CHEMICAL CHARACTERISTICS OF MESOZOIC COAST RANGE OPHIOLITE IN CALIFORNIA

By E. H. BAILEY and M. C. BLAKE, JR., Menlo Park, Calif.

Abstract.—Sixty-four major element analyses of rocks representative of the Coast Range ophiolite in California were compared with analyses of other onland ophiolite sequences and those of rocks from oceanic ridges. The rocks can be classed in five groups—harzburgite-dunite, clinopyroxenite-wehrlite, gabbro, basalt-spilite, and keratophyre-quartz keratophyre—which on various diagrams occupy nonoverlapping fields. The harzburgite-dunite from onland ophiolite and ocean ridges are comparable and very low in alkalis. Possible differentiation trends defined on AFM diagrams by other rocks from onland ophiolites and ocean ridges suggest two lines of descent: (1) A trend much like the calc-alkalic trend, though shifted somewhat toward higher iron, and (2) an iron-enrichment trend defined chiefly by the more iron-rich gabbros and amphibolite. MgO-variation diagrams for rocks from the Coast Range ophiolite further distinguish the iron-rich gabbros and amphibolite from the other rock groups and indicate that the iron enrichment, unlike that of the Skaergaard trend, is related to the formation of amphibole. Ophiolite sequences that include the most silicic rock types, such as quartz keratophyre, also exhibit the most pronounced dual lines of descent, suggesting that the silicic rocks and the amphibole-rich gabbros are somehow related. Although the major element chemistry of the Coast Range ophiolite is clearly like that of rocks dredged from oceanic ridges, it is not sufficiently diagnostic to discriminate among the choices of a spreading ridge, an interarc basin, or perhaps even the root zone of an island arc as the site of ophiolite formation.

A succession of igneous rocks ranging upward from peridotite through gabbro to mafic and keratophyric lavas directly underlies the late Mesozoic Great Valley sequence of marine sedimentary rocks in western California. In an earlier paper, we described this igneous pile as a typical ophiolite and interpreted it as the Mesozoic oceanic crust on which the Late Jurassic (Tithonian) sedimentary rocks were deposited (Bailey, Blake, and Jones, 1970). Radiometric dating by Lanphere (1971) indicated that this ophiolite was only a few million years older than the basal Great Valley sediments, and Bezore (1971), Page (1972), and Hopson and others (1973), following detailed studies of individual areas, also have concluded the ophiolite is indeed Mesozoic ocean crust.

This paper presents chemical analyses of rocks in the Coast Range ophiolite and compares their major chemical characteristics with those of ancient ophiolites from other areas and with dredged rocks believed to represent today's oceanic crust and upper mantle. The analytical data support the contention

that the Coast Range ophiolite is a fragment of oceanic crust and upper mantle and permit some speculations regarding the petrogenesis of the major lithologies. The data seem inadequate to establish clearly whether the Coast Range ophiolite formed at a spreading ridge, in a marginal or interarc basin, or possibly even at the roots of a volcanic island arc.

CHEMICAL ANALYSIS

Of the 64 chemical analyses of samples representative of the various kinds of rocks in the Coast Range ophiolite listed in tables 1-5, 43 are new and 21 are published. Collection localities are shown in figure 1, and columnar sections depicting the major rock types at these localities are shown in an earlier paper (Bailey and others, 1970, fig. 2). Most of the rocks analyzed were selected on the basis of their freshness from among samples collected during reconnaissance investigation. As a result, even with the fairly large number of analyzed rocks, no locality has been sampled systematically, and no locality is represented by analyses of all the diverse lithologic types found in the Coast Range ophiolite.

Most of 43 new analyses were done by rapid-rock analysis method (Shapiro and Brannock, 1962) in the laboratories of the U.S. Geological Survey. The 21 published analyses are of rocks formerly regarded as part of the Franciscan Formation or believed to be intruded into Franciscan rocks (Bailey and others, 1964; Himmelberg and Coleman, 1968; Maddock, 1964; Case, 1963). Only analyses of those rocks that we are confident are part of the ophiolite lying below the Great Valley sedimentary sequence were selected for inclusion here. Some other published analyses of igneous rocks from Franciscan terrane may be fragments of the Coast Range ophiolite that have been tectonically displaced (Blake and Jones, 1974), but they are excluded here because the fragments are so isolated that their origin is uncertain.

DESCRIPTION OF MAJOR ROCK TYPES

The Coast Range ophiolite can be conveniently subdivided into the following five major rock groups:

1. Harzburgite and dunite, which are nearly everywhere at least somewhat serpentinized.

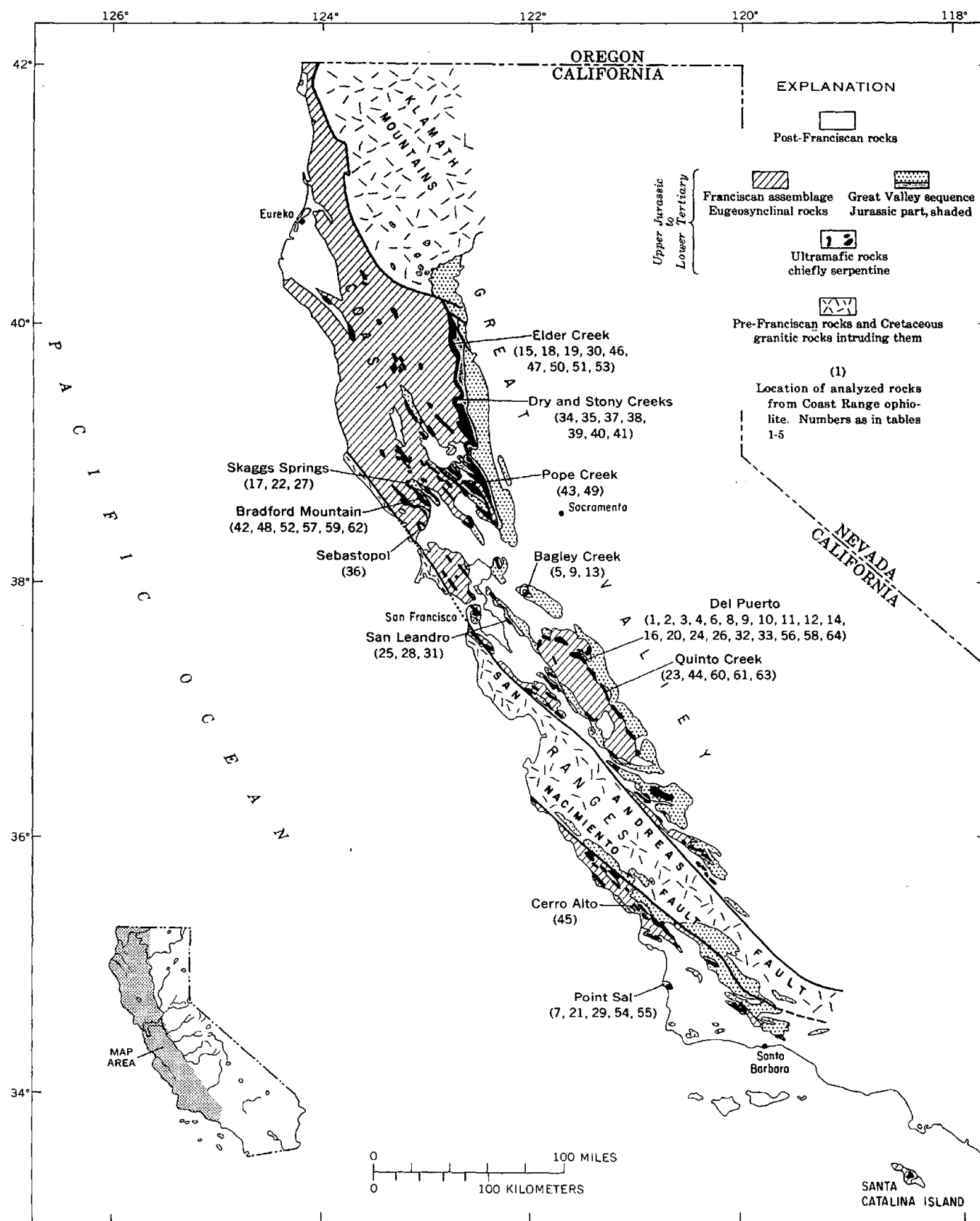


Figure 1.—Generalized geologic map of western California showing location of analyzed rocks from Coast Range ophiolite; numbers are as in tables 1–5.

2. Clinopyroxene-bearing rocks, including clinopyroxenite, wehrlite, and lherzolite(?).
3. Gabbro, including a range of varieties, some of which are cumulates.
4. Basalt, diabase, spilite, including agglomerate and aquagene tuff.
5. Keratophyre, quartz keratophyre, and coarser intrusive equivalents.

The analyses are grouped according to these subdivisions in tables 1–5 and designated by differentiating symbols on the diagrams accompanying this report.

Harzburgite and related rocks

Harzburgite, with some dunite and very minor chromitite, makes up the bulk of the ultramafic portion of the Coast Range ophiolite. These rocks are partly to completely serpentinized, and texturally they range from massive to intensely sheared. Massive varieties and blocks in the sheared varieties have a pronounced metamorphic fabric due to orthopyroxenes being concentrated into layers having preferred crystal orientation (Nicolas, 1968, 1969). Chromite grains are commonly arranged in linear trains, but this is generally difficult to

detect. Typically the metamorphic fabric cannot be related to the fabric in either underlying Franciscan metamorphic rocks or in overlying parts of the ophiolite succession; it seems clearly to have originated when the ultramafic rocks were in a different environment.

The primary minerals in the harzburgites are olivine, orthopyroxene, minor clinopyroxene, and accessory chromian spinel. Alteration minerals in addition to serpentine include magnetite, brucite, and tremolite. Plagioclase has not been noted in any of these rocks. For the harzburgites of Del Puerto yielding analysis 12 in table 1, Himmelberg and Coleman (1968) report a modal composition of: olivine ($For_{90.4}$), 61.4 percent; orthopyroxene ($En_{90.6}$), 27.2 percent; clinopyroxene ($Ca:Mg:Fe=48.4:48.6:3$), 4.5 percent; chromian spinel ($Cr:Al:Fe:Mg=30:38:16:16$), 1.5 percent; and serpentine (lizardite and chrysotile), 5.4 percent.

The dunite is largely composed of coarse- to medium-grained olivine but includes minor amounts of orthopyroxene, exsolved clinopyroxene, and chromian spinel, plus the same alteration products as in harzburgite. Microprobe analyses of olivine from dunite at Del Puerto showed a range of $For_{87.4}-For_{90.9}$ (Himmelberg and Coleman, 1968), similar to the olivine in nearby harzburgite.

Table 1.—Chemical analyses of harzburgite, dunite, and serpentinite from the ophiolite at base of Great Valley sequence

	1	2	3	4	5	6	7	8	9	10	11	12
SiO ₂	35.7	35.7	35.9	36.1	36.57	39.0	39.9	40.0	40.50	42.75	43.2	44.9
Al ₂ O ₃19	.28	.43	.76	.95	.04	.70	.58	.78	.35	.58	.91
Fe ₂ O ₃	5.3	3.8	4.5	3.7	7.29	2.8	6.5	3.2	4.01	1.72	1.7	.80
FeO	4.9	3.2	3.7	4.5	0.37	5.0	2.0	4.0	2.04	7.03	5.6	7.0
MgO	41.3	42.6	42.2	41.7	40.27	46.1	34.6	41.8	37.43	45.40	41.5	43.0
CaO22	.30	.30	.85	.14	.00	2.3	.30	.39	.037	.73	1.5
Na ₂ O00	.00	.00	.08	.31	.00	.0	.00	.28	.01	.00	.02
K ₂ O04	.00	.05	.63	.01	.23	.10	.04	.16	.00	.12	.08
H ₂ O+	11.3	12.6	11.7	10.3	12.43	5.6	11.5	9.0	10.94	1.60	5.9	1.0
H ₂ O-55	.57	.65	.45	.94	.50	1.1	.65	2.81	.09	.16	.09
TiO ₂00	.00	.02	.02	---	.02	.0	.00	---	.01	.02	.02
P ₂ O ₅07	.06	.07	.03	---	.03	.0	.06	---	.00	.06	.03
MnO18	.12	.14	.12	.10	.11	.08	.12	.13	.10	.15	.12
CO ₂34	.24	.32	.08	---	.21	.23	.25	---	.74	<.05	<.05
NiO15	.24	.24	.22	.31	.35	---	.32	.11	.04	.28	.32
Cr ₂ O ₃16	.94	.67	.93	.33	.44	---	.60	.41	.28	.58	.47
Sum	100.4	100.6	100.9	100.5	100.02	100.4	99.0	100.9	99.99	100.16	100.6	100.3
Density ...	2.72	2.67	2.71	2.72	---	2.83	2.65	2.80	---	---	3.14	3.22

1. Serpentinized dunite (65-R-3), Del Puerto, Stanislaus County, Calif. (Himmelberg and Coleman, 1968, p. C21).
2. Serpentinized dunite (65-R-12), Del Puerto, Stanislaus County, Calif. (Himmelberg and Coleman, 1968, p. C21).
3. Serpentinized dunite (65-R-1), Del Puerto, Stanislaus County, Calif. (Himmelberg and Coleman, 1968, p. C21).
4. Serpentinized dunite (66-R-6), Del Puerto, Stanislaus County, Calif. (Himmelberg and Coleman, 1968, p. C21).
5. Bastitic serpentine, Bagley Creek, Contra Costa County, Calif. (Turner, 1891, p. 406).
6. Partly serpentinized dunite (66-R-22), Del Puerto, Stanislaus County, Calif. (Himmelberg and Coleman, 1968, p. C21).

7. Serpentinized peridotite (71-EB-101), Point Sal, Santa Barbara County, Calif. Analysis by Lowell Artis.
8. Partly serpentinized harzburgite (65-R-10), Del Puerto, Stanislaus County, Calif. (Himmelberg and Coleman, 1968, p. 21).
9. Partly serpentinized harzburgite(?), Bagley Creek, Contra Costa County, Calif. (Turner, 1891, p. 406).
10. Harzburgite, Del Puerto, Stanislaus County, Calif. (Bodenlos, 1950, p. 233).
11. Harzburgite (65-R-9), Del Puerto, Stanislaus County, Calif. (Himmelberg and Coleman, 1968, p. C21).
12. Harzburgite (66-R-20), Del Puerto, Stanislaus County, Calif. (Himmelberg and Coleman, 1968, p. C21).

Twelve analyses of dunite and harzburgite from the Coast Range ophiolite are given in table 1. These ultramafic rocks are characterized by very low Al_2O_3 and CaO , each generally less than 0.5 percent, consistent with the absence of plagioclase and the nearly complete absence of clinopyroxene. On a normalized water-free basis, SiO_2 shows a small range of 40.3 to 42.2 (avg 40.9) percent in the dunite, and 43.4 to 47.0 (avg 45.0) in the harzburgite. MgO ranges from 46.4 to 48.8 (avg 47.5) percent in the dunite, and 43.3 to 46.1 (avg 44.5) in the harzburgite. The ratio of total iron (as FeO) to MgO ranges only from 0.15 to 0.19, except for one value of 0.23, the average being equivalent to a ratio of 14.5 FeO to 86.4 MgO , slightly lower than in the principal minerals because of small amounts of accessory clinopyroxene and spinel. All samples are very low in alkalis; only old, possibly suspect, analyses show more than 0.12 percent K_2O . These rocks are generally believed to represent a residuum left after removal of a partial melt from parent mantle material having a composition such as pyrolite or lherzolite (Green and Ringwood, 1967; Coleman, 1971).

Clinopyroxenite and related rocks

Coarse-grained clinopyroxene-rich rocks occur in minor amounts as crosscutting dikes, locally as massive lenses in the harzburgite, and as cumulate layers in the gabbro. As far as we can determine, these rocks everywhere postdate the harzburgite and dunite.

Most of the analyzed rocks are composed entirely of coarse-grained clinopyroxene that generally contains exsolution lamellae of orthopyroxene. Analyzed clinopyroxene from pyroxenite in the Del Puerto area is nearly identical in composition to that from harzburgite (Himmelberg and Coleman, 1968). Minor brown amphibole was seen in a few thin sections of clinopyroxenite. Serpentine minerals are commonly found in the clinopyroxene-rich rocks as thin veinlets, and secondary tremolite and carbonate occur locally; however, the degree of alteration in these rocks, especially serpentinization, is much less than in the harzburgite-dunite group.

The other ultramafic rocks grouped here with the clinopyroxenite are less common; these include wehrlite, lherzolite, and amphibole peridotite, all of which generally occur as thin veins or layers in harzburgite or dunite. Cumulate textures, in which rounded and vermicular grains of clinopyroxene are enclosed by serpentinized olivine, can be recognized in some of the wehrlites, but most of the rocks have a later metamorphic fabric that makes positive identification of cumulate textures difficult. Brownish hornblende is fairly common, and calcic plagioclase is a rare constituent in some of the wehrlites.

The five clinopyroxenite analyses (table 2) are all similar to one another and to the mineral analyses presented by Himmelberg and Coleman for clinopyroxene from the Del

Puerto area (1968, table 5, p. C23). As compared with the harzburgites, CaO is much higher, and this, together with low Al_2O_3 , reflects the abundance of clinopyroxene. Alkalies are very low in these rocks, and TiO_2 content is generally nearly an order of magnitude greater than in the harzburgite-dunite group. The other analyses in the group of clinopyroxene-rich rocks are of wehrlites, amphibole peridotite, and perhaps lherzolite. The only possible lherzolite (analysis 22) contains enough olivine and orthopyroxene to be chemically transitional between the harzburgite-dunites and the clinopyroxenites.

Gabbro

Gabbros in the Coast Range ophiolite have a wide range of occurrences, doubtless a variety of origins, and a correspondingly large range in chemical composition. Gabbro occurs as dikes cutting harzburgite and dunite, as complex lenticular masses lying above the ultramafic rocks, and as small irregular pegmatitic masses. The gabbros are much less abundant than the ultramafic rocks but are present at most ophiolite localities. The largest masses are only about 600 m (2,000 ft) thick, and although one mass has an exposed length of 8 km (5 mi), most are much less extensive.

The relations of gabbros to ultramafic rocks are still poorly understood. So far as is known, the gabbros, in contrast to the harzburgites, generally do not possess the tectonite fabrics that are unrelated to their surroundings. Gabbro dikes cutting serpentinized harzburgite, however, have been stretched, pulled apart, and locally converted to isolated tectonic blocks by shearing parallel to the borders of the harzburgite bodies. Gabbroic cumulates locally show some planar deformation parallel to compositional layering, which initially was defined by rounded crystals of olivine or clinopyroxene enveloped in calcic plagioclase. In addition, these layered cumulates commonly have mineral graded bedding similar to that described for the Papuan ophiolite (Davies, 1971, pl. 7, fig. 2 and pl. 8, fig. 1).

Primary minerals in the gabbros are olivine, clinopyroxene, calcic plagioclase, green or brown hornblende, and opaque minerals; the more common secondary minerals are serpentine, hydrogrossular, prehnite, epidote, and calcite. The mineral composition of gabbros in dikes and layered masses at Del Puerto is olivine ($\text{Fo}_{75.2}$ – $\text{Fo}_{79.5}$) and plagioclase (An_{91}) with some clinopyroxene and minor secondary amphibole (Himmelberg and Coleman, 1968). Mineralogically and texturally, some gabbros of the Coast Range ophiolite resemble the gabbroic and anorthositic rocks adjacent to the San Andreas fault as carefully described by Ross (1970). Pegmatitic gabbros, in contrast to the layered gabbros, are nonfoliated and commonly contain large randomly oriented crystals of hornblende and a little quartz.

Where hornblende is dominant over clinopyroxene, the gabbros grade into amphibolite (analysis 23), but in the rocks

Table 2.—*Chemical analyses of clinopyroxenite and related rocks from the ophiolite at base of Great Valley sequence*

	13	14	15	16	17	18	19	20	21	22
SiO ₂	53.25	52.5	51.5	50.8	49.4	49.1	48.4	46.5	44.6	41.3
Al ₂ O ₃	2.80	1.2	2.2	2.4	2.1	5.8	3.3	7.0	2.0	3.4
Fe ₂ O ₃69	.70	1.2	1.2	2.2	1.4	1.3	2.6	3.7	5.9
FeO	5.93	5.0	3.7	4.5	4.2	4.4	3.9	6.5	3.6	5.7
MgO	19.91	20.6	17.0	20.7	21.6	15.7	23.7	21.6	27.5	28.9
CaO	16.22	18.8	20.9	18.7	16.9	19.7	15.4	11.0	11.5	6.4
Na ₂ O19	.00	.15	.06	.16	.06	.12	.43	.12	.13
K ₂ O01	.24	.08	.05	.02	.07	.0	.14	.08	.01
H ₂ O+24	.47	1.1	1.1	3.2	2.1	4.0	2.7	5.6	7.8
H ₂ O-05	.11	.26	.10		.27	.26	.16	.36	
TiO ₂	---	.00	.18	.10	.15	.21	.20	.25	.04	.08
P ₂ O ₅	---	.06	.02	.04	.04	.04	.0	.06	.0	.05
MnO09	.18	.14	.15	.14	.19	.12	.18	.09	.19
CO ₂	---	.05	.58	---	.11	.0	.01	---	.04	.13
NiO07	.02	---	---	---	---	---	---	---	---
Cr ₂ O ₃54	.17	---	---	---	---	---	---	---	---
Sum	99.99	100.1	99.01	99.90	100.2	99.04	100.71	99.12	99.23	100.0
Density	---	3.25	3.12	3.24	3.13	3.15	3.20	3.16	2.96	2.91

13. "Pyroxenite with some olivine," Bagley Creek, Contra Costa County, Calif. (Turner, 1891, p. 406).
 14. Clinopyroxenite cumulate (65-R-7), Del Puerto, Stanislaus County, Calif. (Himmelberg and Coleman, 1968, p. C21).
 15. Clinopyroxenite (69-EB-50), Elder Creek, Tehama County, Calif. Analysis by G. Chloe, P. Elmore, J. Glenn, J. Kelsey, and H. Smith.
 16. Clinopyroxenite (70-CLE-34), Del Puerto, Stanislaus County, Calif. Analysis by G. Chloe, P. Elmore, J. Glenn, J. Kelsey, and H. Smith.
 17. Clinopyroxenite cumulate (59-349), Skaggs Springs quadrangle, Sonoma County, Calif. (Bailey and others, 1964, p. 84).

18. Clinopyroxenite (69-EB-51), Elder Creek, Tehama County, Calif. Analysis by G. Chloe, P. Elmore, J. Glenn, J. Kelsey, and H. Smith.
 19. Wehrlite cumulate (69-B-33a), Elder Creek, Tehama County, Calif. Analysis by Sam Botts.
 20. Amphibole peridotite (70-CLE-35), Del Puerto, Stanislaus County, Calif. Analysis by I. H. Barlow, S. D. Botts, Gillison Chloe, P. D. L. Elmore.
 21. Wehrlite cumulate (71-EB-103), Point Sal, Santa Barbara County, Calif. Analysis by Lowell Artis.
 22. Lherzolite(?) (59-347), Skaggs Springs quadrangle, Sonoma County, Calif. (Bailey and others, 1964, p. 84).

with abundant hornblende it is not clear if the amphibole is primary, replaces pyroxene as suggested by Thayer (1967, 1972) and Southwick (1970), or is metasomatic (Knipper, 1970). Most of the hornblende gabbro appears to be of igneous origin, based on intrusive contacts and lack of replacement textures. At one locality, along the South Fork of Elder Creek (fig. 1), we noted very coarse grained amphibole gabbro enclosed in clinopyroxenite with very fuzzy contacts separating the two, suggesting metasomatic replacement of the clinopyroxenite.

Chemical analyses of eleven gabbros are given in table 3. SiO₂ ranges from 39.4 to 48.7 percent. Total iron as FeO ranges from less than 4 percent to nearly 20 percent, the high iron values reflecting abundant amphibole and iron enrichment, as discussed in the section on differentiation trends. Na₂O is low in these rocks, averaging about 1.0 percent, and K₂O is less than 0.3 percent except in gabbros that appear to have been altered extensively after solidification. TiO₂ shows a wide range, 0.08 to 2 percent, probably reflecting the diverse origins of the different rock types included.

Basalt, diabase, and spilite

Basalt occurs chiefly as pillow lava, agglomerate, and breccia in a sequence generally between 300 and 1,500 m

(1,000–5,000 ft) thick overlying gabbro or ultramafic rock. Basaltic tuff is a rare component of the ophiolite, but diabase is commonly found as dikes and minor intrusive bodies. Locally, as along Stony Creek in the Stonyford quadrangle (fig. 1), both diabase and pillow basalt are remarkably fresh and consist of calcic plagioclase, pinkish (probably titaniferous) augite, and opaque minerals with only minor secondary celadonite and carbonate. In many places, however, the basalt or diabase has undergone spilitic alteration to albite, pumpellyite, chlorite, epidote, calcite, and minor amounts of other secondary minerals. Olivine is an uncommon constituent of most of these rocks, even where fresh, and where once present, it is generally serpentinized. Many of the basalts had a glassy groundmass that is typically altered to chlorite.

Chemical analyses of 21 basalts and related rocks from 11 widely separated localities are given in table 4. On a normalized calcite- and water-free basis, SiO₂ ranges from 49 to 58 percent, and less than one-third of the analyses show normative olivine. Al₂O₃ ranges from 11.9 to 16.6 percent, as compared to the range of 12 to 18 percent for ocean-ridge basalts reported by Kay, Hubbard, and Gast (1970). CaO is unusually low and has a wide range of about 5 to 11 percent, as compared with average contents of 10 to 13 percent in ocean-ridge basalts. Na₂O and K₂O are generally higher than

Table 3.—Chemical analyses of gabbro from the ophiolite at the base of Great Valley sequence
[N.d., not determined]

	23	24	25	26	27	28	29	30	31	32	33
SiO ₂	39.4	42.0	43.75	45.1	45.7	46.01	46.9	47.7	47.91	48.0	48.7
Al ₂ O ₃	14.9	11.0	19.71	16.9	17.5	15.41	20.6	18.9	17.99	19.3	15.0
Fe ₂ O ₃	6.2	2.1	7.08	4.4	.2	2.30	.40	.30	2.70	.81	1.0
FeO	13.8	7.6	6.20	8.9	3.3	5.77	4.1	1.9	4.88	6.9	3.8
MgO	2.9	19.3	5.79	9.3	11.4	13.09	9.0	7.2	10.21	9.8	10.8
CaO	15.8	12.0	13.56	12.6	15.7	15.73	14.2	19.4	14.33	13.3	15.7
Na ₂ O	1.1	.71	1.69	.45	.80	.79	1.4	1.0	.82	.55	1.7
K ₂ O22	.07	.13	.30	.96	.01	.14	.20	.03	.08	.12
H ₂ O+	1.8	3.3	1.30	.79		.86	1.6	3.5	.85	.88	2.5
H ₂ O-16	.32	.32	.12	4.4	.23	.13	.26	.19	.12	.19
TiO ₂	2.0	.82	.65	.54	.08	.22	.06	.03	.13	.08	.29
P ₂ O ₅68	.04	.06	.06	.02	.08	---	---	.09	.02	.02
MnO15	.16	.12	.18	.08	.11	.04	.61	.11	.03	.09
CO ₂	---	.16	---	---	.06	N.d.	.04	.02	N.d.	---	<.05
NiO	---	.11	---	---	---	---	---	---	---	---	.02
Cr ₂ O ₃	---	.25	---	---	---	---	---	---	---	---	.24
Sum	99.1	99.9	100.36	99.6	100.0	100.61	98.6	100.4	100.24	99.87	100.2
Density	3.16	3.00	---	---	2.96	---	2.84	3.03	---	3.00	3.04

23. Amphibolite (70-CLE-6), Quinto Creek, Stanislaus County, Calif. Analysis by G. Chloe, P. Elmore, J. Glenn, J. Kelsey, and H. Smith.
 24. Olivine gabbro (66-R-5), Del Puerto, Stanislaus County, Calif. (Himmelberg and Coleman, 1968, p. C21).
 25. Hornblende clinopyroxene gabbro (R-501-10), San Leandro quadrangle, Alameda County, Calif. Analysis by M. Chiba.
 26. Norite (MB-1A), Del Puerto, Stanislaus County, Calif. Analysis by G. Chloe, P. Elmore, J. Glenn, J. Kelsey, and H. Smith.
 27. Gabbro cumulate (59-348), Skaggs Springs quadrangle, Sonoma County, Calif. (Bailey and others, 1964, p. 84).
 28. Olivine clinopyroxene gabbro (R-501-54), San Leandro quadrangle, Alameda County, Calif. Analysis by M. Chiba.

29. Olivine clinopyroxene gabbro (71-EB-104), Point Sal, Santa Barbara County, Calif. Analysis by Lowell Artis.
 30. Olivine clinopyroxene gabbro (69-B-31), Elder Creek, Tehama County, Calif. Analysis by Lowell Artis.
 31. Hornblende clinopyroxene gabbro (R-501-55), San Leandro quadrangle, Alameda County, Calif. Analysis by M. Chiba.
 32. Hornblende gabbro (70-CLE-31), Del Puerto, Stanislaus County, Calif. Analysis by G. Chloe, P. Elmore, J. Glenn, J. Kelsey, and H. Smith.
 33. Hornblende clinopyroxene gabbro (66-R-10), Del Puerto, Stanislaus County, Calif. (Himmelberg and Coleman, 1968, p. C21).

in the ocean-ridge basalts; this, along with the low CaO, may be a result of spilitization.

On an alkali-silica plot (fig. 2), most of the analyses fall in the tholeiite field of Macdonald and Katsura (1964) and Irvine and Baragar (1971). Using the curves of Kuno (1968), however, only one of the analyses is of tholeiite and the others are about equally divided between high-alumina basalt and alkali basalt.

On the basis of TiO₂ content, the basalt and diabase analyses can be divided into two groups. The high-titanium group includes all samples that plot less than 53.3 percent SiO₂ in figure 2, and it also is characterized by higher iron and calcium. Most of these high-titanium basalts and diabases are from the Stonyford area and are the freshest of the samples studied. On a TiO₂:P₂O₅ plot, the high-titanium basalts lie within the oceanic island basalt field, whereas those with low TiO₂ plot well within the field of ocean-ridge basalts.

Keratophyre and related rocks

In the upper part of the ophiolite in several areas in the Coast Ranges are light-colored, silica-rich extrusive and intrusive rocks which have generally been called keratophyre, quartz keratophyre, albite granite, or trondhjemite. The finer

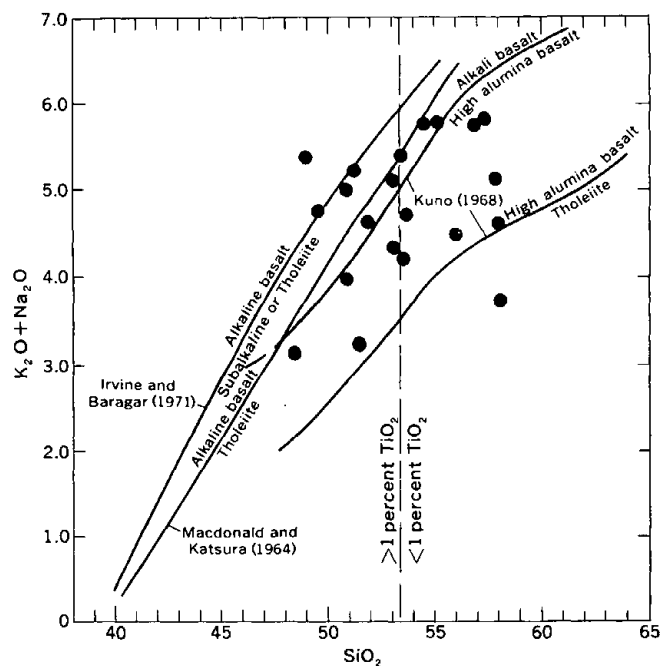


Figure 2.—Total alkali-silica plot of basalts and related rocks from the Coast Range ophiolite. (Based on analyses recalculated to 100 percent after deducting water and CaCO₃.)

	34	35	36	37	38	39	40	41	42	43
SiO ₂	46.2	46.5	46.60	47.5	48.2	49.0	49.2	49.5	49.7	50.2
Al ₂ O ₃	16.6	14.6	15.28	13.5	13.2	14.8	13.0	13.0	14.3	14.0
Fe ₂ O ₃	6.3	5.0	3.98	3.3	3.4	3.4	4.6	4.7	5.1	2.3
FcO	4.2	6.4	8.17	7.3	8.4	6.1	8.1	8.6	1.3	9.4
MgO	5.2	6.8	5.4	4.0	5.5	7.2	5.2	5.7	8.4	6.4
CaO	8.5	7.9	10.68	11.0	9.7	7.9	9.3	8.3	6.4	7.7
Na ₂ O	4.2	2.2	2.26	3.3	3.4	4.2	2.8	4.3	2.4	4.3
K ₂ O82	2.3	.85	.54	.32	.78	.24	.53	.27	.15
H ₂ O+	---	4.2	3.63	2.3	---	---	2.0	---	3.7	3.3
H ₂ O-	4.8	---	.24	.67	3.9	4.1	.73	2.40	7.3	.43
TiO ₂	2.3	2.5	2.87	2.5	2.3	1.9	3.0	2.3	.57	1.8
P ₂ O ₅44	.34	.36	.31	.26	.32	.11	.27	.10	.05
MnO20	.38	.08	.25	.18	.19	.22	.27	.04	.37
CO ₂34	.70	.06	3.8	.15	.27	.25	.14	---	.01
Sum	<u>100.1</u>	<u>99.8</u>	<u>100.46</u>	<u>100.3</u>	<u>98.9</u>	<u>100.2</u>	<u>98.7</u>	<u>100.0</u>	<u>99.6</u>	<u>100.4</u>
Density	2.73	2.76		3.00	2.84	2.86	3.00	2.94	2.38	3.00
<hr/>										
34.	Spilite (BSO-108), Dry Creek, Glenn County, Calif. Analysis by I. Barlow, S. Botts, G. Chloe, and P. Elmore.				39.	Spilite (BSO-94), Stony Creek, Colusa County, Calif. Analysis by I. Barlow, S. Botts, G. Chloe, and P. Elmore.				
35.	Diabase (BSO-91), Stony Creek, Colusa County, Calif. Analysis by I. Barlow, S. Botts, G. Chloe, and P. Elmore.				40.	Diabase (SF-70-2), Stony Creek, Colusa County, Calif. Analysis by Sam Botts.				
36.	Basalt, Sebastopol quadrangle, Sonoma County, Calif. (Switzer, 1945, p. 7).				41.	Spilite (BSO-90), Stony Creek, Colusa County, Calif. Analysis by I. Barlow, S. Botts, G. Chloe, and P. Elmore.				
37.	Basalt (SF-70-1), Stony Creek, Colusa County, Calif. Analysis by S. Botts.				42.	Zeolitized basaltic tuff (B69-4), 2 mi (3 km) SE. of Bradford Mountain, Sonoma County, Calif. Analysis by L. Artis, G. Chloe, P. Elmore, J. Glenn, J. Kelsey, and H. Smith.				
38.	Basalt (BSO-107), Stony Creek, Colusa County, Calif. Analysis by I. Barlow, S. Botts, G. Chloe, and P. Elmore.				43.	Spilite (70-B-102), Pope Creek, Napa County, Calif. Analysis by Sam Botts.				

	44	45	46	47	48	49	50	51	52	53	54
SiO ₂	50.5	50.7	51.0	51.7	51.8	52.0	52.1	52.5	53.8	54.7	55.5
Al ₂ O ₃	15.8	14.8	16.3	15.7	15.0	13.5	14.8	14.0	15.0	15.2	15.1
Fe ₂ O ₃	4.5	3.9	3.9	1.4	2.8	1.7	1.5	2.6	3.0	3.5	1.2
FeO	2.7	7.5	6.1	5.7	7.1	6.8	6.3	4.6	7.2	4.8	6.1
MgO	7.1	5.3	6.1	7.1	4.9	9.8	7.0	6.4	5.8	5.5	6.4
CaO	8.2	6.4	7.7	5.5	6.7	7.3	6.1	10.1	5.1	4.9	6.4
Na ₂ O	4.6	4.7	3.6	4.0	4.7	3.7	4.4	2.8	5.1	4.6	4.0
K ₂ O47	.10	.39	1.2	.66	.54	.80	.40	.50	.19	.34
H ₂ O+	2.8	2.2	3.7	4.0	3.0	3.2	3.9	3.5	1.9	3.8	2.4
H ₂ O-.....	.79	.76	.32	.57	.45	.63	.60	.50	.49	.37	.51
TiO ₂86	1.8	.10	.48	.86	.50	.72	.62	.53	.80	.55
P ₂ O ₅12	.01	.01	.05	.10	---	.08	.08	.05	.11	.05
MnO11	.17	.17	.14	.19	.14	.13	.10	.14	.11	.11
CO ₂61	.27	.02	1.7	1.1	.02	2.7	2.8	.30	.06	.08
Sum	99.2	98.6	99.4	99.2	99.4	99.8	101.1	101.0	98.9	98.6	98.7
Density	---	2.84	3.00	2.76	2.78	2.92	2.76	2.76	2.81	2.76	2.82
44. Spilite (CP-1B), Quinto Creek, Stanislaus County, Calif. Analysis by G. Chloc, P. Elmore, J. Glenn, J. Kelsey, and H. Smith.						49. Basalt (70-B-100), Pope Creek, Napa County, Calif. Analysis by Sam Botts.					
45. Spilite (70-EB-301), "Cuesta diabase," 1½ mi NW. of Cerro Alto, San Luis Obispo County, Calif. Analysis by Lowell Artis.						50. Spilite (69-B-38), Elder Creek, Tehama County, Calif. Analysis by Lowell Artis.					
46. Coarse diabase agglomerate (69-B-34), Elder Creek, Tehama County, Calif. Analysis by S. Botts.						51. Diabase agglomerate (69-B-37), Elder Creek, Tehama County, Calif. Analysis by Lowell Artis.					
47. Spilite (72-B-44), 1 mi E. of Eagle Peak, Paskenta quadrangle, Tehama County, Calif. Analysis by Lowell Artis.						52. Splitized diabase (69-B-15), Fall Creek, Healdsburg quadrangle, Sonoma County, Calif. Analysis by Lowell Artis.					
48. Spilite (B69-14), Fall Creek, Healdsburg quadrangle, Sonoma County, Calif. Analysis by L. Artis, G. Chloc, P. Elmore, J. Glenn, J. Kelsey, and H. Smith.						53. Spilite agglomerate (69-B-35), Elder Creek, Tehama County, Calif. Analysis by Lowell Artis.					
						54. Spilite (70-B-302), Point Sal, Santa Barbara County, Calif. Analysis by Lowell Artis.					

grained varieties may petrographically resemble andesite, dacite, or rhyolite but are richer in Na_2O and poorer in K_2O and CaO . The keratophytic rocks occur as pillow lavas in the Quinto Creek area and as massive flows(?) or local tuff-breccias in other areas. Coarser varieties seem to be dikes or sills that generally occur in the same areas as the finer keratophyre. These siliceous rocks lie above the gabbros, and in the Del Puerto, Quinto Creek, and Bradford Mountain areas they are apparently more common than basaltic rocks that normally occur at this level in the ophiolite. Their occurrence in the Coast Ranges is virtually confined to localities in an ophiolite sequence, and their field relations make it clear that they should be regarded as an integral part of this sequence.

These rocks in hand specimen generally show conspicuous euhedral phenocrysts of quartz and feldspar. In thin section, the extrusive varieties are characterized by glomeroporphyritic textures defined by clots of euhedral plagioclase (An_{50-62}), generally with pronounced zoning, in a fine-grained recrystallized matrix of quartz and albite. Quartz phenocrysts have the high-temperature β form and are typically much corroded. The keratophyre represented by analysis 61 (table 5) contains phenocrysts of sanidine. Primary mafic minerals have not been recognized in the more siliceous varieties, but secondary minerals such as epidote, Fe-rich pumpellyite, and chlorite

appear to pseudomorph original biotite or hornblende. At several localities veins of deep-green to gray volcanic glass cut by veinlets of heulandite have been noted.

The intrusive types range from quartz porphyry, consisting of phenocrysts of quartz and albitized plagioclase in a much altered fine-grained matrix, to coarse-grained granular granitic rocks (hornblende quartz diorite?) that locally are interlayered or show complex intrusive relations with gabbro and amphibolite. The freshest samples contain relatively abundant hornblende and minor biotite, largely replaced by chlorite, prehnite, and epidote.

Chemical analyses of 10 keratophyres and related rocks from 4 localities are listed in table 5. We have somewhat arbitrarily designated as keratophyre all rocks with SiO_2 between 56 and 65 percent and used quartz keratophyre for those with $\text{SiO}_2 > 65$ percent. Most of these rocks are characterized by a higher ratio of $\text{Na}_2\text{O}:\text{K}_2\text{O}$ than found in normal calc-alkaline igneous rocks. Their chemical relation to calc-alkaline rhyolite, dacite, and other silicic extrusive rocks based on normative feldspar plots (O'Connor, 1965) is shown in figure 3. These chemical data plus the petrographic descriptions suggest that the keratophyre and quartz keratophyre may represent albitized andesite, dacite, and rhyolite, and their intrusive equivalents.

Table 5.—Chemical analyses of keratophyre and quartz keratophyre from ophiolite at base of Great Valley sequence

	55	56	57	58	59	60	61	62	63	64
SiO_2	57.5	58.2	65.4	68.04	70.0	72.5	72.6	72.9	74.1	77.08
Al_2O_3	14.5	16.4	14.3	12.09	13.6	14.0	14.4	12.5	12.0	12.43
Fe_2O_3	1.7	3.7	2.9	3.81	2.6	.77	1.5	2.0	1.8	1.48
FeO	5.3	4.8	3.6	3.21	2.4	3.3	.60	2.6	1.4	.55
MgO	3.3	3.2	1.2	1.97	.73	1.0	.40	.35	1.61	.23
CaO	5.5	6.8	3.3	3.41	2.7	2.5	1.2	2.4	1.5	.88
Na_2O	5.2	3.3	5.4	5.04	5.2	3.7	5.2	4.7	3.7	6.13
K_2O20	.54	.52	---	.35	.33	1.1	.20	1.3	.15
H_2O^+	2.6	1.1	2.1	1.89	.93	1.5	1.4	.86	1.7	.92
H_2O^-28	.24	.39	.54	.37	.08	.46	.24	.45	.31
TiO_261	.77	.65	.46	.62	.21	.20	.30	.37	.22
P_2O_506	.12	.12	.05	.18	.06	.03	.08	.08	.02
MnO08	.16	.07	.10	.05	.06	---	.04	.05	.07
CO_2	3.5	---	---	---	---	---	.02	.05	---	---
Sum	100.3	99.3	99.9	100.61	99.7	100.0	99.1	99.2	100.0	100.47
Density	2.70				2.70		2.60	2.66		

55. Keratophyre (71-EB-105), Point Sal, Santa Barbara County, Calif. Analysis by L. Artis.

56. Hornblende keratophyre (MB-1B), Del Puerto, Stanislaus County, Calif. Analysis by G. Chloe, P. Elmore, J. Glenn, J. Kelsey, and H. Smith.

57. Quartz keratophyre (B69-8), 1 mi NE. of Bradford Mountain, Healdsburg quadrangle, Sonoma County, Calif. Analysis by L. Artis, G. Chloe, P. Elmore, J. Glenn, J. Kelsey, and H. Smith.

58. Quartz keratophyre (DP-2), Del Puerto, Stanislaus County, Calif. (Bailey and others, 1964, p. 55 from Maddock, 1955).

59. Quartz keratophyre (B69-7), 1½ mi ESE. of Bradford Mountain, Healdsburg quadrangle, Sonoma County, Calif. Analysis by L. Artis, G. Chloe, P. Elmore, J. Glenn, J. Kelsey, and H. Smith.

60. Quartz keratophyre (CP-6), Quinto Creek, Stanislaus County, Calif. Analysis by G. Chloe, P. Elmore, J. Glenn, J. Kelsey, and H. Smith.

61. Quartz keratophyre (70-B-4), Quinto Creek, Stanislaus County, Calif. Analysis by L. Artis.

62. Quartz keratophyre (B69-16), Fall Creek, Healdsburg quadrangle, Sonoma County, Calif. Analysis by L. Artis, G. Chloe, P. Elmore, J. Glenn, J. Kelsey, and H. Smith.

63. Quartz keratophyre (CP-5), Quinto Creek, Stanislaus County, Calif. Analysis by G. Chloe, P. Elmore, J. Glenn, J. Kelsey, and H. Smith.

64. Quartz keratophyre (DP-1), Del Puerto, Stanislaus County, Calif. (Bailey and others, 1964, p. 55 from Maddock, 1955).

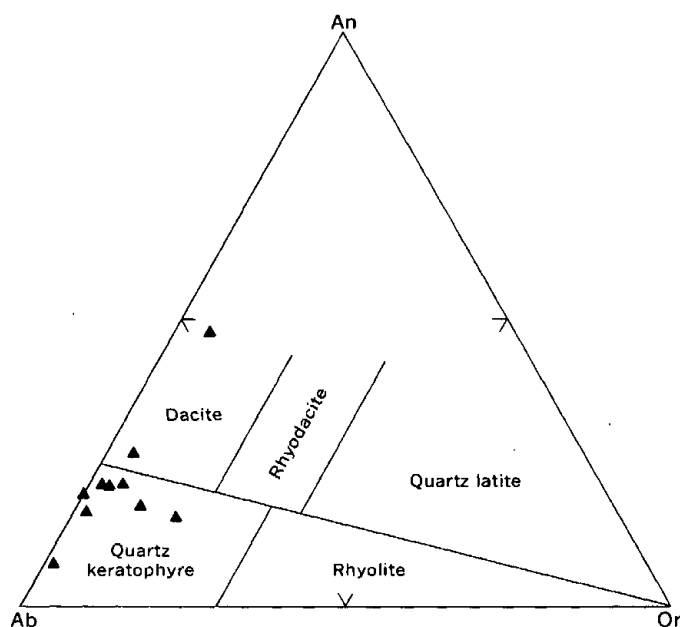


Figure 3.—Normative feldspar ratio plot of keratophyres and related rocks from the Coast Range ophiolite.

RELATIONS AMONG MAJOR ROCK TYPES

The chemical relations among the major kinds of rocks making up the Coast Range ophiolite can be visualized by the use of several of the more commonly used ternary diagrams.

AFM diagram

Figure 4A shows the adjusted analyses plotted on an AFM diagram, which is often used to display pictorially differentiation trends in a suite of rocks (Wager and Deer, 1939; Hess, 1960). In this plot $A = K_2O + Na_2O$, $F = \text{total iron calculated as FeO}$, and $M = MgO$. The most striking feature of the analyses when plotted on this diagram is the virtually complete separation of the five major rock groups.

The field of harzburgite and related rocks shows very little overlap with the field of clinopyroxene-bearing rocks. Both groups are nearly lacking in alkalis, but the fields are separated because of the greater Fe:Mg ratio in the clinopyroxene-bearing rocks.

Especially noteworthy is the separation of basaltic and related rocks from gabbros despite the wide range in composition of both lithologic types. The main difference here is a result of calcic plagioclase in gabbro and sodic plagioclase in basalt. The greater total alkalis in the basaltic group might be attributed entirely to alkali enrichment through seawater reaction (Hart, 1970). However, the alkali enrichment shown by the basalt analyses is largely a result of increased Na_2O , whereas the most striking chemical change in the rinds of pillow basalts is almost everywhere an enrichment in K_2O . The presence of secondary minerals such as albite, pumpellyite,

chlorite, epidote, prehnite, and calcite suggests that the primary chemistry may have been altered by soda metasomatism during low-grade metamorphism.

The keratophyric rocks, with their very high total alkali content, occupy a field distinct from that of basalt and spilite. Although MgO and total iron are unusually low in these rocks, the Fe:Mg ratio for most is somewhat greater than in the basalts.

Or-Ab-An diagram

Figure 4B, based on normative orthoclase, albite, and anorthite, shows the same separation of the keratophyre, basalt, and gabbro fields seen in the AFM diagram. The ultramafic rocks are not plotted because their alkali content is so low that analytical error becomes significant. If they were shown, however, most of the pyroxene-rich rocks would plot within the gabbro field. For all the plotted rocks, the very low normative orthoclase, reflecting low K_2O , is striking and is an earmark of the ophiolitic suite.

QFM diagram

Figure 4C shows the analyses plotted on a QFM diagram, which is based on essentially normative values of quartz (Q), alkalis plus CaO in feldspar (F), and the ferromagnesian components of mafic minerals (M). In this plot the ultramafic rocks lie close to the Q-M side of the triangle, with clinopyroxene-bearing varieties separated from the low-silica harzburgite-dunite group. The gabbro, basalt, and keratophyre groups all lie in a narrow band extending from the F-M base to near the Q apex, suggesting their kinship and indicating little difference in alkalis plus CaO (F) throughout a compositional range from very mafic to very silicic lithologies. In this plot, contrary to figures 4A and 4B, there is considerable overlap of the fields of basalt and gabbro.

ACF diagram

Figure 4D, the analytical data plotted on an ACF diagram, compares excess Al_2O_3 over that used for feldspar plus ferric iron (A), CaO (C), and the ferromagnesian oxides (F). Here, as in figure 4C, the gabbro and basalt occupy nearly the same field, which is slightly overlapped by the more mafic keratophyres. The gabbro, basalt, keratophyre, and clinopyroxenite fields are approximately centered on a line extending from a point on the C-F base near $1/3$ C and $2/3$ F to the A apex, indicating a nearly constant ratio of lime to ferromagnesian oxides through rocks having a range in normative feldspar content from 0 to more than 50 percent. The harzburgite-dunite rocks cluster in the F apex and are clearly separated from the clinopyroxenites, reflecting the near absence of lime in the orthopyroxene-olivine rocks. A similar relation was shown in a $CaO-Al_2O_3$ plot by Coleman (1971, fig. 3, p. 1216), who suggested that partial melting of

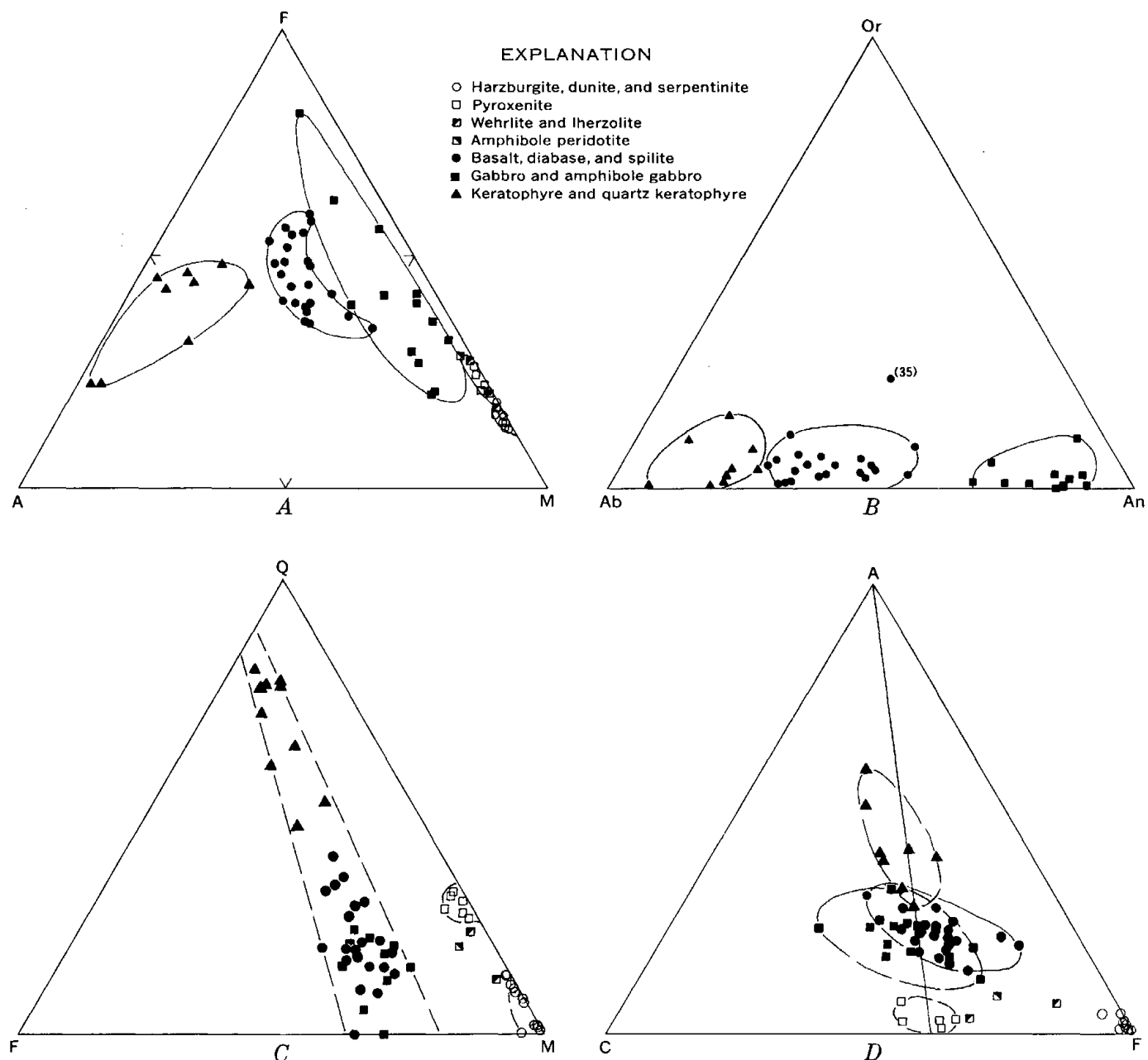


Figure 4.—Ternary diagrams of analyzed rocks from the Coast Range ophiolite. A, AFM diagram with $A = \text{Na}_2\text{O} + \text{K}_2\text{O}$, $F = \text{total iron as FeO}$, and $M = \text{MgO}$. B, Or-Ab-An diagram based on normative feldspars. C, QFM diagram based on calculated SiO_2 in quartz, cations in feldspar, and ferromagnesian oxides in mafic minerals. D, ACF diagram based on calculated Al_2O_3 not in feldspar plus ferric iron indicated by A, CaO indicated by C, and ferromagnesian oxides indicated by F.

Iherzolite might produce a harzburgite-dunite component plus basaltic liquid, which with differentiation and crystal settling could yield both keratophyre and gabbro.

MgO variation diagram

MgO variation diagrams of the Coast Range ophiolite are shown in figure 5. This kind of diagram has been used elsewhere in determining the petrologic process responsible for

chemical variations in a suite of igneous rocks. For example, Wright (1971) demonstrated that for some basalt suites in Hawaii chemical variation can be explained simply by the addition or subtraction of olivine phenocrysts, while in others a more complicated process involving olivine, hypersthene, augite, and plagioclase seems to be required. Similarly, for some differentiated lavas from Kilauea Volcano, mixing of magmas has been shown to be the most reasonable process (Wright and Fiske, 1971).

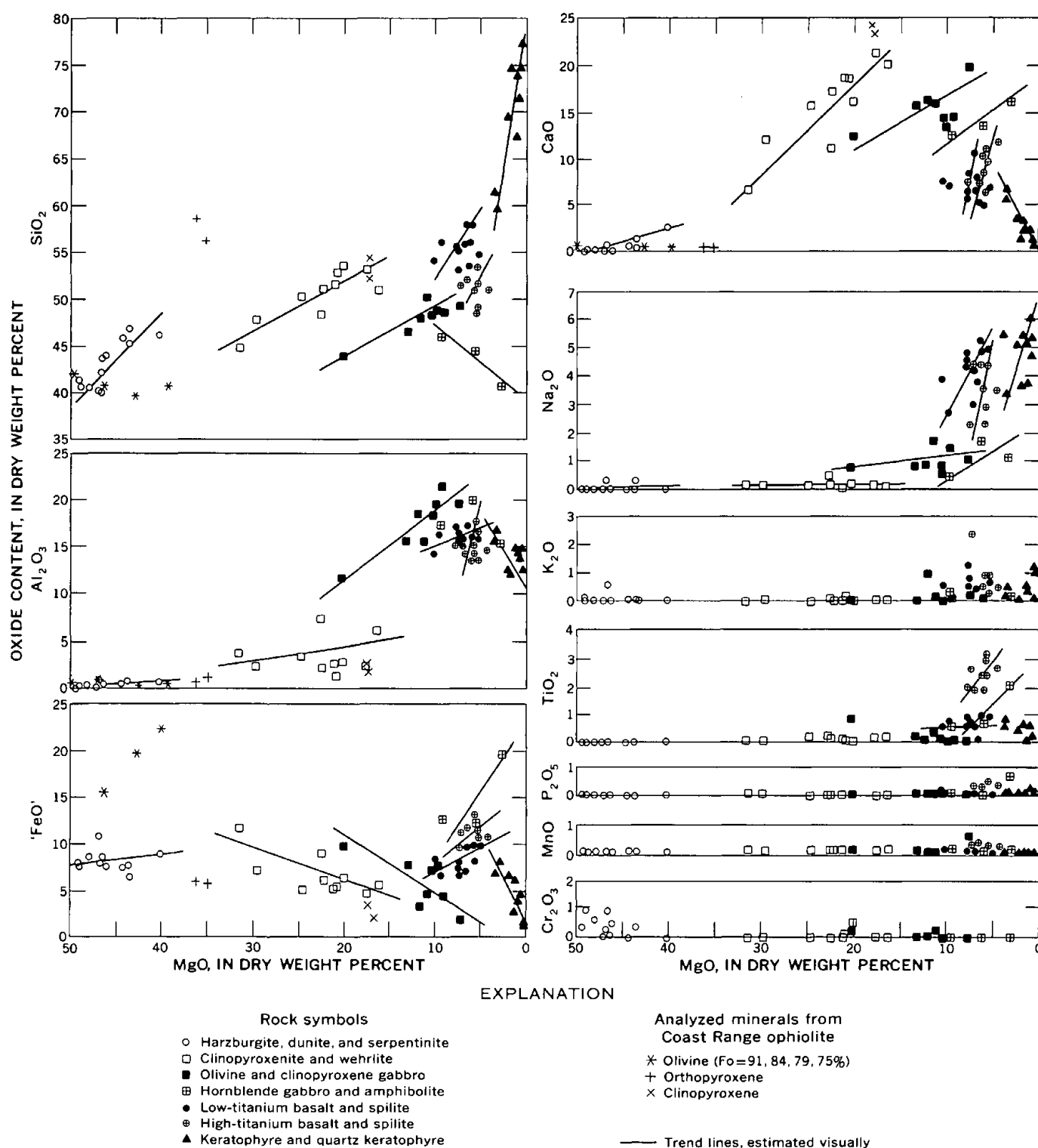


Figure 5.—MgO variation diagrams for rocks from the Coast Range ophiolite. 'FeO' is total iron expressed as sum of FeO and $0.9 \text{ Fe}_2\text{O}_3$.

For figure 5, analyses were normalized to 100 percent dry weight, and 'FeO' is total iron expressed as the sum of FeO and $0.9 \text{ Fe}_2\text{O}_3$. A few analyzed minerals that might control

the chemical variation have been plotted. These are from Himmelberg and Coleman (1968) and include olivines from harzburgite-dunite (maximum range), clinopyroxene, and

mafic gabbro; orthopyroxenes from harzburgite (maximum range); and clinopyroxene from clinopyroxenite and harzburgite.

The plotting of trend lines using the fivefold grouping of the rocks proved to be difficult owing to the scatter of points, and at first it seemed necessary to omit from the variation diagrams analyses that were felt to represent either altered rock or atypical samples. However, after subdividing the gabbro group into two subgroups based on amount of total iron and separating the basalts into high and low titania subgroups, a second computer run yielded the more meaningful results shown in figure 5.

Within the ultramafic groups, chemical variation yields approximately linear plots, but for many oxides the harzburgite-dunite and clinopyroxene-wehrlite trends are unconnected but roughly parallel. In both groups, the variation is largely olivine controlled, because the trend lines for each group roughly project through the field of the analyzed olivines. The composition of the olivine involved, however, is markedly different for each ultramafic group.

In the gabbro group the much greater scatter of points is undoubtedly due to the diverse origins of the different rock types included. The iron-rich gabbros (analyses 25, 26) and the one amphibolite (analysis 23) behave differently from the others, showing reversed $\text{FeO}:\text{MgO}$ and $\text{SiO}_2:\text{MgO}$ trends, as well as anomalously high values of several other oxides. The most mafic gabbro (analysis 24) also is somewhat different from the others; however, we have included it because its high Cr_2O_3 and NiO content (Himmelberg and Coleman, 1968) suggest that it is possibly a bridge between the ultramafic and mafic rocks. The trend lines suggest that differences between the more magnesian gabbros are olivine controlled, but by an olivine considerably lower in forsterite than in the ultramafic groups. Trend lines drawn through the three iron-rich gabbros indicate that relative to increasing MgO , the FeO , CaO , and TiO_2 all decrease while SiO_2 increases. These trends are clearly not related to any of the plotted control minerals and suggest some other process. Two possible mechanisms to explain the high-iron rocks are magmatic iron enrichment, such as that described for the Skaergaard Intrusive Complex, and late magmatic or postmagmatic metasomatism, ascribed by Thayer (1972) to hornblende gabbros (epidiorites) from other ophiolite complexes. Because the Coast Range gabbros do not appear to contain either Fe-rich pyroxene or olivine but do grade to amphibolite, we assume that the process leading to the enrichment in iron was not similar to that of the Skaergaard.

For the basalt-diorite-spilite group the nongradational nature of the high- and low-titanium basalts is clearly shown by the $\text{TiO}_2:\text{MgO}$ diagram. The trends of both groups are distinctly different from those of the ultramafic rocks and the gabbros. This can be seen clearly in the greater slope of all the trend lines, and in particular in the reversed trend of $\text{FeO}:\text{MgO}$, which is very similar to ocean-ridge basalts (Kay and others, 1970, fig. 4, p. 1596). The steepness of trend lines

for alkalis, CaO , and especially SiO_2 suggests the effect of some process such as spilitization.

Trend lines in the keratophyres and quartz keratophyres also appear to be similar to those seen in residual glasses left over from crystallization of basaltic magma. Here again, however, the steepness of the slopes for $\text{Na}_2\text{O}:\text{MgO}$ and $\text{SiO}_2:\text{MgO}$ may indicate that these rocks have been altered by albitization.

In conclusion, the MgO variation diagrams in general show a good separation of all five major rock groups similar to that seen on the AFM diagram. The two ultramafic groups, while clearly separate in detail, could have formed largely as a result of differential removal of forsteritic olivine from some less primitive magma composition. The gabbros show two very different trends, one suggesting removal of olivine and the other a secondary, probably metasomatic, iron enrichment. The basalt-spilites are clearly separated into high-titanium and low-titanium varieties and other oxides are correspondingly different. Finally, the keratophyre-quartz keratophyre group is distinctly different from the basalts.

COMPARISON WITH OTHER OPHIOLITES

In order to compare the suite of rocks making up the Coast Range ophiolite with other similar sequences, we have prepared several AFM diagrams using chemical analyses reported from other well-known ophiolite localities (fig. 6). These include the Troodos massif, Cyprus; Vourinos, Greece; Bay of Islands and Lush's Bight Complexes, Newfoundland; Hatay, Turkey; Macquarie Island; Papua; and the Baltimore complex, Maryland.

The Troodos massif on Cyprus, with its outstanding development of parallel dikes forming the Sheeted Intrusive unit, is perhaps the best known example of ophiolite that can be directly compared with current concepts of ocean-ridge crust and upper mantle. We have used in our plot (fig. 6A) 55 analyses as given by Bear (1960), Wilson and Ingham (1959), Gass and Masson-Smith (1963), and Moores and Vine (1971). These analyses are from a wide spectrum of rock types ranging from dunite to "quartz-albite microporphyry" (keratophyre?) and trondhjemite. Included are intermediate rock types termed "micro-diorite," "quartz gabbro," "trachybasalt," and "andesite" not distinguished in most ophiolites, including the Coast Range ophiolite. Some rocks referred to as epidiorite obviously have greatly altered chemistry and have been omitted from the plot.

The Vourinos ophiolite complex of northern Greece has a range of rock types from dunite through gabbro, norite, basalt, quartz diorite, and soda pegmatite. Both gabbro and basalt are unusually low in alkalis, and spilites are absent. We have included in our plot (fig. 6B) 24 analyses as given by Brunn (1956) and Moores (1969).

Ophiolites from Newfoundland are represented by a plot (fig. 6C) that is a composite of gabbro and peridotite from the Bay of Islands Complex (Irvine and Findlay, 1972), gabbro

and mafic pillow lava and breccia from the same complex (Williams and Malpas, 1972), mafic volcanic rocks from Lush's Bight (Papezik and Fleming, 1967; Smitheringale, 1972, and written commun., 1973) plus three analyses of soda granites from Bay of Islands and Notre Dame Bay (Harold Williams, unpub. data, 1973). Some unspecified rock types from the Lush's Bight Complex are shown only by "X" on the AFM diagram, and others designated by symbol as keratophyre might be classed as meta-andesite, according to W. G. Smitheringale.

The Hatay ophiolite belt of southeastern Turkey and northwestern Syria is represented by 28 analyses given by Dubertret (1955) and Majer (1960); most are in the compositional range from dunite to basalt (fig. 6D). Majer (1960, p. 18) also lists two analyses of "quartz-diorite-aplite" which he regards as a differentiate from the magma that was the source of the predominantly mafic and ultramafic rocks of this ophiolite suite. The aprites are very minor in volume, and rocks of composition intermediate between basalt and aplite are notably absent.

The ophiolite of Macquarie Island, 200 km (700 mi) south of New Zealand on the Macquarie Ridge, is spatially more closely related to an oceanic spreading axis than most on-land ophiolites (Varne and others, 1969). It also contains a well-developed swarm of parallel dikes, similar to the Troodos Sheeted Intrusive. On our plot (fig. 6E), the Macquarie Island ophiolite is represented by 21 analyses ranging in composition from harzburgite to basalt and soda-gabbro. Most of the analyses are of rocks from the island itself (Mawson, 1943), but some are from dredge hauls on the nearby oceanic ridge (Watkins and Gunn, 1970). As in most oceanic-ridge areas, this ophiolite does not contain more differentiated silicic or iron-rich rock types.

The ophiolite of eastern Papua, made famous by studies of Davies (1971), is the classic example of an obduction zone where oceanic crust is thrust over continental crust. Using Davies' data, we show a plot (fig. 6F) of 31 analyses of rocks ranging in composition from harzburgite to tonalite and dacite. On the AFM diagram, the wide separation of basalts from gabbros, chiefly reflecting a difference in Fe:Mg ratio, is an unusual feature of this ophiolite, perhaps accentuated by an inadequate number of analyses.

The Baltimore complex, supposed by some to be an ophiolite, is represented by a plot (fig. 6G) of 23 analyses from Herz (1951), Hopson (1964) and Southwick (1970). Included are serpentinites that were possibly derived from harzburgite, pyroxenites, many gabbros, quartz diorite, and one analysis of the Relay "quartz-diorite" (trondhjemite). Some of the gabbroic rocks unusually high in iron were termed bojiite by Herz (1951) and possibly represent iron enrichment related to magmatic processes. Southwick (1970), however, has pointed out that many of these iron-rich gabbros are strongly uraltized and that one has to be very cautious in relating this enrichment to magmatism. No basalts have been

identified, and only one siliceous differentiate possibly related to this extensively metamorphosed and dismembered ophiolite was analyzed.

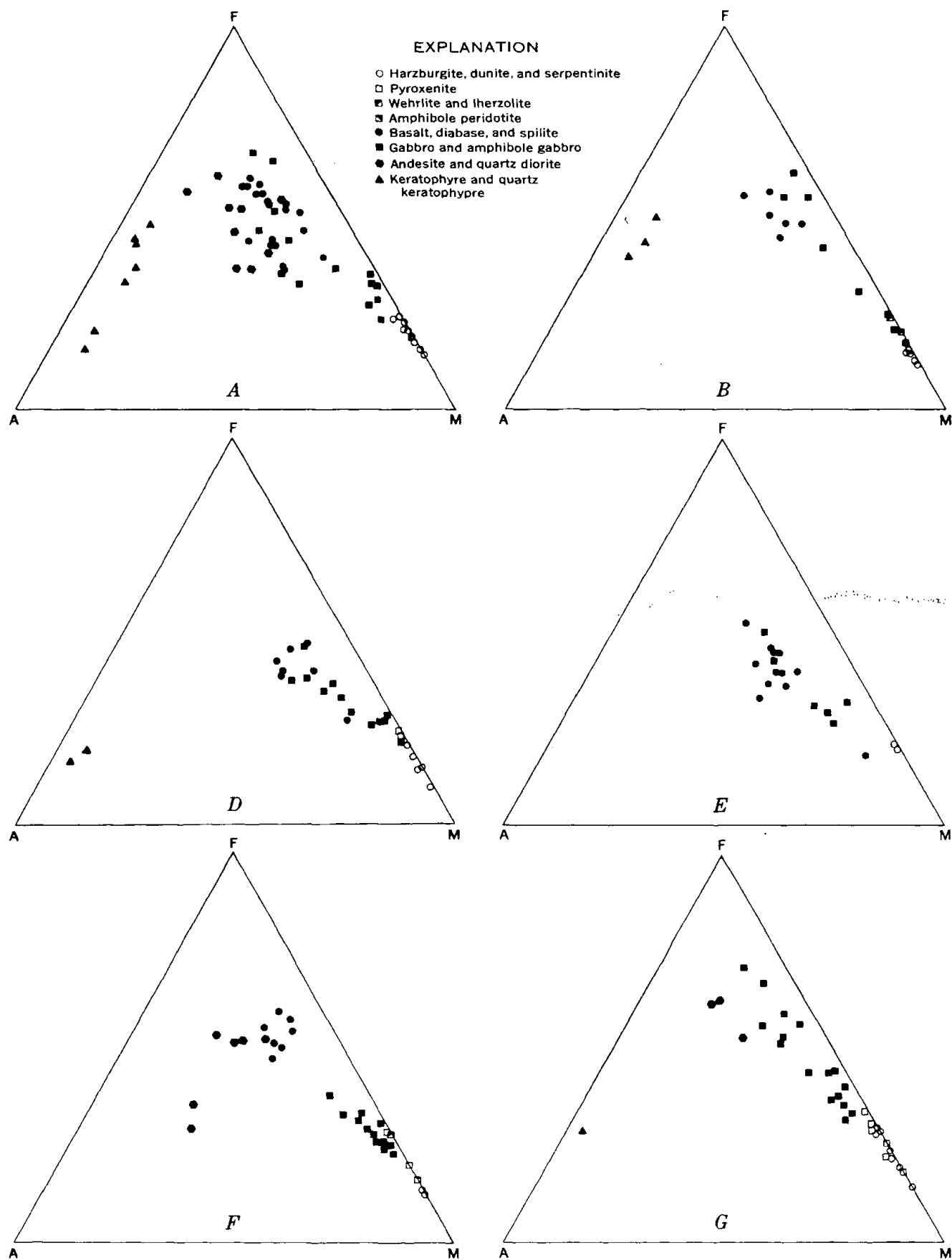
COMPARISON WITH OCEANIC-RIDGE ROCKS

Onland ophiolites have been compared with oceanic crust and upper mantle because they are similar in lithology and sequential order, and the major units are roughly comparable in thicknesses (Bailey and others, 1970; Coleman, 1971; Moores and Vine, 1971; Peyve, 1969; Knipper, 1970; Sabyushev and Usmanov, 1971). In order to compare gross chemical relations between the Coast Range ophiolite and rocks representative of oceanic crust and upper mantle, we have plotted AFM diagrams from analyses of rocks dredged from the mid-Atlantic Ridge (Aumento, 1969, 1972; Engel and Engel, 1964a; Engel and others, 1965; Melson and others, 1968; Miyashiro, 1970; Miyashiro and others, 1969; Nicholls and others, 1964); the East Pacific Rise (Engel and Engel, 1964b; Engel and others, 1965; Engel and Fisher, 1969); Galapagos Rift (K. Nishimori, written commun., 1973); and Indian Ocean Rise (Engel and Fisher, 1969; Vinogradov and others, 1969). A summary AFM diagram showing the fields occupied by the major rock types from the three oceanic ridges (fig. 7) reveals some differences between comparable rock types, especially gabbro, but we believe that additional sampling would eliminate most, if not all, of these differences.

The oceanic rocks chemically show both similarities to, and differences from, the Coast Range ophiolite, as well as other onland ophiolites. The harzburgite-dunite-serpentine rocks from different oceans are all essentially identical in AFM plots, having almost no alkalis, and MgO:FeO ratios of 80–88. Harzburgites and dunites from the Coast Range ophiolite plot almost identically (MgO:FeO=82–88), and only those in the ophiolites of the Troodos massif (MgO:FeO=76–87) and the Baltimore complex (MgO:FeO=70–86) lie a little outside the range of oceanic ultramafic rocks.

The AFM plots of oceanic gabbros show less spread than plots of gabbros in the Coast Range ophiolite (fig. 8A). Many of the Coast Range gabbros are less alkalic than their oceanic counterparts. Gabbros from other onland ophiolites show similar relations to the oceanic gabbros, and like the Coast Range gabbros, generally include some rocks poorer in alkalis and richer in magnesium than any yet dredged from the ocean floor. One might speculate that the dredged oceanic gabbros have been skimmed from only the upper parts of thick bodies, whereas the samples from land include cumulates from the lower parts of such bodies.

The basaltic rocks of the oceanic crust plot on an AFM diagram (fig. 8B) in a small elliptical field, whereas basaltic rocks from onland ophiolites exhibit a greater spread. A medial point for the ophiolitic basalts selected visually has the same Fe:Mg ratio as the mean oceanic basalt but lies about 4 percent closer to the alkali apex, perhaps reflecting postdeposi-



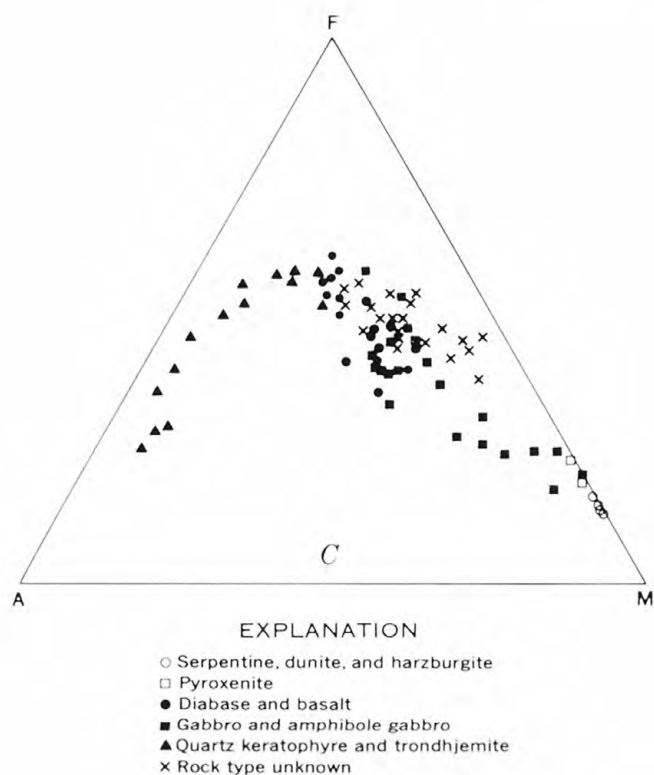


Figure 6.—AFM diagrams of ophiolite suites exposed in A, Troodos, Cyprus; B, Vourinos, Greece; C, Bay of Islands, Newfoundland; D, Hatay, Turkey; E, Macquarie Island; F, Papua; and G, The Baltimore complex.

tional alteration. The crescentic field of the Coast Range basaltic rocks half encircles the elliptical plot of the oceanic basalts with almost no overlap, suggesting either more advanced differentiation or greater postcooling alteration. Analyses of basalts from Troodos, Macquarie Island, and Newfoundland (mostly Lush's Bight) show a similar shift toward the alkaline apex; basalts from Hatay are more magnesian than many of the other ophiolitic or oceanic basalts.

Rocks more silicic than basalt are so rarely recovered from ocean ridges that there are few analyses with which the silicic rocks of onland ophiolites can be compared. Aumento (1969) gives analyses of two "diorites" from the mid-Atlantic Ridge, which he compares with quartz-diorites and trondhjemites of the Alpine or Ophiolite Complex, and in a later paper (1972) he lists a composite of analyses of five similar rocks. An analysis of an aplite from the mid-Atlantic Ridge is given by Miyashiro, Shido, and Ewing (1969). These few analyses of oceanic silicic rocks suggest that locally magmatic differentiation has advanced far enough to produce rocks comparable to keratophyres and related rocks of onland ophiolites. Such rocks, however, seem to be much less abundant along oceanic ridges than in such ophiolites as the Coast Range, Troodos, and Vourinos.

In a summary of AFM plots (figure 9), we have shown the fields of the five major lithologic groups in each of the better studied ophiolite areas, and we have added lines to show possible differentiation trends. The rocks of the Coast Range ophiolite apparently show a dual line of descent; one trend is somewhat comparable to the normal calc-alkaline trend, whereas the other, defined by some gabbros, is comparable to the iron-enrichment part of the Skaergaard trend. Other ophiolite suites having silicic rocks, such as Troodos and Vourinos, show this dual trend, suggesting derivation of the keratophyres and iron-rich gabbros by fractionation of a normal tholeiitic basalt magma, although metasomatic alteration has undoubtedly accentuated the separation of the basalt-gabbro stem. Where silicic rocks are not present, as in Hatay or Macquarie Island, the gabbros do not show iron enrichment, and their fields are similar to those of the basalts.

Rocks from the ocean ridges also show the dual line of descent, though not as markedly as some of the onland ophiolites. On these diagrams at least, the trend lines of the onland ophiolites are comparable to those of the oceanic ridges, supporting the belief that ophiolites are truly onland oceanic crust.

CONCLUSIONS

The 64 rock analyses included here are believed to provide a representative sample of the California Coast Range ophiolite. The rocks are divisible into five major groups: harzburgite-dunite, clinopyroxenite-wehrlite, gabbro, basalt-spilite, and keratophyre-quartz keratophyre. On an AFM diagram the five groups occupy virtually nonoverlapping fields; on an Or-Ab-An diagram, they are nonoverlapping except for gabbro and pyroxenite. Most varieties of rocks from the Coast Range ophiolite are chemically similar to rocks from other onland ophiolites and to rocks recovered from the oceanic ridges, although the basalts tend to be richer in Na_2O and K_2O , possibly as a result of postdepositional alteration.

Possible differentiation trends for the ophiolitic rocks, defined by AFM plots, suggest two lines of descent with a bifurcation point equivalent to a high-magnesia olivine basalt. One trend from olivine basalt to quartz keratophyre is much like the typical calc-alkaline trend; the other represented by the iron-rich and amphibole-bearing gabbros is an iron-enrichment trend. Ophiolite suites containing the most siliceous rocks also show the greatest iron enrichment in associated gabbros. Oceanic-ridge rocks also define the same double line of descent, although only a few rocks more silicic than basalt have been analyzed.

MgO variation diagrams for the Coast Range ophiolite have more complicated trend lines than the AFM plots. Rather than a relatively smooth line extending from the depleted rocks through the gabbro, each of these groups had a unique trend line which is subparallel to the others and suggests a strong olivine control during crystallization. The iron-rich gabbro and

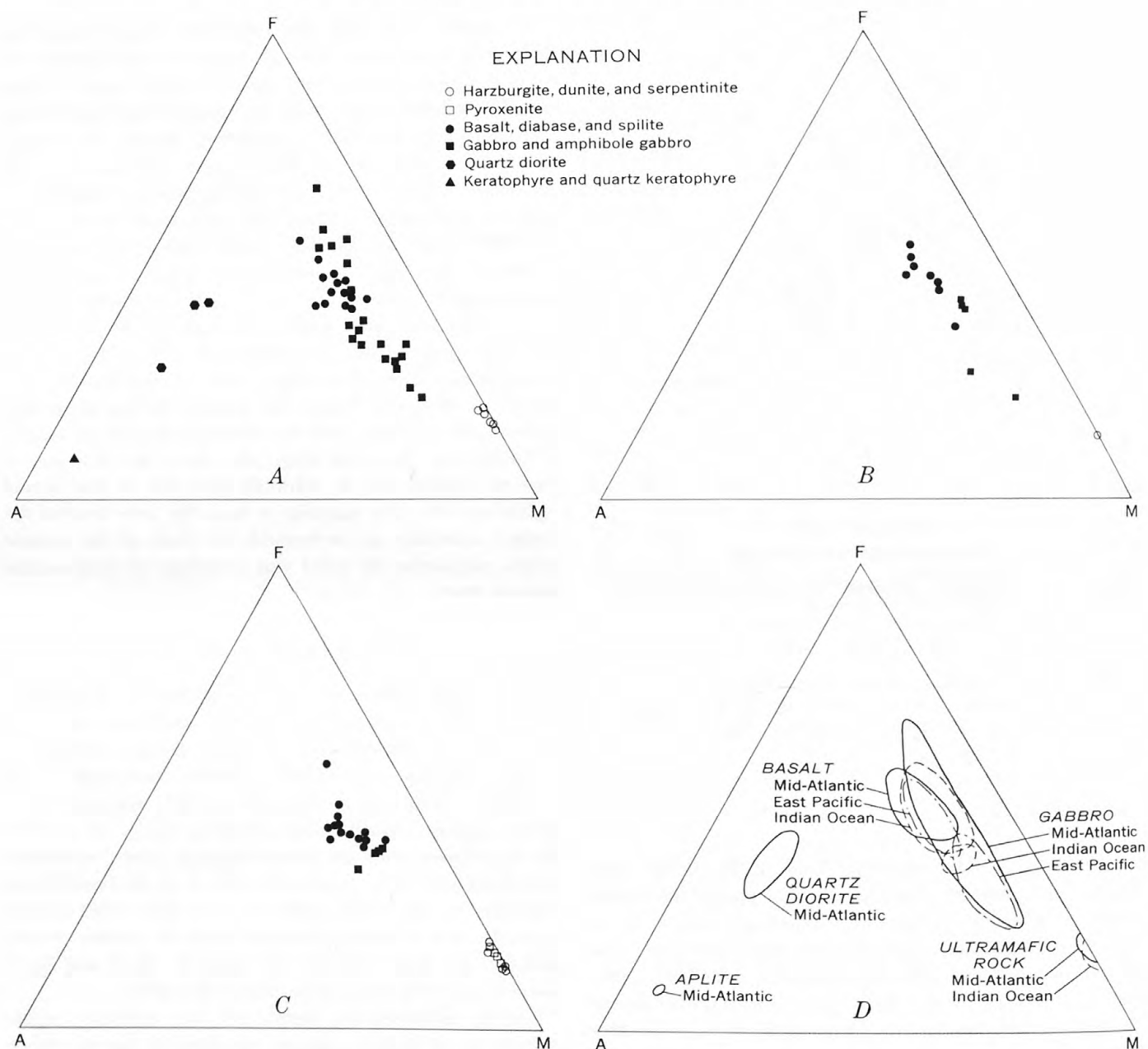


Figure 7.—AFM diagrams from ocean ridge areas showing fields of rock types. A, Mid-Atlantic Ridge. B, East Pacific Rise and Galapagos Rise and Rift Zone, C, Indian Ocean Rise. D, Composite showing field of rock types.

amphibolite trend lines are divergent indicating that their generation is not olivine-controlled but rather the result of increasing crystallization of hornblende, as shown by a decrease in SiO_2 with increasing $\text{FeO}:\text{MgO}$. The basalts also contain two distinctive subrends defined by high- and low-titanium varieties.

The Coast Range ophiolite, like other ophiolites, resembles oceanic crust and upper mantle in rock types and sequential order, though the basaltic and gabbroic layers seem nearly everywhere to be thinner than in oceanic areas (Coleman,

1971). Various models suggested for the buildup of oceanic crust at spreading axes postulate: (1) removal of basaltic magma from lherzolite or related mantle material to yield a residual, harzburgitic upper mantle, (2) coeval extrusion of the basaltic magma to form an overlying cover of pillow basalt, into which a related swarm of parallel dikes is intruded, and (3) intrusion of mafic magma at or near the base of the basalt layer to fill chambers in which the magma differentiates by crystal settling to yield layered cumulates of gabbroic to anorthositic rocks and a small amount of silicic magma that

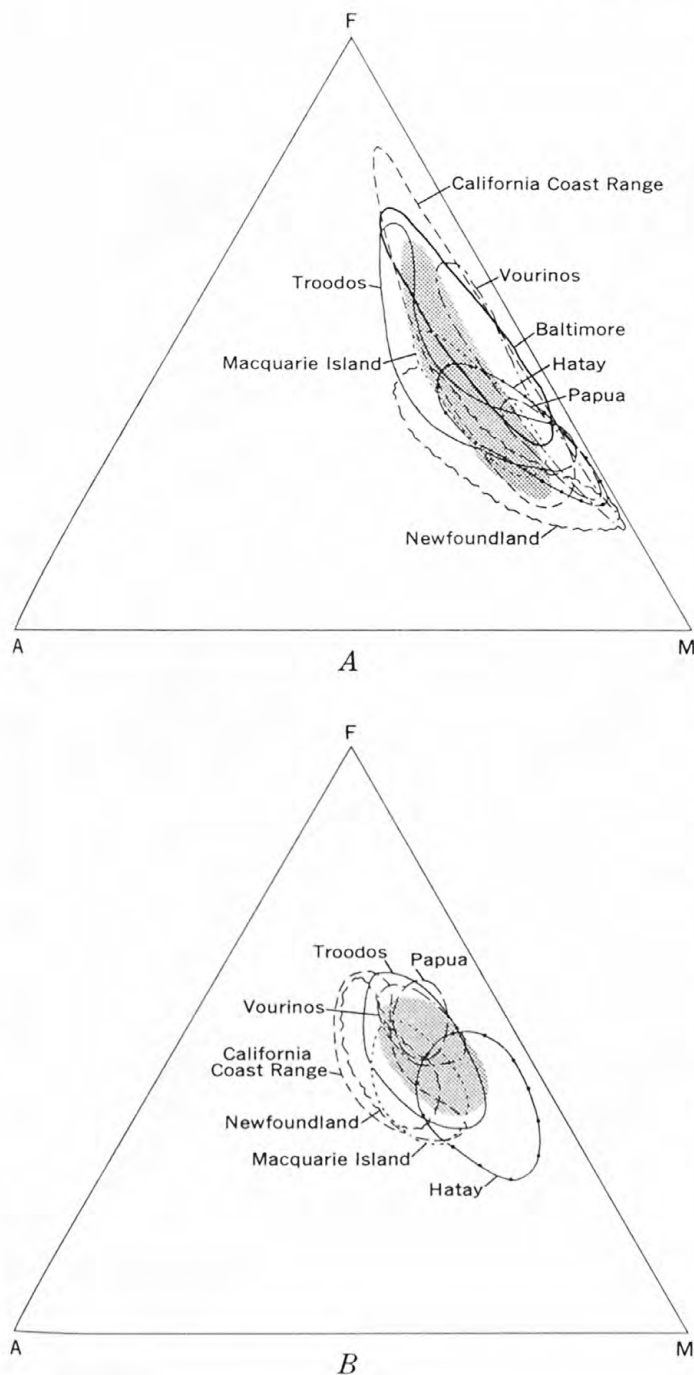


Figure 8.—AFM diagram showing fields occupied by gabbros (A), basalts (B) from oceanic ridges (shaded areas) and onland ophiolites.

may be extruded to form keratophyre or consolidate in situ as trondhjemite. It has been suggested that similar sequences of rocks can be developed in interarc basins (Karig, 1972; Slater and others, 1972) or even at the roots of island arcs built on oceanic crust (Ewart and Bryan, 1972). As the resulting rock sequence would be much the same in all these environments, the major element content of the Coast Range ophiolite,

though clearly suggesting direct comparison with oceanic crust and upper mantle, does not provide clues for distinguishing between a spreading ridge, an interarc basin, or perhaps even the root zone of an island arc as the site of formation of this ophiolite.

ACKNOWLEDGMENTS

We appreciate the kindness of W. G. Smitheringale and Harold Williams, of Memorial University of Newfoundland, in providing us with unpublished data on Newfoundland rocks and are equally grateful to K. Nishimori, of Scripps Institution of Oceanography, for unpublished analyses of rocks dredged from the East Pacific. We are also grateful to R. D. Brown, Jr., U.S. Geological Survey, for unpublished basalt analyses from the Stony Creek area, California. In addition, we wish to acknowledge the considerable help given by Deborah Harden who carefully calculated and plotted the parameters for hundreds of analyses. Finally, sincere thanks go to our colleagues, K. J. Murata, D. A. Swanson, T. P. Thayer, and T. L. Wright, who reviewed the manuscript and provided much valuable criticism.

REFERENCES CITED

- Aumento, Fabrizio, 1969, Diorites from the mid-Atlantic Ridge at 45° N.: *Science*, v. 165, p. 1112–1113.
- , 1972, The oceanic crust of the mid-Atlantic Ridge at 45° N., in *The ancient oceanic lithosphere*: Canada Dept. Energy, Mines and Resources, Earth Physics Br. Pub., v. 42, no. 3, p. 49–53.
- Bailey, E. H., Blake, M. C., Jr., and Jones, D. L., 1970, On-land Mesozoic oceanic crust in California Coast Ranges in *Geological Survey research 1970*: U.S. Geol. Survey Prof. Paper 700-C, p. C70–C81.
- Bailey, E. H., Irwin, W. P., and Jones, D. L., 1964, Franciscan and related rocks, and their significance in the geology of western California: *California Div. Mines and Geology Bull.* 183, 177 p.
- Bear, L. M., 1960, The geology and mineral resources of the Agros-Apisou area: *Cyprus Geol. Survey Dept., Mem.* 7, pt. 1, p. 1–50.
- Bezore, S. P., 1971, Ophiolitic and associated rocks near Mount St. Helena—Geologic guide to the northern Coast Ranges Point Reyes Region: *Geol. Soc. Sacramento Guidebook*, p. 23–27.
- Blake, M. C., and Jones, D. L., 1974, Origin of Franciscan mélanges in northern California: *Soc. Econ. Paleontologists and Mineralogists, Spec. Pub.* (In press.)
- Bodenlos, A. J., 1950, Geology of the Red Mountain magnesite district, Santa Clara and Stanislaus Counties, California: *California Jour. Mines and Geology*, v. 46, p. 223–278.
- Brunn, J. H., 1956, Contribution à l'étude géologique du pinde septentrional et d'une partie de la Macédoine Occidentale, in *Annales Géologiques des Pays Helleniques*: Athens, Laboratoire de géologie de l'université, 358 p.
- Case, J. E., 1963, Geology of a portion of the Berkeley Hill and San Leandro Hills, California: *Berkeley, California Univ., Ph. D. thesis*, 155 p.
- Coleman, R. G., 1971, Plate tectonic emplacement of upper mantle peridotites along continental edges: *Jour. Geophys. Research*, v. 76, no. 5, p. 1212–1222.

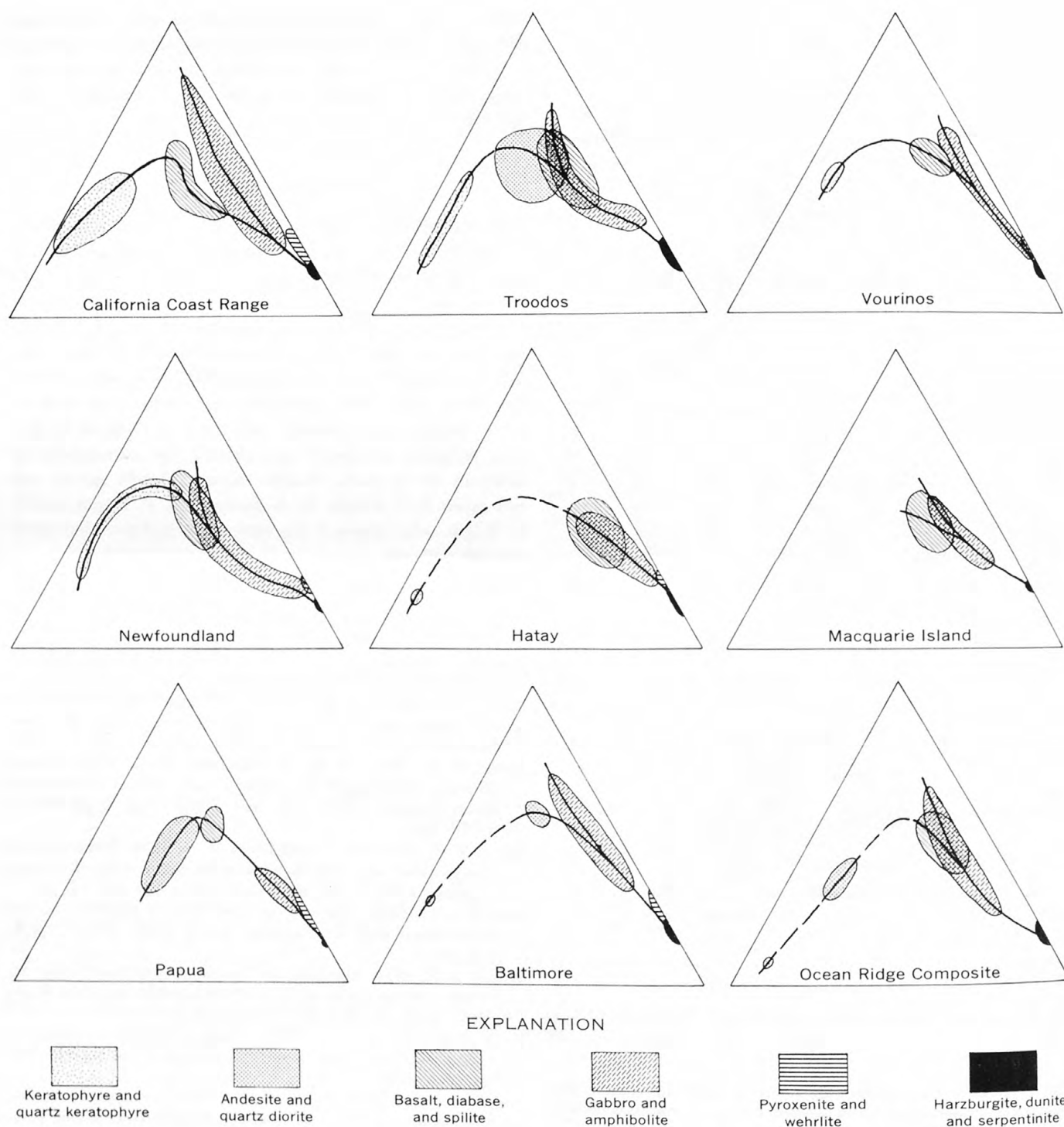


Figure 9.—Summary AFM diagrams showing fields occupied by rock types in various ophiolites and a composite of ocean-ridge samples. Possible differentiation trend lines are indicated in each diagram.

- Davies, H. L., 1971, Peridotite-gabbro-basalt complex in eastern Papua—An overthrust plate of oceanic mantle and crust: *Australia Bur. Mineral Resources, Geology and Geophysics Bull.* 128, 48 p.
- Dubertret, Louis, 1955, *Géologie des roches vertes du Nord-Ouest de la Syrie et du Hatay (Turquie)*: Mus. Natl. Historie Nat., Mém. 6, 179 p.
- Engel, A. E. J., and Engel, C. G., 1964a, Composition of basalts from the mid-Atlantic Ridge: *Science*, v. 144, p. 1330–1333.
- , 1964b, Igneous rocks of the East Pacific Rise: *Science*, v. 146, p. 477–485.
- Engel, A. E. J., Engel, C. G., and Havens, R. G., 1965, Chemical characteristics of oceanic basalts and the upper mantle: *Geol. Soc. America Bull.*, v. 76, no. 7, p. 719–734.
- Engel, C. G., and Fisher, R. L., 1969, Lherzolite, anorthosite, gabbro, and basalt dredged from the mid-Indian ocean ridge: *Science*, v. 166, p. 1136–1141.
- Ewart, Anthony, and Bryan, W. B., 1972, Petrography and geochemistry of the igneous rocks from Eua, Tongan Islands: *Geol. Soc. America Bull.*, v. 83, p. 3281–3298.
- Gass, I. G., and Masson-Smith, D. J., 1963, The geology and gravity anomalies of the Troodos massif, Cyprus: *Royal Soc. London Philos. Trans.*, ser. A. 255, p. 417–467.
- Green, D. H., and Ringwood, A. E., 1967, The stability fields of aluminous pyroxene peridotite and garnet peridotite and their relevance in upper mantle structure: *Earth and Planetary Sci. Letters*, v. 3, p. 151–160.
- Hart, Roger, 1970, Chemical exchange between sea water and deep ocean basalts: *Earth and Planetary Sci. Letters*, v. 9, no. 3, p. 269–279.
- Herz, Norman, 1951, Petrology of the Baltimore gabbro, Maryland: *Geol. Soc. America Bull.*, v. 62, p. 979–1016.
- Hess, H. H., 1960, Stillwater igneous complex, Montana: *Geol. Soc. America Mem.* 80, 230 p.
- Himmelberg, G. R., and Coleman, R. G., 1968, Chemistry of primary minerals and rocks from the Red Mountain-Del Puerto ultramafic mass, California, in *Geological Survey research 1968*: U.S. Geol. Survey Prof. Paper 600-C, p. C18–C26.
- Hopson, C. A., 1964, The crystalline rocks of Howard and Montgomery Counties, in *Geology of Howard and Montgomery Counties*: Baltimore, Maryland Geol. Survey, p. 27–215.
- Hopson, C. A., Frano, C. J., Pessagno, Emile, and Mattinson, J. M., 1973, Late Jurassic ophiolite at Point Sal, Santa Barbara County, California [abs.]: *Geol. Soc. America Abs. with Programs*, v. 1, no. 5, p. 58.
- Irvine, T. N., and Baragar, W. R. A., 1971, A guide to the chemical classification of the common volcanic rocks: *Canadian Jour. Earth Sci.*, v. 8, p. 523–548.
- Irvine, T. N., and Findlay, T. C., 1972, Alpine-type peridotite with particular reference to the Bay of Islands igneous complex: *Canada Dept. Energy, Mines and Resources Earth's Physics Br. Pub.*, v. 42, no. 3, p. 97–128.
- Karig, D. E., 1972, Remnant arcs: *Geol. Soc. America Bull.*, v. 83, p. 1057–1068.
- Kay, R. W., Hubbard, N. J., and Gast, P. W., 1970, Chemical characteristics and origin of oceanic ridge volcanic rocks: *Jour. Geophys. Research*, v. 75, p. 1585–1613.
- Knipper, A. L., 1970, Gabbroidy ofiolitovoy "formatsii" v razreze okeanicheckoy kory [Gabbros of ophiolite "formations" in oceanic crust]: *Geotektonika*, no. 2, March-April, p. 112–120 (in Russian).
- Kuno, Hisashi, 1968, Differentiation of basalt magmas, in Hess, H., and Poldervaart, A., eds., *Basalts—The Poldervaart treatise on rocks of basaltic composition*, v. 2: New York, Interscience, p. 623–688.
- Lanphere, M. A., 1971, Age of the Mesozoic oceanic crust in the California Coast Ranges: *Geol. Soc. America Bull.*, v. 82, no. 11, p. 3209–3211.
- Macdonald, G. A., and Katsura, Takeshi, 1964, Chemical composition of Hawaiian lavas: *Jour. Petrology*, v. 5, p. 82–133.
- Maddock, M. E., 1955, *Geology of the Mount Boardman quadrangle*: Berkeley, California Univ., Ph. D. thesis.
- , 1964, *Geology of the Mount Boardman quadrangle*, Santa Clara and Stanislaus Counties, California: California Div. Mines and Geology Map Sheet 3, scale 1:62,500.
- Majer, V., 1960, Magmatic rocks in the region of Bassit between Latakia and Kessab in northwestern Syria: *Fac. Sci. Univ. Skopje, Yugoslavia Spec. Ed.*, no. 10, p. 1–37.
- Mawson, Douglas, 1943, Macquarie Island, its geography and geology: Australian Antarctic Expedition 1911–1914, Sci. Rept. Sec. A 5, Govt. Printing Office, Sydney.
- Melson, W. G., Thompson, Geoffrey and Van Andel, T. H., 1968, Volcanism and metamorphism in the mid-Atlantic Ridge, 22° N. latitude: *Jour. Geophys. Research*, v. 73, no. 18, p. 5925–5941.
- Miyashiro, Akiho, 1970, Crystallization and differentiation in abyssal tholeiites and gabbros from mid-ocean ridges: *Earth and Planetary Sci. Letters*, v. 7, p. 361–365.
- Miyashiro, Akiho, Shido, Fumiko, and Ewing, Maurice, 1969, Composition and origin of serpentines from the mid-Atlantic Ridge near 24° and 30° N. lat.: *Contr. Mineralogy and Petrology*, v. 23, p. 117–127.
- Moore, E. M., 1969, Petrology and structure of the Vourinos ophiolitic complex of northern Greece: *Geol. Soc. America Spec. Paper* 118, 74 p.
- Moore, E. M., and Vine, F. J., 1971, The Troodos massif, Cyprus, and other ophiolites as oceanic crust; evaluation and implications: *Royal Soc. London Philos. Trans.*, ser. A, v. 268, no. 1192, p. 443–466.
- Nicholls, G. O., Nalwalk, A. J., and Hays, E. E., 1964, Nature and composition of rock samples dredged from the mid-Atlantic Ridge between 22° N. and 52° N.: *Marine Geology*, v. 1, p. 333–343.
- Nicolas, Adolphe, 1968, Relations structurales entre le massif ultrabasique de Lanzo, ses satellites et la zone de Sesia Lanco: Nantes, France, *Bull. Suisse de Minéralogie et Pétrographie*, v. 48/1, p. 145–156.
- , 1969, Pétrographie—une vue unitaire concernant l'origine des massifs ultrabasiques des Alpes occidentales internes: *Acad. Sci. Comptes Rendus, [Paris] Sér. D*, v. 269, p. 1831–1834.
- O'Connor, J. T., 1965, A classification for quartz-rich igneous rocks based on feldspar ratios, in *Geological Survey research 1965*: U.S. Geol. Survey Prof. Paper 525-B, p. B79–B84.
- Page, B. M., 1972, Oceanic crust and mantle fragment in subduction complex near San Luis Obispo, California: *Geol. Soc. America Bull.*, v. 83, p. 957–972.
- Papezik, V. S., and Fleming, J. M., 1967, Basic volcanic rocks of the Whaleback area, Newfoundland: *Geol. Assoc. Canada Spec. Paper* No. 4 (Hugh Lilly memorial volume), p. 181–192.
- Peyve, A. F., 1969, Oceanic crust of the geologic past: *Geotektonika*, no. 4, p. 5–23; also *Geotectonics*, no. 4, p. 210–224.
- Ross, D. C., 1970, Quartz gabbro and anorthositic gabbro; markers of offset along the San Andreas fault in the California Coast Ranges: *Geol. Soc. America Bull.*, v. 81, p. 3647–3662.
- Sabdyushev, Sh. Sh., and Usmanov, R. R., 1971, Tectonic sheets, mélange, and the ancient oceanic crust in Tamdytau (Western Uzbekistan): *Geotectonics*, no. 5, p. 283–287.
- Sclater, J. G., Hawkins, J. W., Jr., Mammerickx, Jacqueline, and Chase, C. G., 1972, Crustal extension between the Tonga and Lau Ridges—Petrologic and geophysical evidence: *Geol. Soc. America Bull.*, v. 83, p. 505–517.
- Shapiro, Leonard, and Brannock, W. W., 1962, Rapid analysis of silicate, carbonate, and phosphate rocks: *U.S. Geol. Survey Bull.* 1144-A, 56 p.

- Smitheringale, W. G., 1972, Low-potash Lush's Bight theoleiites: Ancient oceanic crust in Newfoundland?: *Canadian Jour. Earth Sci.* v. 9, no. 5, p. 574-588.
- Southwick, D. L., 1970, Structure and petrology of the Harford County part of the Baltimore-State line Gabbro-Peridotite complex, in Fisher, G. W., and others, ed., *Studies of Appalachian geology—central and southern*: New York, Interscience Publishers, p. 397-415.
- Switzer, George, 1945, Eclogite from the California glaucophane schists: *Am. Jour. Sci.*, v. 243, no. 1, 8 p.
- Thayer, T. P., 1967, Chemical and structural relation of ultramafic and feldspathic rocks in alpine intrusive complexes, in Wyllie, P. J., ed., *Ultramafic and related rocks*: New York, John Wiley and Sons, p. 222-239.
- , 1972, Gabbro and epidiorite versus granulite and amphibolite: A problem of the ophiolite assemblage: *Caribbean Geol. Conf.*, 6th, Palomar, Venezuela 1972, *Proc.* p. 315-320.
- Turner, H. W., 1891, The geology of Mount Diablo, California: *Geol. Soc. America Bull.*, v. 2, p. 384-402.
- Varne, Richard, Gee, R. D., and Quilty, P. G. J., 1969, Macquarie Island and the cause of the oceanic linear magnetic anomalies: *Science*, v. 166, p. 230-233.
- Vinogradov, A. P., Udintsev, G. S., Dmitriev, L. V., Kanaev, V. F., Neprochnov, Y. P., Petrova, G. N., and Rikunov, L. N., 1969, The structure of the mid-ocean rift zone of the Indian Ocean and its place in the World Rift System: *Tectonophysics*, no. 8, p. 377-401.
- Wager, L. R., and Deer, W. A., 1939, Geological investigations in East Greenland, pt. III, the petrology of the Skaergaard intrusion, Kanegard-lugssuaq, East Greenland: *Medd. Grønland*, v. 105, no. 4, 352 p.
- Watkins, N. D., and Gunn, B. M., 1970, Petrology, geochemistry, and magnetic properties of some rocks dredged from the Macquarie Ridge: *New Zealand Jour. Geology and Geophysics*, v. 14, p. 153-168.
- Williams, Harold, and Malpas, John, 1972, Sheeted dikes and brecciated dike rocks within transported igneous complexes, Bay of Islands, Western Newfoundland: *Canadian Jour. Earth Sci.*, v. 9, no. 9, p. 1216-1229.
- Wilson, R. A. M., and Ingham, F. T., 1959, The geology and mineral resources of the Xeros-Troodos area: *Cyprus Geol. Survey Dept. Mem.* 1, 184 p.
- Wright, T. L., 1971, Chemistry of Kilauea and Mauna Loa lava in space and time: *U.S. Geol. Survey Prof. Paper* 735, 40 p.
- Wright, T. L., and Fiske, R. S., 1971, Origin of the differentiated and hybrid lavas of Kilauea volcano, Hawaii: *Jour. Petrology*, v. 12, no. 1, p. 1-65.

ULTRAMAFIC ROCKS OF THE EAGLE QUADRANGLE, EAST-CENTRAL ALASKA

By HELEN L. FOSTER and TERRY E.C. KEITH,
Menlo Park, Calif.

Abstract.—More than 97 separate occurrences of ultramafic rocks, some of which are included in a northwest-trending zone of alpine-type ultramafic rocks, have been mapped in the Eagle quadrangle, east-central Alaska. They are divided into three groups primarily on the basis of degree of serpentinization. Group I consists of lens-shaped bodies of serpentinite 1 m² (10 ft²) to several 100 m² (1,000 ft²) in area. Relict textures and presence of bastite indicate that the original rock was harzburgite and dunite. Group II consists of bodies composed of partially serpentinized harzburgite and dunite and includes the large Mount Sorenson and American Creek bodies. Group III is dominantly hornblende and pyroxenite, probably intrusive and not genetically related to groups I and II. The authors believe that the ultramafic bodies of groups I and II are alpine-type peridotites and may include dismembered ophiolite. The Tintina fault system could have provided a zone of weakness along which mantle material was tectonically emplaced or it may have been a plate boundary in late Paleozoic time. If it represents a plate boundary, the metamorphic terrane which lies between the Tintina and Denali fault systems would have to be allochthonous, perhaps originating as a northward-moving slice of continental crustal material. During the course of the movement as the two continental masses approached and perhaps collided, mantle peridotite and oceanic crustal material were squeezed up along the continental margin onto the continental slice.

More than 97 separate occurrences of ultramafic rock were found south of the Yukon River in the Eagle quadrangle, east-central Alaska, during the course of reconnaissance geologic mapping (figs. 1, 2, 3). The size of outcrops of ultramafic rock ranges from 1 m² (10 ft²) to 41 km² (16 mi²), but most outcrops are small. Although these rocks have not yet been studied in detail, it seems appropriate to record the known data as a background for future studies and for comparison with ultramafic rocks elsewhere.

GEOLOGIC SETTING

The Eagle quadrangle (USGS map, 1:250,000) is in the northeastern part of the Yukon-Tanana Upland, a maturely dissected mountainous terrain lying between the Yukon and Tanana Rivers (fig. 1). The highest elevations are about 1,900 m (6,200 ft) and relief is commonly 500 m (1,640 ft) or more. The Seventymile, Fortymile, and Charley River systems, tributaries to the Yukon River (fig. 2), drain most of the area.

The Tintina fault (or trench) (Roddick, 1967, p. 23) is a major northwest-trending structure that crosses the northeast

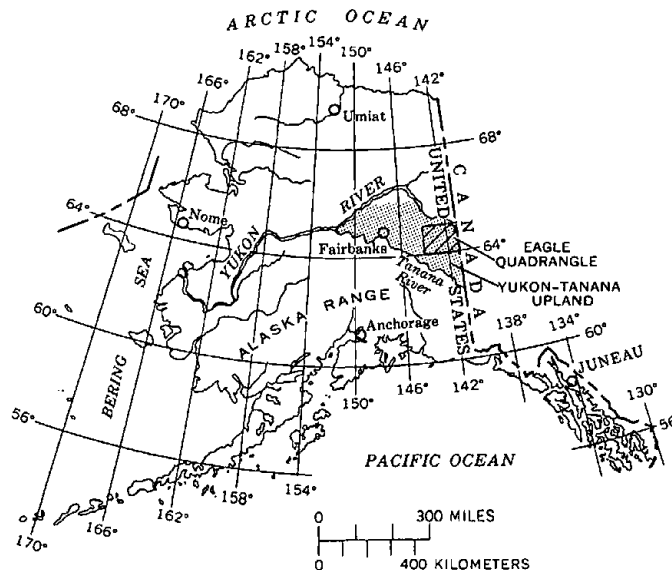


Figure 1.—Index map of Alaska showing location of the Yukon-Tanana Upland.

corner of the quadrangle, separating unmetamorphosed Precambrian, Paleozoic, and Mesozoic sedimentary rocks on the northeast from metamorphic rocks on the southwest (Foster, 1972). Throughout much of its length, it is not a single fault but a complex zone of faults. The metamorphic terrane extends southward across the Yukon-Tanana Upland, beneath the Tanana River valley, and into the Alaska Range as far as the Denali fault (fig. 2) (Foster, 1970). The Denali fault separates these metamorphic rocks on the northeast from late Paleozoic volcanic rocks and Mesozoic sedimentary rocks on the southwest (Richter, 1973).

The metamorphic rocks range in grade from the prehnite-pumpellyite to the amphibolite facies and many are polymetamorphic. Some facies changes are gradational; others are sharp as a result of faulting. The metamorphic rocks are mostly of sedimentary origin but locally include rocks of igneous origin. The sediments were probably deposited in Paleozoic time (Foster, 1972). Granitic plutons (fig. 3) were intruded in Mesozoic and Tertiary time, and Cenozoic(?) volcanic rocks and Cretaceous(?) and Tertiary sedimentary rocks crop out locally (Foster, 1972).

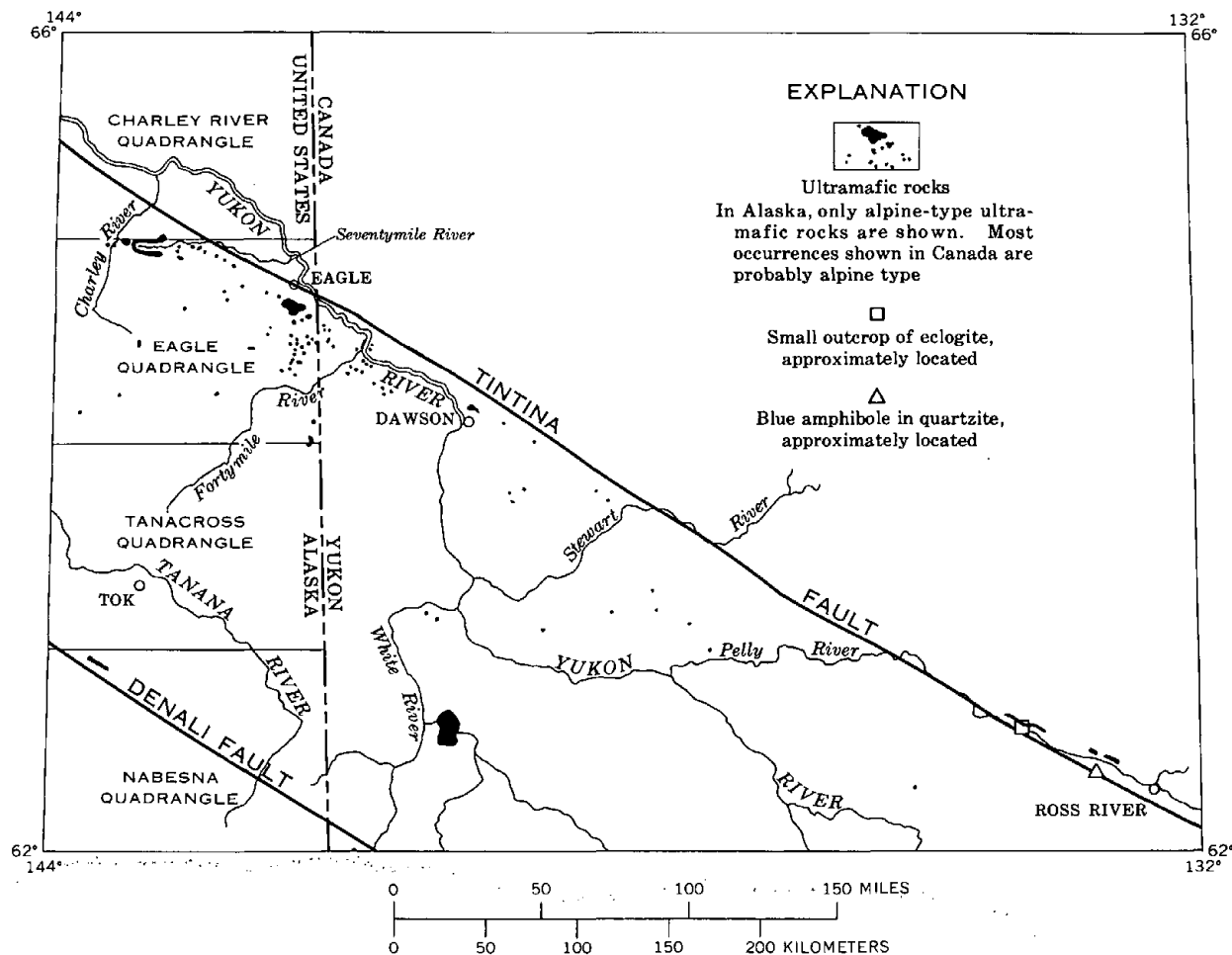


Figure 2.—Distribution of ultramafic rocks south of the Tintina fault. Data from Bostock (1964), Douglas (1968), Foster (1972), Geological Survey of Canada (1957), Green (1972), and Tempelman-Kluit (1970, 1972b).

Several faults, probably splays of the Tintina, are south of the main fault zone; the principal fault is shown on the map (fig. 3) as the Seventymile fault and herein referred to by that name. There are several prominent northeast-trending faults. A zone of serpentinized ultramafic masses trends northwestward more or less parallel to the Tintina fault. This zone of ultramafic rocks continues southeastward into the Yukon Territory, Canada, and northwestward into the Charley River quadrangle. The total length of the ultramafic zone, as included in this discussion, is about 550 km (340 mi) (fig. 2). Ultramafic bodies in line with the northwest and southeast extension of this zone may be a part of it but are not considered in this report.

Ultramafic bodies are found throughout the Eagle quadrangle. The Tanacross quadrangle to the south contains a few small ultramafic bodies, mostly not serpentinized. Ultramafic bodies, including several large serpentinized ones, are known to the west in the Big Delta quadrangle (Mertie, 1937, pl. 1). None are mapped north of the Tintina fault zone in the Charley River quadrangle (Brabb and Churkin, 1969).

On the basis of field observations and aeromagnetic data (Veach, 1972) flown with a $\frac{3}{4}$ -mi spacing of flightpaths, most of the ultramafic bodies are believed to be separate masses or lenses that are not connected beneath the surface. The size of the outcrop is probably indicative of the relative size of the body.

DESCRIPTION OF THE ULTRAMAFIC ROCKS

The ultramafic rocks of the Eagle quadrangle are here divided into three groups for description and discussion: group I, those that are completely serpentinized or altered to talc, magnesite, and, rarely, dolomite; group II, those that are partially serpentinized; and group III, several types of hornblendites and pyroxenites.

The rocks of groups I and II are related in origin and differ only in their degree of serpentinization. In group I, the rocks, though thoroughly serpentinized, have relict textures indicating that they were originally harzburgite and dunite. The original modal composition of the rocks in group II can be fairly well estimated; these rocks also were mostly harzburgite

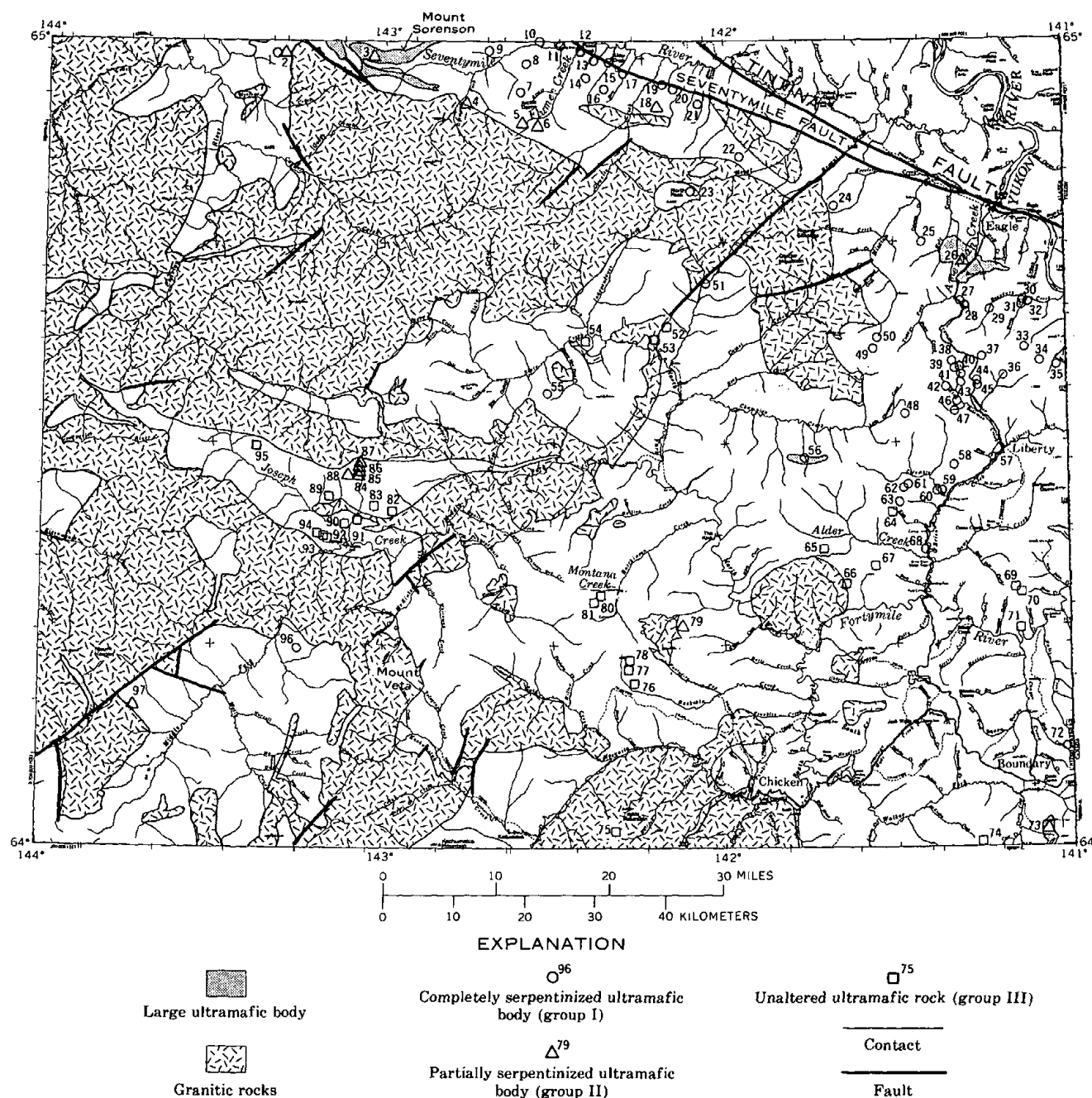


Figure 3.—Ultramafic rocks in the Eagle quadrangle.

and dunite. The rocks of group III probably are not genetically related to those of groups I and II. Some ultramafic bodies in the quadrangle have not yet been mapped owing to the reconnaissance nature of the fieldwork.

The mineralogy and textures of the ultramafic rocks have been determined by field examination and by preliminary study of more than 150 thin sections and more than 130 X-ray diffraction traces. Not all exposures have been studied and some have been examined in considerably more detail than

others. Rocks from approximately 62 percent of the outcrops were X-rayed, sectioned, or both. Semiquantitative spectrographic analyses were made of more than 96 specimens, and fire assay and spectrographic analyses for the platinum group elements were made of 73 specimens (Keith and Foster, 1973). Detailed notes on the mineralogy of the three groups of ultramafic rocks and complete semiquantitative spectrographic analyses are available in a U.S. Geological Survey open-file report (Keith and Foster, 1973).

Group I

The ultramafic rocks of group I, serpentinite, or, in a few places, talc derived from serpentinite, occur as small (1 to several 100 m² or 10 to several 1,000 ft²) lenslike bodies. The bodies are scattered through the quadrangle (fig. 3), but there is a concentration in a zone about 12 km (7.5 mi) wide south of the Seventymile fault and another concentration in a zone about 27 km (17 mi) wide that extends southeastward from 6 km (3.7 mi) south of the Tintina fault for a distance of about 44 km (27 mi). In the zone south of the Seventymile fault, seven of the bodies occur along the fault itself or immediately south of it. The country rock in the zone south of the Seventymile fault is only slightly metamorphosed, mostly quartzite, argillite, and marble. Most of the ultramafic bodies farther south from the Seventymile fault are in greenschist-facies terrane; a few are in epidote-amphibolite- or amphibolite-facies terrane.

Most contacts of the group I ultramafic bodies are obscured by vegetation, colluvium, or, less commonly, rubble, but in places fibrous actinolite and slip-fiber serpentinite are found at the boundary, indicating local shearing.

The ultramafic rocks of group I are mostly massive, green to black serpentinite. In the northern part of the area (loc. 1, 7–17, 19–25, fig. 3), the serpentinites consist of a fine-grained mixture of lizardite and clinochrysotile that have a crude mesh texture after olivine and serpentine pseudomorphs after orthopyroxene (bastite). Antigorite has been identified at locality 14 (fig. 3). Brucite, magnetite, and, at a few places, magnesite and chromite occur sporadically in amounts generally less than 1 percent. Bastite and mesh textures produced by the serpentinization of olivine indicate that these rocks were originally harzburgite or dunite with orthopyroxene constituting 0 to 15 percent or more of the rock.

The small serpentinite bodies in the eastern part of the area consist of antigorite with minor amounts, commonly less than 1 percent, of magnetite, magnesite, and, in places, actinolite and talc. In most of these bodies, original textures have been completely obliterated and there are no late veinlets of serpentinite. The antigorite forms a dense, finely crystalline mass; anhedral fine-grained aggregates of magnetite and of magnesite are scattered irregularly throughout the antigorite as closely associated clots. A few small bodies containing bastite indicate that these rocks also were originally harzburgite and dunite.

Veinlets of serpentinite crosscut some of the small bodies of group I in a random fashion. The veinlets are very thin, generally 1 mm (0.04 in.) or less, and rarely have cross-fiber development. At least some of these late veinlets are chrysotile, although the massive serpentinite may be antigorite. Magnetite grains, and in places associated brucite, are found aligned along but not within the veinlets.

One isolated body (loc. 55, fig. 3) in the Eagle C-2 quadrangle, about 9,000 m² (97,000 ft²) in area, contains

veinlets 3 to 25 mm (0.125–1 in.) thick of well-developed cross-fiber asbestos of commercial quality (Foster, 1969a). The massive serpentinite cut by the asbestos veinlets is antigorite, but it has some bastite, indicating that the original rock may have been harzburgite. A layer of magnetite grains 1 to 2 mm (0.04–0.08 in.) thick occurs at the contact of the veinlet with massive antigorite.

Good quality cross fiber in closely spaced veinlets has not been found in other bodies, although narrow veinlets of cross fiber have been observed in a few places. Slip fiber is locally found in many bodies along joints and small faults.

Fine-grained antigorite in a few of the bodies of group I in the eastern part of the quadrangle (locs. 49, 56, 58, and 68, fig. 3) is associated with significant amounts of talc, actinolite, chlorite, magnesite, and less commonly, dolomite. Field and petrographic observations indicate that these minerals formed from antigorite during low-grade metamorphism or hydrothermal activity.

Massive white quartz-carbonate veins have been found in association with serpentinite bodies of several localities (Nos. 12, 41, and near 62, fig. 3) in group I and in the Mount Sorenson body of group II (No. 3, fig. 3). The carbonate is dominantly magnesite with or without minor dolomite. Bright-green mica and green stain color the surface of some of these rocks.

The largest body in group I, about 0.25 km² (2,700 ft²) or more in area, is on Flume Creek (loc. 12, fig. 3) just south of the Seventymile fault. The outcrops at locality 13 (fig. 3) may be part of this body. Flume Creek cuts through the body, exposing serpentinite, a 12-m (40-ft)-wide quartz-carbonate zone and altered diorite that may be a tectonic inclusion. Rodingite occurs as a very fine-grained, light-colored rock; its contacts are concealed. It is a fine-grained mixture consisting predominantly of hydrogrossularite with subordinate clinopyroxene (diopside), chlorite, and prehnite. The texture of the sample suggests that it may originally have been an aphanitic volcanic rock.

The Flume Creek serpentinite is massive, fine-grained lizardite and clinochrysotile. Less than 1 percent each of primary chromite and secondary magnesite is present in some specimens. Large grains of bastite are evident in hand specimen, indicating that the original rock was harzburgite.

Flume Creek has been mined for placer gold near its mouth, and lode gold has been found in shear zones near the downstream contact with the serpentinized body (Saunders, 1956). Clark and Foster (1971, p. 6–10) suggest that the lode gold exists in small amounts in quartz veins and silica-carbonate rock associated with the serpentinized rock.

Semiquantitative spectrographic analyses of several samples showed silver in amounts as much as 1.5 ppm; analysis by atomic absorption indicated as much as 11 ppm gold in the silica-carbonate rock. This is the only ultramafic body in the Eagle quadrangle with which both gold and silver are known to be associated, although silver was detected in the small masses

of serpentine at localities 22 and 23 (fig. 3). Several small outcrops of much altered basalt are found between Flume and Alder Creeks. Chert is known along the Seventymile River a few kilometers to the northwest and near localities 9 and 10 (fig. 3).

Group II

The ultramafic rocks of group II are partially serpentinized harzburgite and dunite. Eight of the group II ultramafic occurrences, including the large Mount Sorenson (loc. 3, fig. 3) and American Creek (loc. 26, fig. 3) bodies are in the northwest-trending zone of ultramafic bodies south of the Tintina fault. The others are scattered throughout the Eagle quadrangle.

Olivine (Fo₈₅₋₉₅) is the dominant primary mineral in the rocks of group II; orthopyroxene (enstatite) makes up 0 to 50 percent of the rocks; and clinopyroxene occurs locally. Accessory amounts of chromite (less than 1 percent) are found in the Mount Sorenson and American Creek bodies.

Most of the rocks in group II have been at least 50 percent serpentinized; lizardite and clinochrysotile mixtures are the most common serpentines. Serpentine from localities 2, 3, 79, 84, and 86 (fig. 3) was positively identified as a mixture of lizardite and clinochrysotile. Antigorite was positively identified by X-ray diffraction traces at localities 26, 57, and 73 (two large bodies and one small one, all in the eastern part of the quadrangle) and at locality 97 in the southwestern part of the quadrangle. Some crosscutting veinlets of chrysotile are found in nearly all of the group II bodies. The veinlets, fairly abundant to scarce in different exposures, are commonly 1 mm (0.04 in.) or less wide and locally show some cross-fiber development. Secondary minerals associated with the serpentine are actinolite, penninite, green chlorite, talc, magnetite, and brucite.

Mount Sorenson body

The Mount Sorenson body (loc. 3, fig. 3) is the largest in the Eagle quadrangle, about 41 km² (16 mi²), but it is remote and access has been limited. It consists of northern and southern east-west-trending arms, connected at their western end.

The body appears to be massive, partially serpentinized peridotite with some variation in orthopyroxene content relative to olivine content. The eastern part is mostly highly serpentinized dunite with about 5 percent orthopyroxene (or bastite). The western part is partially serpentinized harzburgite containing as much as 35 percent orthopyroxene.

Olivine throughout the body is forsteritic (Fo₈₀₋₉₅) as determined optically. The grains are fractured and serpentinized to different degrees and kink banding is common. Relatively fresh olivine grains (less than 20 percent serpentinized) from the western part of the southern limb are granulated.

The orthopyroxene is enstatite. In the northwestern part of the body, the orthopyroxene grains are in small clusters. In the eastern part, the orthopyroxene, completely replaced by serpentine (bastite), occurs as separate grains 3 to 4 mm (0.12–0.16 in.) long. Schiller texture formed by exsolving reddish-brown blades of an unidentified mineral is fairly common. No distortion of orthopyroxene grains was found.

Clinopyroxene occurs in a few samples from the western part of the northern arm. One sample appears to be from a nearly monomineralic pyroxenite lens. Chromite in amounts less than 1 percent is associated with the least serpentinized rock as small anhedral grains and as large poikilitic or embayed grains, as much as 1.5 mm (0.14 in.) long.

Serpentine is by far the most abundant secondary mineral, but actinolite, penninite, talc, magnetite, and brucite are found. On fresh surfaces the serpentine, a mixture of lizardite and clinochrysotile, is dark green to black and massive and is commonly cut by tiny veinlets of fibrous clinochrysotile about 1 mm (0.04 in.) thick. No antigorite has been identified in this body. Most of the serpentine has been derived from olivine and has crudely developed to well-developed mesh texture. Serpentine has replaced orthopyroxene beginning along cleavages and grain boundaries. Serpentine slip fiber is found on massive blocks.

Actinolite (tremolite) is a fairly common secondary mineral present in amounts as much as 20 percent. It is colorless in thin section and consists of relatively coarse to fine radiate groups of needles. In places fine-grained talc is associated with actinolite in amounts as high as 8 percent. Penninite is also found in the actinolite-bearing rocks, probably more widely distributed but less abundant than talc. Brucite, which is minor in amount, is not closely associated with actinolite, talc, and penninite but rather occurs with the serpentine and magnetite, having formed from replacement of olivine and orthopyroxene. Tiny disseminated grains of magnetite are derived from the serpentinization of olivine and orthopyroxene and are commonly concentrated along microfractures where serpentinization has taken place.

A vertical quartz-carbonate (magnesite) vein with small patches of bright green stain cuts through massive peridotite in the north-central part of the mass. It is about 1.1 m (3.3 ft) wide, 3 m (10 ft) long, and trends N. 80° W.

Diabase, probably as tectonic inclusions incorporated into the peridotite during emplacement through the crust, is found in many places throughout the peridotite body. The outcrop pattern is irregular and each outcrop is small, 3 to 20 m (10–65 ft) in longest dimension. No contact effects were noted, but the diabase is considerably altered, especially in the eastern part of the body, and shape and size of the inclusions suggest that they could have been dikes. The alteration may be from metasomatism during serpentinization. Diabase in the eastern part of each limb has microveinlets of prehnite with associated actinolite and light-green chlorite. Tectonic inclusions in a similar serpentinite environment are described by

Foster (1967, p. D120–D122) in the northwestern part of the Yukon-Tanana Upland.

Nonfoliated hornblendites of unknown extent are found at the extreme northwestern and southwestern margins of the peridotite body where it is in contact with low-grade metamorphic rocks. Patches of gabbros and basalts, altered in different degrees, are in contact with the Mount Sorenson peridotite (Foster, 1972), but these rocks have not been studied for this report. Argillite, metagraywacke, metatuff, and other low-grade metasedimentary rocks border the body on both the north and south and have the same general northwesterly trend as the outcrop of the ultramafic body.

American Creek body

The American Creek ultramafic body, about 31 km² (12 mi²) in area, is the second largest serpentinized peridotite body (loc. 26, fig. 3) in the Eagle quadrangle. The body is a massive peridotite, black on fresh surfaces and dark reddish brown on weathered surfaces, which are rough from resistant orthopyroxene. No lineation of orthopyroxene grains was observed.

There is little variation in primary mineralogy throughout the body. The rock is harzburgite with minor dunite. Olivine is the dominant mineral and orthopyroxene constitutes 5 to 35 percent of the rock. Clinopyroxene and chromite constitute less than 5 percent and less than 1 percent, respectively, of the rock. Composition of olivine has been determined optically as 80 to 90 percent forsterite. Kink banding is common. The olivine is commonly granulated at grain boundaries and within the grains. In a few places unaltered olivine fragments are included in small serpentine-filled veinlets. The orthopyroxene is enstatite (En_{92–95}). The orthopyroxene grains are commonly 2 to 4 mm (0.07–0.16 in.) long; in some places they are concentrated in small clusters of 10 to 15 large grains. Deformation of orthopyroxene grains is common and ranges from slight bends to tight folds. Clinopyroxene has been found only near the southern border of the body, where it is associated with groups of orthopyroxene grains. Sporadically distributed anhedral grains of chromite are as much as 1 mm (0.04 in.) across and locally are extensively embayed.

All the peridotite body is serpentinized to some extent, from 5 to 100 percent. In thin section the serpentine, antigorite, is seen to generally consist of fairly coarse radiating blades and fibrous bundles. Veinlets less than 1 mm (0.04 in.) wide of clinochrysotile crosscut the peridotite. In some places traces of cross-fiber development can be seen in the veinlets, and near the southern boundary along the road, there are local thin veinlets of well-developed cross fiber.

Fine-grained acicular actinolite forms alteration rims on pyroxene in places. Talc and chlorite are found locally with actinolite in amounts generally less than 1 percent. The chlorite is commonly pale green to colorless in thin section. Some penninite is present. Brucite, in amounts less than 1

percent, is found with secondary magnetite. Magnetite is commonly disseminated as tiny grains concentrated along microfractures or in pockets; it also occurs sporadically as large anhedral grains. Total magnetite may in places be as high as 3 percent.

Large massive inclusions of country rock, metasedimentary rocks, are found along the southern boundary of the American Creek body. Some inclusions are intensely deformed and sheared. At the northern boundary of the peridotite along the east side of the road is a white and gray-green, fine-grained laminated rock which becomes blotchy in color and increases in grain size away from the peridotite. The gray-green laminae are almost entirely actinolite with minor penninite, and the white bands are a cloudy fine-grained aggregate of several minerals, among which plagioclase and zoisite have been identified by an X-ray diffraction trace. Outward from the peridotite the laminae are increasingly distorted, broken, and twisted, resulting in the blotchy color. Texture and mineral assemblage indicate that the rock may have been a large slab of sedimentary rock that was metasomatically altered by processes similar to those described by Coleman (1967, p. 40) during emplacement and serpentinization of the peridotite. A small, extensively altered granitic inclusion within the peridotite near the northern boundary is coarse grained and consists almost entirely of altered plagioclase and muscovite with minor intergranular carbonate.

The metamorphic grade of the rocks surrounding the American Creek peridotite is greenschist facies, probably upper greenschist facies. The American Creek peridotite is very similar to the Mount Sorenson peridotite, except that the dominant serpentine is antigorite in the American Creek and lizardite and clinochrysotile in the Mount Sorenson. Deformation of olivine is similar in both, but orthopyroxene in the American Creek body is highly deformed whereas that in the Mount Sorenson body is not. These differences may relate to the metamorphic history of the areas during or after the emplacement of the ultramafic bodies, the Sorenson area undergoing a less intense degree of metamorphism than the American Creek area.

Boundary body

The third large ultramafic body is located near Boundary (loc. 73, fig. 3) and is south of the main concentration of ultramafic bodies. There are no significant outcrops of ultramafic rock to the south of it in the Tanacross quadrangle (Foster, 1970). The Boundary body has an approximate area of 8 km² (3 mi²) but contacts are not exposed. Metamorphic rocks surrounding it are of upper greenschist to amphibolite facies (Foster, 1969b). The serpentine, antigorite, has been so sheared, squeezed, and altered to talc, chlorite, magnesite, and actinolite that original textures and mineralogy have been obliterated in all but a few places. Poorly developed bastite indicates that the body may have originally been a harzburgite

with a low percentage of orthopyroxene. Slip fiber and long stiff fibers (picrolite) of serpentine are found locally.

Group III

The ultramafic rocks of group III crop out here and there in the southern two-thirds of the Eagle quadrangle. Rock types are predominantly hornblende and pyroxene hornblende to hornblende pyroxenite and pyroxenite. Biotite is locally abundant. Gabbroic dikes are not included with the ultramafic rocks. For discussion, group III, which includes rocks of several types, modes of occurrence, and probably of diverse ages and origins, is subdivided into two groups: group IIIA includes the largest bodies, which are generally fairly coarse grained and probably intrusive; group IIIB consists of small, fairly fine grained bodies believed to be mostly dikes or small intrusive bodies.

Group IIIA

Group IIIA comprises six different occurrences of coarse-grained, probably intrusive ultramafic rocks (figs. 3, 4). They are predominantly hornblende but locally clinopyroxene or biotite is abundant. Apatite is a common accessory mineral, and secondary minerals include actinolite and chlorite (from hornblende and clinopyroxene), albite, epidote-group minerals, sphene, antigorite, magnetite, and rarely garnet. At least some of these ultramafic rocks have been metamorphosed along with surrounding country rocks, although no foliation has developed.

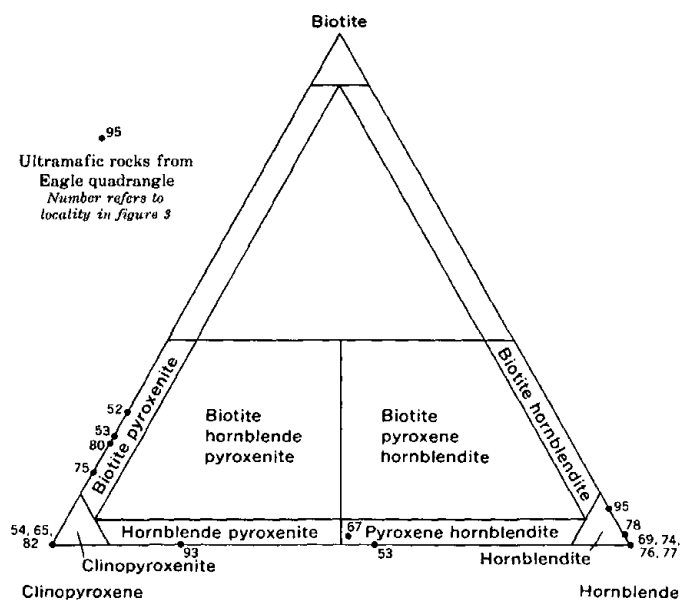


Figure 4.—Ternary diagram showing the dominant primary mineralogy for the group IIIB ultramafic bodies, Eagle quadrangle, Alaska. Primary silicate minerals not included are olivine at localities 65 and 75 (both less than 10 percent), and orthopyroxene at locality 67 (less than 1 percent). The group IIIA ultramafic bodies cover nearly the entire range shown by the diagram, including segregations of pure end members. Two separate rock types are plotted for locality 53.

The easternmost occurrences of group IIIA are two ultramafic masses north of the Fortymile River, localities 70 and 71 (fig. 3). Locality 70 is predominantly biotite pyroxenite and pyroxene hornblende. Diopside augite makes up 5 to 80 percent of the body, hornblende 0 to 20 percent, biotite 0 to 12 percent, and olivine 0 to 2 percent. Secondary minerals include actinolite (mostly from clinopyroxene), green chlorite (mostly after biotite), chlorite (penninite), antigorite, sphene, calcite, magnetite, hematite, and local concentrations of epidote. Some serpentinization was observed near the margin of the mass. Veinlets of pegmatite and granitic rock cut the mass. A small hornblende body included in group IIIB (loc. 69, fig. 3) occurs a few 100 m to the northwest.

Rock of locality 71 (fig. 3), exposed in cliffs on the north side of the Fortymile River, is primarily biotite hornblende with minor hornblende pyroxenite. Exceptionally large crystals of biotite and dark-green hornblende, 50 to 75 mm (2–3 in.) in length, compose much of the body. Locally, more than 80 percent of the rock consists of clinopyroxene. Euhedral crystals of apatite as much as 3 mm (0.12 in.) long make up nearly 2 percent of a few rocks.

The rocks at locality 80 (fig. 3), south of Montana Creek in the south-central part of the Eagle quadrangle, are primarily hornblende pyroxenite with minor biotite hornblende. They intrude coarse-grained marble and can be seen to be infolded and metamorphosed with the marble. Epidote, garnet, and albite in the ultramafic rock are indicative of metamorphism. Sills of ultramafic rock emanate from the main mass and penetrate between the layers of marble.

The country rock is probably Paleozoic for some of the marble contains crinoid columnals, but the time of the metamorphism is unknown. The ultramafic body could therefore be either Paleozoic or Mesozoic in age. The small nearby body, locality 78 (fig. 3), may be a part of it.

The body of locality 89 (fig. 3), composed primarily of clinopyroxene hornblende, hornblende, and clinopyroxenite, is unique in that a sample from the north-central part of the body consists dominantly of green amphibole grains, many of which have rims of blue amphibole. The development of blue amphibole rims is local and may be a metasomatic effect of fluids from a nearby granitic intrusion.

The body at locality 90 (fig. 3), one of the largest in group III, about 0.4 km² (0.15 mi²), consists primarily of hornblende, hornblende pyroxenite, biotite hornblende, and biotite pyroxenite. The rock is mostly coarse grained with hornblende and biotite grains more than 40 mm (1.6 in.) in diameter. Biotite grains are unusually large in biotite hornblende, and hornblende is exceptionally large in other rock types. An age determination by the K⁴⁰/Ar⁴⁰ method on the hornblende from this locality (by Donald Turner at the Potassium Argon Lab., Alaska Univ.) gave 170.7 m.y. on hornblende and 180.9 m.y. on biotite (Donald Turner, oral commun., 1973). This is close to the age of 177±5 m.y. on hornblende from hornblende syenite near Mount Veta, 24 km

to the southeast. (Potassium argon age report No. 54, Menlo Park, 1969. Potassium analysis by Lois Schlocker and argon analysis and age calculation by J. Von Essen.) Intrusive rocks containing abundant hornblende crop out from south of Mount Veta northward through the Joseph Creek area to the vicinity of the hornblendite at locality 54 (fig. 3).

Group IIIB

Group IIIB consists of 19 small ultramafic bodies that crop out in the southern half of the Eagle quadrangle. Rock types include pyroxenite, biotite pyroxenite, olivine pyroxenite, hornblende pyroxenite, hornblendite, and biotite hornblendite (fig. 4). Secondary minerals that are generally minor in amount include actinolite, chlorite, albite, hornblende, and magnetite. Minor serpentine was found at two localities (Nos. 64 and 67, fig. 3). More detailed information on the mineralogy of the individual bodies is given in an open-file report (Keith and Foster, 1973).

Most of these bodies are probably dikes or small intrusive bodies that are somewhat metamorphosed. Their age is not known but probably ranges from Paleozoic through Mesozoic.

Geochemical Data

Semiquantitative spectrographic analyses for 36 elements and gold analyses by atomic absorption were made for 29 randomly selected samples of group I rocks, 16 of group II rocks, and 35 of group III rocks (Keith and Foster, 1973). No consistent pattern was detected for any element or group of elements or for ultramafic bodies in any given area. Nickel ranged from 5 ppm to more than 5,000 ppm in groups I and II, but was 1,000 to 5,000 ppm in most specimens. Vanadium commonly has an inverse relation to nickel, generally being higher in specimens comparatively low in nickel. Nickel was generally low in rocks of group III, being less than 300 ppm in all but two localities.

Platinum group minerals were analyzed by fire assay and spectrographic methods for 24 group I specimens, 23 group II specimens, and 26 group III specimens. Platinum was detected in only 9 specimens from groups I and II, and 0.010 ppm was the highest amount contained. In group III, however, 7 specimens contained platinum and one specimen (loc. 52, fig. 3) contained 0.300 ppm platinum and 0.200 ppm palladium. The complete analyses for all elements analyzed are given in a U.S. Geological Survey open-file report (Keith and Foster, 1973).

DISCUSSION AND CONCLUSIONS

Petrologic Relations

We have shown that Groups I and II are serpentinized harzburgite and dunite or massive serpentinite for which the original mineralogy cannot be determined. We believe that

these rocks have a different origin from those of group III. They exhibit many of the features of alpine-type ultramafic complexes as described by Jackson and Thayer (1972, p. 290). The mineralogy of the original rock types, shown in figure 5, closely corresponds to Jackson and Thayer's harzburgite subtype (1972, p. 290, 291, 294) and also falls, for the most part, into the common alpine-type grouping of Coleman (1971a, p. 906). The two plots of the Mount Sorenson body (No. 3, fig. 5), which are outside the normal alpine-type range, are local concentrations of clinopyroxene-rich rocks within the body.

The ultramafic rocks of the Eagle quadrangle have other features of alpine-type rocks. Foliation can be recognized in several exposures. Layering such as that described by Taylor and Noble (1960, p. 176; Noble and Taylor, 1960, p. 188) has not been found, although there are clinopyroxene segregations

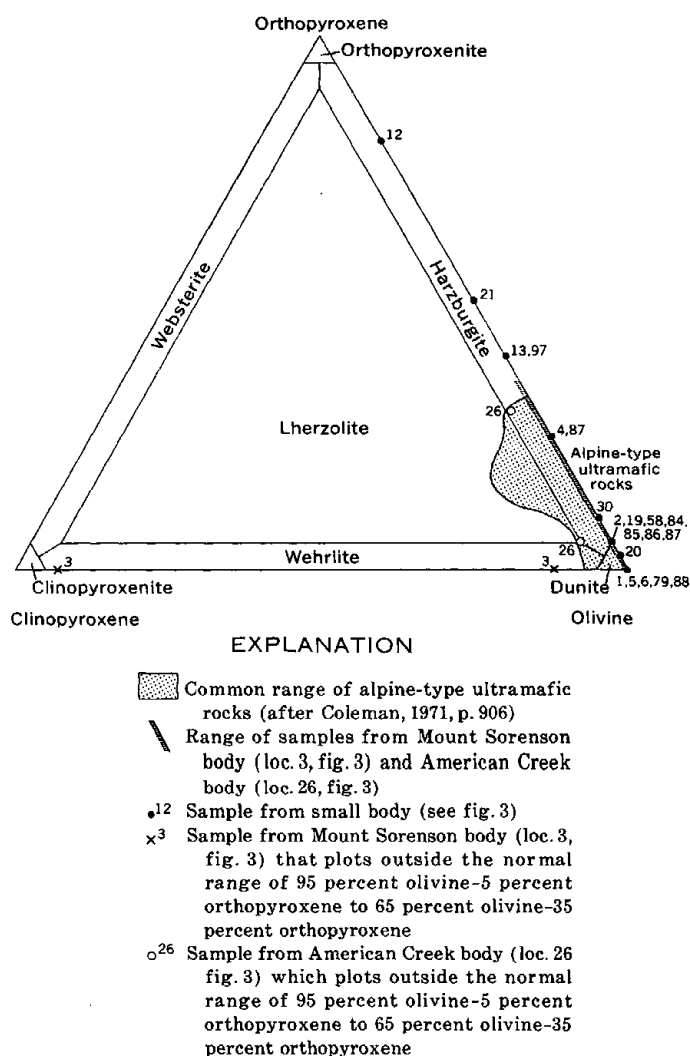


Figure 5.—Ternary diagram showing estimated modes of the original mineralogy of the partially serpentinized alpine-type ultramafic rocks of the Eagle quadrangle, Alaska, relative to the modal range of the most common alpine-type worldwide occurrences.

or lenses in the Mount Sorenson body. There is no evidence of cumulus textures. Orthopyroxene grains are deformed in the American Creek body. Olivine grains are kink banded and granulated in both the American Creek and Mount Sorenson bodies. Contact metamorphic effects are not evident in the country rock adjacent to the ultramafic bodies and most of the boundaries that can be observed are fault contacts. Hard green fibrous actinolite or serpentine is found along some boundaries. The bodies are irregular in shape and some of the smaller bodies are lenticular.

The characteristics of the Mount Sorenson ultramafic mass and other bodies in the northwest-trending zone suggest that they might also be considered as part of an ophiolite, probably a dismembered ophiolite. According to the criteria established by the Penrose Ophiolite Conference (Coleman, 1973, p. 4), the Mount Sorenson ultramafic mass has the following characteristics of an ophiolite:

1. Rock type is predominantly serpentinized harzburgite and dunite.
2. Slightly metamorphosed gabbroic rocks are in close proximity to the Mount Sorenson mass.
3. Small amounts of much altered basalt crop out nearby. Massive greenstone that may have been derived from basaltic rock is adjacent to and near the ultramafic rocks. Pillow structures have not been observed in the greenstone near Mount Sorenson but possible pillows have been recognized in it near localities 56 and 59 (fig. 3).
4. Green and gray banded chert, argillite, and some marble crop out in minor amounts in the vicinity of Mount Sorenson.
5. Fault contacts are common.
6. Diabase is present as tectonic inclusions.

The ultramafic rocks in Yukon Territory, Canada, which appear to be the southeastward extension of the zone of ultramafic rocks in the Eagle quadrangle, are alpine type and probably include dismembered ophiolite. Green (1972, p. 119) describes the ultramafic rocks southwest of the Tintina in the Dawson map area as small highly sheared serpentinite (principally antigorite) bodies, some of which are associated with greenstone and basic igneous rock.

Still farther southeast along this trend in the vicinity of Ross River is serpentinite and peridotite described by Tempelman-Kluit (1972b, p. 17, 18, 19) as a narrow continuous belt along the Vangorda fault (part of the Tintina fault zone, fig. 2). The dominant rock type is serpentinite, mostly antigorite pseudomorphous after olivine and orthopyroxene. Locally, where the rocks are not completely serpentinized, it is clear that the original rock was harzburgite. The ultramafic bodies are bounded by faults and are closely associated with basaltic rocks, including pillow lavas. Cherty rocks and recrystallized limestone are mapped in the same unit as the basalt.

A single small outcrop of eclogite is known in the area north of the Vangorda fault in terrane considered to be Precambrian in age (fig. 2). About 40 km (25 mi) southeast of the eclogite

outcrop along the same fault, blue amphibole has been reported in quartzite (Tempelman-Kluit, 1970, p. 19–22) (fig. 2). So little is known of these small, single occurrences of eclogite and blue amphibole that it cannot be determined at present whether or not they are related to the origin of the ultramafic rocks.

Alpine-type ultramafic rocks are now most commonly considered to be of mantle origin; ophiolites are regarded by many as slabs of oceanic crust and mantle tectonically emplaced at continental margins (Bailey and others, 1970, p. C77; Dewey and Bird, 1971, p. 3179; Coleman, 1971b, p. 1212). Although the ultramafic bodies described in this report have been studied only in reconnaissance fashion, the number of characteristics in common with many well-known alpine-type bodies and ophiolite complexes is sufficient to consider that their origins may be similar.

Structural Relations

To aid the discussion of the origin of these rocks, certain aspects of their tectonic setting are summarized.

The Tintina fault, also known as the Tintina trench (Roddick, 1967, p. 23) is an exceptionally long (more than 950 km or 590 mi) straight feature that may be linked with structures along the northern Rocky Mountain trench (Tempelman-Kluit, 1972a, p. 39; Roddick, 1967, p. 23). The rocks on the northeast side of the Tintina have been part of a relatively stable continental cratonic terrane since Precambrian time. The rocks in the metamorphic terrane southwest of the Tintina differ from those on the northeast primarily by their greater degree of recrystallization and their maximum age, in most of the area probably no greater than early or middle Paleozoic. They seem to typify a continental rather than an island arc or oceanic crustal assemblage; andesite has not been found, and the metamorphic rocks are predominantly of sedimentary origin. We cannot rule out that some may be the metamorphosed equivalents of those on the northeast side of the fault. Large Mesozoic granitic intrusions are numerous.

Richter and Jones (1973, p. 408) have referred to this metamorphic terrane bounded on the north by the Tintina fault system and on the south by the Denali fault system as part of "an old dissected craton***." They believe that the Denali fault system came into existence in Miocene and Pliocene time at the margin of this craton as a ridge-arc dextral transform fault along a suture that originally marked the site of an ancient subduction zone. An island arc system lay to seaward, resting on the margin of an oceanic plate.

Manner of Emplacement

Assuming that the alpine-type ultramafic rocks of the Eagle quadrangle are of mantle origin, there seem to be two principal situations in which they might have originated. One assumes that alpine-type ultramafic rocks are emplaced tectonically at or near plate margins, the other that such mantle material may

be emplaced within a crustal plate and not necessarily at its margins.

The great length of the Tintina fault system and the fact that it juxtaposes two different terranes throughout much of its length suggests to us the possibility that it is a geosuture that originated as a plate boundary. Following the time relations suggested by Richter and Jones (1973), the rocks composing the terrane between the Tintina and Denali fault systems must have been deposited or accreted to the continental margin by about Permian time.

The source of this terrane is enigmatic. It could be an allochthonous slice or wedge of continental crust rifted or otherwise detached from the North American plate (Monger and Ross, 1971, p. 273). Such a slice could have originated to the south or southeast and moved northward in late Paleozoic time (Jones and others, 1972, p. B214). As the slice neared or pushed along the continental plate margin, trapped oceanic crustal and mantle material might have been shoved onto the slice or pushed up along marginal fractures. The process involved a continent-continent collision similar to that of the concept described by Dewey and Bird (1970, p. 2641–2643). In Alaska the collision was between the North American continental plate and a smaller continental mass along what is now the site of the Tintina fault zone. The alpine-type ultramafic rocks of the Eagle quadrangle could have been derived from overridden and plowed up ocean-mantle material caught up in a narrowing suture at the leading edge of the continental slice (fig. 6).

Ultramafic rocks in Vermont and southern Quebec are in some respects similar to those of the Eagle quadrangle and are examples of alpine-type ultramafic rocks that seem to occur within continental crust and may not necessarily be associated with a plate margin. In the Roxbury district, Vermont, Jahns (1967) has described alpine-type ultramafic rocks in a folded and metamorphosed Paleozoic terrane. The elongate ultramafic sheets and tabular form of some of the bodies resemble the form of those in the Ross River area, Yukon Territory. The sequence of events, including later partial steatization and formation of quartz-carbonate rock, are characteristic of the Eagle quadrangle ultramafic rocks. Jahns (1967, p. 156) states that the Roxbury ultramafic rocks "seem best explained as tectonically emplaced masses of crystalline serpentinite, perhaps derived from olivine-rich rock during upward movement of the crust." The Roxbury district ultramafic

rocks are not known to be directly associated with any large ancient or modern fault system.

In southern Quebec, the dominant ultramafic rock type is serpentinitized harzburgite associated with some dunite, pyroxenite, and gabbro (Riordon and Laliberté, 1972, p. 1). Asbestos has formed locally in commercial amounts, and later alteration includes the formation of talc-carbonate rocks. The country rock consists of folded, faulted, and metamorphosed Paleozoic eugeosynclinal rocks. It is suggested that the ultramafic rocks were intruded in Late Ordovician time along a zone of weakness (Riordon and Laliberté, 1972, p. 3) or extruded on a eugeosynclinal ocean floor through a major zone of distensional fractures (Lamarche, 1972, p. 65). In Vermont and Quebec, of course, it is possible that plate margins as old as Paleozoic have not and perhaps cannot be recognized.

If, however, the Tintina fault system is not a plate boundary, the Eagle quadrangle ultramafic rocks may have aspects of origin in common with rocks of Vermont and Quebec. Perhaps the Eagle quadrangle ultramafic bodies were somehow tectonically derived from depth along a zone of weakness (Tintina fault system) in the continental crust, possibly involving "deep seated" faulting. Study and mapping of the serpentinitized ultramafic bodies in the Big Delta quadrangle (directly west of the Eagle quadrangle) may aid in the interpretation of the Eagle quadrangle ultramafic rocks. It has been suggested that the Big Delta ultramafic rocks are at the margin of a major but ancient (Paleozoic) thrust fault (F.R. Weber, oral commun., 1973).

Serpentinization

Whatever the tectonic setting for emplacement of the ultramafic rocks, we suggest that peridotite derived from the mantle was moved upward as elongate blocks or sheets in the vicinity of the present Tintina fault zone. The process of serpentinitization of the peridotite (Coleman and Keith, 1971, p. 323) began as the rising peridotite came into contact with water contained within sedimentary rocks in the crust (Coleman, 1971a) and continued throughout final emplacement in the upper crust.

The peridotite, upon reaching the upper crust, probably consisted of several large serpentinitized masses, such as the Mount Sorenson and American Creek bodies and other highly serpentinitized bodies. Most of the serpentinitization was

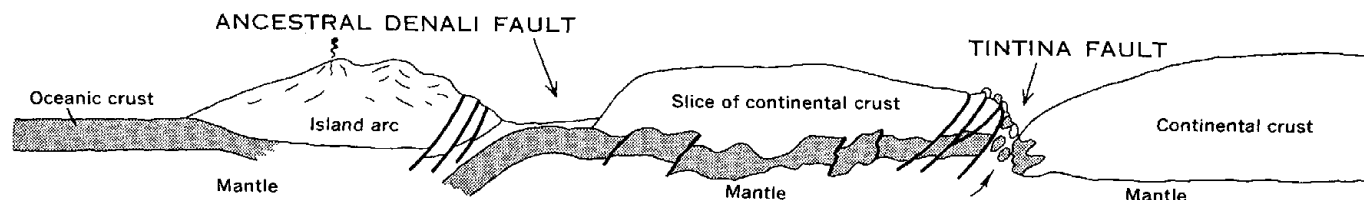


Figure 6.—Schematic cross section showing postulated relations across the Denali and Tintina faults in late Paleozoic time and possible situation for emplacement of the alpine-type peridotites. Parts of diagram modified from Richter and Jones (1973, p. 418).

probably complete by this time, but metamorphism and deformation continued and the more highly serpentized parts of the peridotite were stretched out to form lenses.

The serpentine group minerals that are present in most places in the Eagle quadrangle, correlate with the metamorphic grade of the adjacent country rock; that is, lizardite and clinochrysotile-bearing bodies are generally surrounded by country rock that is slightly metamorphosed, whereas the antigorite-bearing bodies are generally enclosed in country rock of a higher metamorphic grade; that is, upper greenschist or amphibolite facies. In a few places where polymetamorphism and (or) other factors have complicated the mineralogy, this relation may not exist.

Chernosky (1971) has determined experimentally that antigorite does not form directly from other serpentine; however, this does not definitely preclude the possibility of its doing so in nature. The formation of antigorite requires higher temperature-pressure conditions than does the formation of lizardite and chrysotile (Deer and others, 1962, p. 186; Wenner and Taylor, 1970; Coleman, 1971a, p. 907). The antigorite could have formed either directly from the mantle peridotite as it entered the upper crust or by the recrystallization of lizardite and clinochrysotile to antigorite during greenschist- or amphibolite-facies metamorphism after emplacement (Coleman, 1971a, p. 901). Evidence of both processes are seen in thin section. The thin veinlets of chrysotile formed after emplacement of the serpentized bodies and may be now forming as a result of the activity of groundwater (Barnes and others, 1967; Barnes and O'Neil, 1969).

The serpentine in some ultramafic bodies in the Eagle quadrangle has been replaced to different degrees by talc and magnesite. The formation of such talc-rich rocks with associated magnesite is discussed by Deer, Howie, and Zussman (1962, p. 127–128) as steatization due to hydrothermal alteration of ultramafic rocks (including serpentinite). Jahns (1967, p. 157–158) in his study of the serpentinite of the Roxbury district, Vermont, indicates that replacement of serpentinite by talc-carbonate rock could have been accomplished relatively simply through introduction of CO_2 and loss of H_2O . It has been shown by Deer, Howie, and Zussman (1962, p. 127) that in some areas steatization has taken place subsequent to serpentization during a period of greenschist metamorphism.

In the Eagle quadrangle, the serpentine that is partially replaced by talc and magnesite is fine grained and massive and the magnesite veinlets cut the serpentine, indicating that the steatization is definitely a late alteration of serpentine. It could have resulted from regional greenschist metamorphism or hydrothermal solutions.

Silica-carbonate veins are associated with a few of the ultramafic bodies as late alteration products. The silica phase is well crystallized quartz; the carbonate is magnesite associated at a few places with dolomite. Deer, Howie, and Zussman

(1962, p. 128) describe the progressive alteration of serpentine to a talc and magnesite assemblage and then to a magnesite and quartz assemblage as the CO_2 in the rock increases and H_2O decreases.

Barnes, O'Neil, Rapp, and White (1973) describe in detail the conditions for formation of silica-carbonate veins from serpentine in the presence of CO_2 -rich waters at surface conditions. They conclude that this process is not limited to surface conditions. The presence of quartz as the silica phase in the rocks of the Eagle quadrangle rather than chalcedony or opal indicates that the alteration here took place at a temperature and pressure higher than those of surface conditions. The quartz-carbonate veins could be a product of late low-grade metamorphism (Mount Sorenson body) or greenschist metamorphism (loc. 41, fig. 3) in the presence of excess CO_2 .

Age Relations

Little data is available for determining the time of emplacement of the peridotite in the Eagle quadrangle, but the relation of the peridotite bodies to the Paleozoic metasedimentary rocks and to the Mesozoic intrusive rocks, their deformation and tectonic setting, and their involvement in regional metamorphism suggest a late Paleozoic or early Mesozoic age. Ultramafic rocks near Ross River are considered to have been emplaced in Triassic time (Tempelman-Kluit, 1972b, p. 19). All the alpine-type ultramafic rocks along the Tintina fault may not have been emplaced at the same time, and the Eagle rocks are not necessarily the same age as those near Ross River.

Although several metamorphic events affected the Eagle area, the times of metamorphism are unknown. Metamorphism may have begun in late Paleozoic time in connection with orogenic activity resulting from the collision of the continental slice and continental plate and may have continued into early Mesozoic time. Radiometric age determinations on the metamorphic rocks of the Eagle quadrangle yield dates within the Mesozoic (Wasserburg, Eberlein, and Lanphere, 1963, p. 258–259; Donald Turner, oral commun., 1973) and probably reflect primarily thermal events related to the intrusion of granitic plutons. The rocks of the granitic plutons are not metamorphosed.

Although the suture, the position of which is now marked by the Tintina fault or trench, probably came into existence in Paleozoic time, right-lateral transcurrent movement is postulated along the Tintina fault in the Cretaceous (Roddick, 1967, p. 30), and there may have been vertical movement. Minor vertical movement, with perhaps limited strike-slip movement, took place during the Tertiary in the Yukon Territory (Tempelman-Kluit, 1972a, p. 39), and in the Eagle quadrangle movement was sufficient to form thick breccia and gouge zones.

Summary

Although we can identify many of the ultramafic rocks of the Eagle quadrangle as alpinotype, there is no clear indication of how they were transported from the mantle. The Tintina fault system could have provided a zone of weakness along which mantle material was tectonically emplaced or it may represent a plate boundary in late Paleozoic time. If it does represent a plate boundary, the metamorphic terrane that lies between the Tintina and Denali faults would have to be allochthonous, perhaps originating as a northward-moving slice of continental material. During the course of the movement as the two continental masses approached and perhaps collided, mantle peridotite and oceanic crustal material were squeezed up along the continental margin onto the continental slice.

During the upward rise of mantle peridotite, serpentinization took place and the process was probably mostly complete when the peridotite reached its surface or near-surface crustal position. During later regional deformation, some of the serpentinized peridotite was fragmented and pieces of it were incorporated as pods into the metasedimentary sequence. Minor serpentinization and local alteration continued as a result of contact metamorphism and hydrothermal activity. Groundwater may still be an active agent of local minor serpentinization.

REFERENCES CITED

- Bailey, E.H., Blake, M.C., Jr., and Jones, D.L., 1970, On-land Mesozoic oceanic crust in California, in *Geological Survey research 1970*: U.S. Geol. Survey Prof. Paper 700-C, p. C70–C81.
- Barnes, Ivan, LaMarche, V.C., Jr., and Himmelberg, Glen, 1967, Geochemical evidence of present-day serpentinization: *Science*, v. 156, p. 830–832.
- Barnes, Ivan, and O'Neil, J.R., 1969, The relationship between fluids in some fresh alpine-type ultramafics and possible modern serpentinization, western United States: *Geol. Soc. America Bull.*, v. 80, p. 1947–1960.
- Barnes, Ivan, O'Neil, J.R., Rapp, J.B., and White, D.E., 1973, Silica-carbonate alteration of serpentine: Wall rock alteration in mercury deposits of the California Coast Ranges: *Econ. Geology*, v. 68, p. 388–398.
- Bostock, H.S., 1964, *Geology*, McQuesten, Yukon Territory: Canada Geol. Survey Map 1143A, scale 1:253,440.
- Brabb, E.E., and Churkin, Michael, Jr., 1969, *Geologic map of the Charley River quadrangle, east-central Alaska*: U.S. Geol. Survey Misc. Geol. Inv. Map I-573, scale 1:250,000.
- Chernosky, J.V., 1971, Minerals of the serpentine group: *Carnegie Inst. Ann. Rept.* 1970-71, p. 153–157.
- Clark, S.H.B., and Foster, H.L., 1971, *Geochemical and geological reconnaissance in the Seventymile River area, Alaska*: U.S. Geol. Survey Bull. 1315, 21 p.
- Coleman, R.G., 1967, Low temperature reaction zones and alpine ultramafic rocks of California, Oregon, and Washington: U.S. Geol. Survey Bull. 1247, 49 p.
- 1971a, Petrologic and geophysical nature of serpentinites: *Geol. Soc. America Bull.*, v. 82, p. 897–918.
- 1971b, Plate tectonic emplacement of upper mantle peridotites along continental edges: *Jour. Geophys. Research*, v. 76, no. 5, p. 1212–1222.
- 1973, Ophiolite conference combines field trips, seminars: *The Geologist*, v. 8, no. 2, p. 1–4.
- Coleman, R.G., and Keith, T.E., 1971, A chemical study of serpentinization—Burro Mountain, California: *Jour. Petrology*, v. 12, no. 2, p. 312–328.
- Deer, W.A., Howie, R.A., and Zussman, J., 1962, *Rock-forming minerals, in Sheet silicates*, v. 3: New York, John Wiley and Sons, 270 p.
- Dewey, J.F., and Bird, J.M., 1970, Mountain belts and the new global tectonics: *Jour. Geophys. Research*, v. 75, no. 14, p. 2625–2647.
- 1971, Origin and emplacement of the ophiolite suite: Appalachian ophiolites in Newfoundland: *Jour. Geophys. Research*, v. 76, no. 14, p. 3179–3206.
- Douglas, R.J.W., 1968, *Geology and economic minerals of Canada*: Canada Geol. Survey, 838 p.
- Foster, H.L., 1969a, Asbestos occurrence in the Eagle C-4 quadrangle, Alaska: U.S. Geol. Survey Circ. 611, 7 p.
- 1969b, Reconnaissance geology of the Eagle A-1 and A-2 quadrangle, Alaska: U.S. Geol. Survey Bull. 1271, p. G1–G30.
- 1970, Reconnaissance geologic map of the Tanacross quadrangle, Alaska: U.S. Geol. Survey Misc. Geol. Inv. Map I-593, scale 1:250,000.
- 1972, Preliminary geologic map of the Eagle quadrangle, Alaska: U.S. Geol. Survey Misc. Field Studies Map MF-358, scale 1:250,000.
- Foster, R.L., 1967, Tectonic inclusions from a serpentinite, east-central Alaska: U.S. Geol. Survey Prof. Paper 575-D, p. D120–D122.
- Geological Survey of Canada, 1957, *Geological map of Yukon Territory*: Canada Dept. Mines and Tech. Surveys Map 1048A, scale 1:125,000.
- Green, L.H., 1972, *Geology of Nash Creek, Larsen Creek, and Dawson. Map areas, Yukon Territory*: Canada Geol. Survey Mem. 364, 157 p.
- Jackson, E.D., and Thayer, T.P., 1972, Some criteria for distinguishing between stratiform, concentric, and alpine peridotite-gabbro complexes: *Internat. Geol. Cong.*, 24th, Montreal 1972, sec. 2, Petrology, p. 289–296.
- Jahns, R.H., 1967, II. Serpentinites of the Roxbury District, Vermont, in *Wyllie, P.J., ed., Ultramafic and related rocks*: New York, John Wiley and Sons, p. 137–160.
- Jones, D.L., Irwin, W.P., and Ovenshine, A.T., 1972, Southeastern Alaska—A displaced continental fragment?, in *Geological Survey research 1972*: U.S. Geol. Survey Prof. Paper 800-B, p. B211–B217.
- Keith, T.E.C., and Foster, H.L., 1973, Basic data on the ultramafic rocks of the Eagle quadrangle, east-central Alaska: U.S. Geol. Survey open-file rept.
- LaMarche, R. Y., 1972, Ophiolites of Southern Quebec, in *Irving, E., ed., The ancient oceanic lithosphere*: Canada Earth Physics Branch Pub., v. 42, no. 3, p. 65–69.
- Mertie, J.B., Jr., 1937, *The Yukon-Tanana region, Alaska*: U.S. Geol. Survey Bull. 872, 276 p.
- Monger, J.W.H., and Ross, C.A., 1971, Distribution of Fusulinaceans in the western Canadian Cordillera: *Canadian Jour. Earth Sci.*, v. 8, no. 2, p. 259–278.
- Noble, J.A., and Taylor, H.P., Jr., 1960, Correlation of the ultramafic complexes of southeastern Alaska with those of other parts of North America and the world, in *Petrographic provinces, igneous and metamorphic rocks*: *Internat. Geol. Cong.*, 21st, Norden 1960, pt. 8, p. 188–197.
- Richter, D.H., 1973, Preliminary bedrock geologic map of the Nabesna quadrangle, Alaska: U.S. Geol. Survey open-file map, 2 sheets.
- Richter, D.H., and Jones, D.L., 1973, Structure and stratigraphy of eastern Alaska Range: *Am. Assoc. Petroleum Geologists Mem.* 19, Arctic Geology, p. 408–420.
- Riordon, P.H., and Laliberté, R., 1972, Asbestos deposits of southern

- Quebec, in *Guidebook to excursion B-08: Internat. Geol. Cong. 24th, Montreal 1972*, 21 p.
- Roddick, J.A., 1967, Tintina trench: *Jour. Geology*, v. 75, no. 1, p. 23-33.
- Saunders, R.H., 1956, Report on the Flume Creek lode-gold prospect, Eagle quadrangle: Alaska Terr. Dept. Mines open-file rept., 7 p.
- Taylor, H.P., Jr., and Noble, J.A., 1960, Origin of the ultramafic complexes in southeastern Alaska, in *Petrographic provinces, igneous and metamorphic rocks: Internat. Geol. Cong., 21st, Norden 1960*, pt. 8, p. 175-187.
- Tempelman-Kluit, D.J., 1970, An occurrence of eclogite near Tintina trench, Yukon: Canada Geol. Survey Paper 70-1, pt. B, p. 19-22.
- 1972a, Evidence for timing and magnitude of movement along Tintina Trench [abs.], in *Faults, fractures, lineaments and related mineralization in the Canadian cordillera: Geol. Assoc. Canada Programme and Abs., Cordilleran Sec.*, p. 39.
- 1972b, Geology and origin of the Faro, Vangorda, and Swim concordant zinc-lead deposits, central Yukon Territory: Canada Geol. Survey Bull. 208, 73 p.
- Veach, N.J., 1972, Aeromagnetic survey, east Alaska Range, Eagle, Alaska: Alaska Dept. Nat. Resources, Geol. and Geophys. Surveys, 24 maps, scale 1:63,360.
- Wasserburg, G.J., Eberlein, G.D., and Lanphere, M.A., 1963, Age of the Birch Creek schist and some batholithic intrusions in Alaska [abs.]: *Geol. Soc. America Spec. Paper* 73, p. 258-259.
- Wenner, D.B., and Taylor, H.P., Jr., 1970, Temperatures of serpentinization of ultramafic rocks based on O^{18}/O^{16} fraction between coexisting serpentine and magnetite [abs.]: *Geol. Soc. America Abs. with Programs*, v. 2, no. 7, p. 718-719.

BARIUM IN HYBRID GRANITOID ROCKS OF THE SOUTHERN SNAKE RANGE, NEVADA

By DONALD E. LEE and WILLIS P. DOERING, Denver, Colo.

Abstract.—In a magmatic environment, barium usually substitutes for potassium in the crystallizing silicates, and the two increase together in rocks late in the differentiation sequence. Results of this study show the opposite trend in an equivalent of a large part (63–76 percent SiO_2) of the classic differentiation sequence that resulted mainly from assimilation of chemically distinct host rocks. The barium content of the hybrid granitoid rock appears to be controlled mainly by the barium contents of the various sedimentary rock types assimilated.

In a magmatic environment, most of the trace elements are taken up by the crystallizing silicates, substituting for the major elements largely on the basis of ionic size. The substitution of barium for potassium has been cited as a particularly good example of this principle, with the two increasing together in rocks late in the differentiation sequence (Krauskopf, 1967, p. 587–589). Moreover, eight studies cited by Puchelt (1972, p. 56–E–7) found that barium concentrations increase during progressing differentiation. The present paper (1) describes the opposite trend in an equivalent of a large part (63–76 percent SiO_2) of the classic differentiation sequence that resulted mainly from assimilation of chemically distinct host rocks, and (2) presents data on the barium content of an unusual muscovite-rich hybrid rock that formed through assimilation of argillite.

The Jurassic granitoid rocks studied crop out a few miles north of the Mount Wheeler mine in the southern part of the Snake Range, about 50 mi (80 km) southeast of Ely, Nev. These same rocks are the subject of a comprehensive field and laboratory study (Lee and Van Loenen, 1971) that includes both a geologic map that shows sample localities and tables of complete chemical data for all the specimens discussed in the present report. The sample numbers used here are the same as in the comprehensive study, where rocks are numbered in order of increasing CaO content; that is, from most felsic to most mafic. The field numbers used in earlier papers cited in this report are keyed to these sample numbers by Lee and Van Loenen (1971, p. 11).

The samples were analyzed by X-ray fluorescence using a General Electric XRD-6¹ spectrograph. A chromium X-ray tube produced the radiation, and a LiF analyzing crystal having a 2-*d* spacing of 2.848 Å was used. The barium $L\beta_2$ line was selected to measure the amount of barium in the samples because it gave a low background count and the least interference with adjacent lines. The net counts of the unknown samples were compared to those of the U.S. Geological Survey standard rocks to obtain the concentrations in parts per million. The values used for these standards are those recommended by De Laeter, Abercrombie, and Date (1969), who determined the concentrations by the stable isotope dilution method. These standard samples were alternated with the unknown ones about 30 times. The uncertainty of X-ray determinations compared to the isotope dilution values is 2.5 percent, at the 1- σ confidence level.²

Results of semiquantitative spectrographic analyses are based on their identity with geometric brackets whose boundaries are 1.2, 0.83, 0.56, 0.38, 0.26, 0.18, 0.12, and so forth, and are reported arbitrarily as midpoints of these brackets: 1, 0.7, 0.5, 0.3, 0.2, 0.15, and 0.1, respectively. The precision of a reported value is approximately plus or minus one bracket at 68-percent confidence, or two brackets at 95-percent confidence.

SNAKE CREEK—WILLIAMS CANYON AREA

The influence of host rock on the chemistry and mineralogy of intrusive rocks of the southern Snake Range is most clearly shown in the Snake Creek—Williams Canyon area. There the intrusive is undeformed, probably has not been eroded to a depth of much more than 1,000 ft (300 m), and is well exposed in contact with quartzite, shale, and limestone. Within a horizontal distance of 3 mi (5 km) the intrusive grades from a quartz monzonite (76 percent SiO_2 , 0.5 percent CaO) where the host rock is quartzite to a granodiorite (63 percent SiO_2 ,

¹ Use of trade name in this paper is for descriptive purposes only and does not constitute an endorsement of the product by the U.S. Geological Survey.

² 1 σ = confidence level of 67-percent uncertainty.

4.5 percent CaO) where the host rock is limestone. Other major elements vary as one would expect in a normal differentiation sequence. Most minor elements show a similar variation, the notable exceptions being the rare earths (Lee and Bastron, 1967; Lee and Van Loenen, 1971, p. 25, 44) and barium.

Quantitative barium analyses of the rocks are listed in table 1. In figure 1, barium is plotted against CaO and the equivalent

Table 1.—Quantitative barium analyses, in parts per million, of granitoid rocks from the Snake Creek—Williams Canyon area

[W. P. Doering, analyst. Method of analysis explained in text. Complete analyses of rocks listed by Lee and Van Loenen (1971, table 5). Samples 71, 72, 77, 81, and 85 are xenoliths]

Sample	Ba	Sample	Ba	Sample	Ba
1	353	30	1,528	59	1,136
2	260	31	1,482	60	1,115
3	309	32	1,501	61	1,034
4	328	33	1,466	62	1,683
5	336	34	1,625	63	1,186
6	498	35	1,624	64	1,016
7	334	36	1,481	65	1,070
8	301	37	1,676	66	1,017
9	815	38	1,617	67	1,159
10	467	39	1,505	68	1,221
11	437	40	1,633	69	1,255
12	825	41	1,679	70	1,144
13	655	42	1,102	71	1,191
14	933	43	1,670	72	697
15	1,086	44	1,413	73	1,239
16	1,124	45	1,563	74	1,168
17	1,094	46	1,725	75	1,178
18	1,122	47	2,382	76	1,310
19	1,157	48	1,698	77	1,019
20	1,126	49	1,586	78	1,353
21	1,182	50	1,670	79	1,255
22	1,016	51	1,533	80	1,016
23	1,110	52	1,675	81	1,630
24	1,036	53	1,547	82	1,120
25	1,307	54	1,543	83	1,018
26	1,408	55	1,532	84	1,132
27	915	56	1,712	85	581
28	989	57	1,726	86	1,073
29	1,492	58	1,670		

ranges of K_2O and SiO_2 are indicated. It is apparent in figure 1 that the most felsic part of the Snake Creek—Williams Canyon exposure contains the least barium, less than 400 ppm. The trend rises sharply to a maximum barium content of more than 1,600 ppm where the rock contains 2.0–2.5 percent CaO (3.8–3.0 percent K_2O). A secondary trend, also indicated in figure 1, branches from the main trend where the rock contains 2.0–2.5 percent CaO.

It is probably significant that the maximum barium contents are found where the rock contains 2.0–2.5 percent CaO. Lee and Van Loenen (1971, p. 20) stated:

We cannot be sure where to project the western edge (Pioche Shale) of the main syncline across the igneous outcrop; but were it not for the intrusive, the Pioche Shale probably would crop out on the present erosion surface somewhere between or near the 2.0- and 2.5-percent-CaO contours on plate 1. This deduction is based partly on

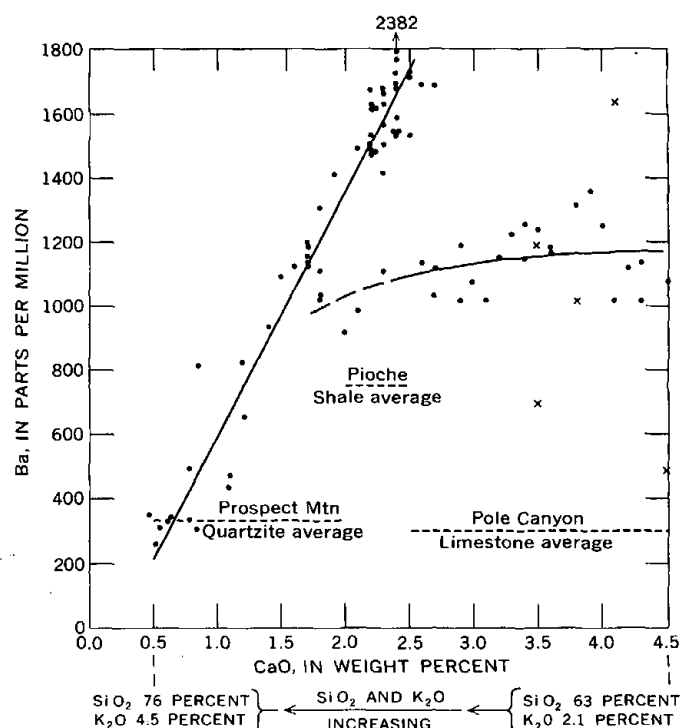


Figure 1.—Relation between CaO and Ba contents in granitoid rocks of the Snake Creek—Williams Canyon area. Equivalent ranges of contents of SiO_2 and K_2O , in weight percent, are indicated. Average Ba contents of sedimentary rocks indicated on parts of diagram representing assimilation of those rocks. Based on tables 1 and 2 and data listed by Lee and Van Loenen (1971, tables 5, 9). •, main intrusive; x, xenolith. See text for discussion.

the fact that Pioche Shale abuts the intrusive in this position and partly on the fact that the intrusive is almost devoid of (Pioche Shale) xenoliths west of the 2.0-percent-CaO contour, whereas these xenoliths are common to abundant east of this contour. Whatever the structural interpretation, it is clear that lower CaO contents in the granitoid rock are near the quartzite country rock, and higher CaO contents are near the shale and limestone.

Complete analyses of 34 samples of the sedimentary rocks that are in contact with (and were assimilated by) these hybrid granitoid rocks were listed by Lee and Van Loenen (1971, p. 8, 9). For the present study, splits of the quartzites and shales were analyzed for barium. The quantitative results are listed in table 2, and the averages are indicated on those parts of figure 1 that presumably represent assimilation of the respective rocks. The average for the Pole Canyon Limestone (fig. 1) is based on semiquantitative data for nine samples (Lee and Van Loenen, 1971, p. 36). In a general way, average barium contents of the quartzite, shale and limestone assimilated appear to relate to the trends indicated for the mass of granitoid rock (fig. 1), but they do not account for the concentrations of points above 1,400 ppm barium.

The distribution of potassium in these hybrid rocks is apparent from the opposite trends for biotite and microcline summarized in figure 2 and described in detail by Lee and Van

Table 2.—Quantitative barium analyses, in parts per million, of Prospect Mountain Quartzite and Pioche Shale

[W. P. Doering, analyst. Method of analysis explained in text. Complete analyses of rocks listed by Lee and Van Loenen (1971, table 1)]

Sample	Ba	Sample	Ba
Prospect Mountain Quartzite		Pioche Shale—Continued	
Q1	300	S3	508
2	465	4	514
3	421	5	921
4	133	6	1,078
Average	330	7	1,336
Pioche Shale		8	1,403
S1	527	9	240
2	274	Average	756

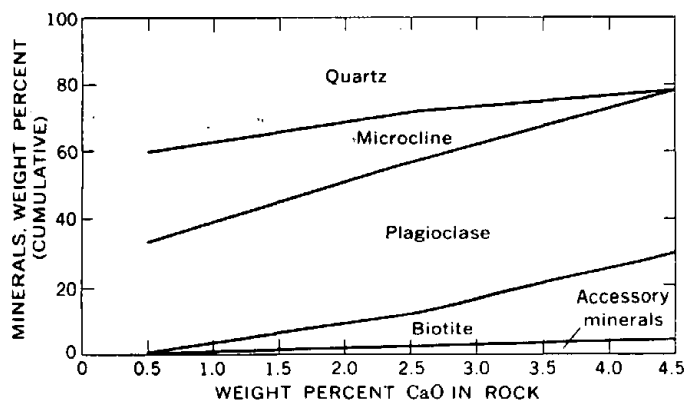
¹ Semiquantitative value from Lee and Van Loenen (1971, table 1).

Figure 2.—General relations between CaO content and mineralogy, for granitoid rocks of the Snake Creek—Williams Canyon area. (From Lee and Van Loenen, 1971, fig. 11.)

Loenen (1970, p. D198; 1971, p. 27). On the basis of data in table 3, the distribution of barium is approximated in figure 3;

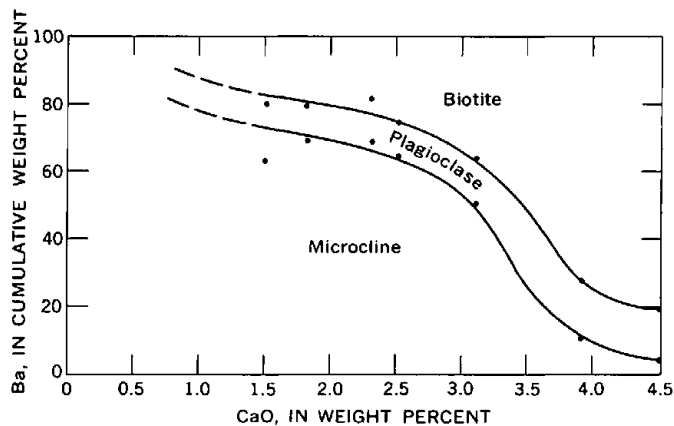


Figure 3.—Distribution of Ba among minerals in granitoid rocks of the Snake Creek—Williams Canyon area, based on data in table 3. See text for discussion.

this figure does not consider the very minor amounts of barium present in the constituent sphene (Lee and others, 1969), epidote (Lee and others, 1971), and apatite (Lee and others, 1973).

The mineral totals in table 3 are generally less than the barium value obtained directly by rock analysis. The discrepancies may be due to one or more of the following factors, listed in order of decreasing probability:

1. The semiquantitative determination of barium in microcline and (or) plagioclase may be low.
2. Minor amounts (as much as 0.50 percent) of muscovite were detected during mineral separation work on these rocks. The muscovite recovered from sample 79 contains 6,322 ppm barium.
3. During systematic mineral separation work on 30 of these rocks, a few grains of a mineral identified optically as barite fractionated with the zircon from sample 78. This is the only sample in which barite was detected, and it probably makes up much less than 0.01 percent of the rock (0.01 percent barite would be equivalent to about 66 ppm barium in the rock).

POLE CANYON—CAN YOUNG CANYON AREA

In the Pole Canyon—Can Young Canyon area of the southern Snake Range there is an exposure of an unusual hybrid rock that has developed through assimilation of argillite. This rock is distinguished in part by large phenocrysts of muscovite, many of which contain euhedral crystals of biotite. The rock is described in detail by Lee and Van Loenen (1971, p. 5, 38–39). Chemical differences in the rock from place to place are relatively small, with no systematic spatial distribution of values for either major or minor elements. The distribution of barium in three samples of this rock is summarized in table 3.

Chemical analyses of six samples (AR 1–6) of the argillite assimilated by this hybrid rock are listed by Lee and Van Loenen (1971, p. 8). For the present study, splits of these same samples were analyzed for barium, and quantitative results were 884, 140, 1,482, 1,019, 474, and 630 ppm, respectively. The average of these determinations is 771 ppm, perhaps fortuitously close to the values obtained for the granitoid rock itself (table 3).

DISCUSSION

The hybrid granitoid rocks of the southern Snake Range are of petrologic interest for two main reasons:

1. In the Snake Creek—Williams Canyon area, the equivalent of a large part of the classic differentiation sequence has developed mainly from assimilation of chemically distinct host rocks.
2. The Pole Canyon—Can Young Canyon area intrusive body is an unusual muscovite-bearing hybrid rock that has developed through assimilation of argillite. The distinct-

Table 3.—Distribution of barium among minerals in granitoid rocks of the Snake Creek—Williams Canyon area and the Pole Canyon—Can Young Canyon area

[Quantitative Ba analyses (biotite, muscovite, and rock) by W. P. Doering. Semiquantitative analyses (microcline and plagioclase) by R. E. Mays. Values for plagioclase based on analysis of 1:1 mixture of quartz and plagioclase; values listed are twice those determined on the mixture, assuming no Ba present in the quartz. Methods of analysis explained in text.]

Sample	CaO in rock (wt percent)	Mineral in rock (wt percent)				Ba in pure mineral (wt percent)				Contribution to Ba content of the rock (wt percent)					Total Ba in rock (wt percent)				
		Biotite	Micro-cline	Musco-vite	Plagio-clase	Biotite	Micro-cline	Musco-vite	Plagio-clase	Biotite	Micro-cline	Musco-vite	Plagio-clase	Total ¹	Biotite	Micro-cline	Musco-vite	Plagio-clase	Total
Snake Creek—Williams Canyon area																			
15	1.5	10	18	38	0.1703	0.3	0.04	0.0170	0.054	0.0142	0.0852(0.1086)	19.9	63.4	16.7	100.0
22	1.8	7	17	40	.3566	.503	.0250	.085012	.1220(.1016)	20.5	69.7	9.8	100.0
39	2.3	8	14	43	.2314	.503	.0185	.070129	.1014(.1505)	18.3	69.0	12.7	100.0
55	2.5	11	16	41	.2903	.503	.0320	.080123	.1243(.1532)	25.7	64.4	9.9	100.0
66	3.1	10	10	45	.3609	.503	.0361	.050135	.0996(.1017)	36.3	50.2	13.5	100.0
78	3.9	19	2	49	.3513	.503	.0668	.010147	.0915(.1353)	73.1	10.9	16.0	100.0
86	4.5	26	1	48	.3081	.503	.0801	.0050144	.0995(.1073)	80.5	4.4	15.1	100.0
Pole Canyon—Can Young Canyon area																			
89	6	19	6	35	0.0633	0.3	0.0399	0.014	0.0038	0.057	0.0024	0.0048	0.0648(0.0760)	5.6	83.8	3.5	7.1	100.0
90	5	17	9	36	.0871	.3	.0491	.014	.0044	.051	.0044	.005	.0648(.0741)	6.8	78.7	6.8	7.7	100.0
93	4	19	5	40	.0590	.3	.0485	.014	.0024	.057	.0024	.0056	.0674(.0689)	3.6	84.5	3.6	8.3	100.0

¹ Totals in parentheses are by rock analysis.

ive nature of this exposure is especially striking inasmuch as it is separated from the Snake Creek—Williams Canyon area intrusive by a septum of sedimentary rocks a mile long and only about 1,000 ft (300 m) wide.

These features of the granitoid rocks of the southern Snake Range are evident not only from the chemistry and mineral content of the rocks, but also from systematic laboratory study of the constituent minerals themselves, as described in the papers already cited.

Data for barium also reflect the different magmatic affinities of these two discrete, but closely adjacent outcrops of granitoid rock. In rocks of the Pole Canyon—Can Young Canyon area, more of the barium is in microcline and muscovite and less is in biotite and plagioclase.

In considering the data for granitoid rocks of the Snake Creek—Williams Canyon and the Pole Canyon—Can Young Canyon areas (fig. 1), recall that we are dealing with a crystallized magma, the results of liquid \rightleftharpoons crystal equilibria, regardless of whether our "original, uncontaminated" magma was formed by palingenesis of sediments or by differentiation from some more basic magma at depth. This conclusion is based on the fact that analyses of rocks concentrate in and near Bowen's (1937) thermal valley on the liquidus surface in the system $\text{NaAlSi}_3\text{O}_8\text{--KAlSi}_3\text{O}_8\text{--SiO}_2$ (Lee and Van Loenen, 1971, fig. 15, p. 33). As emphasized by Tuttle and Bowen (1958), such a concentration is readily explained if the chemical compositions are controlled by liquid \rightleftharpoons crystal equilibria but would be a remarkably fortuitous result of any mechanism not involving a magma. Except for barium, the major- and minor-element concentration gradients in the contaminated rocks of the Snake Creek—Williams Canyon area

are regular and well defined. In an extended discussion, Lee and Van Loenen (1971, p. 37) concluded that these gradients were effected by a combination of diffusion and mechanical mixing in the magmatic environment. The data for barium (table 1, fig. 1) are difficult to explain, not only because the general trend is the opposite of what one would expect in normally differentiated rocks (also true of the trends for zirconium, fluorine, and the rare earths), but also because the main trend splits into a secondary trend where the rock contains 2.0–2.5 percent CaO (fig. 1). We speculate as follows:

1. For some reason, the Ba^{+2} ion was relatively immobile in the magmatic environment, and thus the barium content of the granitoid rock strongly reflects the barium content of the sedimentary rock assimilated. This would imply that the barium content of the Pioche Shale samples (table 2, fig. 1) is too low to be representative of much of the Pioche Shale that was assimilated.
2. The distribution coefficient ($D=\text{Ba concentration in the crystal/Ba concentration in the melt}$) is high for K-feldspars (Puchelt, 1972, p. 56–D–15). Perhaps conditions were such that this coefficient was especially high at the time this part of the granitoid rock was crystallizing. Our data for microcline (table 3) are inadequate to test this idea.

Our unpublished quantitative data for rubidium (which also substitutes for potassium in crystallizing silicates) in these rocks show a regular increase with increasing K_2O (decreasing CaO) as one would expect in normally differentiated rocks. Nonetheless, these data also suggest the influence of the shale, for $\text{K/Rb} > 230$ where the rock contains 2.0–2.5 percent CaO (3.8–3.0 percent K_2O) and $\text{K/Rb} \leq 230$ in both the most mafic

and most felsic parts of the Snake Creek-Williams Canyon exposure. We note finally that a mineralogical study of the igneous biotites recovered from these rocks (Lee and Van Loenen, 1970) shows a number of regular chemical changes from the mafic to felsic parts of the exposure, indicating complete reworking of the detrital mica present in the assimilated Pioche Shale.

REFERENCES CITED

- Bowen, N. L., 1937, Recent high-temperature research on silicates and its significance in igneous geology: *Am. Jour. Sci.*, v. 33, no. 193, p. 1-21.
- de Laeter, J. R., Abercrombie, I. D., and Date, R., 1969, Mass spectrometric isotope dilution analyses of barium in standard rocks: *Earth and Planetary Sci. Letters*, v. 7, p. 64-66.
- Krauskopf, K. B., 1967, *Introduction to geochemistry*: New York, McGraw Hill Book Co., 721 p.
- Lee, D. E., and Bastron, Harry, 1967, Fractionation of rare-earth elements in allanite and monazite as related to geology of the Mt. Wheeler mine area, Nevada: *Geochim. et Cosmochim. Acta*, v. 31, no. 3, p. 339-356.
- Lee, D. E., Mays, R. E., Van Loenen, R. E., and Rose, H. J., Jr., 1969, Accessory sphene from hybrid rocks of the Mount Wheeler mine area, Nevada, in *Geological Survey research 1969*: U.S. Geol. Survey Prof. Paper 650-B, p. B41-B46.
- 1971, Accessory epidote from hybrid granitoid rocks of the Mount Wheeler mine area, Nevada, in *Geological Survey research 1971*: U.S. Geol. Survey Prof. Paper 750-C, p. C112-C116.
- Lee, D. E., and Van Loenen, R. E., 1970, Biotites from hybrid granitoid rocks of the southern Snake Range, Nevada, in *Geological Survey research 1970*: U.S. Geol. Survey Prof. Paper 700-D, p. D196-D206.
- 1971, Hybrid granitoid rocks of the southern Snake Range, Nevada: U.S. Geol. Survey Prof. Paper 668, 48 p.
- Lee, D. E., Van Loenen, R. E., and Mays, R. E., 1973, Accessory apatite from hybrid granitoid rocks of the southern Snake Range, Nevada: *U.S. Geol. Survey Jour. Research*, v. 1, no. 1, p. 89-98.
- Puchelt, H., 1972, Barium, in Wedepohl, K. H., ed., *Handbook of geochemistry*: Springer-Verlag, v. II/3, p. 56-D-1-56-E-9.
- Tuttle, O. F., and Bowen, N. L., 1958, Origin of granite in the light of experimental studies in the system $\text{NaAlSi}_3\text{O}_8$ - KAlSi_3O_8 - SiO_2 - H_2O : *Geol. Soc. America Mem.* 74, 153 p.

DISTRIBUTION AND OCCURRENCE OF RARE EARTHS IN THE THORIUM VEINS ON HALL MOUNTAIN, IDAHO

By MORTIMER H. STAATZ, VAN E. SHAW, and JAMES S. WAHLBERG, Denver, Colo.

Abstract.—Rare earths, although equal to or more abundant than thorium in many thorium veins, are much less abundant than thorium in the veins on Hall Mountain, Idaho. Total rare-earth content of these veins ranges from 0.00111 to 0.197 percent in 12 samples from 10 veins; the thoria (ThO_2) content, from 0.011 to 5.84 percent. The rare-earth oxide to thoria ratios range from 0.0019 to 3.22. Only two samples contained more rare earths than thorium, and these two samples came from veins related to a fault near the base of a thick sill; the others came from veins near the top of the same sill.

The relative amounts of the individual lanthanides are remarkably similar in the Hall Mountain veins, although cerium, gadolinium, or dysprosium are the most abundant in different samples. These veins differ in lanthanide distribution both from the Earth's crust and from the thorium veins of the Lemhi Pass district, Idaho and Montana, in that they contain chiefly yttrium-group rare earths. Most of the rare earths occur in thorite, whose atomic structure will accommodate wide-ranging proportions of the rare earths. Cenosite, one of the few minerals with a high content of the yttrium group of rare earths, was found in one vein.

Rare earths are present in all the known thorium veins in the United States. This association is due in part to the similarity of the ionic radius of thorium (Th^{4+}) to those of the rare earths (RE^{3+}). A study of the distribution and occurrence of the rare earths in the thorium veins of the Lemhi Pass district, Idaho and Montana (Staatz and others, 1972), showed that the rare earths there are almost as abundant as thorium. It was also found that the distribution patterns of the lanthanides differed from vein to vein and also from that derived from crustal abundance data. The Lemhi Pass veins consist principally of quartz or a quartz-microcline gangue cut by abundant iron-oxide veinlets that contain thorite, commonly monazite, and some brockite. They are similar in gross mineralogy to thorium veins in the Powderhorn and Wet Mountains districts, Colorado, the Capitan Mountains, N. Mex., the Mountain Pass area, California, and the Wausau district, Wisconsin. Mineralogically, all these veins differ considerably from the thorite veins at Hall Mountain in northernmost Idaho, which do not contain microcline and have only sparse amounts of iron oxides (Staatz, 1972, p. 246-247). Hall Mountain veins commonly are richer in thorite and allanite than those at Lemhi Pass, but have only minor monazite and no brockite. Because the

mineralogical differences between the Hall Mountain and Lemhi Pass areas are considerable, samples from the Hall Mountain thorium veins were analyzed for rare earths to see if the amounts of these elements and their proportions varied from those at Lemhi Pass.

The rare earths consist of 16 elements that have similar chemical properties. Fifteen of these elements, atomic numbers 57 through 71, make up the lanthanide group of elements—lanthanum (La), cerium (Ce), praseodymium (Pr), neodymium (Nd), promethium (Pm), samarium (Sm), europium (Eu), gadolinium (Gd), terbium (Tb), dysprosium (Dy), holmium (Ho), erbium (Er), thulium (Tm), ytterbium (Yb), and lutetium (Lu). One of these, promethium, is known chiefly as an artificially produced element and will not be mentioned again in this paper. In addition to the lanthanides, the element yttrium (Y), atomic number 39, which has chemical similarities to, and is found in many minerals along with, the lanthanides, is classed as a rare-earth element. The rare-earth group is divided into the "light" rare earths of cerium subgroup, which consists of the first seven lanthanides (La through Eu), and the "heavy" rare earths or yttrium subgroup, which consists of yttrium and the last eight lanthanides (Gd through Lu).

The rare earths are a closely related group of elements, generally with the same valence ($3+$) and with similar ionic radii. The lanthanides have a unique atomic arrangement in that with an increase in atomic number electrons are added to an inner ($4f$) level rather than to an outer level. Consequently, the elements have nearly identical chemical properties, and so they maintain a relatively coherent group and are found in many rocks and minerals in approximately the same proportions as in the crust of the Earth. Various rare-earth elements can be separated from the other rare earths by several geologic processes (Adams, 1969, p. C38; Fleischer and Altschuler, 1969, p. 725); this separation of rare earths is called fractionation. If the proportion of individual rare-earth elements is different from that of the Earth's crust, then fractionation probably has taken place.

GEOLOGIC SETTING

Thorium veins occur in an area of about one-half square mile on the west side of Hall Mountain, just south of the Canadian

border. This area is a steep mountainside with a moderately thick soil cover supporting abundant brush and trees. Fourteen thorium-bearing veins have been found in this area. The greater part of Hall Mountain is underlain by the lower part of the Prichard Formation of the Belt Supergroup, which consists principally of a light-gray fine-grained quartzite containing 20–30 percent biotite and muscovite. In the area containing the thorium veins, the quartzite is intruded by a thick sill of quartz diorite (one of the Purcell sills, which are widespread in northern Idaho and southeastern British Columbia) (fig. 1). The lower boundary of the sill in this area is formed by a large fault; the upper boundary is a normal contact, which is offset in several places by northeast-trending cross faults. The thorium veins are found in both the quartzite and the quartz diorite, and most occur adjacent to the upper contact of the sill. The veins range in known length from 6 to 700 feet (2 to 213 m) and in thickness from a thin seam to 13 feet (4 m). They strike from N. 42° W. to N. 30° E. and dip steeply. Most veins are sheared and brecciated. Thirty minerals have been identified in these veins, but most are found only in minor quantities and only in a few veins. The mineralogy of these veins is erratic, both among the several veins and within individual veins. The principal gangue minerals are quartz and calcite; the principal thorium mineral is thorite. In addition, chlorite, magnetite, lepidocrocite, pyrite, and biotite commonly are present. Other less common minerals noted, in the general order of decreasing abundance, are: goethite, sphene, zircon, apatite, plagioclase, allanite, chalcophyllite, rutile, actinolite, pyrrhotite, muscovite, hematite, epidote, ilmenite, malachite, chrysocolla, monazite, cenosite, jarosite, dolomite, fluorite, and an unknown brown thorium mineral. A more detailed description of the mineralogy of these veins has been published previously (Staatz, 1972).

ANALYTICAL PROCEDURE

Twelve samples from 10 different veins (fig. 1) were chosen for the present study. Three of the samples (31-70, 33-70, 34-70; table 1) are chip samples from the Wawa No. 2, the longest vein in the area. One sample (4-70, table 1) is a grab sample of the most radioactive part of the Golden Sceptre vein. The rest are chip samples from other veins, ranging in length from 0.3 to 11.0 ft (0.09 to 3.4 m); these samples were cut at right angles to the veins.

A chemical separate that contained all the rare earths and thorium was first made by Shaw; then the amounts of thorium and individual rare earths were determined by X-ray fluorescence by Wahlberg using the following method. The results, computed as percentages of the original total sample weight, are given in table 1.

The method of separating the rare earths and thorium from the sample was the same as that used on ore samples from the Lemhi Pass district, described by Staatz, Shaw, and Wahlberg (1972, p. 75). The X-ray fluorescence procedure differed from

that used on samples from Lemhi Pass and is as follows. First, a 20 scan was made of each rare-earth element and of thorium in the chemical separate. Elements other than the rare earths and thorium occur in minor amounts in the separate, and the amounts of these minor elements differ between samples. To minimize this matrix effect, a dilution was made in a second sample by taking 1–30 mg of the separate and fusing it with 1 g of lithium tetraborate. This diluted fusion was ground and made into a 1-1/8-inch (2.86-cm) disk. Standards are prepared by fusing known amounts of rare earths and thorium with lithium tetraborate and preparing similar disks. All disks are scanned by X-ray fluorescence. The amounts of rare-earth elements in the separates that formed peaks on the scan of the diluted disks are determined by comparison with that of the standards. Some of the rare-earth elements that formed peaks on the original scan do not form peaks on the scan of the diluted disks. The quantities of these rare earths are determined by comparing their peak heights on the original scan with those of the rare earths whose amounts have been determined. Spectral interference was determined by adding known amounts of an interfering element to known amounts of the element to be determined. A correlation was made with the peak height after the quantity of interfering element was determined. No correction was made for enhancement effects, but such a correction would be small at the large dilutions used.

RESULTS OF ANALYSIS

The total content of rare-earth oxides in the 12 samples ranges from 0.00111 to 0.197 percent (table 1) and averages 0.0426 percent. Although this low average figure does not represent the grade of any particular vein, it does give a reasonable median figure of the percentages of the rare earths one might expect in other samples of veins in the Hall Mountain area. The content of thorium in the samples ranges from 0.011 to 5.84 percent and averages 1.55 percent, making the average thorium content about 30 times greater than that of the total rare-earth oxides.

The sample (31-70) with the least amount of rare-earth oxides also contains the least amount of thorium; the sample (22-70) with the most rare-earth oxides contains the second largest amount of thorium. The only vein sampled more than once (the Wawa No. 2, fig. 1) is represented by three samples that range in rare-earth oxides content from 0.00111 to 0.11 percent and in thorium content from 0.019 to 5.84 percent; the sample lowest in rare-earth oxides and thorium (31-70) is from a quartz-poor and calcite-rich part of the vein. Although the amount of thorite, the principal thorium- and rare-earth-bearing mineral in this vein, varies considerably, those parts of the vein that were both low in quartz and high in calcite were uniformly low in thorite. A part of the Wawa No. 2 vein consists mainly of sheared quartz; a meter or so farther along the vein the visible minerals consist of quartz, chlorite, lepidocrocite, and abundant thorite; a short distance from here

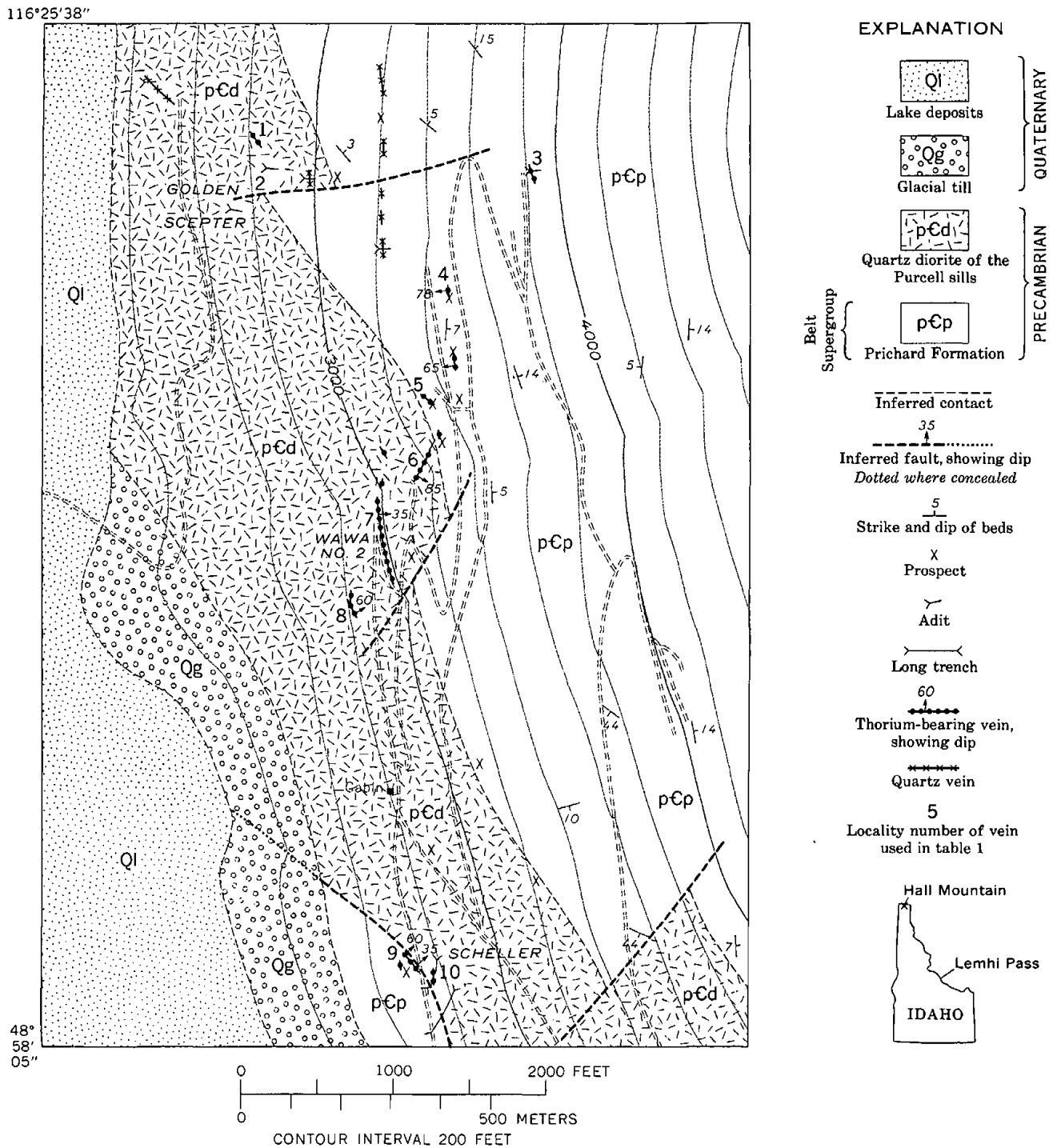


Figure 1.—Geologic map of the area containing the thorium-bearing veins on Hall Mountain.

the composition of the vein may change to calcite, actinolite, apatite, and a little thorite. The long quartz vein exposed underground in the Golden Sceptre also has a spotty distribution of thorium, and probably also of rare earths. Testing of this vein where exposed in the tunnels indicates that most of

the vein is not radioactive and that the radioactivity is confined to several small shoots. The erratic variance in mineralogy in these veins, which may change both along and across veins, is paralleled by the variance in chemical composition.

Table 1.—Rare-earths and thorium analyses, in percent, of samples from Hall Mountain, Idaho

Locality (fig. 1)	Sample	La ₂ O ₃	Ce ₂ O ₃	Pr ₂ O ₃	Nd ₂ O ₃	Sm ₂ O ₃	Eu ₂ O ₃	Gd ₂ O ₃	Tb ₂ O ₃	Dy ₂ O ₃
1	4-70 Golden Sceptre . .	0.00074	0.0027	<0.00013	0.0011	0.00080	<0.00034	0.0016	<0.00034	0.0011
2	7-70 . . . do00052	.0024	<0.00026	.00079	.00079	<.0013	.0034	<.0013	.0021
3	22-70 T.M.U. No. 10085	.028	.00037	.0037	.0018	<.0031	.014	<.0031	.012
4	28-7000032	.0019	<.000096	.00080	.00048	<.00080	.0016	<.00080	.0016
5	21-7000036	.0012	.000049	.00052	.00029	<.000041	.0011	<.000041	.00092
6	25-70 Wawa No. 100042	.0014	<.000084	.00070	.00014	<.00070	.0018	<.00070	.0015
7	31-70 Wawa No. 2	<.000015	.00021	<.00030	.00030	.00030	<.00015	<.00018	<.00015	<.00030
	33-70 . . . do0016	.0080	<.00056	.0048	.0032	<.0040	.010	<.0040	.0056
	34-70 . . . do00013	.00042	<.00021	<.00084	.00084	<.0021	.0017	<.0021	.00084
8	43-7000010	.00053	.000023	.00023	.00015	<.00013	.0013	<.00013	.0016
9	17-70 Scheller00033	.0021	<.0033	<.0033	<.0033	<.0044	<.0044	<.0044	<.011
10	16-70 . . . do00012	.0040	<.00061	<.00098	<.00098	<.0012	<.0012	<.0012	<.0031

Locality (fig. 1)	Sample	Ho ₂ O ₃	Er ₂ O ₃	Tm ₂ O ₃	Yb ₂ O ₃	Lu ₂ O ₃	Total lantha- nides	Y ₂ O ₃	Total ¹ RE ₂ O ₃	ThO ₂	¹ RE ₂ O ₃ / ThO ₂
1	4-70 Golden Sceptre . .	<0.00027	0.0011	<0.00034	0.00067	<0.00034	0.00981	0.0087	0.0185	0.47	0.039
2	7-70 . . . do	<.0010	.0021	<.0013	.0018	<.0013	.0139	.0020	.0159	1.94	.0062
3	22-70 T.M.U. No. 10018	.0079	.0031	.0061	<.0031	.0873	.11	.197	4.76	.041
4	28-70	<.00016	.0011	<.00048	.0011	<.00080	.00890	.012	.0209	1.22	.017
5	21-7000016	.00032	.000081	.00024	<.00041	.00524	.0051	.0103	.061	.17
6	25-70 Wawa No. 1	<.00014	.00098	<.00042	.00084	<.00071	.00778	.011	.0188	1.12	.017
7	31-70 Wawa No. 2	<.00030	<.00030	<.00090	<.00030	<.00015	.000810	.00030	.00111	.019	.058
	33-70 . . . do	<.00080	.0048	<.0024	.0080	.0040	.0460	.064	.110	5.84	.0019
	34-70 . . . do	<.00042	.00084	<.0013	.0013	<.0021	.00523	.021	.0262	3.07	.0085
8	43-70000052	.00075	.000075	.00050	<.00013	.00531	.016	.0213	.12	.18
9	17-70 Scheller	<.0055	<.0055	<.0055	<.0055	<.00055	.00243	.033	.0354	.011	3.22
10	16-70 . . . do	<.0012	<.0012	<.0012	<.0012	<.00031	.00412	.032	.0361	.026	1.39

¹ RE₂O₃ stands for rare-earth oxides.

DISTRIBUTION OF RARE EARTHS COMPARED TO DISTRIBUTION OF THORIUM

As previously noted, thorium and rare earths commonly occur together in the same minerals, although the proportions of each vary greatly in different minerals. For example, bastnaesite has a very high rare-earth content compared to its thorium content; thorite, on the other hand, has a high thorium content compared to its rare-earth content. The thorium and rare-earth minerals found in the Hall Mountain area are thorite, allanite, monazite, cenosite, and an unknown brown thorium mineral. Thorite is by far the most common, making up over 90 percent of the thorium-bearing and rare-earth-bearing minerals. Allanite, which in this area contains over 30 times as much rare earths as thorium, is common only in certain parts of some veins. The other three minerals are extremely rare and were noted in small amounts in only one sample each. In only two samples (16-70 and 17-70) is the rare-earth oxide content higher than the thorium content. These two samples came from veins on the Scheller property that lie adjacent to a fault bounding the west side of the quartz diorite sill (fig. 1). All the other samples came from veins occupying small fractures near the east side of the sill.

In general, then, veins are very low in rare-earth content as compared to their thorium content. The ratio of the total rare-earth oxides to thorium (RE₂O₃/ThO₂) for all samples ranges from 0.0019 to 3.22 (table 1). The wide range in RE₂O₃/ThO₂ indicates that there is little relation between the

amount of RE₂O₃ and of ThO₂ in the Hall Mountain veins, which may be due to several, perhaps interdependent, causes. The striking difference in the RE₂O₃/ThO₂ ratios between the two samples from the Scheller property and the other samples may be due to fractionation of vein fluids at depth, fluids from each group following a separate fracture or fractures to their present site. The lack of correlation in other veins may in part also be due to fractionation at depth, or it may be due to differences in chemical and physical conditions at vein sites. These differences would be reflected in varying proportions of the rare-earth and thorium minerals (for example, thorite and allanite).

DISTRIBUTION OF INDIVIDUAL RARE EARTHS

The differences between the relative amounts of the lanthanides are most easily seen on a plot of their distribution (Semenov and Barinskii, 1958, p. 416). Graphs showing the lanthanide distribution were made from the analytical data (table 1) of samples in which most of the lanthanides are present in measurable amounts. In three of the samples the total amount of rare earths was so small that many of the elements were below the limit of detection. Figure 2A shows a graph of the crustal distribution of the lanthanides prepared from data by Taylor (1964, p. 1280–1281). Figures 2B–D show typical distribution patterns of the lanthanides in the Hall Mountain veins. The major difference between the

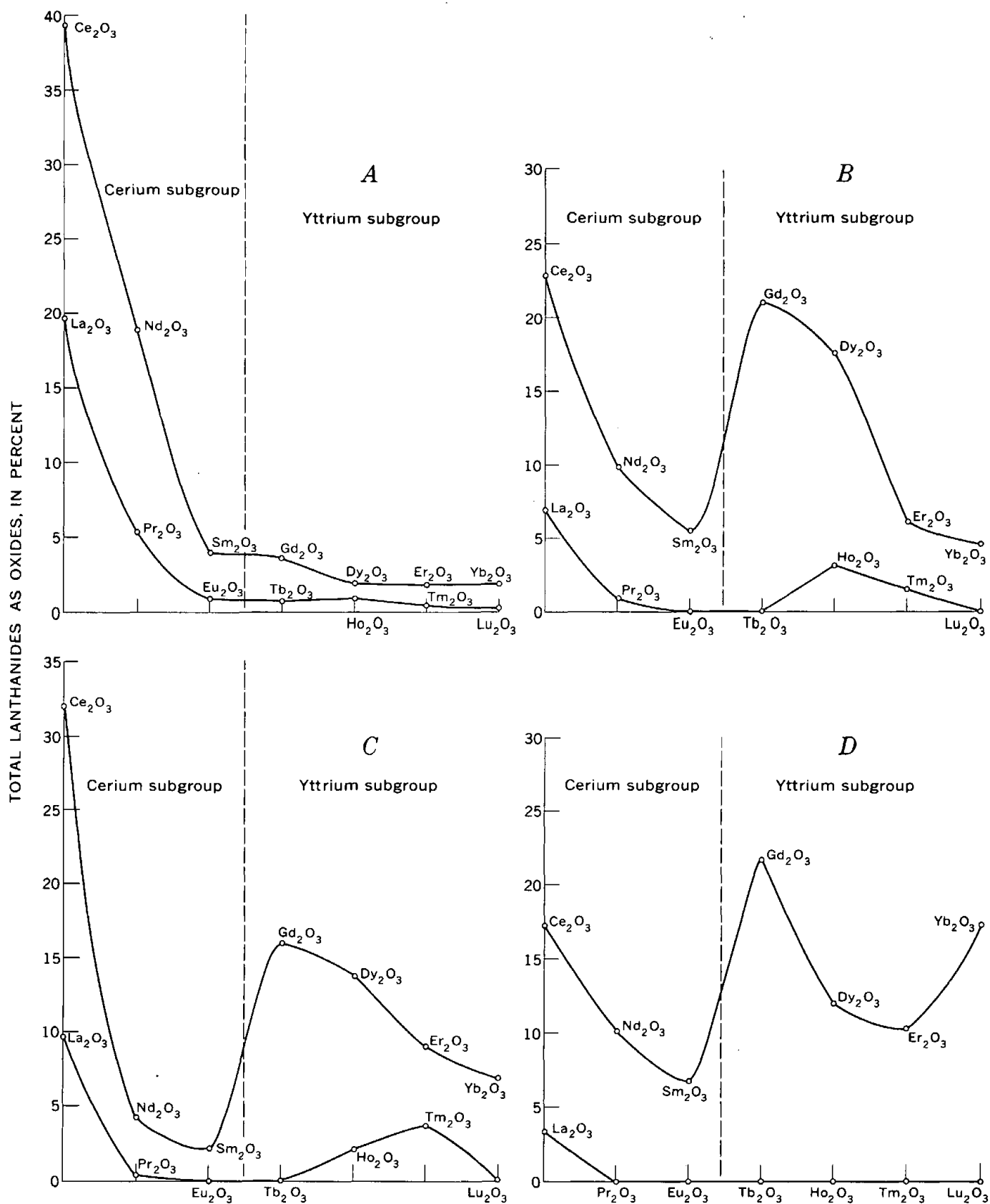


Figure 2.—Distribution of lanthanides. A, Crustal abundance. B, C, and D represent samples from Hall Mountain: B, sample 21-70; C, sample 22-70; and D, sample 33-70. Upper line, even-atomic-numbered lanthanides; lower line, odd-atomic-numbered lanthanides.

lanthanide distribution in the Earth's crust and that in the Hall Mountain district is the preponderance of the yttrium group of lanthanides in the Hall Mountain district. Generally this group makes up but a small percentage of the total rare earths (fig. 24). Yet at Hall Mountain, the yttrium group in 11 of 12 samples accounts for 71–98 percent of the total rare earths found in the veins. In one sample (31-70) the yttrium group apparently makes up only 27 percent, but this sample contained only a very small amount of rare earths and the amount separated for X-ray fluorescence was only 5 mg, near the limit of detection.

In studies of the proportions of the lanthanides to one another, the amount of each lanthanide as a percentage of the total lanthanide content is calculated. If this percentage is plotted against the atomic number of the lanthanide element, a zigzag line is obtained, because the even-atomic-numbered elements generally are more abundant than the odd-atomic-numbered elements. Because the zigzag line tends to mask the similarities and differences among the various lanthanides, Semenov and Barinskii (1958) suggested a plot in which the odd- and even atomic-numbered elements were graphed separately on the same diagram. This plot makes the similarities and differences in the lanthanide distribution much easier to detect, and it is the plot used in this paper.

The dominant lanthanide is cerium in some samples, gadolinium in some, and dysprosium in one. All samples, however, have a high gadolinium content. All graphs of the even-atomic-numbered lanthanides are somewhat similar. They show a high cerium content followed by decreasing contents of neodymium and samarium, then an abrupt increase to gadolinium to form a high, although in sample 43-70 the high is formed by the next element, dysprosium (table 1). The percentages of the rest of the even-atomic-numbered lanthanides decrease, generally, with increasing atomic weight, but in samples 33-70 (fig. 2D) and 34-70 (table 1) a sharp increase occurs with ytterbium. The relative amounts of the lanthanides of odd atomic number, shown on the lower curves of the graph, commonly reflect those of their even-atomic-numbered neighbors. This parallelism is not well shown in the diagrams of the Hall Mountain samples because the total amount of rare earths was so small that the amounts of some of the odd-atomic-numbered lanthanides were below the sensitivity of the method. The sensitivity decreases as the amount of total rare earths in the sample decreases.

The plots of the lanthanide distribution in the veins at Hall Mountain do not resemble those of most of the samples from the Lemhi Pass district (Staatz and others, 1972, p. 79–80). In the Lemhi Pass area most of the samples have a Nd_2O_3 maximum; some also have a Ce_2O_3 high. In addition, many samples have a secondary Eu_2O_3 high. Most of the samples are rich in the cerium subgroup of rare earths. Only 5 out of 31 samples from Lemhi Pass have maximums of Gd_2O_3 or Dy_2O_3 . Therefore, the fluids that formed the veins in the two

areas probably contained widely different proportions of the different rare-earth elements.

The mineralogy of the rare-earth minerals is partly, but not entirely, dependent on the relative amounts of the several lanthanides available in the vein fluids. For example, bastnaesite forms from fluids rich in the "light" lanthanides, and the quantity of each of these elements incorporated into the bastnaesite structure is similar to that of the Earth's crust (Adams, 1969, p. C40). In bastnaesite, lanthanum, cerium, praseodymium, and neodymium make up over 90 percent of the total lanthanides. Xenotime, on the other hand, forms from fluids rich in the "heavy" lanthanides, although the element incorporated in the largest amount may be any one of several of the heavy even-atomic-numbered lanthanides. The structure of some minerals, however, is such that they will accept whatever lanthanides are available. In most environments the relative abundance of the lanthanides will be the same as that in the Earth's crust (fig. 24), but in some, fractionation will have changed the relative proportions of the lanthanides in the vein fluids. For example, in a compilation by Michael Fleischer (written commun., 1969) of nearly 400 monazite analyses, all but two had cerium maximums; the two exceptions had neodymium as the dominant lanthanide. Thorite, which is by far the most important thorium and rare-earth mineral in the Hall Mountain veins, has not been well studied and we were able to locate only nine analyses in the literature. Five of these analyses (Semenov and Barinskii, 1958, p. 406; Heinrich, 1963, p. 207; Kalita, 1969, p. 92; Yes'kova and Ganzeyev, 1964, p. 1271; Mineev, 1968, p. 122) show cerium highs; two (Khvostova, 1969, p. 332; Turovskiy and others, 1968, p. 1180) show neodymium highs, and two others (Pavlenko and others, 1959, p. 369; Mineev, 1968, p. 123) show dysprosium highs. None of these thorites came from veins. Because thorite is by far the most common rare-earth-bearing mineral in the Hall Mountain veins, the lanthanide distribution patterns (figs. 2B–D) are virtually those of this mineral. Some are high in cerium, some in gadolinium, and one in dysprosium, and all, except for sample 31-70, have a preponderance of yttrium-group rare earths. The variation in the proportions of the rare earths in different thorites indicates that the thorite structure is not markedly selective in its acceptance of rare-earth ions and so the proportions of the several rare earths in a thorite probably reflect the rare-earth content of the vein-forming fluids.

A mineral that reflects the high content of yttrium-group rare earths in the vein fluids is cenosite, a hydrous calcium yttrium carbonate silicate. This mineral, which has been described in only nine other localities, was found at one spot in the Wawa No. 2 vein (loc. 7, fig. 1). Its occurrence at the Wawa No. 2 has been described by Adams, Staatz, and Havens (1964). Although this mineral is rare, it is one of the few minerals that is made up principally of the yttrium group of rare earths and hence is a mineralogic marker for veins or rocks rich in this rare-earth group.

REFERENCES CITED

- Adams, J. W., 1969, Distribution of lanthanides in minerals, in Geological Survey research 1969: U.S. Geol. Survey Prof. Paper 650-C, p. C38-C44.
- Adams, J. W., Staatz, M. H., and Havens, R. G., 1964, Cenosite from Porthill, Idaho: *Am. Mineralogist*, v. 49, no. 11-12, p. 1736-1741.
- Fleischer, Michael, and Altschuler, Z. S., 1969, The relationship of the rare-earth composition of minerals to geologic environment: *Geochim. et Cosmochim. Acta*, v. 33, no. 6, p. 725-732.
- Heinrich, E. W., 1963, Xenotime and thorite from Nigeria: *Am. Mineralogist*, v. 48, no. 1-2, p. 206-208.
- Kalita, A. P., 1969, Features of the distribution of lanthanides and yttrium in rare earth granitic pegmatites of the eastern part of the Baltic Shield, in Features of the distribution of rare earths in pegmatites: Moscow, Isdat, Nauka, p. 79-100.
- Khvostova, V. A., 1969, [Rarer-element distribution in metamorphic conglomerates of the Urals]: *Geokhimiya*, no. 3, p. 328-334; (in Russian); translated in *Geochemistry Internat.*, v. 6, p. 288-294, 1969.
- Mincev, D. A., 1968, [Geochemistry of apogranites and rare metal metasomites of northwestern Tarbagatai]: *Akad. Nauk SSSR Inst. Mineral. Geokhim. Kristallogchim. Redk. Elementov*, p. 1-183 (in Russian).
- Pavlenko, A. S., Vainshtein, E. E., and Turanskaya, N. V., 1959, Certain regularities in the behavior of rare earths [and] yttrium in magmatic and postmagmatic processes: *Geochemistry*, no. 4, p. 357-380.
- Semenov, E. I., and Barinskii, R. L., 1958, The composition characteristics of the rare earths in minerals: *Geochemistry*, no. 4, p. 398-419.
- Staatz, M. H., 1972, Thorium-rich veins of Hall Mountain in northernmost Idaho: *Econ. Geology*, v. 67, no. 2, p. 240-248.
- Staatz, M. H., Shaw, V. E., and Wahlberg, J. S., 1972, Occurrence and distribution of rare earths in the Lemhi Pass thorium veins, Idaho and Montana: *Econ. Geology*, v. 67, no. 1, p. 72-82.
- Taylor, S. R., 1964, Abundance of chemical elements in the continental crust—a new table: *Geochim. et Cosmochim. Acta*, v. 28, no. 8, p. 1273-1285.
- Turovskiy, S. D., Usmanov, U. U., and Nikolayeva, A. V., 1968, [Distribution of rare earths in a series of progressively crystallizing minerals]: *Akad. Nauk SSSR Doklady*, v. 178, no. 5, p. 1179-1181 (in Russian); translated in *Acad. Sci. USSR Doklady, Earth Sci. Sec.*, v. 178, no. 1-6, p. 218-219, 1968.
- Yes'kova, Ye. M., and Ganzeyev, A. A., 1964, [Rare earth elements in accessory minerals of the Vishnev Mountains]: *Geokhimiya*, no. 12, p. 1267-1279 (in Russian); translated in *Geochemistry Internat.*, v. 1, p. 1152-1163, 1964.

ORIGIN OF SPONGY CHERTS

By BETH M. MADSEN, Denver, Colo.

Abstract.—The spongy-textured surface in some cherts, visible on electron micrographs, is inherited from authigenic cristobalite. Spongy bedded cherts were originally bedded porcelanites similar to the porcelanite in the Miocene Monterey Formation of California.

Electron-microscope studies of the surface textures of chert have shown that there are two distinct varieties. Folk and Weaver (1952) initially recognized these two textures and named them novaculite type and spongy. In subsequent studies, Monroe (1964) and Oldershaw (1968) also recognized the two textures and called them granular and spongy. The granular or novaculite type of chert consists of equigranular subhedral grains that are free of inclusions. Spongy chert consists of irregular grains with surfaces that resemble swiss cheese or a sponge due to the numerous bubblelike holes that pepper the grain surfaces. Folk and Weaver (1952), on the basis of index of refraction, specific gravity, and chemical analyses, interpreted these bubblelike holes as tiny fluid inclusions of water. Typical spongy chert and granular chert are shown in figures 1 and 2, respectively.

Folk and Weaver (1952) concluded that the development of chert textures was controlled by the spacing and abundance of the initial centers of crystallization. They reasoned that many evenly spaced centers would generate a granular texture and fewer unevenly spaced centers would form the spongy texture. Oldershaw (1968), from his study of the Namurian bedded chert of North Wales, suggested that the amount of impurities and the concentration of silica in solution controls the texture. He found an increase in argillaceous and organic content in spongy cherts over granular cherts. A correlation between refractive index and the surface texture of cherts was found by Folk and Weaver (1952). Cherts composed of microcrystalline quartz and chalcedonic quartz with a normal quartz index of refraction (ordinary ray) were of the granular type. Cherts made up of chalcedonic quartz with an index of refraction below normal quartz were of the spongy-textured type.

The Miocene Monterey Formation of California was characterized by Bramlette (1946) as very siliceous. A major

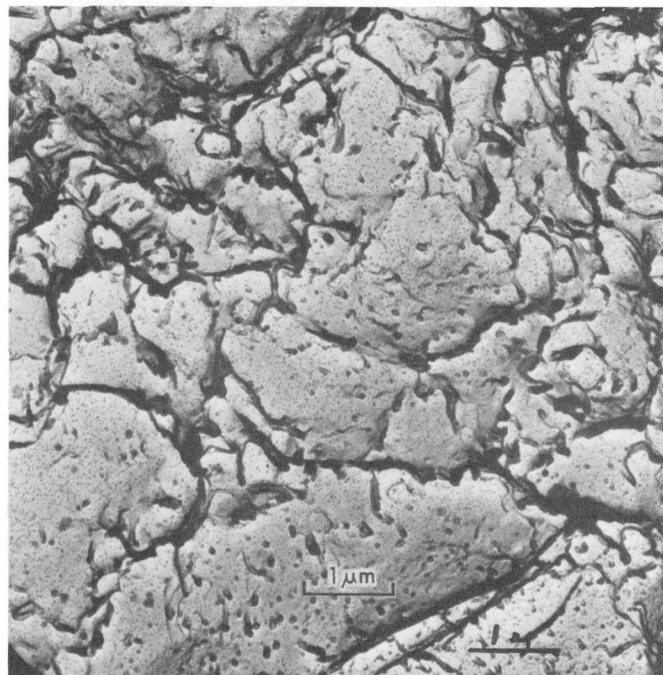


Figure 1.—Electron micrograph of a spongy-surface chert. The chert is from Ordovician rocks in East Northumberland Canyon, Nye County, Nev., and is interbedded with bedded barite rock.

rock type in the Monterey Formation is porcelanite which consists mainly of very fine grained cristobalite. Experiments by Ernst and Calvert (1969) on porcelanite from the Monterey Formation showed that the conversion of cristobalite to quartz is a zero-order reaction and that at a temperature of 20°C in relatively pure water the transformation would take about 180 m.y. If the temperature is raised to 50°C, the conversion period would be 4–5 m.y.

Electron micrographs of cristobalite from the porcelanite of the Monterey Formation show irregular grains with a spongy texture (fig. 3). A comparison of figure 1 with figure 3 shows the similarity of the spongy-textured chert to the spongy-textured cristobalite.

Conversion by a solid-solid transformation with time of cristobalite to quartz could result in cherts with spongy textures. Preservation of even the tiny bubblelike holes suggests

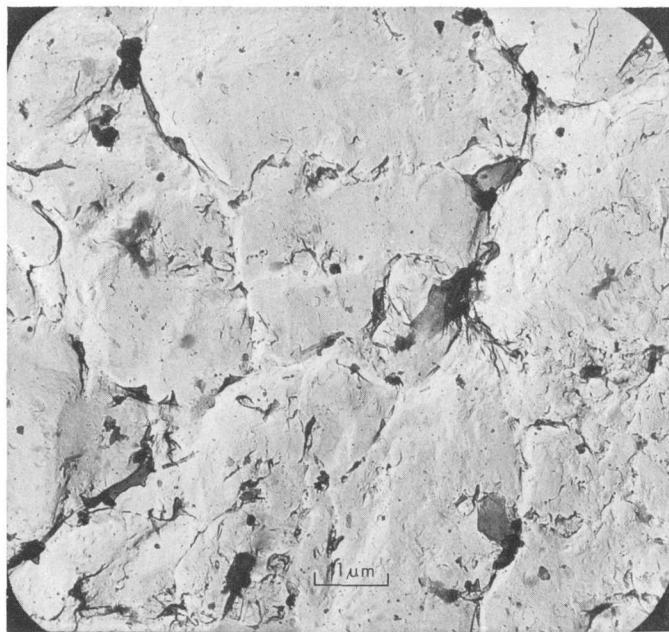


Figure 2.—Electron micrograph of a chert nodule with granular surface. The chert nodule is from the Getaway Limestone Member of the Cherry Canyon Formation, southwest Texas.

that solution and redeposition of silica did not occur. The density difference between quartz and cristobalite could be the cause of some of the shrinkage cracks and intricate crumbling commonly observed in marine-bedded cherts. The granular texture probably is the result of solution of silica and redeposition as quartz, as suggested by Bramlette (1946), Folk and Weaver (1952), and Oldershaw (1968). Mixtures of the textures could result if both processes occurred.

Pimm, Garrison, and Boyce (1971) described chert from the western equatorial Pacific as cryptocrystalline quartz. Their electron micrographs are similar to electron micrographs of spongy chert and porcelainite; their description of the fabric as a “mosaic of highly irregular grains that are peppered with numerous tiny fluid inclusions” indicates that the fabric of chert from the western equatorial Pacific is similar to the fabric of spongy chert and porcelainite. Heath and Moberly (1971) noted the similarity of the siliceous material collected in the western equatorial Pacific to porcelainite of the Monterey Formation.

Weaver and Wise (1972) concluded that deep-sea cristobalite is an authigenic mineral. They found the cristobalite to consist of fine blades, 300–500 Å thick, with a well-developed crystalline form. They found it growing in spherules, 3–10 μm in diameter. Because of the bladed crystals and the free growth of the spherules, they concluded that the cristobalite is authigenic. Similar authigenic spherulites of cristobalite from Tertiary coastal plain sediments of eastern and southeastern United States were described and named “lepispheres” by

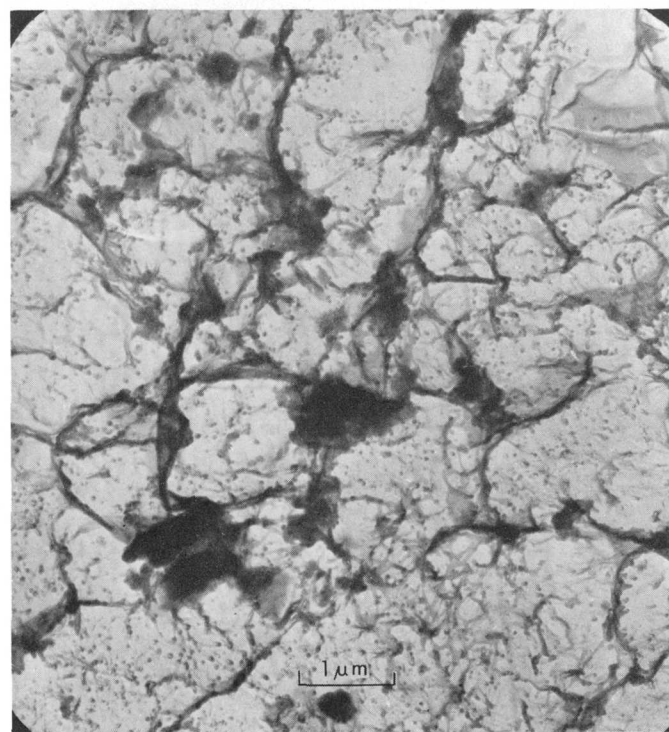
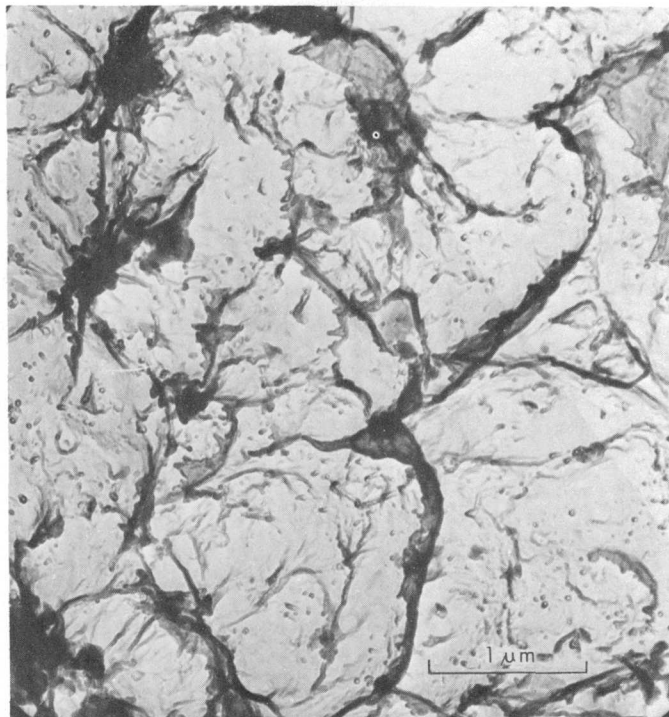


Figure 3.—Electron micrographs of porcelainite showing the typical spongy surface texture. The porcelainite is from the Miocene Monterey Formation, Indian Creek section of San Luis Obispo County, Calif.

Weaver and Wise (1973). Deposition of the cristobalite during authigenesis could explain the scarcity of siliceous fossils in

porcelanite, if solution of the fossils provided some of the silica for the authigenic cristobalite. Lepispheres have not been recognized from the Monterey Formation, probably because the weight of the overlying sediments deformed the delicate spherulites.

In summary, I suggest that spongy-textured cherts, were initially deposited as a cristobalitic porcelanite. The conversion of cristobalite to quartz is a solid-solid transformation that preserved the tiny bubblelike holes of the cristobalite, giving the chert a spongy appearance.

REFERENCES CITED

- Bramlette, M. N., 1946, The Monterey formation of California and the origin of its siliceous rocks: U.S. Geol. Survey Prof. Paper 212, 57 p.
- Ernst, W. G., and Calvert, S. E., 1969, An experimental study of the recrystallization of porcelanite and its bearing on the origin of some bedded cherts: *Am. Jour. Sci.*, v. 267-A (Schairer Volume), p. 114-133.
- Folk, R. L., and Weaver, C. E., 1952, A study of the texture and composition of chert: *Am. Jour. Sci.*, v. 250, no. 7, p. 498-510.
- Heath, G. R., and Moberly, Ralph, Jr., 1971, Cherts from the western Pacific, Leg 7, Deep Sea Drilling Project, in Winterer, E. L., and others, eds., *Initial Reports of the Deep Sea Drilling Project*: Washington, U.S. Govt. Printing Office, v. 7, pt. 2, p. 991-1007.
- Monroe, E. A., 1964, Electron optical observations of fine-grained silica minerals: *Am. Mineralogist*, v. 49, nos. 3-4, p. 339-347.
- Oldershaw, A. E., 1968, Electron-microscopic examination of Namurian bedded cherts, North Wales (Great Britain): *Sedimentology*, v. 10, p. 255-272.
- Pimm, A. C., Garrison, R. E., and Boyce, R. E., 1971, Cherts and radiolarian mudstones, in Fischer, A. G., and others, eds., *Initial Reports of the Deep Sea Drilling Project*: Washington, U.S. Govt. Printing Office, v. 6, p. 1212-1218.
- Weaver, F. M., and Wise, S. W., 1972, Ultramorphology of deep sea cristobalitic chert: *Nature-Phys. Sci.* v. 237, no. 73, p. 56-57.
- , 1973, Chemically precipitated sedimentary cristobalite in Tertiary Atlantic and Gulf coastal plain sediments: *Geol. Soc. America Abs. with Programs*, v. 5, no. 5, p. 449.

ANALYSES AND ECONOMIC POTENTIAL OF MONAZITE IN LIBERIA

By SAM ROSENBLUM, Denver, Colo.

Abstract.—Eleven monazite samples from Liberia, including seven from beach sands, were analyzed by the X-ray fluorescence method. The monazite samples, containing only one-half percent impurities, were obtained by use of a hot Clerici-solution procedure for purification which was devised by the author. The percentage of the rare-earth elements in Liberian monazite concentrates does not differ greatly from that of monazite sands elsewhere in the world. The average of the 11 samples shows less praseodymium and neodymium than Russian and American monazites, but more cerium. Liberian coastal sands apparently contain sufficient reserves of monazite (and other heavy minerals of commerce) to encourage mining. A feasibility study of production and marketing of monazite from Liberian beach sands is recommended.

In a study of more than 2,500 heavy-mineral concentrates, mainly from streams in western and central Liberia, Srivastava and Rosenblum (unpub. data, 1974) indicated that monazite constituted as much as 50 percent of some concentrates in northwestern Liberia, but more commonly the monazite content was 1-5 percent.

Monazite was found by Rosenblum and Srivastava (unpub. data, 1974) to range from a trace to 10.4 percent of the heavy minerals in 60 surficial sands from modern and raised beaches between Robertsport and Harper. Heavy minerals ordinarily range from 0.4 to 12 percent of the beach sand and average about 6.3 percent. Selected samples of beach sand contain as much as 87 percent heavy minerals. Many aeroradioactivity anomalies are correlative with concentrations of monazite and zircon along the beaches (Behrendt and Woterson, 1971); however, no attempt was made in that investigation to estimate the reserves of heavy minerals in the beaches nor to evaluate the monazite therein. Monazite is widely distributed throughout Liberia, but the chances of locating significant monazite deposits are greater on the beaches than inland.

This paper presents the results of X-ray fluorescence analyses of 11 monazite samples from Liberia, West Africa, and discusses the possibility of recovery of monazite from coastal sands. Four monazite concentrates were analyzed in 1968 by semiquantitative spectrographic procedures as part of

a heavy-mineral reconnaissance in Liberia (Rosenblum, 1969). Monazite was concentrated from seven additional samples of surficial beach sands collected between Robertsport and Greenville (fig. 1) during a special study of heavy minerals in the coastal area. These seven concentrates and splits of the four samples analyzed in 1968 were analyzed by a recently developed X-ray fluorescence method that is considered more reliable for determinations of the rare-earth elements than semiquantitative spectrographic analysis. These 11 X-ray fluorescence analyses were sought for comparison with the

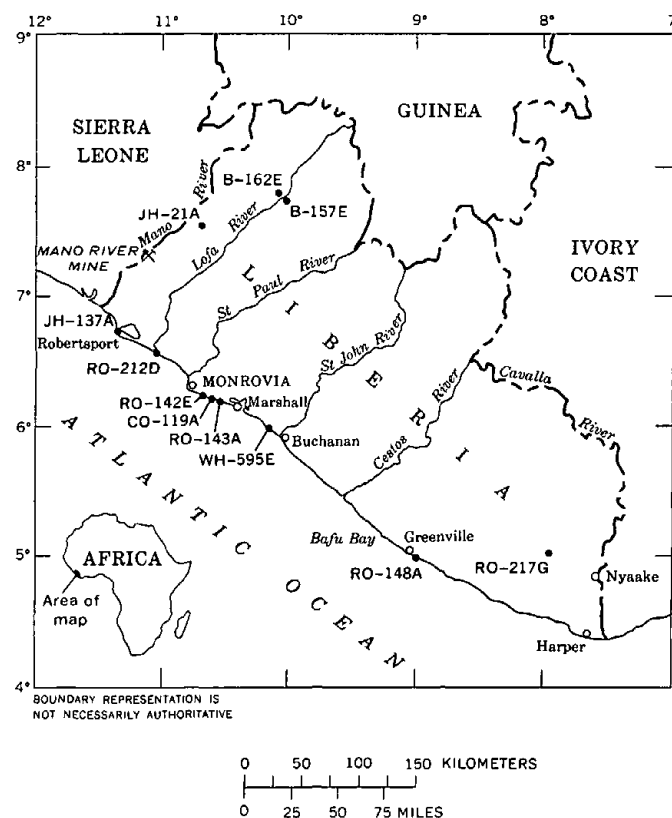


Figure 1.—Map of Liberia showing location of monazite sample sites (solid dots).

semiquantitative spectrographic analyses of 1968, in which lutetium was reported (Rosenblum, 1969) to range from 1,000 to 3,000 ppm or 0.10 to 0.30 percent. Also sought were the major elements, which had been reported as 100,000 ppm (10 percent), or greater than 10 percent. The results of neutron-activation analysis of five monazites for europium and lutetium are also presented.

Considering the value of monazite concentrates and the simple technology required for recovery of monazite, a search of pertinent literature was made to gather information intended to stimulate interest in the mining of monazite from Liberian beach sands. All previous investigations in Liberia involving monazite are cited, and relevant economic data through September 1973 are presented.

This work was done as part of a cooperative project of the U.S. Geological Survey and the Liberian Geological Survey and was sponsored by the Government of Liberia and the Agency for International Development, U.S. Department of State.

PREVIOUS INVESTIGATIONS

Previous studies of monazite in Liberia were mainly in connection with investigations of heavy minerals in stream and beach sands. The Columbia-Southern Chemical Corp. (USA) (unpub. data, 1957) indicated that monazite averaged 1.3 percent of the heavy minerals recovered from 109 drill holes in beach sand between Monrovia and Buchanan. The heavy-mineral content of the sands averaged 6.4 percent and locally was as much as 32 percent.

Between 1962 and 1966, the Diamond Mining Corp. of Liberia reported many occurrences of monazite in stream concentrates, mainly in western Liberia, in many unpublished periodic reports submitted to the Government of Liberia.

Van Griethuysen (1970), geologist for Wm. H. Muller and Co. (Netherlands), published a conservative estimate of 100,000 metric tons (equal to 2 percent) of heavy minerals in beach sands extending from Greenville 30 km west to Bafu Bay. He indicated that the heavy minerals are normally dispersed in beach sands but also occur here and there in lenses as much as 1 m thick, 15 m wide, and 100 m or more long, dipping about 5° toward the ocean; these lenses contain as much as 75 percent of heavy minerals in places, including 0–5 percent monazite.

In 1971, Wm. H. Muller and Co. (written commun.) indicated reserves of 300,000 metric tons of heavy minerals in beach sands 20–33 km west of Greenville; this figure includes 0–5 percent monazite, among other economic minerals.

United Nations geologist Valto Veltheim reported (oral commun., 1972) that exploration of beach sands in the Marshall area indicated 100,000–150,000 metric tons of heavy minerals, including 2.8 percent monazite. Continued exploration westward to Monrovia and Robertsport will probably increase these reserves by several times the above amount.

SAMPLE PREPARATION

The monazites analyzed were purified from selected heavy-mineral concentrates, most of which were prepared by panning samples of sand from beaches and streams. One sample (RO-148A) was a grab sample from black sand on the surface of a beach; another (RO-217G) was a grab sample from a black-sand deposit in a stream (fig. 1). All the monazite samples are genetically heterogeneous, the stream samples presumably less so than the beach samples. The purified monazite fractions, however, are considered representative of the respective deposits.

The grains from each concentrate that passed through a 60-mesh (0.25-mm) screen were used for analyses, as was done in the earlier analyses (Rosenblum, 1969, p. 5). The heavy-mineral fraction was first separated in methylene iodide at 3.2 specific gravity; then the monazite was separated from this fraction by a Frantz magnetic separator. Monazite grains that were extracted at amperages less than 0.60 A were minor in amount, and many had hydrous iron oxide coatings; only negligible amounts of monazite were extracted at amperages greater than 0.80 A. The fraction that separated between 0.60 and 0.80 A contained 85 to 95 percent monazite; the remainder was rutile, zircon, and spinel.

Purification of the monazite concentrate was accomplished by means of a hot Clerici solution technique (Rosenblum, 1974). By this method, minerals having a density of less than 4.9 float on a hot Clerici solution of that density and are trapped in the upper part of the solution when it solidifies upon cooling. The nearly pure monazite is recovered by first washing the impurities from the top of the test tube into a filter paper with water and then flushing the monazite concentrate from the bottom of the tube into another filter paper where it is thoroughly washed with warm water. The sample is then rinsed with acetone and dried under a heat lamp. Black impurities remaining with the monazite were estimated to constitute about one-half percent of the sample and were tentatively identified as ilmenorutile. A spectroscopic test of a few black grains picked from a monazite concentrate showed iron and titanium, but niobium and tantalum were not detected. Under the stereomicroscope these grains appear to be dark rutile. At densities above 4.9, they most likely contain niobium and tantalum, but not enough to detect in the spectroscopy at hand.

Most of the monazite grains are well rounded and range from pale yellow to yellow brown. The lighter colored grains are generally transparent, but the darker grains are commonly turbid and have submicron-sized particles, possibly alteration products resulting from radioactivity. There is no apparent relation between shape, color, turbidity, magnetic susceptibility, or other physical properties by which to distinguish two or more types of monazite. Thus, the analytical results cannot be related to specific physical properties but represent averages

Table 1.—X-ray fluorescence analyses of monazite, in weight percent, from Liberia
[Analyst, J. S. Wahlberg, U.S. Geol. Survey]

Field No.	La ₂ O ₃	Ce ₂ O ₃	Pr ₂ O ₃	Nd ₂ O ₃	Sm ₂ O ₃	Eu ₂ O ₃	Gd ₂ O ₃	Tb ₂ O ₃	Dy ₂ O ₃	Ho ₂ O ₃	Er ₂ O ₃	Tm ₂ O ₃	Yb ₂ O ₃	Lu ₂ O ₃	Y ₂ O ₃	ThO ₂	Sum
B-157E	17.6	32.4	2.5	8.3	0.8	0.06	0.4	<0.04	0.05	<0.07	<0.03	<0.04	<0.03	<0.05	0.4	7.5	70.0
B-162E	15.0	29.6	2.4	8.6	1.1	<0.06	.5	.04	.2	<0.07	.1	<0.04	<.03	<.05	.7	8.1	66.3
CO-119A	15.0	30.5	2.9	11.0	1.5	.19	.9	.08	.2	<.07	.05	<.04	<.03	<.05	1.1	7.0	70.4
JH-21A	18.4	32.3	2.4	7.6	.6	.08	.2	.04	<.05	<.07	.04	<.04	<.03	<.05	.2	6.6	68.5
JH-137A-3	14.0	29.0	2.4	9.3	1.3	.17	.8	.09	.2	<.07	.06	<.04	<.03	<.05	.9	7.3	65.6
RO-142E	13.2	28.4	2.8	10.7	1.5	.12	.9	.08	.2	<.07	<.03	<.04	<.03	<.05	.9	6.4	65.3
RO-143A	13.7	29.0	2.5	9.8	1.5	.19	.8	.08	.2	<.07	.1	<.04	<.03	<.05	.9	6.6	65.4
RO-148A	13.6	29.2	2.6	10.2	1.4	<.06	.7	.07	.2	<.07	.07	<.04	<.03	<.05	.6	6.5	65.1
RO-212D	13.2	28.9	2.5	10.7	1.8	.13	1.1	.10	.4	<.07	.09	<.04	<.03	<.05	1.4	7.4	67.7
RO-217G	14.0	29.5	2.6	9.5	1.3	.06	.6	.07	.3	<.07	.07	<.04	<.03	<.05	.6	8.4	67.0
WH-595E	14.7	29.0	2.5	9.2	1.4	.11	.8	.07	.2	<.07	.05	<.04	<.04	<.05	1.0	7.9	66.9
Average	14.8	29.8	2.6	9.5	1.3	.11	.7	.07	.2	<.07	.06	<.04	<.03	<.05	.8	7.2	67.1

Table 2.—Mean composition of rare-earth oxides in monazite, in weight percent

Oxides	USGS (26 samples) ¹	Russian investigators (56 samples) ¹	Lindsay Chemical Co. (many samples) ¹	This report (11 samples) ²
La ₂ O ₃	21.7	24.6	23.8	24.1
CeO ₂	45.5	46.6	47.7	51.0
Pr ₆ O ₁₁	5.1	5.1	6.0	4.3
Nd ₂ O ₃	19.2	18.2	18.8	15.2
Sm ₂ O ₃	4.0	3.5	2.0	2.1
Gd ₂ O ₃	1.9	2.0	.5	1.2
Others	2.6	(³)	1.2	2.1
Sum	100.0	100.0	100.0	100.0

¹ Data from Mertie (1960, p. 624).

² Average, not mean, composition of oxides.

³ Not determined.

Table 3.—Typical analyses of monazite sands, in weight percent

Country	ThO ₂	Rare-earth oxides	U ₃ O ₈
India	8.9	59.4	0.35
Brazil	6.5	59.2	.17
United States	3.1	40.7	.47
South Africa	5.9	46.4	.12
Malagasy Republic	8.8	46.2	.41
Liberia ¹	7.2	59.9	(²)

¹ This report; other data from Baroch (1965, p. 949).

² Not determined.

for heterogeneous monazite concentrates similar to what might be obtained in normal commercial extraction.

RESULTS OF ANALYSES

Table 1 shows the composition of the 11 monazite samples reported as 16 metal oxides. Subtracting the sum of each sample from 100 percent, the remaining oxide, P₂O₅, appar-

Table 4.—Neutron-activation analysis of europium and lutetium in Liberian monazites, in parts per million

[Analyst, Heinrich Stark, Institut für Radiochemie der Technischen Universität, Munich, West Germany]

Field No.	Eu	Lu
RO-212D	620±15	100
RO-217 G	200±15	100
UNMS-5921	830±15	100
UNMS-5922	745±15	100
UNMS-8151	820±15	100

ently ranges from 29.6 to 34.9 percent. The average of the analyses in table 1 was recalculated to 100 percent rare-earth elements as shown in table 2, to permit comparison of the Liberian monazites with the mean percentage of rare-earth oxides in monazites of three different groups of analysts. The category "Others" cited in table 2 includes oxides of europium, terbium, erbium, dysprosium, and yttrium, but not thorium oxide. The thorium oxide and rare-earth oxides of Liberian monazites are compared with typical analyses of monazite sands in table 3.

The results of europium and lutetium determinations obtained by neutron-activation analysis of Liberian monazite by United Nations radioisotope expert R. W. Thiele (written commun., 1972) are presented in table 4.

DISCUSSION

The rare-earth content of the 11 samples from Liberia does not differ greatly from that of other monazite samples in the world (see tables 2 and 3). Cerium is a little greater than average, but the other oxides (especially those of praseodymium and neodymium) are correspondingly lower.

In view of the encouraging prices for rare-earth elements and oxides (table 5), recovery of Liberian monazite from beach sands may be economically feasible. Prices of rare-earth

Table 5.—Prices of high-purity rare-earth oxides and metals in 1971, in U.S. dollars

[Data from United Mineral and Chemical Corp., New York, Tech. Bulls.,
June 1971 (oxides) and July 1971 (rare-earth metals)]

Element	Oxide			Metal (ingot)		
	Per gram (1–99 g)	Per gram (500–999 g)	Per pound (2 lb and up)	Per gram (1–99 g)	Per gram (500–999 g)	Per kilogram (1–10 kg)
Lanthanum	(¹)	0.18	60.00	0.46	0.28	232.50
Cerium	(¹)	.22	72.00	.46	.28	232.50
Praseodymium	(¹)	.32	120.00	1.09	.60	525.00
Neodymium	(¹)	.25	90.00	.60	.42	385.00
Samarium	(¹)	.28	108.00	1.25	1.05	945.00
Europium	7.91	4.80	1,875.00	9.25	12.30	² (12,000.00)
Gadolinium54	.36	150.00	1.54	.92	875.00
Terbium	9.45	6.16	2,400.00	4.20	3.40	3,325.00
Dysprosium	2.50	1.75	675.00	1.61	1.08	875.00
Holmium	1.75	1.23	480.00	3.15	1.65	1,517.00
Erbium	1.05	.63	240.00	1.89	.95	875.00
Thulium	15.75	10.00	3,900.00	19.18	13.43	² (13,000.00)
Ytterbium	1.40	.95	375.00	1.45	1.28	840.00
Lutetium	21.00	13.50	5,250.00	33.25	24.50	² (24,000.00)
Yttrium56	.28	112.00	1.30	.63	605.00
Scandium	4.20	3.36	1,425.00	19.32	14.25	² (14,000.00)

¹Price not quoted.²Price not quoted, but approximately calculated from 500–999 gram unit price.

oxides and elements listed in table 5 represent a 1.7 to 3 times increase over prices quoted in 1968 (Rosenblum, 1969, p. 2). The history of prices since 1957 (Parker and Baroch, 1971, p. 71; Griffith, 1970, p. 4) shows that a sudden rise occurred between 1968 and 1971. The price of domestic (U.S.) monazite sand increased from \$180 to \$200 per long ton, nominal, in 1968 (W. C. Overstreet, written commun., 1969) and from \$180 to \$200 per short ton, nominal, in 1970; prices for Australian monazite, minimum 60 percent rare-earth oxides plus ThO₂, were \$192 to \$216 per long ton in October–December 1970 (Griffith, 1970, p. 3). However, the average declared value of imported monazite concentrate ranged from \$131 to \$142 per long ton. The British monthly publication, "Industrial Minerals," quoted prices of monazite (minimum 55 percent rare-earth oxides, per long ton, cost including freight) as follows:

	British pounds	U.S. dollars
May–July 1968	65–80	156–192
Aug. 1968–Sept. 1969	65–75	156–180
Oct.–Dec. 1969	70–80	168–192
Jan. 1970–Sept. 1973	75–85	180–204

The analyses of table 1 show that Liberian monazites average 59.9 percent rare-earth oxides, contain greater than average percentages of ThO₂, and, depending on production costs, may be competitive in the world market.

According to previous investigations, beach-sand deposits from Greenville west to the Sierra Leone border contain sufficient monazite (among other heavy minerals of commerce) to be minable for monazite alone. The areas of highest potential include the coast from Greenville west to Bafu Bay (30 km),

the Marshal area, the area just west of Monrovia, and the Robertsport area. Personal inspection of these areas and radioactivity anomalies that indicate other monazite areas make the author believe that the reserves of monazite are sufficient to warrant mining. A feasibility study is recommended to evaluate production and marketing of monazite and other commercial heavy minerals in Liberian beach sands.

REFERENCES CITED

- Baroch, C. T., 1965, Thorium, in Mineral facts and problems: U.S. Bur. Mines Bull. 630, p. 947–959.
- Behrendt, J. C., and Wotorson, C. S., 1971, An aeromagnetic and aeroradioactivity survey of Liberia, west Africa: Geophysics, v. 36, no. 3, p. 590–604.
- Griethuysen, H. V. van, 1970, Mineral exploration of Wm. H. Muller & Co. in East Liberia: Geol. Mining Metall. Soc. Liberia Bull., v. 4, p. 88–95.
- Griffith, R. F., 1970, Rare-earth minerals and metals: U.S. Bur. Mines Minerals Yearbook 1970, Preprint, 9 p.
- Mertie, J. B., Jr., 1960, Monazite and related minerals, in Gillson, J. L., and others, eds., Industrial minerals and rocks—nonmetallics other than fuels [3d ed., rev.]: New York, Am. Inst. Mining, Metall., and Petroleum Engineers, p. 623–629.
- Parker, J. G., and Baroch, C. T., 1971, The rare-earth elements, yttrium, and thorium; a materials survey: U.S. Bur. Mines Inf. Circ. 8476, 92 p.
- Rosenblum, Sam, 1969, Preliminary spectrographic analyses of monazite from western Liberia: U.S. Geol. Survey open-file rept., 11 p.; Liberian Geol. Survey Memo. Rept. 42, 11p.
- , 1974, A mineral separation procedure using hot Clerici solution: U.S. Geol. Survey Jour. Research, v. 2, no. 4, p. 479–481.

BUDDINGTONITE, AMMONIUM FELDSPAR, IN THE PHOSPHORIA FORMATION, SOUTHEASTERN IDAHO

By R. A. GULBRANDSEN, Menlo Park, Calif.

Abstract.—Buddingtonite is distributed widely in the rocks of the Meade Peak Member of the Phosphoria Formation in southeastern Idaho and occurs in amounts up to about 50 percent. Most of the buddingtonite is in the middle mudstone interval of the member between two phosphate-rich intervals. The composition of the buddingtonite, in terms of a buddingtonite-K-feldspar series, shows an apparent range of $Bd_{82}KF_{18}$ to $Bd_{13}KF_{87}$, and compositions of $Bd_{72}KF_{28}$ to $Bd_{50}KF_{50}$ may be the most common. The predominant silicate mineral suite consists of buddingtonite-albite-illite. Albite is present in amounts up to about 20 percent. Buddingtonite may have developed directly from volcanic glass in the presence of abundant ammonium, derived from the decomposition of organic matter, in interstitial waters, or it may have formed at some later diagenetic stage from other products of volcanic glass alteration, such as montmorillonite or zeolites.

Buddingtonite was described and named comparatively recently by Erd, White, Fahey, and Lee (1964). It occurs as a reaction product of low-temperature hot-spring water, which contains 460–540 ppm of ammonium, and andesite lava and older rocks at Sulphur Bank mine, Lake County, Calif. Buddingtonite has been synthesized by Barker (1964) at temperatures ranging from 550° to 600°C and a pressure of 2,000 bars. The occurrence of buddingtonite in the Phosphoria Formation is only the second reported natural occurrence and is the first in sedimentary rock.

The Phosphoria Formation, the Park City Formation, and the Shedhorn Sandstone compose the three rock units of Permian age whose nomenclature, lithology, and distribution are described by McKelvey and others (1959). The Phosphoria, present in the States of Idaho, Wyoming, Montana, Utah, and northeastern Nevada, consists of phosphorite, mudstone, and carbonate rock, all typically rich in organic matter, and chert. It includes two phosphatic members, the Meade Peak Phosphatic Shale Member and, stratigraphically higher, the Retort Phosphatic Shale Member. The Meade Peak contains rich deposits of phosphate in southeastern Idaho, where it ranges in thickness from about 110 to 225 ft (33.5–68.6 m). The Retort is much thinner than the Meade Peak, a maximum of 80 ft (24.4 m) in southwestern Montana, but also contains economically important rich beds of phosphorite in west-central Montana.

OCCURRENCE

Buddingtonite was discovered in bed P-24 of the Meade Peak Phosphatic Shale Member of the Phosphoria Formation in southeastern Idaho at Gravel Creek Divide (fig. 1), a stratigraphic section described in Davidson, Smart, Peirce, and

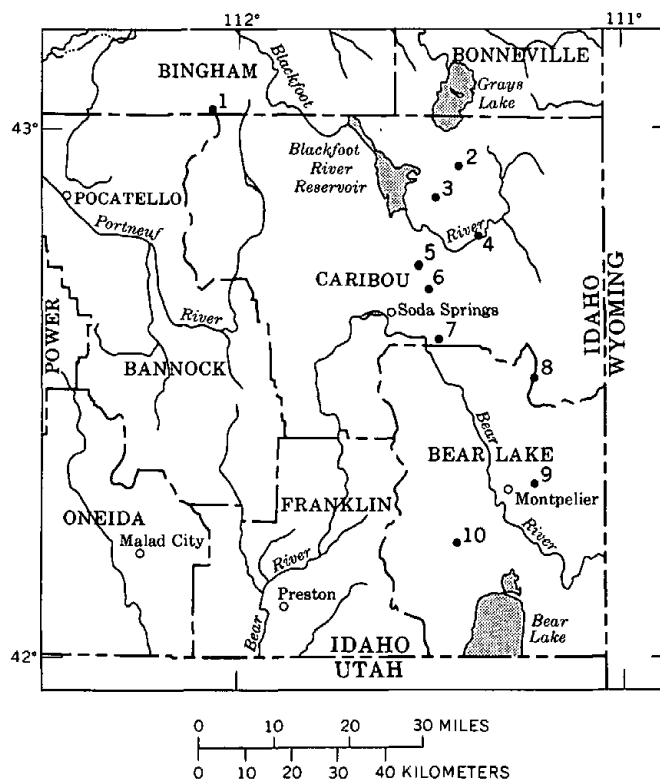


Figure 1.—Map showing location of stratigraphic sections of the Meade Peak Phosphatic Shale Member that are referred to in this report.

1. Fort Hall (Smart and others, 1954; O'Malley and others, 1953).
2. Gravel Creek Divide (Davidson and others, 1953).
3. Henry mine, Monsanto Co.
4. Blackfoot Narrows (O'Malley and others, 1953).
5. Woodall Mountain mine, Simplot Co.
6. Trail Canyon (McKelvey, Armstrong, and others, 1953).
7. Swan Lake Gulch (McKelvey, Davidson and others, 1953).
8. Snowdrift Mountain (Smart and others, 1954).
9. Montpelier Canyon (McKelvey, Armstrong, and others, 1953).
10. Paris Canyon (O'Malley and others, 1953).

Weiser (1953). Bed P-24, about 45 ft (13.7 m) above the base of the Meade Peak, is a 1-ft(0.3-m)-thick, brown, moderately hard fine-grained porous rock that is composed approximately of 48 percent buddingtonite, 32 percent dolomite, 13 percent illite, and 7 percent other constituents. In thin section, buddingtonite appears as light-brown, microcrystalline, barely anisotropic, shapeless masses that are interstitial to comparatively large subhedral dolomite grains (modal size about 50 μ m).

Buddingtonite is present in all the stratigraphic sections of the Meade Peak Member so far examined in southeastern Idaho (fig. 1). It has also been identified in the Meade Peak Member in western Wyoming and southwestern Montana, and in the Rectort Phosphatic Shale Member in southwestern Montana.

In southeastern Idaho the occurrence of buddingtonite within the Meade Peak Member is chiefly in the middle part, the "barren zone" of the mining industry which is the interval between the two phosphate-rich zones of the member. The middle interval is composed principally of mudstone but also includes carbonate rock, phosphorite, and some chert, and it ranges in thickness from about 25 to 145 ft (7.6–44.2 m). Buddingtonite is present in nearly all samples examined by X-ray and ranges in amount from practically zero to about 50 percent and is commonly greater in amount than 10 percent. Correlation of buddingtonite-rich beds or groups of beds between sections has not yet been achieved, but with detailed study the prospects for such correlation are good. One former ash horizon is recognized in sections 1, 3, 5, 6, 7, 8, and 9 of figure 1. It occurs in the lower part of the lower phosphate zone and contains ammonium K-feldspar ($\text{Bd}_{13}\text{KF}_{87}$), rather than buddingtonite (Bd_{50}).

Buddingtonite is always accompanied by illite, and albite, in a maximum amount of about 20 percent and commonly in amounts of about 5–10 percent, is also usually present. Significant amounts of montmorillonite and kaolinite also occur with buddingtonite in some samples.

COMPOSITION AND X-RAY PROPERTIES

The chemical composition of the acid ($\text{HCl}:\text{H}_2\text{O} = 1:3$) insoluble part of the sample of bed P-24 is presented in column 1 of table 1. The analysis is of a mixture composed mainly of buddingtonite and illite, 73.2 percent and 18.6 percent, respectively. These amounts are calculated by using equations relating the values for SiO_2 and Al_2O_3 of column 1 in table 1 with the respective amounts in theoretical buddingtonite ($(\text{NH}_4\text{AlSi}_3\text{O}_8 \cdot 0.5\text{H}_2\text{O})$ (Erd and others, 1964) and illite (Schultz, 1964). The portions of the constituents in the analysis that are combined in illite are listed in column 2. Those attributed to buddingtonite are given in column 3, and they are calculated to a formula of five cations (column 6), excluding water which Erd, White, Fahey, and Lee (1964)

Table 1.—Chemical analysis of buddingtonite-rich sample

[Sample collected from bed P-24 of the Meade Peak Phosphatic Shale Member of the Phosphoria Formation, southeastern Idaho, at Gravel Creek Divide (fig. 1). Analysts: P. L. D. Elmore, J. Kelsey, H. Smith, and J. L. Glenn. $(\text{NH}_4)_2\text{O}$ by F. Brown]

	Weight percent	Percent in illite	Percent in budd- ingtonite	Cation weight equivalent	Cation ratios	Cations ¹
	(1)	(2)	(3)	(4)	(5)	(6)
SiO_2	59.4	9.9	49.5	60.09	0.8238	2.97
Al_2O_3	19.0	5.0	14.0	50.98	.2746	.99
Fe_2O_3	² 3.8	.9
MgO36	.37
CaO11
Na_2O2525	30.99	.0081	.03
K_2O	3.4	1.3	2.1	47.10	.0446	.16
$(\text{NH}_4)_2\text{O}$	6.1	6.1	26.01	.2345	.85
H_2O^+	³ 3.1	.9	2.2	9.00	.2444	.88
H_2O^-86
TiO_268	.19
P_2O_513
MnO04
Organic matter. ⁴	3.1
CO_2	⁵ <.05
Sum	100.33					

¹ Calculated for total of five (5) cations, excluding water. Factor for multiplying cation ratios is: $F = \frac{5}{\text{sum cation ratios}} = \frac{5}{1.3856} = 3.6085$.

² Total iron as Fe_2O_3 . FeO is 1.1 percent.

³ Determined as 9.2 percent (total H_2O^+) – 6.1 percent $(\text{NH}_4)_2\text{O}$.

⁴ Loss on ignition other than CO_2 and H_2O . Another determination by loss on ignition of an HF residue gave 3.2 percent.

⁵ Not included in summation.

found to be of zeolitic character. The amount of water assigned to buddingtonite in this analysis is not considered to be of high accuracy because of the difficulty of determination in the presence of organic matter, as well as having a significant uncertainty in the amount assigned to illite; however, the amount calculated, using the factor for multiplying the cation ratios of column 5, that was derived from the other five cations, is $0.44\text{H}_2\text{O} \left(\frac{0.88\text{H}}{2} \right)$, a value reasonably close to the $0.5\text{H}_2\text{O}$ found by Erd and others (1964). The other cations calculated for one formula of buddingtonite, column 6, check well, considering their dependence upon the assumed composition of illite. Rounding cation values of Si to 3, Al to 1, recalculating Na, K, and NH_4 to 1, and leaving H_2O as 0.44, yields a formula for buddingtonite of $(\text{NH}_{4.0.82}\text{K}_{0.15}\text{Na}_{0.03})\text{AlSi}_3\text{O}_8 \cdot 0.44\text{H}_2\text{O}$. The significant difference between this formula and the one calculated from the data of Erd, White, Fahey, and Lee (1964) $(\text{NH}_{4.0.93}\text{K}_{0.04}\text{Na}_{0.01}\text{Ba}_{0.01}\text{Mg}_{0.01})\text{AlSi}_3\text{O}_8 \cdot 0.51\text{H}_2\text{O}$, is the lesser amount of NH_4 and the greater amount of K in the Phosphoria buddingtonite. The similarity in size of the ionic

radii of NH_4^+ and K^+ , 1.43 Å and 1.33 Å, respectively, provides theoretical support for the large magnitude of NH_4 substitution of K, as indicated above, in the K-feldspar structure, but the role of water in buddingtonite remains a puzzle.

Most of the iron shown in the chemical analysis of table 1 is soluble in concentrated HCl and probably occurs as an oxide, possibly goethite, as suggested by the presence of a broad poorly defined X-ray peak at 21° – 21.8° 2θ ($\lambda = \text{Cu}$) on a pattern of an iron-rich sample fraction. Some iron is in illite, as shown, and a small amount may be in buddingtonite. The calcium and the phosphorus in the sample are due to apatite and most of the titanium occurs as rutile. A spectrographic analysis of the sample, table 2, shows the presence of significant amounts of zinc (0.1 percent), vanadium (0.05 percent),

Table 2.—Spectrographic analysis of buddingtonite-rich sample
[Analyst: Harry Bastron]

Element	Weight percent	Element	Weight percent
Mn.....	0.0070	Pb.....	0.0007
Ag.....	.0010	Sc.....	.0003
B.....	.0300	Sr.....	.0030
Ba.....	.0150	V.....	.0500
Co.....	.0002	Y.....	.0020
Cr.....	.0500	Yb.....	.0003
Cu.....	.0200	Zn.....	.1000
Mo.....	.0070	Zr.....	.0100
Ni.....	.0150		

and chromium (0.05 percent). They are found to be further concentrated in the $<4\text{-}\mu\text{m}$ -size fraction of the sample where organic matter, iron oxide, and illite are concentrated also, and the metals may be adsorbed on those constituents.

X-ray diffraction data of buddingtonite and K-feldspar are presented in table 3. The data for buddingtonite of the Phosphoria and the type buddingtonite of California compare satisfactorily for most d -values and the corresponding relative intensities, but some differences are noteworthy. The strongest peak (3.243 Å) of the Phosphoria buddingtonite does not correspond in d -value to the strongest peak (3.81 Å) of the California buddingtonite. This lack of correspondence is due to the splitting of the 3.243-Å peak of the Phosphoria buddingtonite into two peaks of lesser intensities, the 3.258-Å and 3.225-Å peaks, of the California buddingtonite, and it probably reflects the difference of the $\text{NH}_4:\text{K}$ ratio between the two samples. Two other differences of this type are indicated for the 2.904-Å and the 1.800-Å peaks of the Phosphoria buddingtonite in table 3. Because of ambiguities in indexing owing to peak broadening, the cell dimensions are not calculated.

The differences of X-ray data between monoclinic buddingtonite and monoclinic K-feldspar are clearly shown by the d -values and intensities presented in table 3. The shift of the strong 4.241-Å (201) peak of K-feldspar to 4.32 Å or 4.33 Å in buddingtonite is striking, as well as the very large increase in

Table 3.—X-ray diffraction data for buddingtonite and K-feldspar

Buddingtonite, ¹ Sulphur Bank mine, California			Buddingtonite, ² Phosphoria Fm., Idaho		K-feldspar ³ (high sanidine)		
<i>dA</i>	<i>I</i>	<i>hkl</i>	<i>dA</i>	<i>I</i> ⁴	<i>dA</i>	<i>I</i> ⁴	<i>hkl</i>
6.75	16	110	6.77	12	6.65	6	110
6.52	96	020	6.52	68	6.51	10	020
5.91	33	011	5.92	28	5.869	10	111
4.33	65	101	4.32	71	4.241	50	201
3.98	33	211	3.99	36	3.947	20	111
					3.87	4B	200
3.81	100	130	3.82	76	3.789	80	130
3.63	12	031	3.64	11B	3.623	16	131
3.60	5	131, 121	3.60	4B	3.557	12	221
3.462	23	112	3.474	25	3.459	50	112
3.381	72	220	3.379	58	3.328	100	220
3.314	34	002	3.320	34	3.287	60	202
3.258	62	040	3.258	35	040
			3.243	100			
3.225	69	202	3.223	80	002
3.129	3	212			
3.014	39	140, 231	3.016	35	2.995	50	131
2.954	13	022	2.959	10B	2.932
2.910	20	141			
			2.904	25B	2.905	20	041, 222, 022
2.894	15	222	2.889
2.862	9	211	2.856	5B
2.767	9	132	2.772	8B	2.766	16	132
2.650	12	112	2.647	8B
2.604	23	141	2.606	14B	2.608	12	312
			2.589	5B	2.582	30	221, 241
			2.570	5B
2.515	11	240	2.519	5B
2.432	12	2.430	10B
2.381	7	2.400?	1?B
2.319	6	2.325	2B
			2.250?	2?B
2.175	28	2.166	26B	2.171	20B	060
2.151	8	2.140?	3?B
2.058	6	2.052	6B
1.989	8	1.990	6B
1.979	8	1.974	7B
1.947	3
1.859	7	1.861	6B
1.802	13
			1.800	21B			
1.797	19	1.793	...	204

¹ Erd and others (1964).

² Averages of at least four measurements of concentrates richer in buddingtonite than sample that was chemically analyzed, $\lambda = \text{CuK}\alpha_1 = 1.54051$ Å. Internal standards: CaF_2 (111) = 3.156 Å, CaF_2 (220) = 1.9318 Å, and quartz (1010) = 4.255. Diffractometer traverse rate = $0.5^\circ 2\theta$ per min. Question marks indicate poor accuracy and even doubtful existence.

³ X-ray powder data filecard 10-353. Poorly resolved peaks less than 2.582 Å not measured (Donnay and Donnay, 1952).

⁴ B, broad.

intensity of the (020) peak of buddingtonite in comparison to that of K-feldspar. The (201) peak position was shown by Bowen and Tuttle (1950) to be related to composition, in weight percent, in the K-feldspar–Na-feldspar series. The shift

of the (201) K-feldspar peak owing to ammonium substitution is shown in figure 2. There 2θ values are plotted against mole percent buddingtonite for synthetic buddingtonite (Barker, 1964), California buddingtonite (Erd and others, 1964), Phosphoria buddingtonite, and synthetic K-feldspar (Donnay and Donnay, 1952). A linear relationship is indicated although

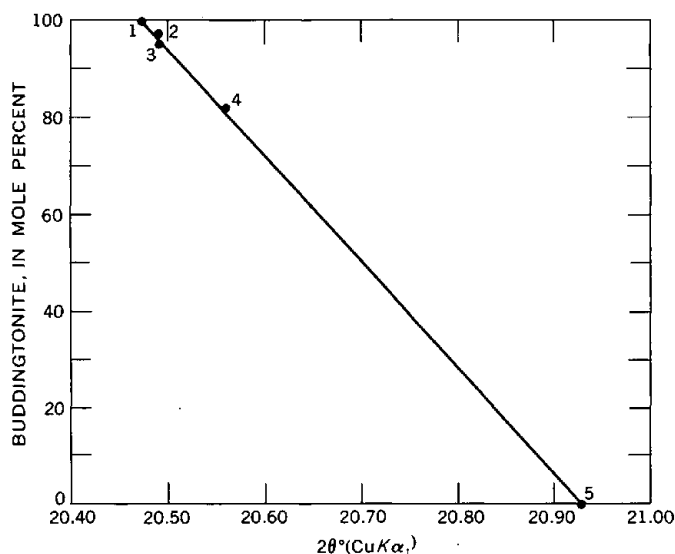


Figure 2.—Relation of composition in the buddingtonite-K-feldspar series with X-ray peak position (201) of K-feldspar.

1. Theoretical buddingtonite, $(\text{NH}_4)\text{AlSi}_3\text{O}_8 \cdot 0.5\text{H}_2\text{O}$.
2. Synthetic buddingtonite ($\text{Bd}_{97.3}\text{Or}_{2.7}$); Barker (1964).
3. California buddingtonite, $(\text{NH}_4+\text{Ba})_{0.954}(\text{K}+\text{Na})_{0.046}\text{AlSi}_3\text{O}_8 \cdot 0.5\text{H}_2\text{O}$, recalculated, excluding Mg; from data of Erd and others (1964).
4. Phosphoria buddingtonite, $(\text{NH}_4)_{0.82}(\text{K}+\text{Na})_{0.18}\text{AlSi}_3\text{O}_8 \cdot 0.44\text{H}_2\text{O}$.
5. Synthetic K-feldspar (sanidine), KAlSi_3O_8 . X-ray powder data filecard 10-353; Donnay and Donnay (1952).

samples of intermediate composition are needed for verification. The extrapolation of the line to 100 percent yields a 2θ value of 20.473° (4.334 Å) for pure buddingtonite and a total peak shift in d -value of 0.093 Å (4.334 Å–4.241 Å), a value remarkably close to the difference in size of the $(\text{NH}_4)^+$ and K^+ ions, 1.43 Å–1.33 Å = 0.10 Å. The closeness of the d -value shift and the ionic radii difference suggests that a linear relationship of peak position with mole percent, rather than weight percent, is likely correct in this instance.

X-ray patterns of many samples of the Meade Peak Member in southeastern Idaho indicate that intermediate compositions in the buddingtonite-K-feldspar series are common. Peak positions in the 2θ range of 20.60 to 20.70 appear to be the most frequent and, using the relationship shown in figure 2, indicate a compositional range of Bd_{72} to Bd_{50} . Because quartz, which is nearly ubiquitous in the samples of the Meade Peak, has a strong peak at 20.86° , peak positions in the range of 20.70° to 20.93° of the buddingtonite-K-feldspar series are

generally obscured and large amounts of quartz can obscure even smaller angle peaks of buddingtonite. Where quartz is present in small amounts, buddingtonite compositions less than Bd_{50} are inferred from the presence of a shoulder on the quartz peak or by an intensity ratio of the buddingtonite peak at about 13.6° to the buddingtonite main peak at about 27.5° of greater than about 0.20. One sample that is free of quartz interference has a peak at 20.87° which, from figure 2, gives a composition of $\text{Bd}_{13}\text{KF}_{87}$, the lowest in the buddingtonite component so far found. Apparent buddingtonite compositions in the Meade Peak, therefore, range from $\text{Bd}_{82}\text{KF}_{18}$ to $\text{Bd}_{13}\text{KF}_{87}$ and compositions in the range of $\text{Bd}_{72}\text{KF}_{28}$ to $\text{Bd}_{50}\text{KF}_{50}$ may be the most common.

SPECIFIC GRAVITY AND REFRACTIVE INDEX

The specific gravity of the main bulk of the Phosphoria buddingtonite of sample P-24 is 2.360 ± 0.005 . The grains are typically clouded with minute inclusions that are presumed to be mostly organic matter but probably include some illite and iron oxide. The organic matter would tend to lower the specific gravity and the others to increase it. Erd, White, Fahey, and Lee (1964) measured a specific gravity of 2.32 ± 0.01 and calculated a density of 2.388 g/cm^3 on the California buddingtonite. The mean refractive index of aggregate grains with included material like that described above is about 1.535.

ORIGIN OF PHOSPHORIA BUDDINGTONITE

In the buddingtonite-rich bed, P-24, of the Gravel Creek Divide section, no textural indication of the origin of the buddingtonite has been recognized. The absence of quartz and the presence of biotite and hornblende among the accessory minerals, however, are key data indicating a derivation of buddingtonite from volcanic glass or intermediate alteration products of glass such as montmorillonite or zeolites. The ammonium required for the buddingtonite was undoubtedly derived from the decomposition of organic matter whose abundance in the brown to black rocks of the phosphatic shale members of the Phosphoria Formation is well known.

Ammonia is a well-known product of the decomposition of organic matter under reducing conditions, but not many data exist on the abundance of ammonia in the bottom and interstitial waters of marine basins. Seawater in general seems to be very low in ammonia with a reported maximum of about 6 mg/l (Redfield and Keys, 1938), and even the stagnant bottom water of the Black Sea is not high, containing only a maximum of 1.3 mg/l of ammonia (Caspers, 1957). The contents of ammonia in interstitial waters, in sharp contrast, are very high; a maximum of 240 mg/l at Saanich Inlet, British Columbia (Nissenbaum and others, 1972), a maximum of about 200 mg/l in the Santa Barbara basin off southern California (Rittenberg and others, 1955), and a similar maximum in Somes Sound, Maine (Berner and others, 1970). Interstitial water in the sediments of Chesapeake Bay contains

as much as about 120 mg/l of ammonia (Bray and others, 1973). These data indicate that the development of buddingtonite would be favored in situ at some distance below the sediment-seawater interface. It is not known if buddingtonite formed directly from volcanic glass or from intermediate products, such as montmorillonite or zeolites, during diagenesis. An unusual seawater composition may have favored the formation of buddingtonite, whether directly or from intermediate products. In continental saline-lake deposits, the development of K-feldspar is from zeolite products of glass alteration (Sheppard and Gude, 1968; Goodwin, 1973).

If the abundance of buddingtonite represents a measure of the minimum amount of glass supplied as volcanic ash during the period of Meade Peak deposition, the contribution was large and practically continuous through much of Meade Peak time. The distribution and concentrations of buddingtonite seem to show that great airfalls of ash did not occur, but that small falls were frequent for a long period of time and that ocean currents may have played an important role in the distribution of the ash. A close relationship between Phosphoria sedimentation and Permian volcanism was postulated by Mansfield (1940) on rather meager evidence. The occurrence of buddingtonite as described in this paper lends strong support to this correlation.

ACKNOWLEDGMENTS

I am especially grateful to R. C. Erd for his help in identifying buddingtonite in this occurrence and in subsequent X-ray work. C. E. Roberson made the first confirmation of ammonium in the mineral. Suggestions by T. L. Wright and R. A. Sheppard have helped to improve the paper, and Wright's recommendations on the organization of the paper are particularly appreciated.

REFERENCES CITED

- Barker, D. S., 1964, Ammonium in alkali feldspars: *Am. Mineralogist*, v. 49, nos. 7-8, p. 851-858.
- Berner, R. A., Scott, M. R., and Thomlinson, Catherine, 1970, Carbonate alkalinity in the pore waters of anoxic marine sediments: *Limnology and Oceanography*, v. 15, no. 4, p. 544-549.
- Bowen, N. L., and Tuttle, O. F., 1950, The system $\text{NaAlSi}_3\text{O}_8\text{-KAlSi}_3\text{O}_8\text{-H}_2\text{O}$: *Jour. Geology*, v. 58, no. 5, p. 489-511.
- Bray, J., Bricker, O., and Troup, B., 1973, Geochemistry of the interstitial waters of the sediments of Chesapeake Bay—nutrients: *Geol. Soc. America Abs. with Programs*, v. 5, no. 2, p. 141.
- Caspers, Hubert, 1957, Black Sea and Sea of Azov, in Hedgpeth, J. W., ed., *Treatise on marine ecology and paleoecology*, V. 1: *Geol. Soc. America Mem.* 67, p. 801-890.
- Davidson, D. F., Smart, R. A., Peirce, H. W., and Weiser, J. D., 1953, Stratigraphic sections of the Phosphoria formation in Idaho, 1949, Pt. 2: *U.S. Geol. Survey Circ.* 305, 28 p.
- Donnay, Gabrielle, and Donnay, J. D. H., 1952, The symmetry change in the high-temperature alkali-feldspar series: *Am. Jour. Sci.*, Bowen Volume, pt. 1, p. 115-132.
- Erd, R. C., White, D. E., Fahey, J. J., and Lee, D. E., 1964, Buddingtonite, an ammonium feldspar with zeolitic water: *Am. Mineralogist*, v. 49, nos. 7-8, p. 831-850.
- Goodwin, J. H., 1973, Analcime and K-feldspar in tuff of the Green River Formation, Wyoming: *Am. Mineralogist*, v. 58, nos. 1-2, p. 93-105.
- Mansfield, G. R., 1940, The role of fluorine in phosphate deposition: *Am. Jour. Sci.*, v. 238, no. 12, p. 863-879.
- McKelvey, V. E., Armstrong, F. L., Gulbrandsen, R. A., and Campbell, R. M., 1953, Stratigraphic sections of the Phosphoria Formation in Idaho, 1947-48, Pt. 2: *U.S. Geol. Survey Circ.* 301, 58 p.
- McKelvey, V. E., Davidson, D. F., O'Malley, F. W., and Smith, L. E., 1953, Stratigraphic sections of the Phosphoria Formation in Idaho, 1947-48, Pt. 1: *U.S. Geol. Survey Circ.* 208, 49 p.
- McKelvey, V. E., Williams, J. S., Sheldon, R. P., Cressman, E. R., Cheney, T. M., and Swanson, R. S., 1959, The Phosphoria, Park City, and Shedhorn formations in the western phosphate field: *U.S. Geol. Survey Prof. Paper* 313-A, p. 1-47.
- Nissenbaum, Arie, Presley, B. J., and Kaplan, I. R., 1972, Early diagenesis in a reducing fjord, Saanich Inlet, British Columbia—I. Chemical and isotopic changes in major components of interstitial water: *Geochim. et Cosmochim. Acta*, v. 36, no. 9, p. 1007-1028.
- O'Malley, F. W., Davidson, D. F., Hoppin, R. A., and Sheldon, R. P., 1953, Stratigraphic sections of the Phosphoria formation in Idaho, 1947-48, Pt. 3: *U.S. Geol. Survey Circ.* 262, 43 p.
- Redfield, A. C., and Keys, A. B., 1938, The distribution of ammonia in the waters of the Gulf of Maine: *Biol. Bull.*, v. 74, p. 83-92.
- Rittenberg, S. C., Emery, K. O., and Orr, W. L., 1955, Regeneration of nutrients in sediments of marine basins [Calif.]: *Deep-Sea Research*, v. 3, no. 1, p. 23-45.
- Schultz, L. G., 1964, Quantitative interpretation of mineralogical composition from X-ray and chemical data for the Pierre Shale: *U.S. Geol. Survey Prof. Paper* 391-C, 31 p.
- Sheppard, R. A., and Gude, A. J., 3d., 1968, Distribution and genesis of authigenic silicate minerals in tuffs of Pleistocene Lake Tecopa, Inyo County, California: *U.S. Geol. Survey Prof. Paper* 597, 38 p.
- Smart, R. A., Waring, R. G., Cheney, T. M., and Sheldon, R. P., 1954, Stratigraphic sections of the Phosphoria formation in Idaho, 1950-51: *U.S. Geol. Survey Circ.* 327, 22 p.

OPTICAL AND X-RAY CRYSTALLOGRAPHIC INVESTIGATIONS OF STRONTIOGINORITES

By RALPH P. CHRISTIAN, G. DONALD EBERLEIN, and JUDITH A. KONNERT,
Washington, D.C., Menlo Park, Calif., Washington, D.C.

Abstract.—Compositional, optical, and unit-cell data are presented for a suite of strontioginorites. These crystals show that Sr:Ca \approx 1 is preferred. Lack of variation in the Sr:Ca resulted in no meaningful correlation between composition and physical properties.

The mineral series with end members $2\text{CaO} \cdot 7\text{B}_2\text{O}_3 \cdot 8\text{H}_2\text{O}$ (ginorite) and $2\text{SrO} \cdot 7\text{B}_2\text{O}_3 \cdot 8\text{H}_2\text{O}$ includes strontioginorite, ideally $\text{SrO} \cdot \text{CaO} \cdot 7\text{B}_2\text{O}_3 \cdot 8\text{H}_2\text{O}$. Because the X-ray diffraction powder patterns of the end members are similar to the pattern given by strontioginorite, all members of the series have been assumed to have essentially the same structure, despite the (Sr,Ca) variation.

The crystal structure of strontioginorite was solved in 1970 by Konnert, Clark, and Christ; the structural formula is $(\text{Sr,Ca})_2\text{B}_{14}\text{O}_{20}(\text{OH})_6 \cdot 5\text{H}_2\text{O}$, and there are four formula units in the monoclinic $P2_1/a$ unit cell: $a = 12.817$ Å, $b = 14.448$ Å, $c = 12.783$ Å, $\beta = 101^\circ 25'$. The two crystallographically distinct cation sites in the structure are different in character, although both cations are included in the borate polyanion sheets by coordination to six oxygen atoms each.

The Ca site is 8-coordinated, the Sr site is 10-coordinated, and the coordinating atoms that are outside the sheet containing the given cations are the key to the orderly stacking of the sheets. Because the two different cation coordinations seem essential to the ordering of the structure, we wished to determine (1) whether the structure could in fact be maintained over the entire (Sr,Ca) range, and (2) whether a variation in physical properties could be noted with a change in the Sr:Ca ratio.

Seven crystals designated strontioginorite from the Königshall-Hindenburg salt mine at Reyershausen near Göttingen, Germany, were made available to us by our colleague, R. C. Erd. We have examined these crystals by X-ray fluorescence analysis methods to determine the Sr:Ca ratio; we have also obtained optical data and cell constants. These data are given in table 1 (after "References Cited"), together with information for the end members. As the data show, there is

not enough variation in the Sr:Ca ratio of the seven crystals to obtain any meaningful correlation between chemical composition and physical properties. Even for the one crystal (No. 1) with a Sr:Ca ratio significantly different from that of the other crystals, the values of the physical constants are the same within the limits of error of the measurements. Therefore, unfortunately, no conclusions concerning the stability of the strontioginorite structure over a range of Sr:Ca values can be made. Perhaps, however, the general lack of variation of the Sr:Ca ratio in the present samples indicates that strontioginorite crystals with Sr:Ca \approx 1 are the most stable, as would be expected from structural considerations.

ACKNOWLEDGMENTS

We are grateful to several of our colleagues at the U.S. Geological Survey: to C. L. Christ for suggesting the problem; to R. C. Erd for supplying the samples; to H. T. Evans, Jr., for the measured powder patterns of synthetic Sr-borate; and to J. R. Clark for reviewing the manuscript and making helpful suggestions.

REFERENCES CITED

- Appleman, D. E., and Evans, H. T., Jr., 1973, Job 9214: Indexing and least-squares refinement of powder diffraction data: U.S. Dept. Commerce, Natl. Tech. Inf. Service, PB-216 188, 67 p.
- Braitsch, Otto, 1959, Über Strontioginorit, eine neue Ginorit-Varietät aus dem Zechsteinsalz: *Contr. Mineralogy and Petrology*, v. 6, p. 366-370.
- Evans, H. T., and Christian, R. P., 1972, Adaptation of the X-ray milliprobe for examination of small single crystals obtained from lunar samples: *Appl. Spectroscopy*, v. 26, p. 313-315.
- Kondrat'yeva, V. V., 1963, [Ginorite]: *Rentgenografiya Mineral'nogo Syr'ya*, v. 3, p. 11-15 (in Russian).
- Konnert, J. A., Clark, J. R., and Christ, C. L., 1970, Crystal structure of strontioginorite $(\text{Sr,Ca})_2\text{B}_{14}\text{O}_{20}(\text{OH})_6 \cdot 5\text{H}_2\text{O}$: *Am. Mineralogist*, v. 55, nos. 11-12, p. 1911-1931.
- Nefedov, E. I., 1955, Neue Minerale: *Geologie*, v. 4, no. 5, p. 526-528.
- Wilcox, R. E., 1959, Use of the spindle stage for determination of principal indices of refraction of crystal fragments: *Am. Mineralogist*, v. 44, nos. 11-12, p. 1272-1293.

Table 1.—Summary of measurements for various strontionorite crystals compared with data for
glinorite and synthetic strontium borate
 [Numbers in parentheses after data are for errors of one standard deviation; that is, 1.512(1) means 1.512±0.001]

	Strontionorites						
	1	2	3	4	5	6	7
Composition: ¹							
Sr	1.34	1.01	1.01	1.01	1.00	1.00	1.02
Ca	0.66	0.99	0.99	0.99	1.00	1.00	0.98
Optics: ²							
α ($n_D^{25^\circ\text{C}}$)	1.512(1)	1.514(1)	1.515(1)	1.515(1)	1.514(1)	1.513(1)	1.513(1)
β ($n_D^{25^\circ\text{C}}$)	1.525(1)	1.525(1)	1.525(1)	1.526(1)	1.526(1)	1.526(1)	1.526(1)
γ ($n_D^{25^\circ\text{C}}$)	1.573(1)	1.574(1)	1.575(1)	1.574(1)	1.575(1)	1.574(1)	1.574(1)
$2V_\gamma$ (obs)	50(2)	50(2)	49(2)	50(2)	49(2)	49(2)	49(2)
$Z \wedge c^*$	+41°	+38°	+42°	+40°	+39°	+40°	40°
$Z \wedge a^*$	-52°	-49°	-54°	-52°	-50°	-52°	-52°
Unit cell: [†]							
a (Å)	12.828(7)	12.845(8)	12.809(8)	12.834(6)	12.816(8)	12.812(25)	12.817(8)
b (Å)	14.451(5)	14.447(6)	14.454(4)	14.439(4)	14.426(5)	14.322(18)	14.448(8)
c (Å)	12.800(4)	12.814(7)	12.793(5)	12.808(8)	12.787(8)	12.803(30)	12.783(8)
β	101°22'(5)	101°19'(5)	101°20'(5)	101°23'(5)	101°18'(5)	101°17'(7)	101°25'(5)
Volume (A^3)	2326.3	2331.7	2322.3	2326.8	2318.3	2303.9	2320.3
ρ (calc) (g/cm^3)	2.30 ₅	2.25 ₅	2.26 ₅	2.26 ₅	2.26 ₅	2.28 ₁	2.26 ₅
Comments	Very good crystal	Good crystal	Good crystal	Twinned	Twinned	Strongly twinned	Used for structure determination; optics not measured.
							Nefedov gave a , b , c in kX units; conversion to A units (1 kX = 1.0026 Å) volume and density calculations by present authors.
							Cell constants from least-square refinement of powder data (Appelman and Evans, 1973) (R. C. Erd, written commun. in advance of publication; sample from Death Valley, Calif.).
							Cell constants from least-square refinement of powder data (Appelman and Evans, 1973).

¹The formula unit was calculated by measuring the Sr:Ca intensity ratios using an X-ray milliprobe with a Cr/W dual-target X-ray tube and a flow proportional detector; all samples were mounted in a holder designed for single crystals (Evans and Christian, 1972). Mixtures of pure CaCO_3 and SrCO_3 were used as standards because the mass absorption coefficient of carbon is close to that of boron, with no absorption edge between them. Very small portions of the synthetic powder mixtures, approximately the size and weight of the average single crystal of strontionorite, were mixed with Duco cement, rolled into small balls, and mounted as the single crystals were. Seven intensity readings of the $K\alpha$ line of each element were taken on each sample, and corrected only for background. The high and low values were discarded; the remaining values were averaged. The precision of the X-ray fluorescence determination of the Sr:Ca ratio has been calculated not to exceed 0.5 percent of the amount based on repeated runs on the smallest crystal (No. 7, 500 μg). The accuracy of the measurement is estimated to be within 1.0 percent of the actual value.

²Indices of refraction were determined by the immersion method in sodium light using a spindle stage (Wilcox, 1959) and 0.002 interval liquids that were checked by

means of an Abbe refractometer at the indicated temperature of measurement. Measurements of $2V_\gamma$ and the relationships between principal indicatrix and crystallographic axes were obtained using a four-axis universal stage and Waldmann hollow-glass sphere filled with an immersion liquid of β index of refraction.

*Orientation: $Y = b$ with $Z \approx [101]$ in all cases. Following Schuster's rule, an extinction angle is given as positive if it is measured to a position in the acute angle between a and c , and negative if it is measured in the obtuse angle. Values are rounded to the nearest degree.

+X-ray measurement of the crystals was carried out using the precession method, and the measurements from the films were refined using least squares methods to get the best possible cell dimensions. Because of the close similarity between the a and c dimensions, it is possible for a type of twinning to occur in which a and c are interchanged, as observed by Braitsch (1959). Three of the crystals showed this twinning on the (010) plane; for these crystals the cell dimensions given are averages for the twins; that is, a is an average of a_1 and a_2 , b is an average of b_1 and b_2 , c is an average of c_1 and a_2 .

SPECTROPHOTOMETRIC DETERMINATION OF VANADIUM IN RUTILE AND IN MAFIC IGNEOUS ROCKS

By JOHN MARINENKO and LEUNG MEI, Washington, D.C.

Abstract.—Minor and major levels of vanadium in rutile are separated from titanium and iron by sample fusion with sodium carbonate followed by water leach and filtration. The filtrate is then acidified with hydrochloric acid. Silicates are decomposed with a mixture of hydrofluoric and hydrochloric acids, and iron is separated by extraction of its chloride with diethyl ether. Sample vanadium in hydrochloric acid is then quantitatively reduced to vanadium(IV) with sulfurous acid. The remaining sulfur dioxide is expelled by heating. Vanadium(IV) then is reacted with excess of iron(III) at reduced acidity (pH 5) in the presence of 1,10-phenanthroline to yield the orange-red iron(II) 1,10-phenanthroline complex. Iron(II) generated by vanadium(IV) is a measure of total vanadium in the sample. The proposed method is free from elemental interferences because the color development cannot take place without the two redox reactions described above, and these are, under the outlined experimental conditions, quantitative only for vanadium.

Vanadium is frequently present in titanium minerals in significant quantities (Watson 1912, 1922; Thornton 1927), and it must therefore be taken into account in the complete analysis of rutile.

A volumetric method by Hillebrand (1919), as applied by Thornton (1927) to vanadium determination in rutiles, is accurate but requires a sample size of about 5 g. The hydrogen peroxide method for vanadium in titanium ores (Codell, 1959) is accurate as well, but also requires large samples. A spectrophotometric phosphotungstovanadate method (Sandell, 1959, as modified by Meyrowitz, 1972), for analysis of vanadium in rutiles, requires matrix matching with respect to iron. Furthermore, at low levels of vanadium (less than 0.4 percent), deviations from Beer's law necessitate the addition of known amounts of vanadium to samples.

West and Conrad (1950) qualitatively estimated vanadium by means of a spot test. They reduced vanadate to vanadyl by heating with hydrochloric acid and then reacted vanadyl with ferric iron and 1,10-phenanthroline at reduced acidity. The orange-red ferrous 1,10-phenanthroline complex indicated a positive test for vanadium. Gottlieb (1951) developed a quantitative method for vanadium by utilizing this approach and applied it to the determination of vanadium in alloys and slags. We have extended this quantitative application to the determination of total vanadium in rutile and basic silicate rocks.

REAGENTS

Sodium carbonate, anhydrous powder.

Hydrochloric acid, 6 *M*.

Ammonium acetate, 50-percent (w/v) aqueous solution.

1,10-phenanthroline, 0.25-percent (w/v) aqueous solution.

Iron(III) solution, 250-ppm Fe_2O_3 . Dissolve 151 mg of ferric alum, $\text{FeNH}_4(\text{SO}_4)_2 \cdot 12\text{H}_2\text{O}$, in 100 ml of 1 *N* H_2SO_4 .

Sulfurous acid. Prepare daily by saturating water with sulfur dioxide.

Concentrated V_2O_5 standard, 250 ppm V_2O_5 , 0.2 *N* in H_2SO_4 . Dissolve 160.8 mg of ammonium metavanadate, NH_4VO_3 , in 50 ml of water containing 2.8 ml of concentrated H_2SO_4 . Transfer to a 500-ml volumetric flask and make up to volume with distilled water.

Working V_2O_5 standard, 10-ppm V_2O_5 , 6 *M* in HCl. Dilute the concentrated standard 25-fold with 6 *M* HCl.

PROCEDURE FOR RUTILE

Fuse 0.100 to 0.200 g of sample with 1 g of Na_2CO_3 in a 30-ml platinum crucible. Cool, add 25 ml of water, cover, and heat on a steam bath for 1 h, with occasional stirring. Filter while hot, using retentive filter paper, into 200-ml volumetric flask. Wash the precipitate several times with distilled water. Add 100 ml of concd HCl to the filtrate and heat on the steam bath for about 1 h to expel carbon dioxide. Cool, and make up to volume with distilled water.

Place a 10.0-ml aliquot of the sample solution and 0 to 100 μg (0–10 ml) of V_2O_5 standards into 50-ml beakers. Add enough 6 *M* HCl as required to the beakers so that each contains 10 ml of acid. Add 1 ml of iron(III) solution, 5 ml of H_2SO_3 , and evaporate to a volume of about 2 ml on a hotplate having a surface temperature of about 250°C. At this stage all the vanadium is converted to the quadrivalent state by sulfur dioxide, excess sulfur dioxide is expelled, and all iron is oxidized to a trivalent state.

Cool, add 1 ml of 1,10-phenanthroline reagent and 10 ml of $\text{CH}_3\text{COONH}_4$ solution and quantitatively transfer the solutions to 25-ml volumetric flasks, washing the beakers several times with small volumes of distilled water. Make up to volume with distilled water and mix. Measure the absorbance

at 510 nm in 1-cm cells, using distilled water as the reference. Compute the vanadium content of the sample by relating sample absorbance to that of standards.

PROCEDURE FOR SILICATES

Weigh a 1.000-g sample into a 50-ml heavy-walled linear polyethylene beaker. Moisten with water, add 100 ml of concd HCl and 20 ml of HF. Stir well with a plastic or platinum stirring rod and evaporate on a steam bath to dryness. Add 10 ml of 1+1 HCl and evaporate to dryness. Repeat this step twice.

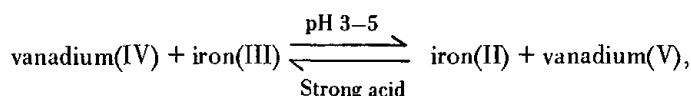
Add 25 ml of 1+1 HCl, cover, and heat on steam bath, stirring occasionally until salts are dissolved. Cool, extract three times with 20 ml of diethyl ether. Discard the organic layer and heat the aqueous layer in a 100-ml Pyrex beaker to expel any of the dissolved ether. Cool, transfer to 50-ml volumetric flask and make up to volume with 1+1 HCl.

Transfer a 5- to 10-ml aliquot of sample solution into a 50-ml Pyrex beaker, add 1 ml of iron(III) solution, and then proceed with the sulfurous acid reduction and color development as described above in the procedure for rutile.

RESULTS AND DISCUSSION

Filtration after sodium carbonate decomposition of rutile separates vanadium from iron and titanium. Mixed acid decomposition of silicates ensures expulsion of silica. Most of the iron in silicate rocks is extracted with diethyl ether. Small amounts of the remaining sample iron do not interfere.

The reversible equilibrium reaction,



yields iron(II) at pH values greater than 3; iron(III) when acidity is increased. The iron(II) thus generated is equivalent to the vanadium(IV) present. Therefore, the iron(II) equivalent of vanadium(IV), determined with 1,10-phenanthroline, is a measure of total vanadium.

The recovery of vanadium by the proposed method was established for pure solutions by measuring the degree of completion of two reactions (reduction of microgram quantities of vanadium(V) to vanadium(IV) by sulfur dioxide in hydrochloric acid, and the color development reaction at reduced acidity with excess of iron(III) and 1,10-phenanthroline). The results are shown in table 1. Columns A and B of the table represent routine total-iron measurement with 1,10-phenanthroline (excess of hydroxylamine hydrochloride is used as reducing agent for iron). This measurement is assumed to be quantitative for iron. Columns C and D represent vanadium measurement by the procedure outlined in this paper in which the standard vanadium serves as reducing agent for iron. It can be seen from the agreement (less than 2-percent difference) of values 1.16 and 1.14 in the note to

Table 1.—Spectrophotometric comparison between iron(II) 1,10-phenanthroline prepared from known iron(III) plus excess hydroxylamine hydrochloride and iron(II) 1,10-phenanthroline prepared from known vanadium plus excess iron(III) as described by the proposed method

Known iron plus excess hydroxylamine hydrochloride		Known vanadium plus excess iron(III)	
$\mu\text{g Fe}_2\text{O}_3$ (A)	$\mu\text{g Fe}_2\text{O}_3/\text{absorbance}^1$ (B)	$\mu\text{g V}_2\text{O}_5$ (C)	$\mu\text{g V}_2\text{O}_5/\text{absorbance}^1$ (D)
40.8	177
81.6	178
102.1	178	30	210
.....	60	203
.....	90	207
.....	100	206

¹ Solution volume, 25 ml; optical cell length, 1 cm; wavelength of absorption, 510 nm; pH of solution, 5.

Note: $\frac{\mu\text{g V}_2\text{O}_5/\text{absorbance}}{\mu\text{g Fe}_2\text{O}_3/\text{absorbance}} = 1.16$; $\frac{\text{mol. wt V}_2\text{O}_5}{\text{mol. wt Fe}_2\text{O}_3} = 1.14$.

table 1 that the effect of the sum of the two reactions used in this procedure, with respect to the vanadium determination, is quantitative. The proposed method is rapid and accurate. As little as 0.05 percent of total vanadium in rutile and 0.005 percent in silicates can be quantitatively determined.

Preliminary data indicate that vanadium in ilmenites can be determined as well. Titanium minerals with high iron content such as ilmenite should be decomposed with a mixture of one part sodium hydroxide to five parts sodium peroxide. Zirconium crucibles should be used for this decomposition. Vanadium is then determined in the water leach according to the procedure described above for rutile.

This method was tested for accuracy and precision on two rutiles and two USGS standard rocks. The data are presented in table 2. Total vanadium found by the proposed method in

Table 2.—Total vanadium content, in percentage, of two rutiles and two USGS standard silicate rocks, as determined by iron (III) 1,10-phenanthroline reagent and by other methods

Sample	Proposed method ¹	Other methods
Total vanadium as V_2O_5		
U.S. Bureau of Mines rutile substitute 1-250-F.	0.39	² 0.30, 0.26
New South Wales Rutile Mining Co., Ltd., rutile concentrate.	.46	² 0.41, 0.44
Total vanadium as V		
Andesite AGV-1	0.0123 .0130 .0124	³ 0.0125
Basalt BCR-10432 .0410 .0413	³ .0399

¹ Five determinations for rutile substitute and six determinations for rutile concentrate. Standard deviation for both samples was 0.01.

² Codell (1959).

³ Flanagan (1973).

rutiles is compared with total vanadium found in these two samples by present authors using the hydrogen peroxide method of Codell. Total vanadium found by the proposed method in silicate rocks is compared with the published values (Flanagan, 1973).

REFERENCES CITED

- Codell, Maurice, 1959, Analytical chemistry of titanium metals and compounds: New York, Interscience Publishers, 378 p.
- Flanagan, F. J., 1973, 1972 values for international geochemical reference samples: *Geochim. et Cosmochim. Acta*, v. 37, no. 5, p. 1189-1200.
- Gottlieb, A., 1951, o-Phenanthroline als Reagens zur quantitativen Bestimmung des Vanadiums: *Mikrochemie*, v. 36-37, p. 360-378.
- Hillebrand, W. F., 1919, The analysis of silicate and carbonate rocks: U.S. Geol. Survey Bull. 700, 285 p.
- Meyrowitz, Robert, 1972, Chemical analysis of rutile—direct spectrophotometric determination of titanium, total iron, niobium, phosphorus, and vanadium: U.S. Geol. Survey Prof. Paper 800-B, p. B157-B164.
- Sandell, E. B., 1959, Colorimetric determination of traces of metals [3d ed.]: New York, Interscience Publishers, 1,032 p.
- Thornton, W. M. 1927, Titanium, with special reference to the analysis of titaniferous substances: *Am. Chem. Soc. Mon. Ser.*, 262 p.
- Watson, T. L., 1912, Vanadium and chromium in rutile and the possible effects of vanadium on color: *Washington Acad. Sci. Jour.*, v. 2, p. 431-434.
- 1922, Rutile-ilmenite intergrowths: *Am. Mineralogist*, v. 7, no. 11, p. 185-188.
- West, P. W., and Conrad, L. J., 1950, Detection of vanadium by means of spot tests: *Mikrochemie*, v. 35, p. 443-448.

RUBIDIUM-STRONTIUM DATING OF THE TRONDHJEMITE OF RIO BRAZOS, NEW MEXICO, AND OF THE KROENKE GRANODIORITE, COLORADO

By FRED BARKER, Z. E. PETERMAN, W. T. HENDERSON,¹ and R. E. HILDRETH, Denver, Colo.

Abstract.—The quartz-eye trondhjemite and associated hornblendite near Rio Brazos, Brazos Peak quadrangle, New Mexico, and the Kroenke Granodiorite of the Mount Harvard quadrangle and Sawatch Range, Colo., lie on an approximate 1,700-m.y. Rb-Sr isochron. Their initial $^{87}\text{Sr}/^{86}\text{Sr}$ ratio is about 0.7026. Six samples of the trondhjemite of Rio Brazos contain 8–43 ppm Rb and 57–194 ppm Sr, and six of the Kroenke intrusive, 53–99 ppm Rb and 314–595 ppm Sr. The Rio Brazos intrusive contains more SiO_2 but less Al_2O_3 and K_2O than does the Kroenke intrusive. The hornblendite contains much MgO and CaO but is low in alkalis; two samples show 2.5–3.2 ppm Rb and 288–431 ppm Sr. These rocks are of the same general age as the much more abundant, typically calc-alkaline Boulder Creek Granodiorite and associated intrusives of Colorado and northern New Mexico.

The intrusive rocks of 1,700- to 1,750-m.y. age of Colorado and northern New Mexico are typically of calc-alkaline type. This terrane, however, does contain a few scattered bodies of trondhjemite or leucogranodiorite, which are now under geochemical study in the U.S. Geological Survey laboratories at Denver. This paper presents results on the Rb-Sr chronology, major elements, and petrography of two of these trondhjemite intrusives—the stock of quartz-eye trondhjemite of Rio Brazos, Brazos Peak quadrangle, in northern New Mexico (lat $36^\circ 50'$ N., long $106^\circ 15'$ W.), and the batholith of Kroenke Granodiorite of the central Sawatch Range, Mount Harvard quadrangle, central Colorado (lat $39^\circ 00'$ N., long $106^\circ 15'$ W.).

The term “trondhjemite” is used to denote rocks that mainly are leucoquartz diorites whose plagioclase is either oligoclase or albite. The mafic silicates may be either biotite or hornblende, or both, although biotite is typical.

TRONDHJEMITE AND HORNBLENDITE OF RIO BRAZOS

The quartz-eye trondhjemite of the Brazos Peak quadrangle, here termed the trondhjemite of Rio Brazos after exposures in that drainage, was discovered and mapped by Muehlberger (1968). This body underlies at least 30 km^2 (12 mi^2) (fig. 1), and its northern extent is not known because of Tertiary cover. The trondhjemite is mostly homogeneous, light gray, and fine

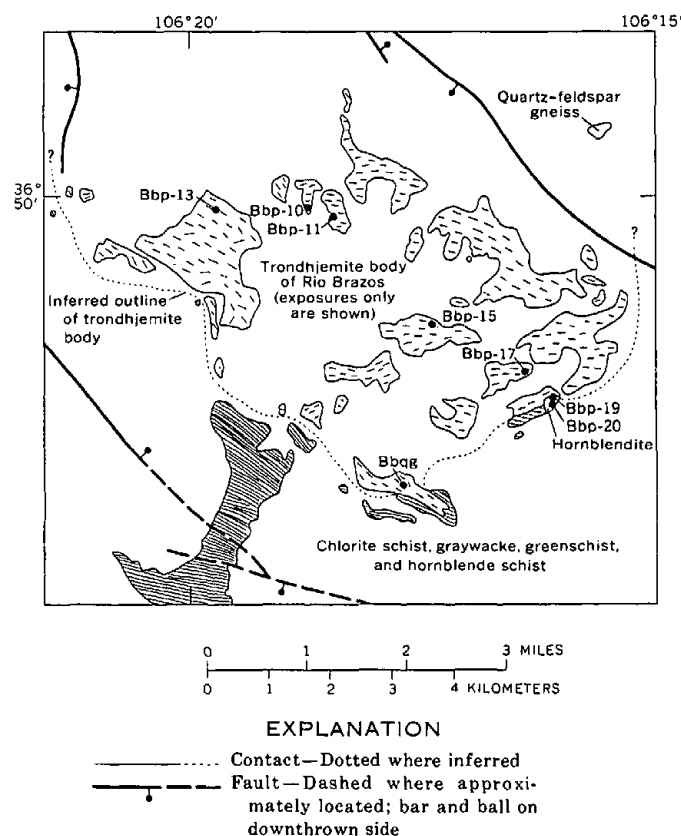


Figure 1.—Geologic sketch map of the Rio Brazos area, New Mexico, (modified from Muehlberger, 1968), showing sample localities. Unpatterned areas indicate Tertiary rocks and surficial deposits. Strike of foliation indicated by direction of trondhjemite pattern. The trondhjemite intrusive body is surrounded by wallrock of chlorite schist, graywacke, greenschist, and hornblende schist. Only exposures of the wallrock (lined pattern) are shown.

to medium grained. Ovoid to subhedral blue-gray quartz eyes, typically 6–12 mm in size but as large as 20 mm, form about 5 percent of most of the trondhjemite. Most of the eyes are recrystallized to aggregates of smaller grains and are interpreted as being relict phenocrysts. Figure 2 shows a quartz eye. Some of the trondhjemite consists of quartz eyes and blocky, subhedral plagioclase (calcic to median albite) grains

¹ Deceased, June 16, 1974.

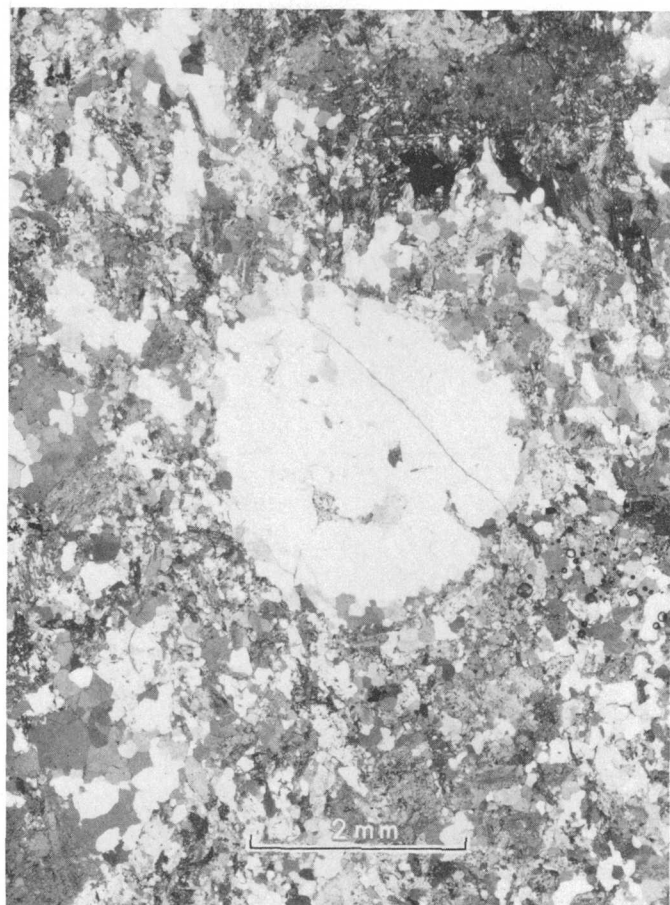


Figure 2.—Photomicrograph of quartz eye in trondhjemite of Rio Brazos. Eye is about 2.6 mm in diameter. Small embayments, as shown in this eye, are common.

set in a fine-grained, wholly recrystallized groundmass; the remainder shows a seriate, inequigranular fabric. The trondhjemite is foliated and has been subjected to metamorphism of lower amphibolite facies. Blue-green hornblende, epidote, biotite, chlorite, microcline, and white mica are other stable phases. Modal compositions are given in table 1. Local zones, as near the sample Bbp-13 (fig. 1), of small inclusions of medium- to dark-gray, fine-grained plagioclase-hornblende-quartz-epidote rock and amphibolite are found.

Attitudes of foliation are parallel or subparallel to schistosity of the wallrocks, which are chlorite schist, graywacke, green-schist, and hornblende schist. We infer that the trondhjemite was deformed and metamorphosed with its wallrocks. We found no exposures of the contact of trondhjemite and wall-rock. The homogeneity, absence of layering, and relatively coarse grain size of the trondhjemite suggest that it was emplaced under hypabyssal or plutonic conditions. Origin as a thick volcanic flow is improbable, but cannot be disproved.

Hornblende forms a small body (fig. 1) at the southeastern margin of the trondhjemite. Its contact with the trondhjemite, however, is not exposed, and so the relative ages of these two

Table 1.—Average chemical and modal analyses of trondhjemite and hornblende of Rio Brazos and of Kroenke Granodiorite

[Analysts: Paul Elmore, James Kelsey, H. Smith, John Glenn, Gillison Chloe, and Violet Merritt. All constituents except Na_2O and K_2O were determined by flame photometer. Tr, trace]

Constituent	Rio Brazos		Kroenke
	Trondhjemite	Hornblende	Granodiorite
Chemical analyses			
[Average of 6 analyses of trondhjemite, 2 of hornblende, and 9 of Kroenke Granodiorite]			
SiO ₂	75.4	46.7	70.4
Al ₂ O ₃	13.7	11.7	16.1
Total Fe as FeO	2.0	10.5	2.1
MgO33	13.3	.65
CaO	1.5	13.8	2.3
Na ₂ O	4.3	.38	4.8
K ₂ O	1.5	.18	2.6
H ₂ O8	1.6	.7
TiO ₂12	.30	.29
P ₂ O ₅04	.09	.08
MnO04	.23	.07
CO ₂18	.07	<.05
Modal analyses			
[Average of 6 analyses of trondhjemite, 2 of hornblende, and 6 of Kroenke Granodiorite]			
Quartz	41	29
Plagioclase	39	49
K-feldspar	4	16
Biotite	4	6
Chlorite	Tr	2	
White mica	8
Hornblende	Tr	72
Epidote	2	25	Tr
Sphene	Tr
Fe-Ti oxides	Tr	Tr	Tr
Apatite	Tr	Tr	Tr
Allanite	Tr
Calcite-Siderite	Tr

rock types are not known. The hornblende is dark green, massive, and homogeneous except for small stringers and irregular concentrations of epidote. It consists almost entirely of stubby prisms of hornblende, 5–15 mm in size, and interstitial anhedral epidote. Table 1 gives the average modal composition. This rock, like the trondhjemite, underwent metamorphism, and all its original plagioclase was transformed to epidote.

Averages of six chemical and modal analyses of the trondhjemite of Rio Brazos are given in table 1, as well as averages of analyses of two hornblende samples. The major element content of the trondhjemite is notable for several features: SiO_2 is high, 75.4 percent; Al_2O_3 is low, 13.7 percent; and K_2O is low, 1.5 percent. The hornblende's composition is different from that of any basaltic or gabbroic rock, especially its Al_2O_3 content of 11.7 percent and its Na_2O content of 0.38. This rock may be a cumulate, formed by the gravitational settling of hornblende and plagioclase from a more sili-

ceous liquid, and so a liquid of this composition may never have existed here.

Abundances of Rb and Sr and ratios of $^{87}\text{Rb}/^{86}\text{Sr}$ and $^{87}\text{Sr}/^{86}\text{Sr}$ of both trondhjemite and hornblende of the Rio Brazos area are given in table 2. These results were determined

Table 2.—Rb-Sr abundances and isotopic ratios

Sample	Rb (ppm)	Sr (ppm)	⁸⁷ Rb/ ⁸⁶ Sr	⁸⁷ Sr/ ⁸⁶ Sr	Regression
Trondhjemite and hornblendite of Rio Brazos					
Bbqg	8.23	132	0.180	0.7073	All samples: 1,724±34 m.y. (⁸⁷ Sr/ ⁸⁶ Sr) ₀ = 0.7026±0.0002
Bbp-10	43.2	68.9	1.820	.7453	
11	39.0	59.8	1.896	
	39.5	59.7	1.925	.7480	
13	13.3	189	.203	
	13.4	194	.200	.7082	Trondhjemite only: 1,690±24 m.y. (⁸⁷ Sr/ ⁸⁶ Sr) ₀ = 0.7032±0.0002
15	19.3	99.4	.564	
	19.1	96.9	.571	.7165	
17	43.3	57.4	2.196	.7569	
19*7030	
	3.22	288	.0324	.7031	
20*	2.5	431	.0234	.7028	
Kroenke Granodiorite					
Bf-176a . . .	52.7	595	0.257	0.7092	1,700±58 m.y. (⁸⁷ Sr/ ⁸⁶ Sr) ₀ = 0.7027±0.0003
301	55.2	582	.275	.7094	
302	77.6	568	.395	.7123	
303	98.8	314	.912	.7246	
304	56.2	518	.314	.7098	
305	69.1	518	.347	.7108	

*Hornblende samples.

by the techniques described by Peterman, Doe and Bartel (1967). All samples give an apparent isochron age of 1,724±34 m.y. and an initial $^{87}\text{Sr}/^{86}\text{Sr}$ ratio of 0.7026±0.0002, as shown in figure 3. Values for the trondhjemite only are 1,690±24 m.y. and 0.7032±0.0002, respectively. Uncertainties are 1σ. These data and the geologic relations do not enable us to say whether the 1,724-m.y. apparent age is an age of metamorphism or of crystallization of the magma.

KROENKE GRANODIORITE

The Kroenke Granodiorite was named by Barker and Brock (1965) from exposures at Kroenke Lake in the Mount Harvard quadrangle; the geologic map of that quadrangle has since been published (Brock and Barker, 1972). The Kroenke Granodiorite forms several small to large plutons of about 125-km² (50-miles²) aggregate area (fig. 4). Scattered masses of similar rock recently have been mapped in reconnaissance to the north and northwest by J. C. Reed, Jr., and R. H. Moench (unpub. data, 1973).

The Kroenke Granodiorite is light gray and typically medium grained, and it ranges in composition from trondhjemite to leucoquartz monzonite (Barker and Brock, 1965). Its average mode is given in table 1. The plagioclase typically is calcic oligoclase. In its wallrocks, which typically are brecciated in a zone 2–30 m (7–100 ft) thick along the contact, the Kroenke sharply crosscuts all structures. Steep contacts are the rule, but attitudes less than 30° are found north of Kroenke Lake (Brock and Barker, 1972). Chilled margins are

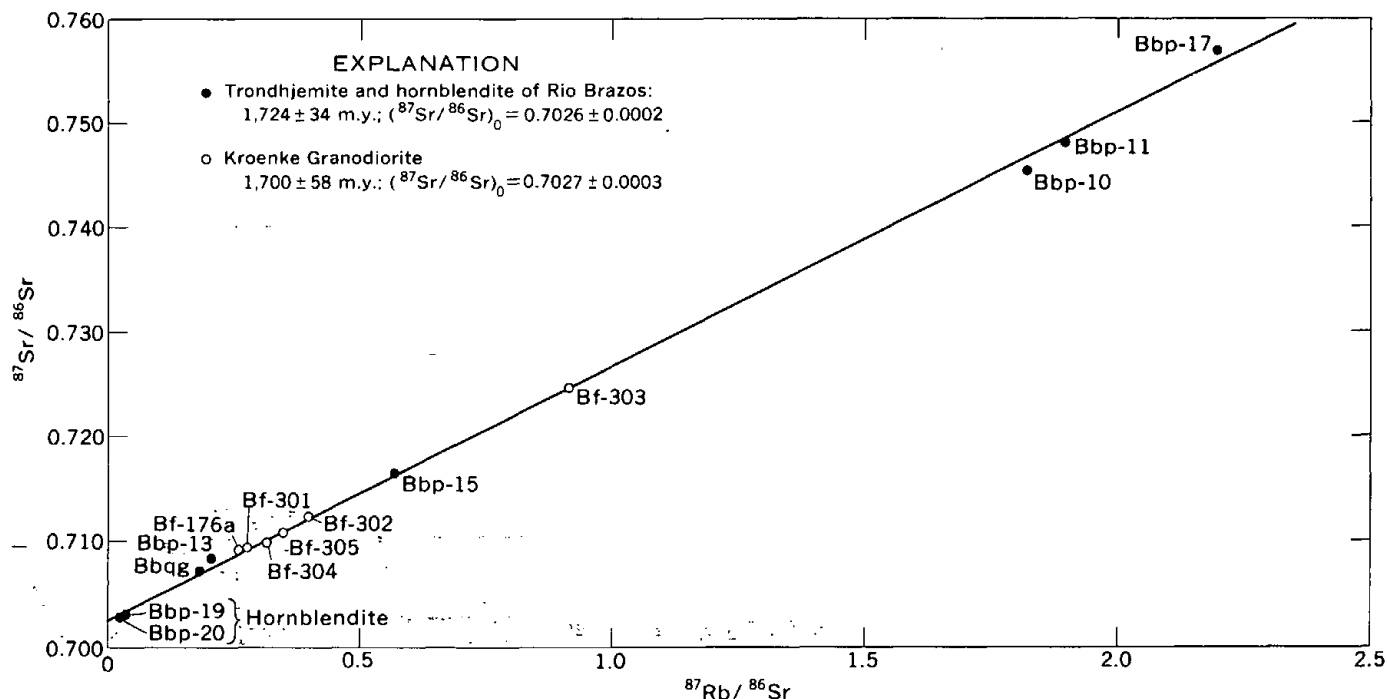


Figure 3.—Rb-Sr isochron diagram of the trondhjemite and hornblende of Rio Brazos, N. Mex., and of the Kroenke Granodiorite, Colo.

found along parts, but not all, of the contact of the Kroenke with its walls. Much of the Kroenke Granodiorite probably is postkinematic.

In many of its outcrops the Kroenke is relatively homogeneous, but small swirl structures that are defined by concentrations of biotite are common. Locally, as in the cliffs 1 km (0.6 mi) southwest of Cloyes Lake, dark biotite-rich, well-foliated bands or lenses of quartz diorite are intimately cross-cut by light-colored biotite-poor, massive trondhjemite. Many of the dark bands are bent. These structures, considered in conjunction with the systematic trend from quartz dioritic to granitic compositions shown by nine samples on a normative quartz-albite-orthoclase plot (Barker and Peterman, unpub. data, 1974), suggest that the darker quartz diorite locally crystallized first, was synkinematically fractured, and that more siliceous and potassic differentiates were injected into these fractures from adjacent and still-liquid regions of the pluton. An excellent example of a similar relationship in the Donegal Granite in Ireland has been documented by Berger (1971).

Synkinematic injection of Kroenke magma also is indicated by the 2-km (1.2 mi)-broad body of trondhjemite in the Ptarmigan Creek drainage, south-central Mount Harvard quadrangle (Brock and Barker, 1972). This mass shows an excellent foliation parallel to that in the wallrocks and also to the contact itself, and its overall shape is antiformal. We interpret it to be a synkinematically injected phacolith.

Tables 1 and 2 indicate that the average Kroenke Granodiorite contains less SiO_2 but more Al_2O_3 , K_2O , CaO , Sr , and Rb than the trondhjemite of Rio Brazos. These differences and other data (Barker, Peterman, and Hansen, 1973; Barker, Arth, and Peterman, 1973) imply genesis of the Rio Brazos magma by partial melting of gabbro at relatively shallow depth and of the Kroenke magma by partial melting of quartz eclogite or garnet amphibolite at depths greater than about 60 km (35 mi).

Our Rb-Sr isotopic data (table 2) indicate that the Kroenke Granodiorite is about 1,700 m.y. old and had an initial $^{87}\text{Sr}/^{86}\text{Sr}$ ratio of about 0.7027. The Rb:Sr ratios of the six measured samples are less than 1 and these samples, considered alone, give an isochron with an uncertainty of almost 60 m.y. (fig. 4).

DISCUSSION OF RESULTS

These two approximate ages of 1,700 and 1,724 m.y. thus place the Rio Brazos and Kroenke intrusives in the Boulder Creek event, which is defined by results on the type, synkinematic, generally calc-alkaline, granodioritic and quartz monzonitic Boulder Creek intrusives of the northern Front Range (T. W. Stern, in U.S. Geological Survey, 1964, p. A95; Stern and others, 1971; Peterman and Hedge, 1968; and Peter-

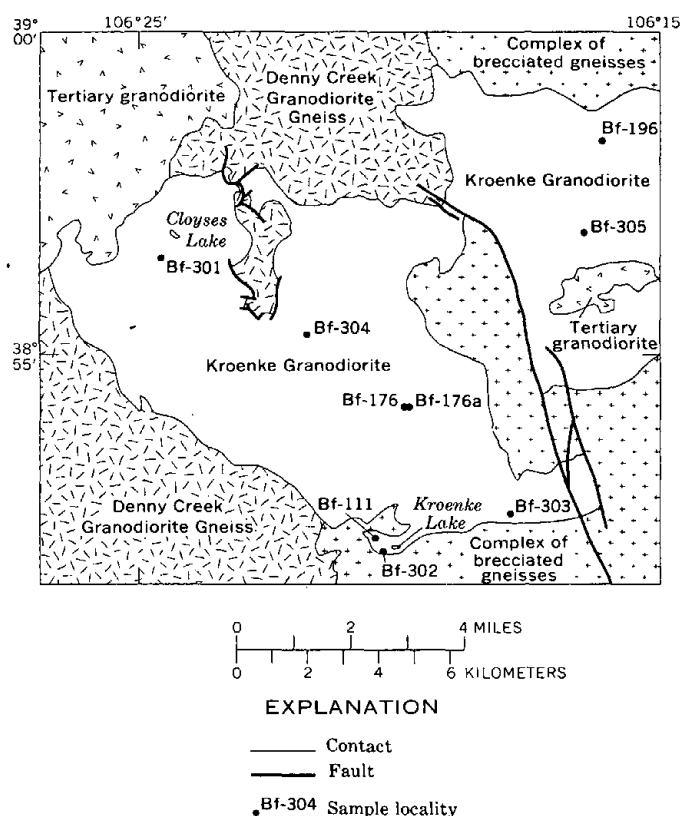


Figure 4.—Geologic sketch map of rocks mostly of Precambrian age in the northeastern part of the Mount Harvard quadrangle, Colorado, showing sample localities (from Brock and Barker, 1972). Samples numbered Bf-111, Bf-176, and Bf-196 are from Barker and Brock (1965).

man and others, 1968). Occurrence of intrusives of this general age has been demonstrated in the Sawatch Range (Wetherill and Bickford, 1965), in the Black Canyon of the Gunnison (Hansen and Peterman, 1968), in the northern Uncompahgre uplift (Hedge and others, 1968), and in the Needle Mountains (Silver and Barker, 1968; Bickford and others, 1969).

Two other masses of trondhjemitic composition are found in southwestern Colorado. The Pitts Meadow Granodiorite of the Black Canyon of the Gunnison was dated by Hansen and Peterman (1968) by the Rb-Sr technique at $1,730 \pm 190$ m.y., and the extrusive Twilight Gneiss was determined by Silver and Barker (1968) by U-Pb analyses of zircon to be $1,760 \pm 20$ m.y. and by Barker, Peterman, and Hildreth (1969) by the Rb-Sr method to be $1,805 \pm 35$ m.y. L. A. Woodward (oral commun., 1973) has reported discovery of trondhjemitic rocks in the Nacimiento uplift of New Mexico. These rocks have not yet been dated, but no trondhjemitic rocks younger than about 1,700 m.y. are known to occur in the Precambrian of Colorado or northern New Mexico.

REFERENCES CITED

- Barker, Fred, and Brock, M. R., 1965, Denny Creek Granodiorite Gneiss, Browns Pass Quartz Monzonite, and Kroenke Granodiorite, Mount Harvard quadrangle, Colorado: U.S. Geol. Survey Bull. 1224-A, p. A23-A26.
- Barker, Fred, Arth, J. G., and Peterman, Z. E., 1973, Geochemistry of Precambrian trondhjemites of Colorado and northern New Mexico—Evidence for subduction? [abs.]: *Am. Geophys. Union Trans.*, v. 54, no. 11, p. 1220-1221.
- Barker, Fred, Peterman, Z. E., and Hansen, W. R., 1973, Trondhjemitic magmatism in the Precambrian of southern Colorado and northern New Mexico: *Geol. Soc. America Abs. with Programs*, v. 5, no. 6, p. 462-463.
- Barker, Fred, Peterman, Z. E., and Hildreth, R. A., 1969, A rubidium-strontium study of the Twilight Gneiss, West Needle Mountains, Colorado: *Contr. Mineralogy and Petrology*, v. 23, no. 4, p. 271-282.
- Berger, A. R., 1971, The origin of banding in the Main Donegal Granite, N.W. Ireland: *Geol. Jour.*, v. 7, pt. 2, p. 347-358.
- Bickford, M. E., Barker, Fred, Wetherill, G. W., and Lee-Hu, Chin-Nan, 1969, Precambrian Rb-Sr chronology in the Needle Mountains, southwestern Colorado: *Jour. Geophys. Research*, v. 74, p. 1660-1676.
- Brock, M. R., and Barker, Fred, 1972, Geologic map of the Mount Harvard quadrangle, Chaffee and Gunnison Counties, Colorado: U.S. Geol. Survey Geol. Quad. Map GQ-952.
- Hansen, W. R., and Peterman, Z. E., 1968, Basement-rock geochronology of the Black Canyon of the Gunnison, Colorado, in *Geological Survey research 1968*: U.S. Geol. Survey Prof. Paper 600-C, p. C80-C90.
- Hedge, C. E., Peterman, Z. E., Case, J. E., and Obradovich, J. D., 1968, Precambrian geochronology of the northwestern Uncompahgre Plateau, Utah and Colorado, in *Geological Survey research 1968*: U.S. Geol. Survey Prof. Paper 600-C, p. C91-C96.
- Muehlberger, W. R., 1968, Geology of Brazos Peak quadrangle, New Mexico: New Mexico Bur. Mines and Mineral Resources Geol. Map 22.
- Peterman, Z. E., Doc, B. R., and Bartel, Ardith, 1967, Data on the rock GSP-1 (granodiorite) and the isotope-dilution method of analysis for Rb and Sr, in *Geological Survey research 1967*: U.S. Geol. Survey Prof. Paper 575-B, p. B181-B186.
- Peterman, Z. E., and Hedge, C. E., 1968, Chronology of Precambrian events in the Front Range, Colorado: *Canadian Jour. Earth Sci.*, v. 5, no. 3, pt. 2, p. 749-756.
- Peterman, Z. E., Hedge, C. E., and Braddock, W. A., 1968, Age of Precambrian events in the northeastern Front Range, Colorado: *Jour. Geophys. Research*, v. 73, no. 6, p. 2277-2296.
- Silver, L. T., and Barker, Fred, 1968, Geochronology of Precambrian rocks of the Needle Mountains, southwestern Colorado—Pt. 1, U-Pb zircon results [abs.]: *Geol. Soc. America Spec. Paper* 115, p. 204-205.
- Stern, T. W., Phair, George, and Newell, M. F., 1971, Boulder Creek batholith, Colorado, Pt. 2—Isotopic age of emplacement and morphology of zircon: *Geol. Soc. America Bull.*, v. 82, no. 6, p. 1615-1634.
- U.S. Geological Survey, 1964, *Geological Survey research 1964*: U.S. Geol. Survey Prof. Paper 501-A, 367 p.
- Wetherill, G. W., and Bickford, M. E., 1965, Primary and metamorphic Rb-Sr chronology in central Colorado: *Jour. Geophys. Research*, v. 70, no. 18, p. 4669-4686.

CONTINENTAL DEPOSITION OF ANTARCTIC TILLITE INDICATED BY CARBON AND OXYGEN ISOTOPES

By D. L. SCHMIDT and IRVING FRIEDMAN, Saudi Arabia, Denver, Colo.

Abstract.—Freshwater deposition of the upper Paleozoic, Gondwana tillite in the Pensacola Mountains is indicated by low δ values of +4.9 to +6.1 permil δO^{18} (SMOW) and -1.8 to -15.9 permil δC^{13} (PDB) in primary sedimentary calcite within the tillite. In contrast, Cambrian marine limestone from the Pensacola Mountains contains heavy isotopic abundances that are entirely characteristic of marine deposition.

The Devonian to Jurassic Beacon sedimentary rocks of the Transantarctic and Ellsworth Mountains, Antarctica (fig. 1), are commonly considered to be mostly continental deposits (Ford, 1964; Adie, 1964). Disagreements arise especially for some deposits below the continental Gondwanan coal measures of the middle and later parts of the Permian (Rigby and Schopf, 1969). Yet the location of transitions between continental and marine facies of the Beacon deposits in Antarctica and similar deposits on other southern continents is important to the reconstruction of Mesozoic Gondwanaland. The upper Paleozoic Gondwana tillites are particularly critical because they occur as widespread stratigraphic markers on all the southern continents (Frakes and Crowell, 1968; Schopf, 1970). These tillites, however, are difficult to interpret because they rarely contain fossils and because the processes of deposition of their principal constituent, diamictite ("pebbly mudstone"), are poorly understood.

In an attempt to determine whether the Carboniferous(?) and Lower Permian Gondwana glacial formation of the Pensacola Mountains, the Gale Mudstone, is of marine or nonmarine origin, 11 calcite samples from the Gale were analyzed for carbon and oxygen isotope abundances (table 1). The glacial origin of the Gale Mudstone (Schmidt and Williams, 1969; Williams, 1969) is not in question; the Gale contains the formational and regional characteristics of a large glacial deposit. The floor of the Gale and several boulder pavements within the formation display uniformly north-south striae that imply a consistent regional iceflow (Frakes and others, 1966). Regional considerations and sedimentary structures in the Gale rocks, notably the disruption of some of the stratified sandstone layers and the common soft-sediment deformational features, have led Frakes and Crowell (1968) to suggest that the diamictites may be reworked mass-movement deposits of glacial marine origin. A marine environment,

however, is inconsistent with the carbon and oxygen abundances of primary calcite in the Gale Mudstone. The massive diamictites therefore are believed to be tillites deposited directly from ice on the continent, and the stratified layers are probably fluvial and lacustrine deposits.

Calcite is a minor primary constituent in the Gale Mudstone, if detrital limestone is excluded. The calcite was penecontemporaneously precipitated by the same water that deposited the stratified sediments in the Gale.

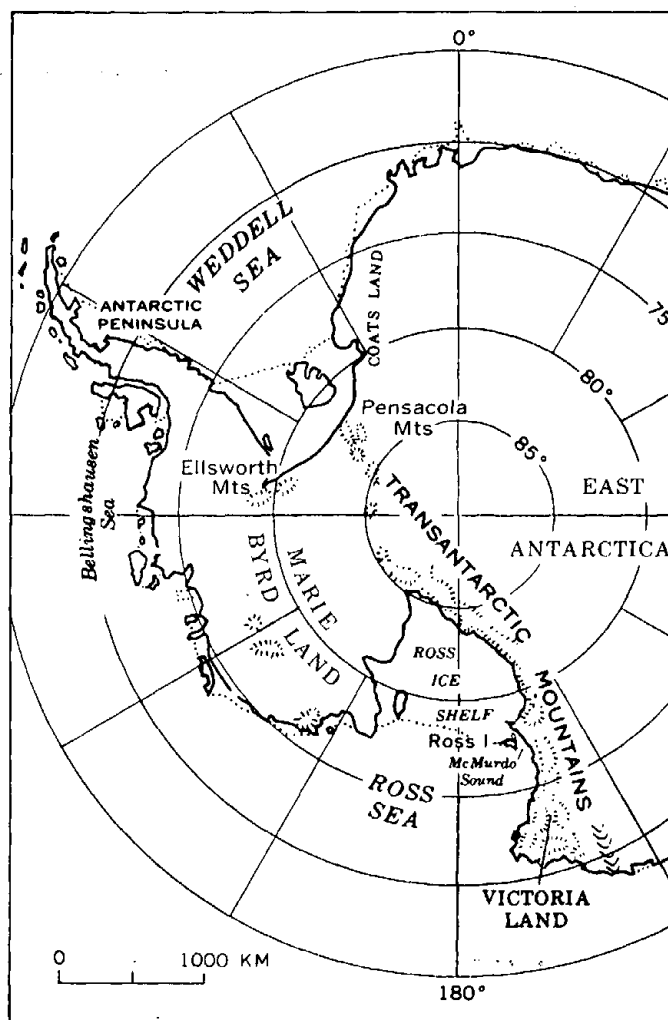


Figure 1.—Location of Pensacola Mountains in Antarctica.

Three petrographically identifiable types of calcite were sampled for carbon and oxygen isotope analysis. **Microcrystalline calcite** (type A, table 1) is clay size, contains clay-sized rock impurities (glacial rock flour), and occurs locally as thin well-laminated beds intimately interbedded with some thin glacial silt beds in the stratified layers. **Fracture-filling calcite** (type B) consists of fine- to medium-grained equigranular crystals filling small, roughly radial, compaction fractures of local origin in massive tillite. **Sparry calcite** (type C) consists of black, coarse-grained poikilitic crystals that locally in part filled initial pore space and in part replaced initial silty matrix in the stratified sandstone and conglomerate.

The black calcic sandstone-conglomerate bodies are small, one to several meters across, angular, and irregularly shaped. A sharp border between calcic and noncalcic rock erratically cuts across obviously more and less permeable layers in the sandstone and conglomerate without regard for permeability. The calcic boundaries were two-solution interfaces whose scale is commensurate with variable local conditions during sediment deposition rather than with regional-scale deuteric alteration.

Abundant petrographic and field evidence suggests that all three types of calcite are primary and most likely have a common origin despite their contrastingly different physical settings. A primary origin is strikingly demonstrated in the field where the stratified layers were broken during superseding glaciation and the transported and rotated blocks of the sandstone and conglomerate occur floating in the overlying tillite. In these blocks the black calcic sandstone-conglomerate bodies have been broken with the blocks, which clearly indicates that the calcite precipitation was prior to breakage and transportation.

A single origin for all three calcite types is best related to calcite precipitation from supersaturated solution during release of hydrostatic pressure at the base of the ice during glacial retreat, as has been demonstrated for Quaternary glaciers (Ford and others, 1970). The microcrystalline calcite, type A, was deposited during sedimentation of the stratified layers. The sparry calcite, type C, was deposited in partially openwork sand and gravel before normal diagenetic infilling and consolidation and positively before the consolidating pressures of the superseding glaciation that are represented by the overlying tillite. The fracture-filling calcite, type B, was precipitated synchronously with a natural volume change in the tillite such as might be caused by decompression and dewatering during deglaciation.

Fourteen other calcite samples from the Pensacola Mountains were analyzed for carbon and oxygen isotope abundances as a control on the isotopic results from the Gale Mudstone. Four calcite samples of dripstone and concretionary carbonate from upper Cenozoic moraines are associated with the present-day continental glaciation in the Pensacola Mountains. Ten calcite samples from Paleozoic sedimentary rocks, older than the Gale Mudstone, are from

ancient nonglacial environments. Also, one calcite sample, collected by Schmidt in 1963 from the Dwyka tillite at Nooitgedacht Farm, Kimberley, Cape Province, South Africa, was analyzed. The isotopic abundances are listed in table 1 and plotted in figure 2.

A composite stratigraphic column of the sedimentary and volcanic rocks of the Pensacola Mountains is shown in figure 2. The rocks comprise three stratigraphic sequences separated by angular unconformities that are related to three well-defined orogenies (Schmidt and others, 1965; Schmidt and Ford, 1970).

Carbon and oxygen isotopic abundances of carbonate sedimentary rocks commonly make it possible to distinguish between marine and nonmarine origins. In figure 2 the ranges of isotopic abundances are shown for each formation tested; the empirical limits (85 percent of all samples analyzed) for marine carbonates are also shown (Keith and Weber, 1964). The O^{18}/O^{16} ratios relative to the ratio for SMOW are given in δO^{18} values permil, and the C^{13}/C^{12} ratios relative to the ratio for the carbon in the reference standard (PDB) are given in δC^{13} values permil. Control samples from the Nelson, a marine limestone, and from modern continental glacial deposits have isotopic abundances that substantiate their known origins.

The δO^{18} value of a limestone depends on four factors: (1) Isotopic composition of the bulk water from which the calcite (or aragonite) is deposited. (2) isotopic equilibrium or disequilibrium between water and $CaCO_3$ during initial disposition. (3) temperature during $CaCO_3$ formation, and (4) postdepositional exchange with water of different isotopic composition and at a temperature possibly different from that of the original deposition. The O^{18} value depends largely on the O^{18} abundance of the bulk water at the time of limestone deposition; with equilibrium between water and calcite, the dependence is direct. Disequilibrium may occur when certain organisms influence carbonate precipitation but the resulting O^{18} values are usually not more than a few permil from the equilibrium value. Precipitation temperature is influential. Limestone formed in equilibrium with marine water at $0^\circ C$ is enriched in O^{18} by 34 permil relative to standard marine water (SMOW), whereas at $25^\circ C$ the enrichment is 28.5 permil. Hence the δO^{18} value of modern marine limestone precipitated at about $+10^\circ C$ is +32 permil.

Ancient marine limestones show a decrease in δO^{18} with increasing age (Keith and Weber, 1964). Recent evidence indicates that this decrease is mainly due to the change in δO^{18} of the oceans through geologic time and is not caused by postdepositional exchange between the carbonate and meteoric water, as had been suggested.

The δC^{13} values of marine carbonate range from -3 to +3 permil and do not ordinarily change significantly with age. The carbon isotope content in freshwater carbonates is much more variable since the sources of carbon chiefly are atmospheric CO_2 and organic carbon as discussed later.

Table 1.—Carbon and oxygen isotope abundances of calcites from upper Paleozoic tillite, Quaternary moraine, and Paleozoic sandstones and limestones from the Pensacola Mountains, Antarctica; one calcite sample from the Dwyka tillite of South Africa

No. ¹	δC^{13} (permil, PDB)	δO^{18} (permil, SMOW)	Calcite type ²	Calcite crystal size (mm)	Calcite content in sample (percent)	Description of calcite and rock	Formation	Age
1	-7.0	+5.6	A	0.004	50-90	Finely laminated microcrystalline limestone and siltstone in stratified layer.	Gale Mudstone . . .	late Paleozoic
2	-12.9	+5.5	A	<0.004	99	Thin microcrystalline limestone bed as a stratified layer. do	Do.
3	-2.6	+5.7	B	0.25	75	Granular calcite as fracture filling do	Do.
4	-1.9	+5.5	C	5	40	Coarse-grained poikilitic calcite matrix in silty sandstone. do	Do.
5	-2.4	+4.9	C	2-5	25	Coarse-grained poikilitic calcite matrix in silty sandstone. do	Do.
6	-10.6	+6.0	C	0.05	30	Granular calcite matrix in sandstone. do	Do.
7	-1.8	+5.9	C	1	99	Coarse-grained calcite nodule in massive tillite. do	Do.
8	-15.9	+5.7	A	<0.004	50	Microcrystalline calcite in stratified sandstone layer. do	Do.
9	-13.3	+5.3	C	1-3	30	Coarse-grained poikilitic calcite matrix in sandstone-conglomerate. do	Do.
10	-15.6	+5.2	C	40	30	Coarse-grained poikilitic calcite matrix in sandstone.	Dover Sandstone. . .	Devonian.
11	-12.2	+5.6	C	1-2	30	Coarse-grained poikilitic calcite matrix in sandstone. do	Do.
12	-3.1	+5.4	B	0.25	80	Granular calcite as fracture filling	Gale Mudstone . . .	late Paleozoic
13	-11.7	+6.1	C	0.5-1	20	Coarse-grained poikilitic calcite matrix in sandstone. do	Do.
15	-20.0	-11.8	≈100	Transported dripstone cementing moraine at base.	Young moraine . . .	Quaternary.
16	-20.2	-9.3	0.05×1	≈100	Transported dripstone cementing moraine at base. do	Do.
17	-28.5	-6.1	0.05	10-50	Transported calcite concretion cementing moraine. do	Do.
18	-12.8	-10.1	0.2	30	Transported calcite nodule cementing moraine. do	Do.
19	-12.8	+3.2	0.5	55	Coarse-grained poikilitic calcite matrix in siltstone at base of boulder tillite.	Dwyka Formation. .	late Paleozoic.
20	-2.8	+8.2	3	27	Coarse-grained poikilitic calcite matrix in sandstone.	Elbow Formation . .	Devonian to Ordovician.
21	-1.1	+10.3	2	33	Coarse-grained poikilitic calcite matrix in sandstone.	Elliott Sandstone . .	Do.
22	-6	+8.1	2	42	Coarse-grained poikilitic calcite matrix in sandstone. do	Do.
23	-6	+12.3	0.5	11	Granular calcite matrix in sandstone do	Do.
24	+7	+15.1	85	Oolitic limestone: 15 percent insolubles.	Wiens Formation . .	Cambrian . . .
25	-1	+14.0	66	Oolitic limestone: 34 percent insolubles. do	Do.
26	+8	+19.0	98	Thick-bedded limestone: 2.29 percent insolubles.	Nelson Limestone . .	Do.
27	+7	+17.5	99	Dense oolitic limestone: 0.67 percent insolubles. do	Do.

¹ U.S. Geological Survey Isotope Laboratory Nos. 3334-1, 3334-2, and so forth.² Calcite types:

- A. . . Microcrystalline, primary sedimentary.
 B. . . Fracture filling, medium crystalline.
 C. . . Sparry, coarse crystalline, poikilitic.

The Nelson Limestone samples have δO^{18} values from +17.5 to +19.0 permil which are to be expected for a Middle Cambrian marine limestone. The δO^{18} of +14.0 to +15.1 permil for the Wiens Formation is somewhat light for the Late Cambrian. The two limestone samples of the Wiens are oolitic, indicating a shallow water environment for their formation and suggesting the influence of some freshwater of low δO^{18} in their environment. The C^{13} values of the Nelson and Wiens samples are well within the range of marine limestone (fig. 2) and a marine origin for both formations is implied.

The carbonate cements in the Elliott Sandstone and Elbow Formation contain δC^{13} values that are marine, but their δO^{18} values of from +8.1 to +12.3 permil are too light to be marine. Marine limestones of Devonian to Ordovician age should have δO^{18} values from +24 to +28 permil. Field

evidence suggests that the Elliott and Elbow clastic rocks were probably deposited in a marine environment; for example, minor, primary phosphorite occurs locally in the Elbow (J. B. Cathcart, written commun., 1970). The lighter δO^{18} values of carbonate cements in the relatively pervious Elliott and Elbow Formations may have been acquired through postdepositional mixing and exchange with lighter O^{18} water from the equally pervious overlying freshwater sandstones.

The two samples of carbonate cement in the Dover Sandstone occur at the contact with the Gale tillite. On the basis of field relations and petrography, this carbonate was precipitated from carbonate solution during the deposition of the tillite and has no relation to the initial sedimentation of the Dover Sandstone. That the light δO^{18} and δC^{13} values in the Dover carbonate are identical to values in the tillite

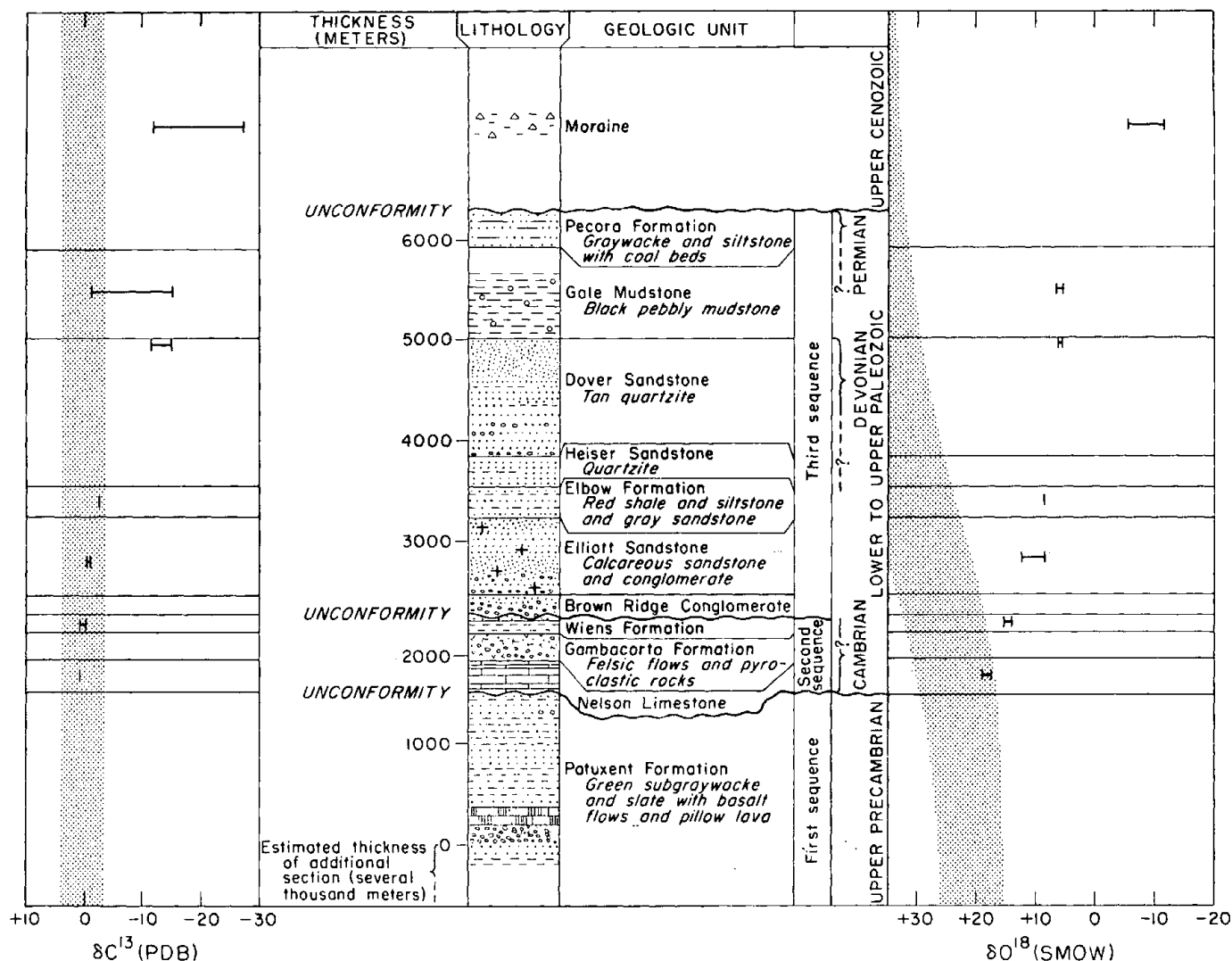


Figure 2.—Composite stratigraphic column and carbon and oxygen isotope abundances in carbonates of sedimentary rocks from the Pensacola Mountains, Antarctica. Bar shows range of isotopic values for each formation tested (table 1). Stipple shows approximate empirical limits of marine carbonates.

carbonate further supports this observation. The two Dover carbonate samples are therefore considered part of the Gale tillite sample.

The carbonates in the Gale tillite samples have both δO^{18} and δC^{13} values that are quite different from those of the preceding samples. The δO^{18} values are light within a small range between +4.9 to +6.1 permil. The δC^{13} values range from -1.8 to -15.9 permil with more than 60 percent of the samples having values lighter than -7.0 permil. The Gale Mudstone contains calcite that is isotopically nonmarine which agrees with field and petrographic evidence presented above.

The carbonate sample from the Dwyka tillite contains δC^{13} and δO^{18} values similar to values in carbonates from the Gale tillite. In addition these Dwyka values agree well with carbon-oxygen isotope analyses of Dwyka carbonates reported by Keith (1969).

Dripstone and concretionary carbonate nodules from upper Cenozoic glacial deposits have δO^{18} values of from -6.1 to

-11.3 permil and δC^{13} values of -12.8 to -28.5 permil. These values substantiate the known freshwater, continental environment in which the carbonate formed and presently occurs.

The different and light δO^{18} values for carbonates from modern and ancient Antarctic glacial deposits suggest that different temperatures were a factor in their formation. The carbonate in the Gale tillite with a δO^{18} content of +5 permil can be precipitated at 0°C from water with a δO^{18} content of -29 permil. Modern Antarctic surface snow has a δO^{18} content of about -26 permil at 1,000 m altitude and about -37 permil at 2,000 m (Confiantini and others, 1963). Hence, the ancient tillite carbonates could have formed at about 0°C from water derived from ice that accumulated as surface snow at about 1,000 m altitude. If the isotopic composition of the oceans were lighter, as previously suggested, then the tillite carbonate could have formed from snow deposited at even lower altitude.

The dripstone carbonate could have formed at 0°C from water with δO^{18} values of from -40 to -45 permil. Modern Antarctic surface snow on the Polar Plateau has δO^{18} values between -37 permil at about 2,000 m altitude and -50 permil at over 3,000 m (Gonfiantini and others, 1963). Hence, the dripstone carbonate probably precipitated from meltwater derived from high-altitude ice.

The source and wide range of the light δC^{13} values in the carbonates from the Gale (-1.9 to -15.9 permil) and the modern dripstone (-12.8 to -28.5 permil) may be complexly related to several factors: (1) Detrital clasts of ancient marine limestone are present in both glacial deposits and empirically contain δC^{13} values from -3 to +3 permil; solution of this detrital limestone could have contributed some carbon having these relatively heavy δC^{13} values, (2) "Soil-zone carbon dioxide" from the decomposition of organic matter contains δC^{13} values from -15 to -25 permil; such carbon, however, is certainly not present in the modern dripstone environment and probably was not a significant factor during the precipitation of the carbonates in the Gale tillite, and (3) carbon from atmospheric CO_2 has a δC^{13} value of about -8 permil and carbon from air CO_2 entrapped in ice may have a similar value; as CO_2 dissolves in water, considerable kinetic fractionation may occur which tends to deplete the bicarbonate in δC^{13} relative to air CO_2 , with the result that the bicarbonate may have δC^{13} values from -8 to about -30 permil (Craig, 1953).

Depending upon the sources of the carbon and the process or processes by which the calcite is dissolved and reprecipitated, the carbon in the resulting calcite can range from about +3 to -30 permil.

Thus, the carbon and oxygen isotope abundances indicate that the Nelson Limestone and Wiens Formation are marine deposits. By contrast the Gale tillite is a nonmarine deposit and probably was formed from freshwater with a δO^{18} value similar to that of the present-day Antarctic snow accumulated at an altitude of about 1,000 m. If the isotopic composition of the Late Devonian-Early Permian ocean was lighter than the present ocean, the freshwater in which the calcite of the Gale tillite formed could have originated as Antarctic snow that accumulated at altitudes lower than 1,000 m.

REFERENCES CITED

- Adie, R. J., 1964, *Antarctic geology*: Amsterdam, North-Holland Publishing Co., 758 p.
- Craig, Harmon, 1953, The geochemistry of the stable carbon isotopes: *Geochim. et Cosmochim. Acta*, v. 3, no. 2, p. 53-92.
- Ford, A. B., 1964, Review of Antarctic geology: *Am. Geophys. Union Trans.*, IG Bull. 82, v. 45, no. 2, p. 363-381.
- Ford, D. C., Fuller, P. G., and Drake, J. J., 1970, Calcite precipitates at the soles of temperate glaciers: *Nature*, v. 226, no. 5244, p. 441-442.
- Frakes, L. A., and Crowell, J. C., 1968, Late Paleozoic glacial facies and the origin of the South Atlantic Basin: *Nature*, v. 217, no. 5131, p. 837-838.
- Frakes, L. A., Matthews, J. L., Neder, I. R., and Crowell, J. C., 1966, Movement directions in late Paleozoic glacial rocks of the Horlick and Pensacola Mountains, Antarctica: *Science*, v. 153, no. 3737, p. 746-749.
- Gonfiantini, R., Togliatti, V., Tongiorgi, E., de Breuck, W., and Picciotto, E., 1963, Geographical variations of oxygen-18/oxygen-16 ratio in surface snow and ice from Queen Maud Land, Antarctica: *Nature*, v. 197, no. 4872, p. 1096-1098.
- Keith, M. L., 1969, Isotopic composition of carbonates from the Karoo and comparison with the Passa Dois group of Brazil, in *Gondwana Stratigraphy* (IUGS Symposium, Buenos Aires, 1967): UNESCO [Paris] Earth Sci. Ser., v. 2, p. 775-778.
- Keith, M. L., and Weber, J. N., 1964, Carbon and oxygen isotopic composition of selected limestones and fossils: *Geochim. et Cosmochim. Acta*, v. 28, no. 11, p. 1787-1816.
- Rigby, J. F., and Schopf, J. M., 1969, Stratigraphic implications of Antarctic paleobotanical studies, in *Gondwana Stratigraphy* (IUGS Symposium, Buenos Aires, 1967): UNESCO [Paris] Earth Sci. Ser., v. 2, p. 91-106.
- Schmidt, D. L., and Ford, A. B., 1970, Geology of the Pensacola and Thiel Mountains, plate V, in Bushnell, V. C., and Craddock, Campbell, eds., *Geologic maps of Antarctica*: Am. Geol. Soc., Antarctic Map Folio Ser., Folio 12.
- Schmidt, D. L., and Williams, P. L., 1969, Continental glaciation of late Paleozoic age, Pensacola Mountains, Antarctica, in *Gondwana Stratigraphy* (IUGS Symposium, Buenos Aires, 1967): UNESCO [Paris] Earth Sci. Ser., v. 2, p. 617-649.
- Schmidt, D. L., Williams, P. L., Nelson, W. H., and Ege, J. R., 1965, Upper Precambrian and Paleozoic stratigraphy and structure of the Neptune Range, Antarctica: U.S. Geol. Survey Prof. Paper 525-D, p. D112-D119.
- Schopf, J. M., 1970, Gondwana paleobotany: *Antarctic Jour. U.S.*, v. 5, no. 3, p. 62-66.
- Williams, P. L., 1969, Petrology of upper Precambrian and Paleozoic sandstones in the Pensacola Mountains, Antarctica: *Jour. Sed. Petrology*, v. 39, no. 4, p. 1455-1465.

REDESCRIPTION OF THE EARLY CAMBRIAN *HELENIA BELLA* WALCOTT, AN APPENDAGE OF *HYOLITHES*

By ELLIS L. YOCHELSON, Washington, D.C.

Abstract.—In accordance with the suggestion of Howell and Stubblefield and subsequent workers, *Helenia* has been reinterpreted as a hyolithid appendage. Isolated specimens of the Early Cambrian *H. bella* Walcott are flattened, are bladelike in cross section, and have an elaborate, irregular ornament covering both surfaces. The specimens are strongly arched and slightly twisted in the third dimension. Presumably these were paired structures which extended outward from openings between the shell and the operculum of the hyolithid and curved down to touch the substrate midway along their length and then upward and posteriorward at the tips. As suggested earlier, their prime function was to provide lateral stability. There is no obvious way that these appendages could have played a major role in locomotion. However, the upper edges of the appendages could have acted as a fulcrum for the operculum; contraction of small muscles running between the operculum and the appendages assisted the ventral part of the operculum to swing upward.

Although the genus *Helenia* Walcott (1890a p. 39; 1890b, p. 616) has been in the literature for many years, it is not well known. Its author provisionally assigned it to the Dentalidae on the assumption that the fossil was a flattened tube open on both ends. In addition to the type species, *H. bella* Walcott, two other species have been assigned to the genus; representative material of them is not available to me and, as I believe they do not belong to the genus, they will be commented upon only briefly. The genus was diagnosed twice in compilations: Grabau and Shimer (1910, p. 7) put *Helenia* in the Hyolithidae, but with possible affinities to the Dentalidae; Shimer and Shrock (1944, p. 525) placed it in Mollusca Incertae Sedis. These treatments are only of historic interest for they did not supply any additional information concerning the genus.

When reporting an Early Cambrian hyolithid specimen that had part of an appendage preserved, and when generally discussing Middle Cambrian hyolithids from the Burgess Shale, Howell and Stubblefield (1950, p. 19) suggested that "... *Helenia* may also be Hyolithid 'fins'." Fisher (1962, p. W124), after diagnosing the genus, noted parenthetically, "I believe that fossils identified as *Helenia* are the supports of a relatively large hyolithid, *Hyolithes princeps*, with which it is

associated." Marek (1963, p. 62-65), in a general discussion of hyolithids independently of Fisher's work, agreed with the remark of Howell and Stubblefield. The interpretation of hyolithid appendages given here in most respects follows that of Marek, and little new of general interest may be added. However, the material upon which *Helenia* was based is so well preserved and so interesting in its own right that no justification is needed for illustrating it.

TYPES AND ILLUSTRATED MATERIAL

After the original description (Walcott, 1890a, p. 39), *Helenia bella* was illustrated by Walcott (1890b, pl. 78, figs. 4, 4a, and 4b) with three line drawings. The first showed a slab (natural size) on which three specimens were exposed, the second showed an enlarged view of what was apparently another specimen, and the third was a drawing of a thin section at natural size. No type specimen or type lot was designated. The drawing of the slab (Walcott, 1890b, fig. 4) was reproduced by Grabau and Shimer (1910) and Shimer and Shrock (1944) in their works on index fossils. *Helenia* is unusual in shape but is so limited in distribution that it is difficult to understand why the genus was ever considered an index fossil. Fisher (1962, fig. 60-4) reproduced the same slab photographically, rotating it 90° to the original drawing but otherwise producing a similar illustration.

Some time after Walcott's (1890a) original description and before his later work, the U.S. National Museum number 18324 was assigned to the figured specimens, plus some additional material. I have not been able to identify either figure 4 or 4a of Walcott (1890b) with any of the available numbered material; I have found a box of thin sections prepared by or for Walcott during 1888-89, but have not been able to associate any of these with figure 4b. However, I feel that the illustrated lot is misplaced rather than lost.

Although it would be perfectly appropriate to designate one of the illustrated specimens or any of the additional material in the collection as a lectotype, there is no need for such a procedure. First, the probability is extremely high—although it remains to be proven by finding a life association—that *Helenia bella* is simply a part of the organism named *Hyolithes*

princeps Billings, 1872; that name based on the shell has clear priority. Second, the concept behind the specific taxon can be clearly formulated from the material, and there is no need for additional clarification by examination of a type. Third, regardless of the merits of this second point, there are no pressing systematic or stratigraphic problems that require a precise knowledge of the type specimen.

The rocks numbered 18324 are from locality 41 of Walcott, taken in 1888 from a railway cut, 1 mile west of Manuels Brook railway bridge, Conception Bay, Newfoundland. Additional material is available from this same locality, which contains more specimens of *Helena bella*, though it was set aside primarily because it shows examples of *Hyolithes princeps* Billings. In my opinion, this lot was collected at the same time as those specimens numbered 18324, but it does not have a museum number and could not be the basis for a lectotype. This second lot corroborates further the proximity—in lieu of the biological association—of conch and appendages. Rare opercula are present in both the numbered and unnumbered lots.

The U.S. National Museum locality register has been changed to indicate that this material was collected from the Brigus Formation. That name was not proposed until 1914. The specimens are in a fine-grained dark-red limestone.

ADDITIONAL OCCURRENCES AND OTHER SPECIES

In 1899, Walcott collected several additional poorly preserved specimens from Smith Sound, Trinity Bay, Newfoundland—his locality 5L. These are also from the Brigus Formation, but so far as I know have not been mentioned previously. For the sake of completeness, it should be noted that Sardeson (1903) mentioned and crudely illustrated a specimen of this species in a somewhat confusing account of phylogeny.

In 1899, Matthew (1899a, p. 192, pl. 2, figs. 7a–e; 1899b, p. 107, p. 6, figs. 7a–e) described a second species of *Helena*, *H. granulata* from Smith Sound. I have not seen the specimens but judging from the description and the outline drawings, this species is quite different from true *Helena*. The tube, if it is a flattened tube, expands at a rapid rate. In addition, the surface is minutely granulated. I suspect strongly that this form is not molluscan. Walcott's specimens from the Brigus Formation at Smith Sound do not show the features mentioned by Matthew.

Cobbold (1921, p. 363, pl. 24, figs. 7a–10) described *Helena cancellata* from the Early Cambrian at Comley in Great Britain. He noted that it was of phosphatic composition, was a collapsed tube, and was covered with a diamond-shaped pattern of ornament; the illustrations suggest that the species is irregular in shape. Cobbold and Pocock (1934, p. 322) indicated that additional material from another Early Cambrian British locality was phosphatic. Undoubted molluscan hard parts are not predominately phosphatic. This species has

nothing to do with *Helena*. More likely it is to be associated with other Early Cambrian material currently being assigned to the Pogonophora.

Poulsen (1932, p. 19, pl. 2, fig. 6) described and illustrated a single fragmentary specimen of *H. bella* from the lower Cambrian Bastion Formation of East Greenland.

GROSS FORM

Specimens of *Helena bella* are best described as curved or arched blades. The curvature shown by larger specimens is remarkably close to the arc of a circle (fig. 1a,b); this is most unusual in mollusks, for growth of hard parts following a fairly obvious logarithmic pattern is the rule. The outline of a *Helena* blade may be approximated by smoothing and joining the arcs of two closely adjacent circles. Because the shape is not allied to a single point, this demonstrates that growth actually follows the pattern of an ellipse or, more likely, a parabola. However even at five times natural size, a close approximation of the outline of many specimens may be constructed by linking and smoothing the arcs of two circles whose centers are separated only by 2 to 2½ cm.

Specimens appear to deviate a bit more from approximate circularity in their earlier growth, but curvature changes remarkably little once this initial stage is passed. This form is to be expected in logarithmic growth; unfortunately, no satisfactory methods are yet available to demonstrate mathematically that the curvature of blades definitely is logarithmic (D. M. Raup, written commun., 1973).

There is virtually no change in curvature between the outer convex edge and the inner concave edge of each blade (fig. 1i, k); the same centers of circles which may be used to approximate the outer edge of a specimen serve equally well to describe the inner edge by using a shortened radius. This feature may be expressed in another manner, by measuring the width at one end of the blade against the width at the other end. Almost all specimens are incomplete, and change in width can only be meaningful with reference to growth; I think that chord length between the two ends of the specimens gives some notion of the growth stage of specimens. A tabulation in millimeters of four specimens is:

Minimum width	Maximum width	Chord length
1.6	2.3	23.2
1.9	2.5	22.3
2.4	3.0	27.7
3.2	4.0	25.5

Measurements of additional specimens are difficult to make because of the shortness of broken segments or their partial burial in matrix. It appears that the minimum width of available specimens is about 1½ mm and that there is a relatively rapid widening to near 2 mm, following which, increase in blade width is at a much slower rate (fig. 1e).

The blades are not two-dimensional arches but are slightly twisted, through a maximum of approximately one quarter of a turn. This amount is on the largest specimen, which has a chord length of 35.5 mm (fig. 1k). Much of the apparent change in blade width seen on photographs of larger specimens is actually foreshortening of perspective (fig. 1k). Smaller specimens show less in the way of a twist, but do express some, being bent 1 to 2 mm into the third dimension. This twisting is not a function of diagenesis or structural effects on the matrix. Regardless of the direction in which the specimens lie within the rock they show the same geometry; most specimens are mainly on a bedding plane, but those that are at a pronounced angle to it show the same regularity.

DETAILED SHAPE AND ORNAMENT

Although *Helenia* was originally described as having an elliptical cross section, this is somewhat inaccurate. The section is nearly subrectangular, except for rounding at the concave and convex edges. The larger blades are about half a millimeter thick. They are composed of white sparry calcite. This material is identical with that of hyolithid shells and opercula in the same samples (fig. 1l); the thickness is comparable with that of the adjacent shells. Only one specimen shows an irregular break and obvious deformation (fig. 1d). I am convinced that the preserved shape is unmodified by diagenesis.

Nothing in any of the material suggests that *Helenia* was a collapsed hollow tube originally open at both ends. Indeed, I am mystified that such a skilled observer as Walcott suggested these features. By the same token, no obvious biologic placement of *Helenia* is apparent, except for a superficial similarity in shape to the scaphopods.

The cross section is minutely thicker at the concave edge than at the convex edge, but this difference is so slight that there is practically no taper of the blade surfaces. A few of the smaller specimens have a faint furrow near the convex edge (fig. 1e), but it cannot be conclusively determined whether this continues through all growth stages and whether the feature occurs on both surfaces of the blade. My impression is that this furrow gradually disappears with increasing size, but when present is symmetrical on both sides.

A thin dark-red layer, presumably of iron oxide, surrounds the sparry calcite (fig. 1b, i). Ornament is preserved on this and on the outer surface of the calcite; no ornament, growth lines, or other indications of periodic growth appear within the calcite (fig. 1c). Hyolithid shells and opercula in the same matrix also have the growth lines and ornament confined to a thin outer layer.

The ornament shows a remarkably high degree of individual variation. This variation is in both the spacing and the direction of ornament and is better illustrated than described. In general, lines may be straight across from one edge to the other, may form a shallow sinus opening toward the narrower end of the specimen, or may be shallowly sigmoidal. They may

be uniform or irregular, and some even coalesce in crossing the blade. There is no consistency of pattern or spacing along an individual specimen or between two specimens of the same width.

The lines of ornament are thin, but rather high and prominent (fig. 1g, j). In the most general terms, the lines are more widely spaced at the narrower edge of the blade than at the wider (fig. 1f, k). Some specimens show a short zone characterized by an abrupt decrease in spacing of these lines relative to most of the blade, concurrent with a slight decrease in their height, and this zone in turn is followed by a smooth region lacking any ornament (fig. 1c, g). Although removal of the outer layer would produce such a smooth surface, that is not the case. The smooth part is also the widest and thinnest part of the blade (fig. 1a). Ornament seems to be both reduced in amplitude and to disappear at the same position on both sides of the blade. The smooth part of a blade is thinner in section than the adjacent ornamented part, even though these parts are of identical width.

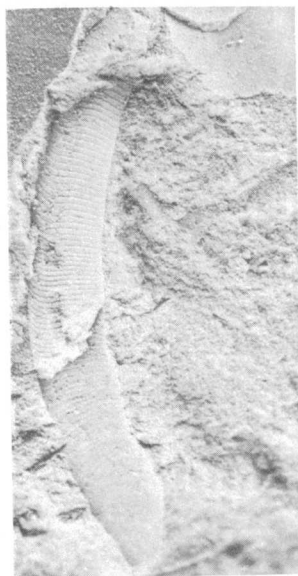
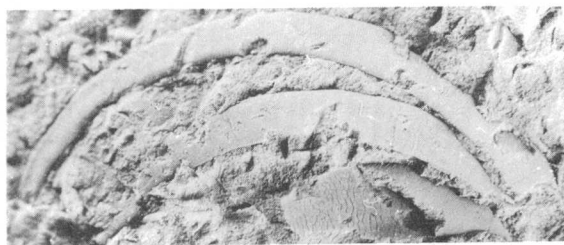
Most specimens are broken, and the shape of the smooth proximal and the ornamented distal ends of the blades is enigmatic. I believe that both terminated in a smoothly rounded curve, though evidence is a bit better for the proximal end (fig. 1a); only one specimen suggests that the distal end was rounded. If this is a correct interpretation, the convex rounding would cut across the lines of ornament.

A few trilobite fragments (fig. 1j) are preserved along with the hyolithid shells and the *Helenia*. Although some of the spine fragments do have a cross section similar to that of the blades, they show a pitted surface internally. Where the material is preserved in full, the Bertillon lines are quite unlike the ornament on the *Helenia* blades.

DISCUSSION

Three general points come to mind in considering this material. First, there is a close similarity between *Helenia bella* and the appendages of the Middle Cambrian *Hyolithes carinatus* Matthew (Yochelson, 1961). Much of the apparent difference in shape is easily ascribed to different growth stages having essentially the same curvature. The relative width of the appendages compared with their length in that occurrence also is similar.

Most fossils in the Burgess Shale have been considerably compressed. Even though the shells of *Hyolithes* show evidence of compaction, by and large the appendages show no indication of deformation, quite in keeping with their flat profile. Those specimens that do show some creasing or bending are a bit larger than most, and this again is reasonably interpreted as a measure of increasing twist with age. Indeed, even though a limited number of hyolithid appendages are known (Marek, 1963, p. 62–63), enough have been found to suggest that they all are virtually the same in general form; what differences are present appear to be the results of preservation.

*a**b**c**d**e**f**g**h**i**j**k**l*

Second, the large size of these appendages is impressive, though it must also be noted that the conch of *Hyolithes princeps* may be more than 100 cm long. The curvature is even more striking, for some of the biggest specimens, if truly circular, would extend through an arc of more than one-third the circumference of a circle. Marek (1963, fig. 11) reconstructed an operculum and appendages in life association which at first sight appears to be somewhat artificial because of the length of appendages, but his interpretation of their dimensions is definitely in keeping with *Helenia bella*.

Third, the elaborate and highly variable ornament on the individual blades is different from that illustrated by Walcott (1890b, pl. 78, fig. 4a), who showed a simple uniform pattern. Apparently the appendages were secreted by mantle folds attached to the operculum; the smooth short distal part of the blade constituted that area within the fold. As the appendage grew laterally, it was extruded from the mantle in a manner comparable in a sense to toothpaste being squeezed from a tube. The individual lines mark the position of the outer edge of the mantle during growth of the appendage. If the mantle edge were not under a stress it would be wrinkled, thereby producing an irregular pattern on the blades. I know of no other mechanism which would produce such an inconsistent ornament on these blades.

Figure 1.—*Helenia bella* Walcott from the Early Cambrian of Manuels

Brook, Newfoundland. All specimens, except *i*, coated with ammonium chloride. Figures *c*, *f*, and *g*, $\times 5$; all others, $\times 3$.

- a. Poorly preserved blade with distal part to right; the curved distal termination is probably unbroken; USNM 18324c.
- b. A broken blade showing the ornament on both surface and external mold; the smooth distal part is to the left, and the lower part of the curved distal tip might not be broken in spite of its proximity to the edge of the slab; USNM 18324a.
- c. External mold and fragment showing crowding of growth lines adjacent to smooth distal part at left; USNM 18324b.
- d. Blade showing obvious crushing; smooth distal part is to the left; USNM 18324a.
- e. Broken blade with smooth distal surface in external mold to extreme left, broken calcite to the left, and the ornamented blade surface preserved along the central part of the arch; USNM 18324b.
- f. Fragment showing irregularities and change in spacing or ornament pattern; USNM 18896o.
- g. Fragment and external mold showing variation in ornament with coalescing lines; smooth distal part is below; USNM 18324d.
- h. Two blades both with distal part to the right; USNM 18324a.
- i. The same slab without a coating; the fragment to the lower right is of a trilobite.
- j. Two fragments, the larger one showing irregularities in the ornament pattern near midlength and the smaller blade and external mold less well preserved but having a faint furrow along the convex margin; the wider object in lower part of photograph is the external mold of a trilobite fragment; USNM 18324e.
- k. Largest specimen available; smooth distal part is to the left on the external mold, and crowding of growth lines may be seen adjacent to this, near the center of the arch; USNM 18324b.
- l. *Hyolithes princeps* Billings ventral surface, also partly present in *g*, showing growth lines extending anteriorward to form the ligula; a fragmentary blade is inclined to the bedding plane in the upper left; USNM 18324b.

FUNCTIONAL INTERPRETATION

The one example of a hyolithid conch, operculum, and appendages in an uncrushed life association (Marek and Yochelson, 1964; Marek, 1967) does not answer all questions regarding the life position of these structures, for the association is incomplete, and the one remaining appendage is broken off close to the operculum. Further speculation is necessary, but it is immediately apparent that the distal ends of the appendages could not rest on the substrate because of the strong curvature of the blades. A sketch made with the points of the blades downward (fig. 2) shows them projecting far below the ventral edge of the operculum; this would require the aperture and anterior part of the shell to be raised above the substrate, a most unlikely life position. Thus the reconstructions (Marek, 1963, fig. 12; Marek and Yochelson, 1964, fig. 2 reproduced here as fig. 3) that show the distal ends curving upward and the convex outer edge of the appendage resting on the substrate are considered to be correct.

Because there is no obvious difference in specimens of *Helenia bella* between the two sides of the blade, one cannot determine the anterior from the posterior and thereby decide objectively whether the twist is toward the aperture or toward the apex. Again, however, the morphology strongly suggests that the twisting is such that the distal end is slightly posterior.

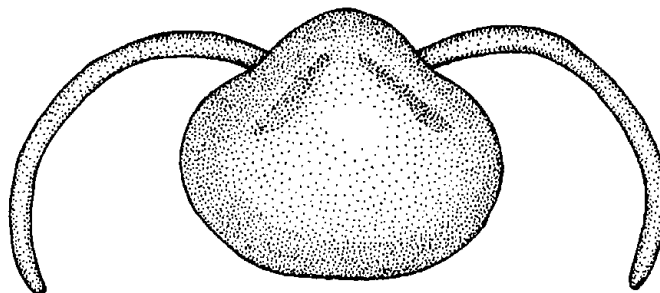


Figure 2.—Inferred reconstruction of appendages and hyolithid operculum. With appendages drawn to the scale of *Helenia* specimens and placed so that they curve point downward, it is obvious that they protrude a significant distance below the ventral edge of the operculum.

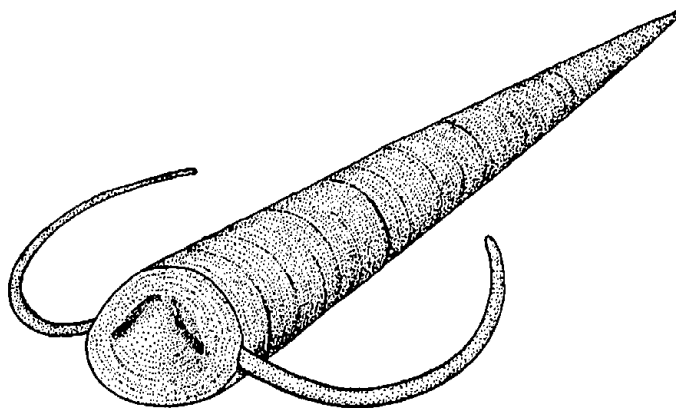


Figure 3.—Reconstruction of hyolithid with operculum and appendages in place (from Marek and Yochelson, 1964). (Copyright 1964 by the American Association for the Advancement of Science.)

Because the operculum surface from which the appendages protrude is arched anteriorward, rather than sunken, it is difficult to envision any way in which these points could extend forward when the operculum was closed. The Burgess Shale occurrence (Yochelson, 1961) does show that all appendages associated with a conch are consistent in having the distal ends directed toward the apex of the conch.

The type of ornament seen throughout most of the length of the blade, combined with the absence of the ornament on the short proximal part, tends to confirm that no soft parts covered the length of the appendage which protruded from the operculum. The size and curvature of *Helenia bella* confirms the ideas expressed earlier by Marek that these structures could not be withdrawn into the shell aperture.

There seems to be little question that the one prime function of the appendages was to provide greater stability for the narrow, elongate hyolithid conch. Should the shell of the hyolithid be inverted, the animal would almost certainly die, for there is no mechanism to flip it back over to life position; the advantages of three-point stability are obvious. Greater stability would be particularly advantageous for this sedentary animal by allowing it to live in an area of shifting strong currents.

More argument surrounds the question of any additional function. Marek (1963, p. 65) has suggested that the appendages might have had the function of oars to assist in locomotion. Although I agree fully that there must have been some sort of mechanism, no matter how inefficient, to move the hyolithid conch, I find it difficult to envision the appendages playing any major active role in movement.

Several points suggest that the appendages played a predominantly passive role. First, if they rested on the substrate with the point downward, they might sink into the substrate. However, because the point is upward, the curved surface is on the substrate; this would distribute the weight so that the appendages probably would not develop a purchase against the bottom sediments. Second, if the animal were to progress, it would be by placing a strain on the anchored blades and pulling forward. I suspect, though I cannot prove, that any such pull would be sufficient to snap these thin blades. Third, for the appendages to assist in moving the animal forward, they would have to be twisted so that they were anterior relative to the operculum. This could only be after the operculum was closed, for otherwise the operculum would move, not the conch. As there is only a slitlike opening between the operculum and edge of the aperture, there would be insufficient space to rotate these blades. These arguments suggest that a functioning of the appendages in a movement such as a "rowing" motion was implausible, though there is nothing that totally rules out this interpretation (Marek, 1963, p. 63).

However, these appendages might have had one other use. A principal difficulty in attempting any reconstruction of hyolithid softparts has to do with the operculum. The difficulty is not in closing the operculum, but in opening it so that the body might then be able to move forward through the aper-

ture. Relaxation of the principal adductor muscles would cause the operculum to gape dorsally but would not necessarily result in any movement on the ventral side of the aperture adjacent to the ligula (shelf).

Marek (1963, 1972) has shown that the inner surfaces of some opercula contain a rather complex pattern of muscle scars, far more than would be expected from adductors that closed the operculum; apparently a series of smaller muscles was also present. I suggest that at least some of these muscles were attached to the appendages. If the two appendages remained in a stationary position relative to the conch, they could act as fulcrum for the operculum. Contraction of muscles running from the dorsal part of the operculum would pull up the ventral part of the operculum slightly. Relaxation of these muscles and contraction of other sets below the appendages would supplement the contraction of main adductors in closing the operculum. This would require no lateral movement of the appendages.

REFERENCES CITED

- Cobbold, E. S., 1921, The Cambrian horizons of Comley, and their Brachiopoda, Pteropoda, Gasteropoda, etc.: Geol. Soc. London Quart. Jour., v. 76, no. 4, p. 325-386.
- Cobbold, E. S., and Pocock, R. W., 1934, The Cambrian area of Rushton (Shropshire): Royal Soc. London Philos. Trans., Ser. B, v. 223, p. 305-409.
- Fisher, D. W., 1962, Small conoidal shells of uncertain affinities, in Moore, R. C., ed., Treatise on invertebrate paleontology, Part W, Miscellanea: New York and Lawrence, Kans., Geol. Soc. America and Univ. Kansas Press, p. W98-W143.
- Grabau, A. W., and Shimer, H. W., 1910, North American index fossils; Invertebrates. Volume 2: New York, A. G. Seiler and Co., 909 p.
- Howell, B. F., and Stubblefield, C. J., 1950, A revision of the fauna of the north Welsh *Conocoryphe viola* beds implying a Lower Cambrian age: Geol. Mag., v. 87, no. 1, p. 1-16.
- Marek, Ladislav, 1963, New knowledge on the morphology of *Hyolithes*: Sborník Geologických Věd, Paleontologie, rada P, v. 1, p. 53-73.
- , 1967, The Class Hyolitha in the Caradoc of Bohemia: Sborník Geologických Věd, Paleontologie, rada P, v. 9, p. 51-113.
- , 1972, Middle Cambrian Hyolithes—*Maxillites* Gen. N.: Prague, Národní Mus., Časopis Národního Muzea, v. 141, p. 69-75.
- Marek, Ladislav, and Yochelson, E. L., 1964, Paleozoic mollusk—*Hyolithes*: Science, v. 146, no. 3652, p. 1674-1675.
- Matthew, G. F., 1899a, Preliminary notice of the Etcheminian fauna of Cape Breton: Nat. History Soc. New Brunswick Bull. 18 (4 pt. 3), p. 198-208.
- , 1899b, The Etcheminian fauna of Smith Sound, Newfoundland: Royal Soc. Canada Proc. Trans., Ser. 2, v. 5, p. 97-119.
- Poulsen, Christian, 1932, The Lower Cambrian faunas of East Greenland: Medd. Grønland, v. 87, no. 6, 66 p.
- Sardeson, F. W., 1903, The phylogenetic stage of the Cambrian Gastropoda: Jour. Geology, v. 11, p. 469-492.
- Shimer, H. W., and Shrock, R. R., 1944, Index fossils of North America: New York, John Wiley & Sons, 837 p.
- Walcott, C. D., 1890a, Descriptive notes of new genera and species from the Lower Cambrian or *Olenellus* zone of North America: U.S. Natl. Mus. Proc., v. 12, p. 33-46.
- , 1890b, The fauna of the Lower Cambrian or *Olenellus* zone: U.S. Geol. Survey Ann. Rept. 10, pt. 1, p. 509-760.
- Yochelson, E. L., 1961, The operculum and mode of life of *Hyolithes*: Jour. Paleontology, v. 35, no. 1, p. 152-161.

EVIDENCE FOR THE PRESENCE OF A HEART IN PALEOZOIC OSTRACODES INCONCLUSIVE

By I. G. SOHN, Washington, D. C.

Abstract.—The presence of a heart in some Paleozoic ostracodes has been inferred by analogy with some living myodocopids that have this organ, and an ordinal classification of the leperditiiids has been proposed because of this inference. A review of the present knowledge of the internal shell structure of living myodocopids indicates that there is no basis for interpreting certain markings preserved on fossil molds and steinkerns as indicating the presence of a heart.

Only one order of living ostracodes, the Myodocopida, has a heart. Kozur (1972) classified the fossil order Leperditiiida with the Myodocopida in the superorder Myodocopamorphes. Adamczak and Weyant (1973) accepted Triebel's (1941) conclusions that anastomosing ridges on steinkerns of leperditiiids represent blood canals, indicating that these (and other) early Paleozoic ostracodes had hearts. It is therefore important to reexamine and evaluate the evidence for the inference of a heart in nonmyodocopid fossil ostracodes.

A review of what is known of the heart in myodocopid ostracodes is pertinent to the inferred presence of a heart in Paleozoic ostracodes. The myodocopid heart is, according to Calman (1909, p. 64), near the dorsal surface just above the mandibles; it has "one pair of lateral ostia and an opening in front through which the blood is expelled. No definite vessels exist, but a network of blood-channels is found in the shell of the Cypridinidae." The position of the heart within the carapace is well illustrated (Claus, 1876, pls. 17, 18; Claus, 1891, pl. 25; Cannon, 1931, 1940; Hartmann, 1967, p. 388, fig. 247). Claus (1876, pl. 17, fig. 2) illustrated on the inside of a left valve of *Asterope oblonga* (Grube, 1861) an anastomosing pattern of thin lines that he labeled as "System von Blutlakunen", here reproduced as figure 1a. The pattern on this illustration is similar to that of *Leperditia* sp. illustrated by Adamczak and Weyant (1973, fig. 1); they called the pattern "vascular markings."

Müller (1894, p. 206, pl. 2, fig. 2) illustrated the inside of a left valve of the living species *Cypridina mediterranea* Costa, 1845, showing "Canale und Nervenstamme"; the same illustration is in Hartmann (1966, p. 161, fig. 98; fig. 1b, this report) showing "Blutlakunen und Nervenstränge." Through the courtesy of L. S. Kornicker, who had borrowed Müller's specimens, I have examined these structures. On the inside of both

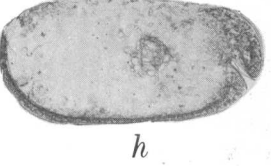
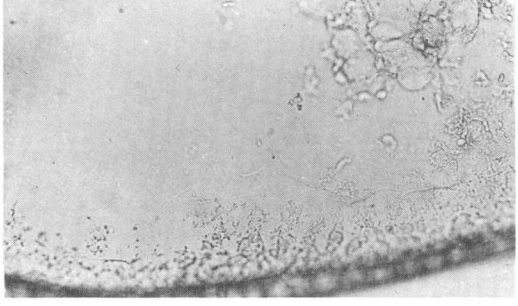
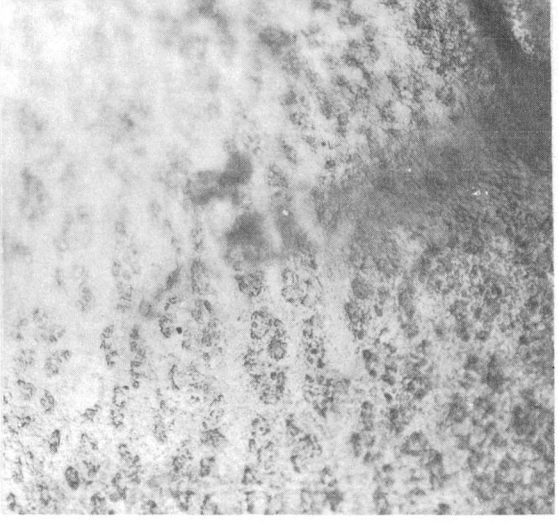
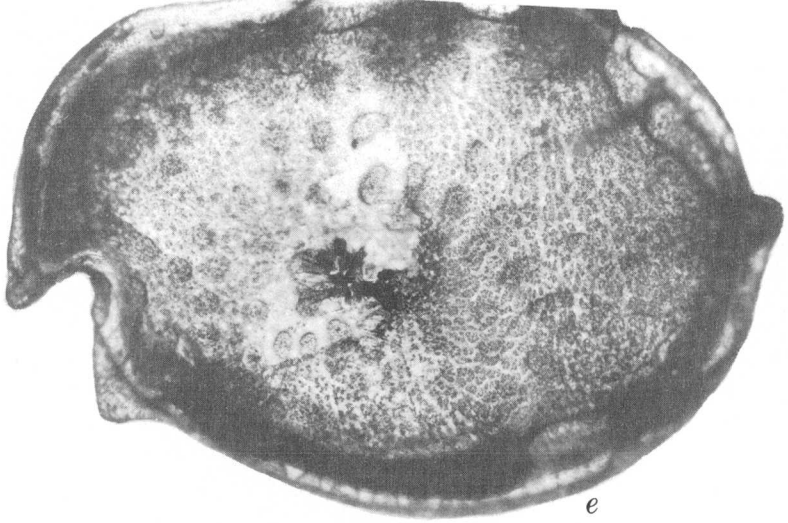
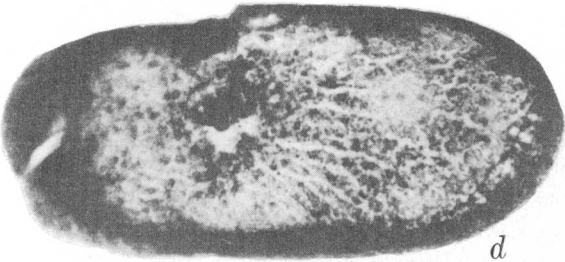
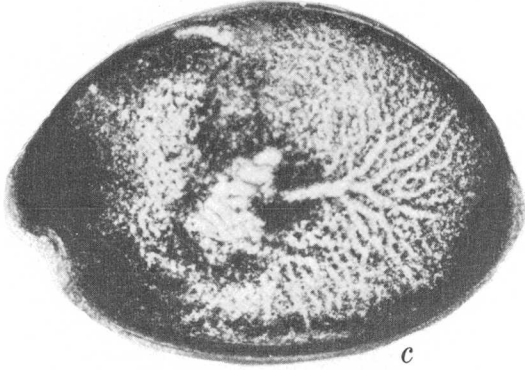
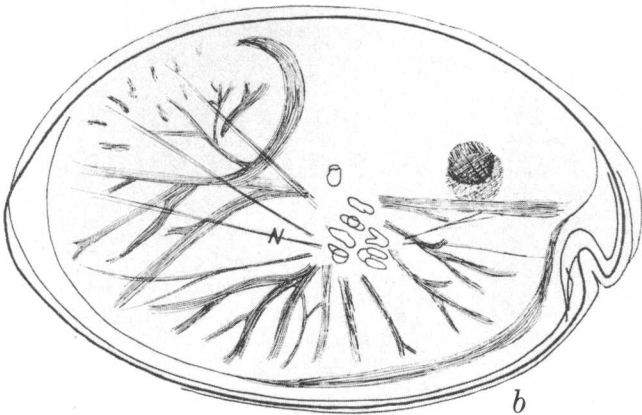
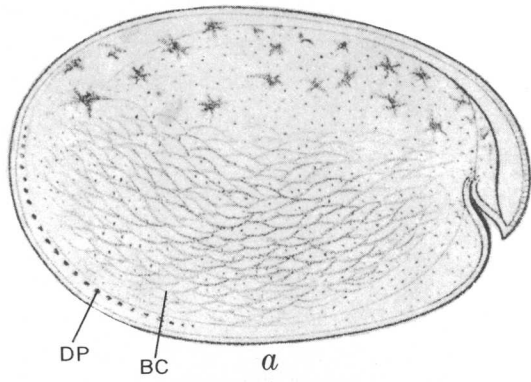
valves crude lineations of a darker color are present among epidermal cells(?). These markings are not as regular and continuous as shown by either Müller or Hartmann; they are not impressed on the inside of the calcified layer and thus would not leave a ridge on an internal mold. Müller (1894, pl. 36, fig. 30) illustrated somewhat similar markings in *Bairdia serrata* Müller, 1894, which he called "Ganglionzellen."

Cannon (1931, p. 456) described the blood system of the myodocopid *Cypridina (Doloria) levis* Skogsberg, 1920 as follows:

Blood enters the carapace directly from the body cavity at the attachment of the adductor muscles. In addition, a tongue of gut parenchyma passes into the valves alongside the adductor muscle, and so blood may pass into the valves from this tissue. From this point there is a system of radiating channels in the thickness of the carapace valves. These were mentioned by Claus (1876, p. 93) in a footnote. They extend outwards to the edges of the valves, where they join to a marginal vessel. This is marked anteriorly and has been figured by Müller (1894, pl. 2, fig. 2) who, however, does not describe it. These marginal sinuses extend up the anterior edges of the valves, past the antennal notches, and open directly into the pericardium at the combined attachment of the aortic and nauplius eye muscles.

The term "thickness" as used by Cannon refers to the body cavity between the inner surface of the valves and the vestment (uncalcified inner lamella) and not to the calcified shell.

Triebel (1941, p. 331, pl. 6, fig. 62) illustrated the inside of a right valve of a juvenile *Cypridina vanhoffeni* Müller, 1908 by a photograph taken with transmitted light that shows the adductor muscle scar located within a dark area which is surrounded by a lighter area extending over the posterior of the valve. This lighter area has a branching structure progressively thinning towards the margins of the valve, with the main, thickest trunk extending into the dark area up to the middle of the upper half of the muscle scar, and additional more vague branchings extend ventrally and posteriorly from the lower part of the muscle scar. Triebel called these branching structures "Blutkanalen." This illustration (fig. 1c) is the basis of some subsequent inferences that the myodocopid heart is associated with a vascular system. Because radiating markings are present on internal molds and casts of certain Paleozoic ostracodes, these markings were interpreted as blood canals that indicate the presence of a heart in the Paleozoic taxa.



I am grateful to Dr. Heinz Malz, Senckenberg Museum, for reexamining the original specimen of Triebel's illustration. He stated (written commun., 1973) that the "vascular system" can be seen on the specimen with transmitted light, that the structure is not engraved on the inside or the outside of the valve, and that adults of this species (Triebel, 1941, pl. 2, fig. 15) do not exhibit this structure because their shells are opaque.

Darby (1965, pl. 19, fig. 6) illustrated without comment a pattern almost similar to Triebel's "vascular system" on the outside view of the left valve of the holotype of *Cylindroleberis psitticina* Darby, 1965. Darby's types were available for examination; the markings can be seen with transmitted light from both the inside and outside of the specimen (fig. 1d), just as Dr. Malz described Triebel's specimen. They are best developed on the left valve, and from the inside they consist of crudely linear areas between clusters of cells that are plastered on top of the inside of the valve. I was able to clean a similar pattern from the inside of a left valve of *Parasterope pollex* Kornicker, 1967, using a camel-hair brush in glycerin (figs. 1g-i).

L. S. Kornicker brought to my attention similar markings on the holotype of a new species of *Asteropteron* he described (L. S. Kornicker, in press), here illustrated as figures 1e, f. A "vascular system" would consist of pipe or veinlike structures with discrete walls and, in order to leave impressions on fossils, they would have to be incised into the shell. The structures in the examined myodocopids are not engraved into the shell and

are definitely not vascular. These suggest that Triebel's "vascular system" may also be nonvascular in structure.

Kozur (1972, p. 6) combined the order Leperditida Pokorny, 1953, and the order Myodocopida Sars, 1866, into his new superorder Myodocopamorphes because of the alleged presence of a heart and vascular system in both and of lateral eyes in the Leperditida. A study of living *Thaumatoocypris* Müller, 1906 and related genera (L. S. Kornicker and I. G. Sohn, unpub. data, 1974), disclosed that, unlike the Halocypridae, this closely related myodocopid group does not have a heart. Because not all myodocopids have a heart, there is no reason to relate the leperditids to the myodocopids in the same superorder.

Adamczak and Weyant (1973) thoroughly reviewed and documented the available literature regarding the alleged blood canals in Paleozoic ostracodes. They rejected Robinson's (1969) statement that somewhat similar markings in *Bernix* Jones, 1884, are not blood canals and his equivocal suggestion that the markings on *Bernix* may represent the chitin network at the base of the shell layer illustrated in Müller (1894, pl. 36, fig. 32). I accept Robinson's conclusions that the markings on *Bernix* are not the result of blood canals. The markings on *Bernix* as illustrated by Robinson (1969, pl. 4) are similar to markings on *Paraconchoecia spinifera* Claus, 1890, illustrated by Claus (1891, pl. 10, fig. 1) that are not blood canals. I question Henningsmoen's (1954) interpretation that markings on steinkerns of *Conchoprimitia* and others interpretations that markings on leperditids and the markings on *Rishona* represent blood canals, and, by inference, I question the presence of a heart in the early Paleozoic ostracode groups.

Markings on *Leperditia* similar to those illustrated by Adamczak and Weyant (1973, fig. 1) were described and illustrated by Jones (1856, p. 85, pl. 6, fig. 4a) on a cast of the interior of a left valve of *Leperditia balthica* (Hisinger, 1831). Berdan (1972, p. 21, pl. 3, fig. 33) illustrated such markings on the outside of a right valve of *Leperditia scalaris* Jones, 1858 which she slightly corroded with acid. Langer (1973, p. 45) discussed such markings as follows: "In many *Hermannina*-species, this system can be seen only faintly after strongly etching the outside of the valve." Because these structures are therefore within the calcified shell, they could not have any relation to those illustrated by Claus on the inside of a myodocopid, suggesting that the "vascular markings" of Adamczak and Weyant are not of the same origin as those illustrated by Claus.

Henningsmoen's illustrations of the "blood canals" in *Conchoprimitia* near the anterior and posterior ends of the adductor muscle scar do not conform with the description by Cannon previously cited and probably cannot be attributed to the tongue of gut parenchyma described in *Doloria levis* Skogberg, 1920. The anastomosing ring of vascular markings illustrated on steinkerns of *Rishona tumida* Adamczak and Weyant, 1973 (fig. 2; pl. 1, figs. 1, 2) also does not fit Cannon's description. Although I have no explanation as to what struc-

Figure 1.—Living myodocopid ostracodes; illustrations upon which the presence of a heart in Paleozoic forms was postulated and photographs that negate the postulate.

- a. *Asterope oblonga* (Grube, 1861). Inside of left valve, magnification not given. BC, system of inferred blood canals (Blutlakunen); DP, pores of the peripheral gland cells (Randdrüsenzellen). From Claus, 1876, pl. 17, fig. 2.
- b. *Cypridina mediterranea* Costa, 1845. Inside of left valve showing inferred blood canals (Blutlakunen), approximately $\times 25$; N, nerves. From Hartmann, 1966, fig. 98, after Müller, 1894, pl. 2, fig. 2.
- c. *Cypridina vanhoeffeni* Müller, 1908. Inside of a juvenile right valve showing inferred blood canals, $\times 28$. From Triebel, 1941, pl. 6, fig. 62.
- d. *Cylindroleberis psitticina* Darby, 1965. Holotype, left valve exterior, $\times 60$. From Darby, 1965, pl. 19, fig. 6. Offshore of Sapelo Island, Ga.
- e, f. *Asteropteron* n. sp. Kornicker (in press), USNM 128680. e, inside of right valve, $\times 35$. f, inside, dorsoposterior area, $\times 135$.
- g-i. *Parasterope pollex* Kornicker, 1967. Left valve of female paratype (USNM 114051) with markings that were partly cleaned using a camel-hair brush in glycerin. g, cleaned area posterior to muscle-scar pattern, $\times 90$. h, inside view of cleaned area posterior and ventral to muscle scar, $\times 22$. i, uncleaned area anterior and ventral to muscle scar showing the same structure as in e and f, $\times 90$.

ture caused the markings in the above two genera, they do not offer conclusive evidence of a heart in the early Paleozoic genera.

It is significant that, although many of the species of fossil myodocopids are based on steinkerns, no markings similar to those which suggest the presence of a heart in fossil ostracodes have been illustrated on fossil Myodocopida.

On the basis of the above discussion, I conclude that the markings illustrated by Müller would not leave impressions on internal molds and on the inside of valves of fossil ostracodes, that the "blood canals" illustrated by Triebel in a myodocopid do not represent vascular structures, and that the markings on leperditids probably represent the organic framework because they are present also within the calcified part of the shell. Because the alleged presence of vascular systems in some Paleozoic ostracodes is based on the misinterpretation of such a system in some extant myodocopids, there is no reliable evidence at this time that Paleozoic ostracodes had a heart. Pending reliable evidence, the classification of Paleozoic taxa on the basis of the presence or absence of a heart is unwarranted.

I am grateful to my colleagues J. M. Berdan and L. S. Kornicker for much information and many fruitful discussions that resulted in this paper. I accept sole responsibility for the opinions expressed.

REFERENCES CITED

- Adamczak, Franciszek and Weyant, Marcel, 1973, *Rishona* Sohn (Ostracoda; Devonian)—Morphology and intercontinental distribution: *Senckenbergiana Lethaea*, v. 53, no. 6, p. 523–541, 3 pls., 8 figs.
- Berdan, J. M., 1972, Brachiopoda and Ostracoda of the Cobleskill Limestone (Upper Silurian) of central New York: U.S. Geological Survey Prof. Paper 730, 47 p., 6 pls.
- Calman, W. T., 1909, Crustacea in Lankester, E. R. ed., A treatise on zoology: London, Adam and Charles Black, pt. 7, fasc. 3, 346 p., 194 figs.
- Cannon, H. G., 1931, On the anatomy of a marine ostracod, *Cypridina (Doloria) levis* Skogsberg: *Discovery Reports*, v. 2, p. 435–482, pls. 6, 7, 12 figs.
- 1940, On the anatomy of *Gigantocypris mülleri*: *Discovery Reports*, v. 19, p. 185–244, pls. 39–42.
- Claus, Carl, 1876, *Untersuchungen zur Erforschung der Genealogischen Grundlage des Crustaceen-System*: Wien, Naturw. Verlag von Carl Gerold's Sohn, 114 p., 19 pls.
- 1891, *Die Halocypriden des Atlantischen Oceans und Mittelmeeres*: Wien, Alfred Holder, 81 p., 26 pls.
- Darby, D. G., 1965, Ecology and taxonomy of Ostracoda in the vicinity of Sapelo Island, Georgia: *Ann Arbor, Michigan Univ., Nat. Sci. Found. Proj. GB-26*, Rept. 2, 76 p., 33 pls., 11 figs.
- Hartmann, Gerd, 1966, Ostracoda, in Gruner, H. E., ed., *Dr. H. G. Bronns Klassen und Ordnungen des Tierreichs*, v. 5, Arthropoda, Abt. 1, Crustacea: Leipzig, Akademische Verlagsgesellschaft Geest und Portig K.-G., Buch 2, Teil 4, Lieferung 1, p. 1–216, 121 figs.
- 1967, Ostracoda in Gruner, H. E., ed., *Dr. H. G. Bronns Klassen und Ordnungen des Tierreichs*, v. 5, Arthropoda, Abt. 1, Crustacea: Leipzig, Akademische Verlagsgesellschaft Geest und Portig K.-G., Buch 2, Teil 4, Lieferung 2, p. 217–408, figs. 122–260.
- Henningsmoen, Gunnar, 1954, Lower Ordovician ostracods from the Oslo region, Norway: *Norsk Geol. Tidsskr.*, v. 33, p. 41–68, pls. 1, 2.
- Jones, T. R., 1856, Notes on the Paleozoic bivalved Entomostraca—No. 3, Some species of Leperditia: *Annals and Mag. Nat. History*, ser. 2, v. 17, p. 81–101, pls. 6, 7.
- Kornicker, L. S., (in press) Antarctic Ostracoda (Myodocopina): *Smithsonian Contr. Zoology*, No. 163, 9 pls., 432 figs.
- Kozur, Heinz, 1972, Einige Bemerkungen zur Systematik der Ostracoden und Beschreibung neuer Platycopida aus der Trias Ungarns und der Slowakei: *Geol. Paläont. Mitt. Innsbruck*, vol. 2, no. 10, p. 1–27, 2 pls.
- Langer, Wolfhart, 1973, Zur Ultrastructure, Mikromorphologie und Taphonomie des Ostracoda-Carapax: *Palaeontographica*, v. 144, Abt. A, p. 1–54, 15 pls., 27 figs.
- Müller, G. W., 1894, Ostracoda—Fauna und Flora des Golfes von Neapel: *Zool. Sta. Neapel, Mon.* 21, 404 p., 40 pls.
- Robinson, J. E., 1969, The history of *Bernix tatei* Jones, 1884, in Neale, J. W., ed., *The taxonomy, morphology and ecology of Recent Ostracoda*: Edinburgh, Oliver and Boyd, p. 14–20, pls. 1–4.
- Triebel, Erich, 1941, Zur Morphologie und Ökologie der fossilen Ostracoden, mit Beschreibung einiger neuer Gattungen und Arten: *Senckenbergiana*, v. 23, no. 4–6, p. 294–400, 15 pls.

PALYNOLOGICAL APPLICATIONS OF PRINCIPAL COMPONENT AND CLUSTER ANALYSES

By DAVID P. ADAM, Menlo Park, Calif.

Abstract.—Two multivariate statistical methods are suggested to help describe patterns in pollen data that result from changes in the relative frequencies of pollen types produced by past climatic and environmental variations. These methods, based on a geometric model, compare samples by use of the product-moment correlation coefficient computed from data subjected to a centering transformation. If there are m samples and n pollen types, then the data can be regarded as a set of m points in an n -dimensional space. The first method, cluster analysis, produces a dendrograph or clustering tree in which samples are grouped with other samples on the basis of their similarity to each other. The second method, principal component analysis, produces a set of variates that are linear combinations of the pollen samples, are uncorrelated with each other, and best describe the data using a minimum number of dimensions. This method is useful in reducing the dimensionality of data sets. A further transformation known as varimax rotation acts on a subset of the principal components to make them easier to interpret. Both methods offer the advantages of reproducibility of results and speed in pattern description. Once the patterns in the data have been described, however, they must be interpreted by the palynologist. An application of the methods in palynology is shown by using data from Osgood Swamp, Calif.

The objective of palynology in paleoecological investigations is the evaluation of past ecological and climatic changes by study of variations in the frequencies of occurrence of pollen grains of different plants through time. The typical result of a pollen investigation is a set of data in which frequencies of many pollen types are recorded for many samples. Once such a set of data is obtained, the patterns of variability within it are identified and then interpreted in terms of environmental and ecological changes.

The traditional method of interpretation relies heavily upon the intuition of the palynologist, usually involving prolonged contemplation of a pollen diagram (a graphical representation of the data set), with much of the time devoted to recognition of patterns present in the data. However, certain alternate methods of pattern recognition are amenable to computer processing, and two of these methods are the subject of this article.

NATURE OF POLLEN DATA

Pollen samples are commonly obtained from small quantities of soil or sediment. Groups of pollen samples are collected so that one may examine either contemporary geographic variability of the kinds and frequencies of pollen grains on the ground (modern surface samples) or changes in frequencies of various pollen types at a given spot through time (fossil samples). Pollen data are accumulated by counting the number of grains of each pollen type under a microscope after the grains are extracted from each sample.

The data are recorded as a matrix of numbers that must always have at least two dimensions to be amenable to the techniques set forth here; single samples cannot be handled. If the basic data matrix has more than two dimensions, as it would for multiple fixed pollen sums (Mehring and Haynes, 1965; Adam, 1967a), it can be summarized in a two-dimensional matrix in which each column corresponds to the best frequency estimate for a pollen type and each row corresponds to a sample.

It is essential that the columns of the data matrix be homogeneous; that is, the frequencies within each column must be based on the same total number of pollen grains for a given pollen sum for each sample, and the number of pollen types included in the sum must remain constant for all samples. If this condition is not met, the data must be converted into percentages to remove the effect of differing sample sizes.

The restriction of homogeneity within columns does not apply between columns. The data for different pollen types may be based on different pollen sums with no adverse effect on the data. This may be desirable when some pollen types tend to dominate a given pollen sum.

Historically, patterns that relate pollen samples to one another have been emphasized, rather than patterns that relate pollen types. This emphasis occurred because pollen samples are readily treated as independent units, whereas it is not possible to consider the frequencies of pollen types independently of each other.

One reason for this difficulty is that pollen counts have customarily been made as proportions, introducing a con-

straint not present in nature into the data. When any type increases in relative frequency, some other type(s) must decrease because the sum of all types always equals 100 percent. One result is that the expected correlation between two unrelated pollen types in a percentage data set is always negative, rather than zero; this obscures the true patterns, which would be observed if the APF (absolute pollen frequencies) in grains per unit area per unit time were known (Mosimann, 1962; 1963; Martin and Mosimann, 1965; Adam, 1967b).

Radiocarbon dating permits accurate estimates of sedimentation rates, and many pollen workers are now basing their data on absolute pollen frequencies in an attempt to avoid the constraint involved in working with percentages (for example, M. B. Davis, 1967, 1969; Davis and Deevey, 1964; Pennington and Bonny, 1970; Waddington, 1969). However, Tauber (1965, 1967a, 1967b) has pointed out that we know very little about the dispersal of pollen grains and that one plant species may directly affect the dispersal of the pollen of other species through physical mechanisms such as the filtration of pollen from the air by leaves and branches; such processes would affect absolute pollen frequencies as well as percentages. This means that it is probably not possible to consider different pollen types as independent entities responding only to ecological competition under varying climatic and edaphic conditions.

The perversity of nature in this respect has left palynologists unable to interpret one pollen type independently of the other types in an analysis. They have therefore focused on pollen spectra (samples) as basic operating units, and because there is no clear, simple relationship between pollen frequencies and the frequencies of the corresponding plants in the surrounding vegetation, they have emphasized the differences between samples, rather than the actual frequencies found.

Implicit in this emphasis is a sort of palynological uniformitarianism: samples resembling each other are presumed to represent plant communities that also resembled each other, and the degree of resemblance is assumed to be monotonically related to the resemblance between the parent plant communities.

The quantitative methods presented here similarly emphasize comparison of pollen samples, rather than relationships between pollen types. Although these methods can be used with equal facility to study the relationships between pollen types, the approach taken here provides results which, in my opinion, are more easily understood in terms of the conventional interpretation of pollen diagrams.

ROLE OF STATISTICS IN PALYNOLOGY

There are two basic approaches to the statistical analysis of pollen-data matrices: descriptive and inferential. The science of statistics has developed largely in response to a need for inferential capabilities in dealing with data, and the statistical

methods developed for that purpose deal with such concepts as confidence limits, distributions, replications, and formal statistical tests of significance.

One major obstacle to the use of inferential methods in palynology is the inherent complexity of any reasonable model of the natural system with which we must deal. Several formal models of this system have been proposed (for example, Fagerlind, 1952; Anderson, 1970; Davis, 1963), and many other informal discussions are in the literature (for example, Faegri and Iversen, 1964; Livingstone, 1969), as well as studies of certain subsystems, including pollen dispersal (Tauber, 1965; 1967a; 1967b) and mixing at the mud-water interface (R. B. Davis, 1967). The complicated nature of these models has precluded any thorough understanding of the statistical distributions followed by pollen data. Some early work was done by Barkley (1934) and Faegri and Ottestad (1948). More recently, Mosimann and his associates (Mosimann, 1962; 1963; 1965; Martin and Mosimann, 1965; Mosimann and Greenstreet, 1971) have considered more complicated pollen distributions at some length, but the results of those studies have not yet been tested widely enough to assess their usefulness fully.

One nonparametric statistical test that has proven useful in palynology is the multinomial chi-square homogeneity test (Faegri and Ottestad, 1948; Deevey and Potzger, 1951; Gray and Guennel, 1961; Mosimann, 1965). This method evaluates the probability that several samples could have come from the same sampling universe. However, the method has its disadvantages in that it cannot account for trends in the data, and trends are of great significance in palynology.

Because the statistical distributions followed by pollen data are not yet properly understood, I consider the usefulness of inferential statistics in palynology to be relatively limited at this time. The techniques used in this work are purely descriptive; they provide only a summarization of the data from various points of view and leave the evaluation of the patterns that are uncovered to the palynologist.

TEST DATA

The techniques described in this paper are illustrated by using pollen data from a core from Osgood Swamp, Calif., described by Adam (1967a). The site is at an altitude of 1,980 m in mixed coniferous forest, near the south end of Lake Tahoe in the central Sierra Nevada; the pollen record includes the entire Holocene and the latest part of the last Pleistocene glaciation.

Although only one data set is used as an example here, these techniques have been applied to several other sets of data and have provided equally good results. I have used common names for plants whenever possible because the exact botanical nature of the pollen types is not of primary importance here; what matters is that the statistical methods presented can simplify the description of a series of observations of many pollen types and many samples.

The Osgood Swamp data set (fig. 1; see also Adam, 1967a) consists of observations of 42 pollen types in 46 samples and is based on four different counts, using the method of multiple fixed sums (Mehring and Haynes, 1965). Pine pollen was recorded as the number of pine grains found in a total count of 200 grains of all pollen. All other pollen types record the number of grains counted in a total of 100 grains of all types except pine. *Isoetes* spores represent twice the number of spores counted in a total of 100 grains of pollen plus *Isoetes*; these figures are doubled to bring them closer to the values

that would have been recovered if *Isoetes* had been counted with the first pollen sum. *Nuphar* leaf hairs are recorded as the number of hairs in a total of 100 leaf hairs plus pollen grains. The differences in scale between the four counts affect the total variance of the data set and the proportions of the variance contributed by the various types but not the basic patterns in the data.

One sample (sample 19) included in the Osgood Swamp data was not included in the original description of the pollen profile. This sample, from a depth of 180 cm, has a very high

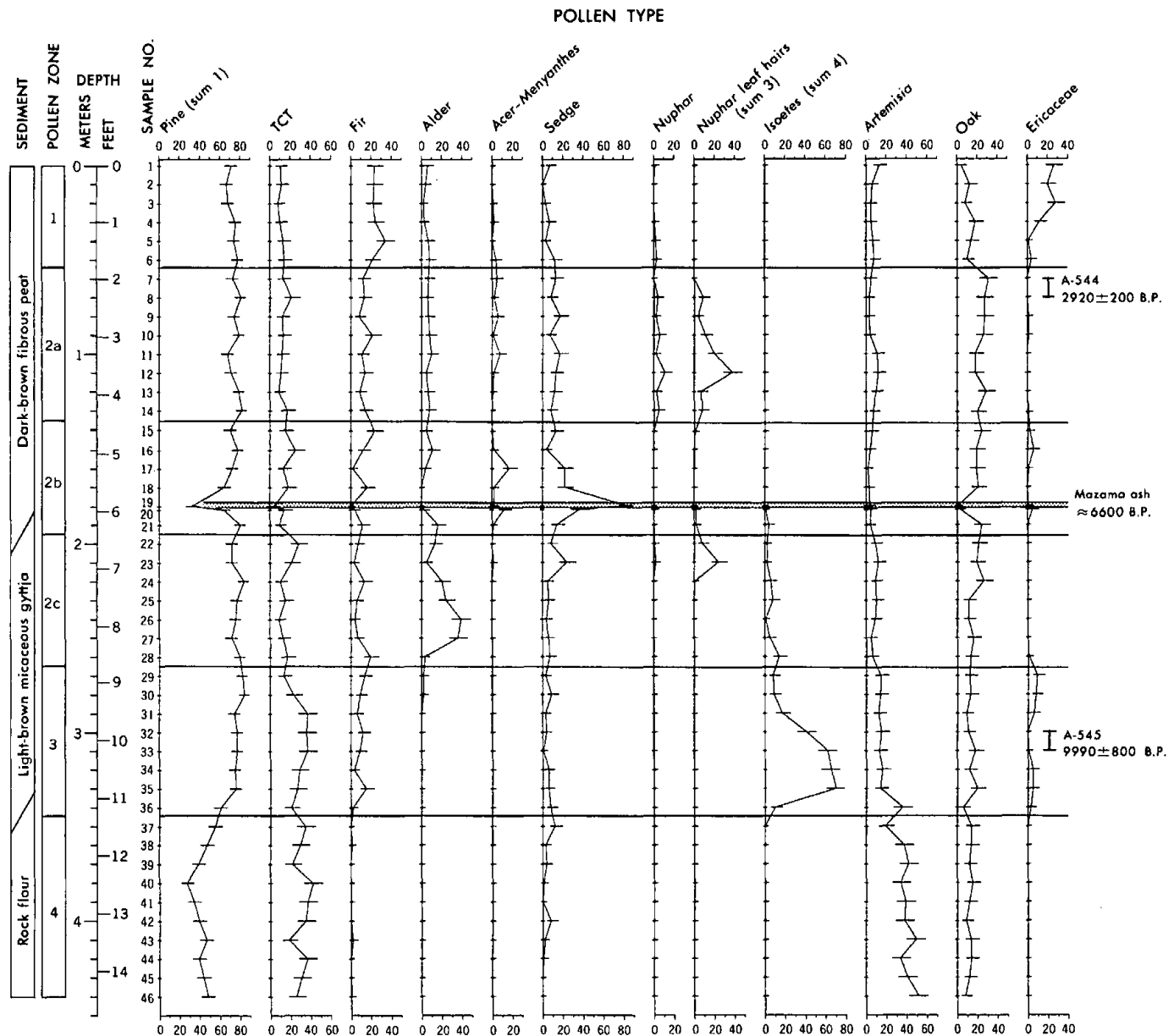


Figure 1.—Pollen diagram from Osgood Swamp, Eldorado County, Calif. Only those pollen types discussed in the text are shown; TCT includes pollen of the families Taxodiaceae, Cupressaceae, and Taxaceae and probably represents mostly juniper and incense cedar. Horizontal bars on frequency curves are 95-percent binomial confidence intervals (Maher, 1972; Mosimann, 1965), and the horizontal scale is in percentage. The two radiocarbon dates are 90 years greater than originally published because of a laboratory correction discovered after initial publication. Figure redrawn with the addition of sample 19 from Adam (1967a, fig. 6).

frequency of sedge pollen, and many of the sedge grains are in clusters. This sample is adjacent to, and includes a part of, the Mazama ash layer. The high sedge frequency is interpreted as a sedge anther that had been included in the sample. That sample was excluded from the original diagram (Adam, 1967a, fig. 6), and a second pollen sample was taken from a depth of 182 cm. The second sample did not show such a high sedge pollen frequency, although the value is still markedly higher than for any other sample on the diagram. The 182-cm sample was included in the original diagram; both samples are included in figure 1. The Osgood Swamp data matrix used in this study may be found in Adam (1970, appendix A).

A GEOMETRIC MODEL

Description

A useful approach to the systematic study of a group of pollen samples is to consider the samples as a set of points in a multidimensional space. If there are m samples and n pollen types, then the frequency data can be regarded as a set of m points in an n -dimensional space. Within this multidimensional space, the structure of the data will be represented as groupings or patterns of points. Samples closely resembling each other will have similar coordinates and be located near each other, whereas unlike samples will be far apart and have dissimilar coordinates.

Such spaces are difficult to visualize when there are more than three dimensions, and graphic representation is not easy with more than two. The example used here has only two dimensions for simplicity of presentation, but the results can be extended to higher order spaces. In this hypothetical example, 15 samples from a core have yielded observations on the frequencies of many pollen types; we will consider only two types, A and B. The traditional mode of presentation of such data is a pollen diagram (fig. 2A), which shows frequencies of occurrence as a function of depth. The geometric model, however, portrays the samples as points whose coordinates are the frequencies of the constituent pollen types (fig. 2B).

Both methods of presentation show that a strong negative relationship exists between pollen types A and B; when A is present in high frequencies, B tends to be present in low frequencies, and vice versa. Most of the variance can be accounted for by a single straight line through the sample points.

An infinite number of sets of coordinate axes can completely describe the variability in the data, even when there are only two dimensions. These other sets of axes represent translations or rotations of the original set, and the sample points possess different coordinates with respect to each set. Some sets of axes may be of greater use for the description of the patterns in the data than the original set.

The standard pollen diagram (fig. 2A) emphasizes pollen types one at a time. In a pollen diagram, consideration of

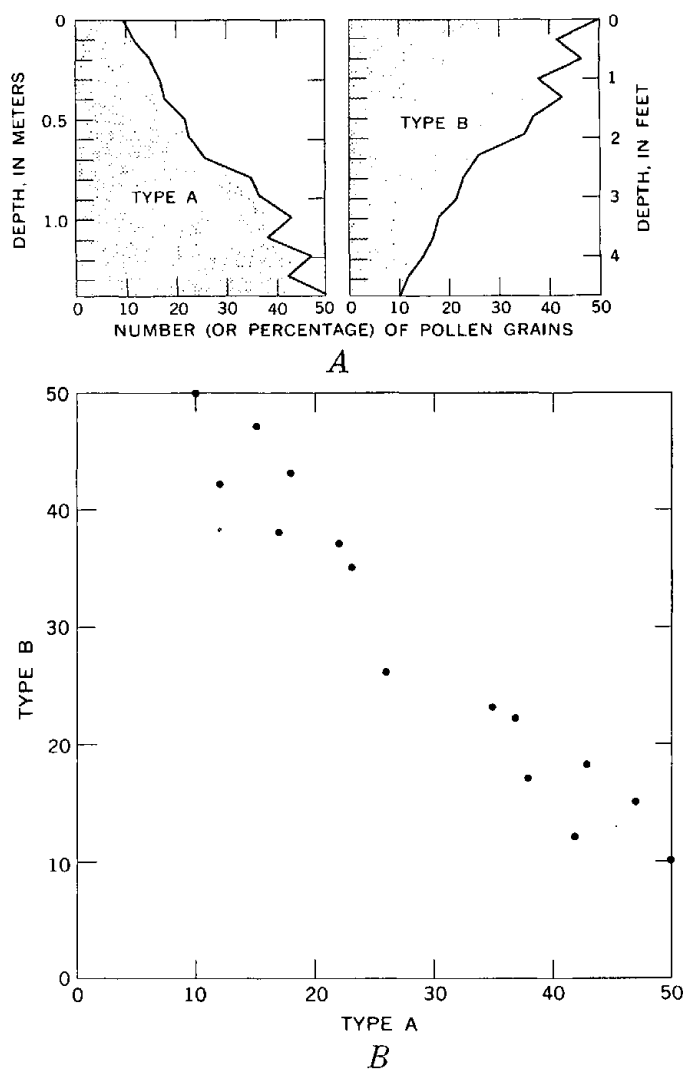


Figure 2.—Alternative representations of hypothetical pollen data. Units along axes may be either pollen grains or percentages. A, Data plotted as a standard pollen diagram. B, Data plotted using the geometric model.

patterns that affect several pollen types at once requires observation of several pollen curves simultaneously. Although such simultaneous observation has been done effectively for many years, it is an art requiring both skill and practice, and it may be unconvincing to the uninitiated.

The geometric model, however, emphasizes patterns between the samples, and interpretation involves relating these patterns to the pollen types. Various statistical techniques permit objective description of the relationships between samples in terms of the original pollen types; in the traditional method the patterns recognized depend on the unformalized criteria and intuition of the observer.

Thinking in terms of a multidimensional space may be as much an art as the traditional method of interpreting pollen diagrams; however, much of the descriptive work that has been

done in the past by the observer can be accomplished by a computer, thus freeing the observer for the more interesting work of relating the (objectively defined) patterns to paleoenvironmental conditions. Computer-defined patterns can be used as a map or guide to the basic data, indicating interesting events.

The justification for introducing a geometric model into palynology thus rests on two main points: (1) The model permits greater objectivity in describing palynological data, so that two workers can independently arrive at the same patterns in a given set of data, and (2) It helps the palynologist to evaluate his diagrams and present his conclusions faster. The latter point is important, for it is doubtful that the advantage of introducing objectivity into part of the interpretive process would alone be sufficient justification for the adoption of a complex methodology. In areas that have been investigated intensively, palynologists have been able to develop large bodies of internally consistent data without using wholly objective methods.

Although palynological examples of geometric models are still rare, geometric models are widely used in multivariate analysis. Of particular interest here are the studies by Orloci (1966) and Pielou (1969) on the use of such models in ecology. Morrison (1967) uses geometric models to good effect in his illustrations of multivariate statistical procedures, and they are implicit in the work of Gnanadesikan and Wilk (1967). At the time this work was completed (Adam, 1970), no other studies applying multivariate statistical techniques to palynology had been published. Since then, a few papers have appeared, including those by Dale and Walker (1970), Webb and Bryson (1972), and Gordon and Birks (1972), and similar techniques have also been applied to deep-sea foraminiferal data (Imbrie and Kipp, 1971). No attempt has been made to integrate the conclusions of these studies with those of this paper.

Applications

Once the basic principle of the geometric model is grasped, there are several techniques that may be applied to yield answers to different sorts of questions concerning a set of data. One approach to the analysis of a set of pollen data is to consider the proximities of the sample points to each other in the n -dimensional geometric model space. Cluster analysis uses such an approach to form a hierarchical grouping of samples, showing how samples resemble each other and the degree of resemblance between them.

Another useful approach is principal component analysis, which describes the variance in the data in an efficient fashion by rotating the coordinate axes about the origin until a set of axes with certain optimum properties is attained. It is then possible to discard axes representing little or no variance and to select a subset of axes that describes most of the variance in

the data using fewer axes than were initially necessary, permitting a reduction in the dimensionality of the data.

Cluster analysis and principal component analysis are powerful tools for the analysis of both modern and fossil pollen data; they require only the initial pollen counts and permit classification and description of the data in an economical form. Hence they are an improvement in palynological methodology over previous intuitive interpretive procedures.

COMPARISON OF SAMPLES

Application of these statistical techniques to pollen data requires the comparison of samples to each other by using some coefficient of similarity. Such a coefficient must be capable of distinguishing samples that are similar to each other from those that are dissimilar.

Many similarity coefficients have been proposed. Those used in palynology include Pearson's product-moment correlation (Martin and Mosimann, 1965; Barkley, 1934) and Spearman's rank-correlation coefficient (Ogden, 1969); Gordon and Birks (1972) have instead used a dissimilarity coefficient. Other promising measures of similarity include cosine-theta (Imbrie, 1964), covariances, and measures of Euclidean distance between sample points in the geometric model space (Parks, 1970). Further discussions of different types of similarity coefficients using biological data include those of Sokal and Sneath (1963) and Greig-Smith (1964).

Because computer programs were already available for principal component and discriminant analyses based on the product-moment correlation coefficient, it was chosen as the most practical measure of similarity between samples in this study. (Webb and Bryson, 1972, have followed the same course of action.) This coefficient is defined as

$$r_{xy} = \frac{\sum_{i=1}^N (x_i - \bar{x})(y_i - \bar{y})}{\sqrt{\sum_{i=1}^N (x_i - \bar{x})^2 \sum_{i=1}^N (y_i - \bar{y})^2}}$$

where x and y are samples and N is the number of pollen types. Note that in this usage, \bar{x} is the frequency of the "average pollen type" in sample x and is equal to the number of grains in the pollen sum divided by N .

When product-moment correlation coefficients are computed for sample pairs from raw pollen frequencies or percentages, the correlations are distributed abnormally, and unreasonably high coefficients are likely (Orloci, 1967; Underwood, 1969). This occurs because the common pollen types are usually present in rather large numbers, whereas many scarce types are present in frequencies near zero (fig. 3).

The points plotted represent the frequencies of individual pollen types in two samples each represented by a coordinate axis. (Note the difference between this and the geometric model outlined above, where the coordinate axes represented pollen types and the data points represented samples.) The

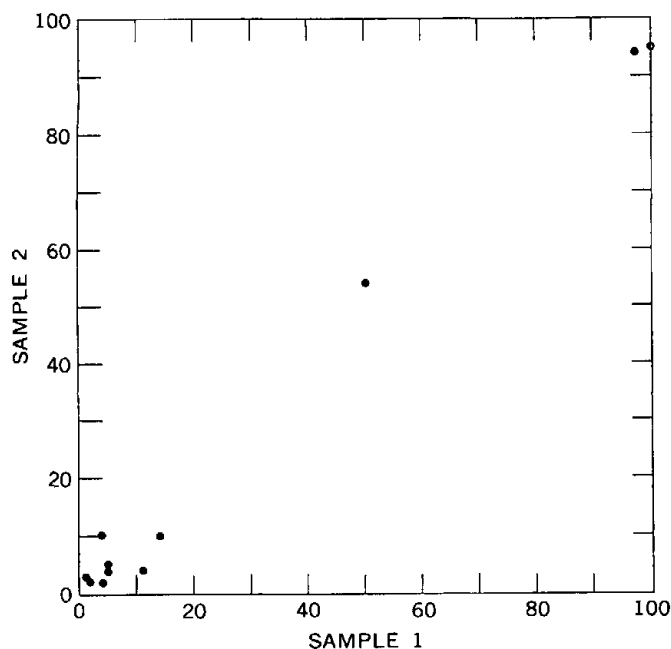


Figure 3.—Scatter graph of frequencies of selected pollen types in samples 1 and 2.

Pollen type	Frequencies (grains)		Pollen type	Frequencies (grains)	
	1	2		1	2
Pine	100	95	High-spine		
Fir	5	4	Compositae	11	4
Oak	14	10	Artemisia	50	54
Sequoiadendron	1	3	Cheno-ams	2	2
Other TCT	97	96	Sarcobatus	4	2
Sedge	5	5	Grass	4	10

correlation of samples 1 and 2 is a measure of how well a straight line fits the data points plotted in figure 3. The differences between the mean frequencies of the various pollen types introduce a large amount of variance that is irrelevant when comparing samples, and this increases the value of the correlation coefficient.

The skewed distribution of the correlation coefficients has been overcome in this study by using a centering transformation of the data (Orloci, 1967; see also Underwood, 1969) before computing the correlations. The mean or expected frequency for each pollen type is calculated for all samples, and each observation is expressed as the departure of the observed value from the expected value for the particular pollen type:

$$z_{ij} = x_{ij} - \bar{x}_j$$

where the z 's represent the transformed data observations, the x 's are the original pollen data, \bar{x}_j is the mean frequency of the j th pollen type, and the subscript i refers to samples. This transformation preserves the meaningful variance intact, while removing the effect of the differing mean frequencies of the

various pollen types. A demonstration of the effect of the transformation on correlations between samples is shown in figure 4. When the data are centered, the distribution of the correlations is much less skewed, and they have a mean value near 0.0.

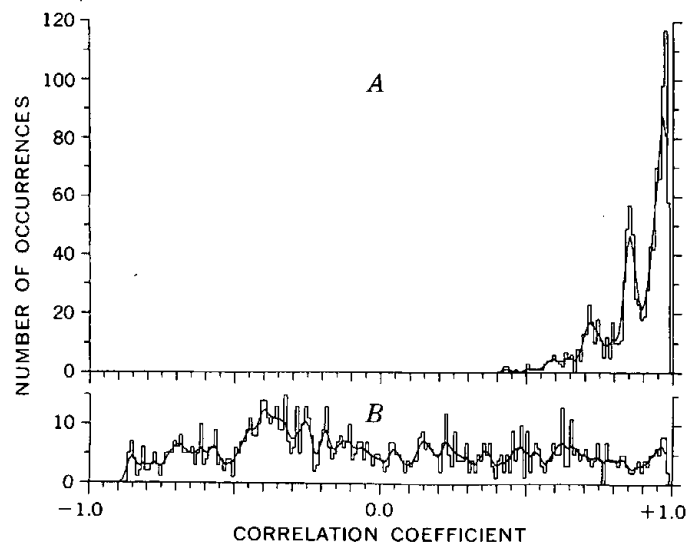


Figure 4.—Effect of a centering transformation on correlation data from Osgood Swamp. Both histograms show frequencies of occurrence of correlation coefficients of various magnitudes. A, Correlations computed from raw percentage data. B, Correlations calculated from the same data after a centering transformation.

A disadvantage of the transformation is that the values of the centered data elements are dependent on the means for the various pollen types, which may vary as samples are added or deleted. It is thus possible for the correlation between two samples to vary depending on what other samples are included in the data set when the means of the pollen types are calculated. In practice, this limits the applicability of conclusions drawn from a given correlation matrix to the samples that are included in it; the results of separate analyses cannot be combined without performing a new analysis on the combined data. Also, samples that are similar in one context may be dissimilar in another. For example, if an analysis includes only postglacial samples from a site, the transformed data values will be controlled by the departures of the observations from the postglacial mean frequencies for the different pollen types, and the correlation matrix will represent major patterns during the postglacial. But if an equal number of glacial-age samples are included, the overall mean frequencies for the pollen types will change, and pollen samples from the postglacial that are dissimilar in terms of the postglacial variability between samples may well be similar in terms of the overall variability between both glacial and postglacial samples.

An alternative transformation would be to normalize the data for each pollen type before comparing samples, which

would assign equal importance to each of the pollen types in the analysis. Although this procedure might be justified for the more common pollen types, the infrequent types have a high proportion of statistical noise in their pollen frequency curves that would be emphasized by increasing the relative importance of the scarce types. The results of analyses of normalized data sets are much less interpretable than when the centering transformation is used.

The general strategy used in comparing samples has been to utilize correlation coefficients as a measure of similarity because of the availability of computer programs, and then to use a centering transformation to make the correlation coefficients behave in a more normal fashion than with untransformed raw counts or percentages.

CLUSTER ANALYSIS

The purpose of cluster analysis is to study the best way in which the samples in a data set may be grouped together. The result is a two-dimensional representation of the relations between the samples, a clustering tree or dendrograph. The tree may be regarded as a classification of the samples based solely on the information contained in the pollen counts.

The mathematical methods of cluster analysis are the simplest used in this study. The nature of the method and its many variants have been amply described (Sokal and Sneath, 1963; Rohlf, 1970). The version used in this study is mean-linkage cluster analysis using a FORTRAN IV computer program written by the author.

The program begins by using the centered data matrix to calculate a matrix of correlation coefficients between pairs of samples. The correlation matrix is searched for the sample pair exhibiting the highest correlation. When identified, the two samples are linked into a group, and the magnitude of the correlation between them when they are linked is recorded. Samples thus linked are considered to be a single, pooled sample for the rest of the analysis until they are linked with still other samples at a lower level of correlation.

The process is repeated until all samples are linked into a single group. However, in all iterations except the first, when there are groups of samples that must be treated as units, the criterion used to determine the level of similarity between two groups is the arithmetic mean of the correlations between each of the members of the first group and each of the members of the second group. Thus, if group A contains samples 1, 3, and

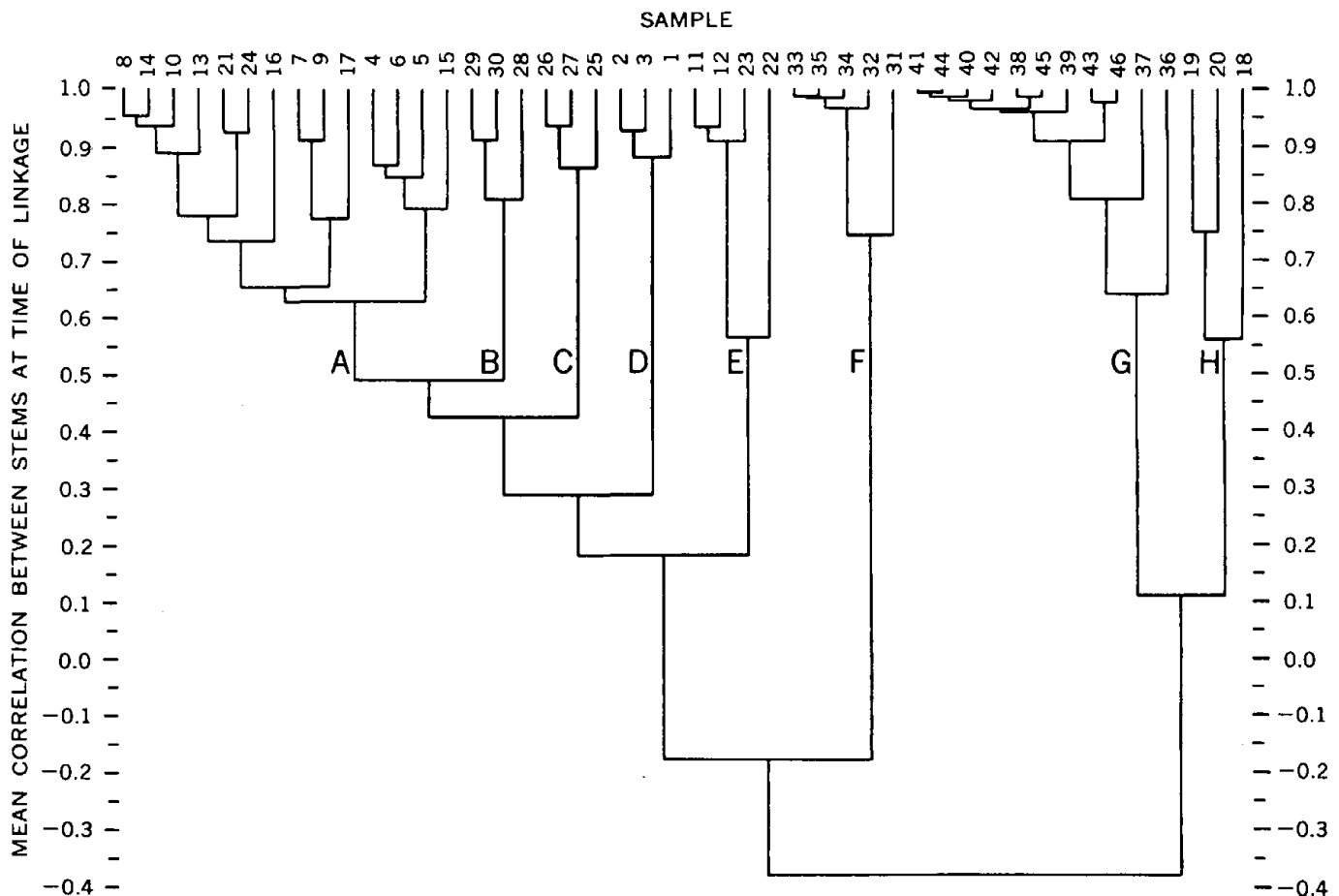


Figure 5.—Mean-linkage clustering tree for the Osgood Swamp data set. A–H are groups within which the mean correlation is 0.5 or greater.

4, and group B contains samples 2, 5, and 7, then the mean correlation between the two groups is

$$r_{AB} = \frac{(r_{12} + r_{15} + r_{17} + r_{32} + r_{35} + r_{37} + r_{42} + r_{45} + r_{47})}{9},$$

where letter subscripts refer to groups and numerical subscripts to individual samples.

The output from such a cluster analysis, the optimum grouping of the samples according to the mean-linkage method, requires no information about the samples other than the data. Cluster analysis thus permits objective comparison of all the samples in a study without regard to their stratigraphic or geographic positions. It is easy even without this technique to spot samples that are physically near each other but dissimilar; however, a method that can compare widely separated samples and objectively assess their degree of similarity is a welcome addition to the palynological toolkit.

Cluster analysis results are shown in the form of a clustering tree, with the samples ordered along the top of the tree so that no branches cross each other (fig. 5). Each branch of the tree is a vertical line representing either a single sample (those which reach the top of the tree) or group of samples (those which bifurcate before reaching the top). Samples or groups that are linked are connected by a horizontal line, the vertical position of which is determined by the degree of similarity (mean correlation) between the linked samples or groups. The order of the samples across the top of the tree is to a certain extent arbitrary; the only restriction is that branches should not cross each other. Reversal of the positions of two groups or samples that stem from any vertical line is permissible and does not alter the information in the tree.

A classification of the samples into groups or clusters is accomplished by arbitrarily choosing some specific level of similarity between groups as cutoff point. These groups are defined as those formed by linkages above the cutoff level and not linked with other groups except below the cutoff. The level of similarity chosen may vary from problem to problem. In the present study, a mean similarity of 0.5 divided the samples into eight groups, which have been designated on figure 5 by the letters A through H. To aid in the discussion of the tree, the samples, their depths, and the groups to which the samples have been assigned are shown in stratigraphic order in table 1.

All the clusters except for A and E are stratigraphically homogeneous; that is, all the samples in the group form a continuous layer in the core, although no stratigraphic information was used in the analysis. Also, group H is the only stratigraphically homogeneous group that interrupts other groups stratigraphically. Group A extends from sample 4 down through sample 24, but it is interrupted twice by samples from group E and once by group H. Apparently, the conditions that produced the group A samples persisted over a long timespan but were interrupted by other events of lesser duration that produced the group E and group H samples.

Table 1.—Stratigraphic listing of Osgood Swamp clusters

[Letters for clusters refer to stems of clustering tree shown in fig. 5]

Sample	Depth (cm)	Cluster
1	0	D
2	10	D
3	20	D
4	30	A
5	40	A
6	50	A
7	60	A
8	70	A
9	80	A
10	90	A
11	100	E
12	110	E
13	120	A
14	130	A
15	140	A
16	150	A
17	160	A
18	170	H
19	180	H
20	182	H
21	190	A
22	200	E
23	210	E
24	220	A
25	230	C
26	240	C
27	250	C
28	260	B
29	270	B
30	280	B
31	290	F
32	300	F
33	310	F
34	320	F
35	330	F
36	340	G
37	350	G
38	360	G
39	370	G
40	380	G
41	390	G
42	400	G
43	410	G
44	420	G
45	430	G
46	440	G

The meaning of the groups in terms of the original pollen types is discussed after the presentation of the principal component and factor analysis results from Osgood Swamp.

PRINCIPAL COMPONENT AND FACTOR ANALYSES

Principal component analysis is a statistical technique for describing the interrelations of a large number of correlated variables in terms of a smaller number of uncorrelated variables that are linear combinations of the initial variables. The object of the analysis is to reduce the dimensionality of the problem under study and thus clarify the patterns that are present in the data.

The methodology of principal component analysis has been described by many authors. Harman (1967) provides a general description as a part of his exhaustive treatment of the larger field of factor analysis. Morrison (1967) gives a general

statistical treatment, and Seal (1964) treats the subject similarly, while relating it to biological data. More specialized treatments include those of McCammon (1966) for geological data and Greig-Smith (1964) and Pielou (1969) for plant ecological data.

In terms of the geometric model, the sample points before analysis are arrayed in a space in which the coordinate axes represent the frequencies of the original pollen types. Reduction of dimensionality is accomplished by rotating the coordinate axes about the origin to find a new set of axes with certain optimum properties. The first axis, or principal component, is selected so that the variance of the coordinates of the sample points along this axis is a maximum. Such an axis amounts to a least-squares line drawn through the sample points and represents the most conspicuous pattern in the data.

Then new axes are selected, one at a time, with the additional restriction that each must be perpendicular to all the previously selected axes. Each new axis is thus uncorrelated with all prior axes and accounts for the largest possible proportion of the residual variance not accounted for by previous axes. After the rotation procedure is finished, there are still as many axes as before, but their orientations have changed.

The output of a principal component analysis is thus a set of rotated coordinate axes, accounting for successively smaller proportions of the variance in the data. If there are conspicuous patterns in the data, it may be possible to describe the data effectively by using only the first few axes, and the remaining axes can then be discarded without much loss of information, as they account for only a small proportion of the variance.

In palynology, however, some pollen types may contribute very little to the total variance yet be very useful in making paleoecological interpretations when present. Principal component analysis considers variance and information to be equivalent, and thus it cannot treat these pollen types properly; the analyst must remember this when interpreting the results.

The lack of emphasis on scarce but significant pollen types could be circumvented by weighting the pollen types in the data differentially according to the observer's evaluation of their relative importance. However, objectivity is one of the main advantages of the technique as it is normally used; once the practice of weighting the pollen types differentially (and subjectively) is adopted, this objectivity is lost, and any desired results could probably be produced simply by selecting the proper set of weighting factors.

While one may argue that a decision not to weight the variables is also subjective, such a decision can be reproduced by independent observers and is therefore to be preferred over a decision to weight the variables.

Another difficulty with the use of weighting factors is that, for a given sample size, the binomial confidence limits (and

hence the sampling errors) are not uniformly distributed over all frequencies. The frequency curves of rare pollen types have a higher ratio of noise to signal than the curves of common types, and any attempt to emphasize the information in scarce pollen types by using large weighting coefficients will also amplify the noise.

Mathematically, principal component analysis is the solution of the matrix equation, $RQ=Q\Lambda$, where, in this study, R is a square, symmetric matrix containing the correlation coefficients between samples, Q is a square matrix in which the columns are the eigenvectors of R , and Λ is a diagonal matrix in which the elements along the principal diagonal are the eigenvalues that correspond to the eigenvectors in the columns of Q (Harman, 1967). The program used for these analyses was BMD03M, one of the University of California biomedical computer programs. A description of that program and the mathematical procedures that it follows are given by Dixon (1968).

The eigenvalues and eigenvectors represent the results of the principal component analysis. The eigenvalues are proportional to the amount of variance accounted for by their associated eigenvectors, and thus the largest eigenvalues identify the eigenvectors that portray the most conspicuous orthogonal patterns in the data.

These eigenvectors contain one weighting coefficient for each pollen sample in the analysis. They are scaled so that the weights may range from -1.0 to $+1.0$, and the absolute value of each weight is proportional to the effect that the particular pattern (eigenvector) has on the corresponding sample. The eigenvectors and weighting coefficients are sometimes referred to as **factors** and **factor loadings**, and these conventions will be adopted here. Once factor loadings on a series of samples have been obtained, they may be plotted as stratigraphic variables in the same way as pollen types are plotted on a pollen diagram. When only a few factors are necessary to explain most of the variance in a data set, the stratigraphic diagram of these few factors is an effective way to present the results of the pollen analysis in a concise form.

The principal components of a data set are ordered so that the first k of them ($k \leq n$, the number of pollen samples) explains the maximum amount of variance that can be accounted for by only k dimensions. This property is useful in determining which of the axes (or factors) can be discarded without loss of useful information, in order to reduce the dimensionality of the problem.

Although the factors that result from simply scaling the eigenvectors are useful for interpretation, they are only one of an infinite number of sets of axes that can be used to describe the same data set. Once the dimensionality of the data has been reduced by selecting the first few principal components, it is possible to make the factors easier to interpret by using a further rotation of the axes. Additional rotation maximizes the variance of the squares of the factor loadings while

preserving the total variance intact and is referred to as **varimax rotation** (Harman, 1967).

The effect of a varimax rotation is to make the larger factor loadings assume values that are close to ± 1.0 and the smaller loadings approach zero. This makes the factors easier to interpret, for the individual pollen samples tend to be either highly affected by a factor or not affected by it at all. Although the varimax axes are orthogonal, the loadings themselves may be correlated and hence nonorthogonal (Matalas and Reiher, 1967). Varimax rotation, it should be repeated, deals only with that part of the variance retained after the principal component analysis.

A new rotation procedure that minimizes the entropy of the factor loadings has recently been suggested by McCammon (1970), but it has not yet been applied to pollen data.

For interpretation, the relations of the original pollen types to each factor must be known; these relations are quantified as **factor amplitudes**. The amplitudes are determined by treating each factor (eigenvector) as a linear equation with one term for each sample and substituting in the transformed (zero mean) data values for a given pollen type for all samples, after normalizing the observations for each sample. Thus,

$$w_{jk} = \sum_{i=1}^m a_{ik} \left[\frac{z_{ij} - \bar{z}_i}{\sigma_i} \right]$$

where the w 's are amplitudes; the a 's are factor loadings; z 's are centered data values; \bar{z}_i is the frequency of the mean pollen type in sample i ; j and k refer to pollen types and factors, respectively; m is the number of samples; and σ_i is the standard deviation of the sample i observations.

The factor loadings may be either positive or negative, and samples whose loadings for a given factor are of opposite sign behave in opposite ways with respect to that factor. The loadings with the greatest absolute value for a factor identify the samples that are most strongly related to that factor. The same relationship is true between factor amplitudes and their associated pollen types.

The 46X46 matrix of correlation coefficients from the pollen profile from Osgood Swamp yielded six factors that accounted for 91.5 percent of the total variance. These six factors were subjected to a varimax rotation. The varimax factors are listed in table 2 and presented graphically in figure 6; the factor amplitudes are listed in table 3. The reader may find it useful to compare figure 6 with the standard pollen diagram from the site (fig. 1).

The loadings on factor 1 (fig. 6) show high positive values below a depth of 330 cm, generally negative values above that level, and particularly high negative values between 330 and 260 cm. This factor is dominated by an inverse relationship between the loadings and the frequency of pine pollen as is shown by the factor amplitude of -97.2 on pine. Other pollen types that possess large negative amplitudes for factor 1 are fir (-15.4) and *Isoetes* spores (-14.0). Pollen types with high

Table 2.—Osgood Swamp factor loadings $\times 1000$

Sample	Depth (cm)	Factors					
		1	2	3	4	5	6
1	0	-160	-26	-6	93	-944	-88
2	10	10	-202	-66	-43	-930	-40
3	20	-101	-78	-33	99	-945	14
4	30	-456	-533	5	-4	-702	-52
5	40	-325	-509	-24	-238	-633	-106
6	50	-523	-474	39	83	-527	-242
7	60	-307	-897	27	69	-102	-191
8	70	-528	-587	467	-178	-81	-112
9	80	-394	-764	304	246	-65	-195
10	90	-508	-544	557	-222	-240	-113
11	100	-18	-172	950	150	-14	-44
12	110	-90	-18	981	-62	-5	92
13	120	-492	-655	422	-83	-47	-186
14	130	-572	-500	446	-166	-202	-206
15	140	-233	-822	56	7	-423	-14
16	150	-429	-520	5	-137	-332	-345
17	160	-296	-601	42	603	-18	-152
18	170	95	-717	-49	506	-189	211
19	180	415	10	2	793	82	154
20	182	14	-133	112	960	-106	25
21	190	-685	-531	122	16	-64	-445
22	200	-156	-404	574	-174	109	-351
23	210	-139	-82	938	150	190	77
24	220	-694	-417	29	-261	-61	-487
25	230	-567	-48	-99	-84	-22	-780
26	240	-230	-181	53	-13	-147	-930
27	250	-241	-153	-23	-15	-52	-934
28	260	-899	-42	-245	-200	-82	-0
29	270	-762	-113	-110	-224	-323	-107
30	280	-785	-99	-119	-142	-106	-60
31	290	-522	414	-374	-247	186	166
32	300	-576	521	-360	-261	376	192
33	310	-530	539	-342	-251	415	183
34	320	-504	600	-342	-172	410	179
35	330	-533	542	-335	-213	380	198
36	340	493	508	-307	-36	174	196
37	350	851	-66	-135	222	150	183
38	360	957	112	-123	-39	87	151
39	370	939	161	-111	43	60	145
40	380	934	173	-121	35	103	181
41	390	952	189	-123	-2	86	166
42	400	948	190	-116	91	93	171
43	410	893	124	-98	-90	49	119
44	420	956	148	-128	-5	98	169
45	430	952	164	-121	-54	69	140
46	440	890	201	-107	-110	38	112

positive amplitudes for factor 1 are *Artemisia* (43.6) and TCT¹ (20.8).

Factor 1 describes the change that takes place at the late glacial/postglacial boundary at Osgood Swamp (Adam, 1967a). During late glacial time, the pollen rain was characterized by higher than average frequencies of *Artemisia* and TCT pollen, while pine and fir pollen and the spores of *Isoetes* were present in less than average amounts. The general interpretation of factor 1 is that high positive loadings identify late glacial samples, while samples with high negative loadings correspond to (early) postglacial time.

¹ TCT includes pollen of the families Taxodiaceae, Cupressaceae, and Taxaceae, and probably represents mostly *Juniperus* and *Calocedrus*.

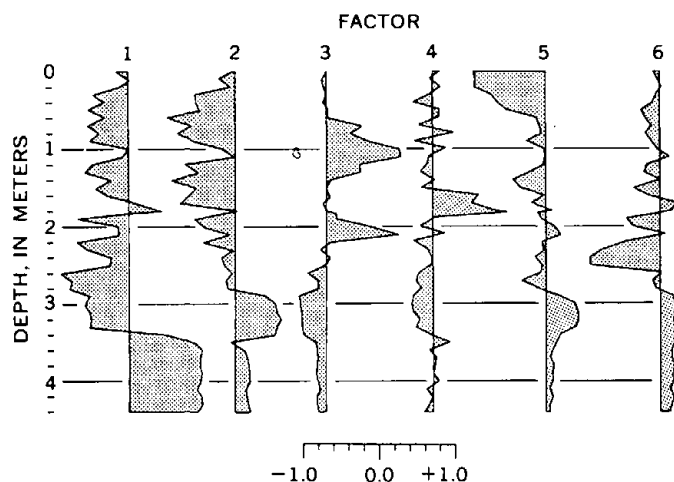


Figure 6.—Varimax factor loadings on samples from Osgood Swamp, plotted against depth.

An exception occurs at about 180 cm. Three samples at this depth have positive loadings because they have such high frequencies of sedge pollen that the frequencies of all other types, and particularly pine, are depressed owing to the constraint effect. Because the amplitude of factor 1 for pine pollen is far larger in absolute value than the amplitudes of all other types, pine pollen frequencies dominate the response of factor 1. The low-pine-content postglacial samples at 180 cm, with positive loadings on factor 1, can be separated from the deeper, late glacial low-pine-content samples on the basis of other factors.

Factor 2 has high negative amplitudes on pine (−38.8), oak (−15.5), fir (−12.6), alder (−7.0), and sedge (−6.8). The types with the largest positive amplitudes are *Isoetes* spores (41.0) and the pollen of *Artemisia* (26.7) and TCT (15.7). All the high loadings of either sign for factor 2 (and all succeeding factors) occur on postglacial samples. The types with high amplitudes for factor 2 involve all three major components of the vegetation: trees (pine, fir, and TCT, probably mostly incense cedar and juniper), shrubs (*Artemisia* and oak, probably mostly the scrub oak *Quercus vaccinifolia*), and aquatic-riparian elements (alder, sedge, and *Isoetes*). An interpretation of factor 2 suggests a shift during postglacial time from an oligotrophic lake surrounded by juniper and *Artemisia* to shallower lake or swamp bordered by sedge and alder in a mixed coniferous forest of pine and fir, with scrub oak replacing *Artemisia* as a montane chaparral element.

The loadings for factor 3 have two pronounced positive peaks at depths of about 1 and 2 m corresponding to samples for which neither factor 1 nor factor 2 has high loadings. The types with high amplitudes are *Isoetes* spores (−21.9) and *Artemisia* (−10.5) on the negative side and *Nuphar* leaf hairs (24.3) and pine (15.7) on the positive; additional positive increments are from oak (7.5), sedge (5.3), and alder (4.1).

Factor 3 displays a pattern in which *Isoetes*, which grows in clear, oligotrophic lakes, contrasts with *Nuphar*, the yellow pond lily, which grows in swamps no more than a few meters

Table 3.—Factor amplitudes on pollen types for Osgood Swamp

Pollen type	Factors					
	1	2	3	4	5	6
Pine	−97.2	−38.7	15.7	−13.0	−19.9	−29.5
TCT	20.8	15.7	−7.2	−3.0	13.3	9.6
Fir	−15.4	−12.6	1.5	−2.6	−17.0	−1.6
<i>Arceuthobium</i>	0.1	−1.9	−0.4	0.4	−2.2	−1.2
Douglas fir	2.3	−0.7	0.0	0.8	−0.8	0.5
Alder	−9.8	−7.0	4.1	−1.7	−1.8	−17.3
<i>Acer-Menyanthes</i>	1.3	−3.6	1.5	5.3	−0.3	0.2
Birch	2.0	−0.3	−0.1	0.4	−0.3	−0.7
Willow	2.5	0.2	−0.2	0.4	0.0	0.5
<i>Shepherdia</i>	2.2	−0.6	−0.2	0.7	−1.6	0.1
Sedge	1.9	−6.8	5.5	14.9	3.1	2.7
Cruciferae	2.2	0.3	−0.8	0.6	−0.1	0.0
<i>Typha-Sparganium</i>	2.1	−0.0	−0.7	1.1	−1.1	0.5
<i>Nuphar</i>	1.3	−1.2	2.3	0.2	−0.6	0.4
Liliaceae	3.4	0.2	−0.9	1.1	0.1	1.0
<i>Artemisia</i>	43.6	26.7	−10.5	−3.5	13.4	13.3
Oak	−7.0	−15.5	7.5	−1.4	0.9	−3.3
Ericaceae	−0.7	1.5	−3.3	0.7	−12.6	1.7
Grass	4.8	0.9	−1.2	0.4	0.7	1.3
High-spine Compositae	4.0	3.7	−3.0	−0.1	2.0	2.5
Low-spine Compositae	2.2	−0.2	−0.3	0.5	−0.6	−0.1
Rosaceae	2.9	0.8	−1.5	0.2	−0.8	0.9
<i>Sarcobatus</i>	4.1	1.9	−1.4	−0.1	0.7	1.1
Cheno-ams	0.2	−1.4	−0.0	0.3	−0.2	−0.5
<i>Castanopsis</i>	1.8	0.5	−1.2	0.5	0.3	0.1
Umbelliferae	1.3	0.2	−0.4	0.3	−0.7	−0.2
<i>Polygonum</i>	2.6	0.1	−0.6	0.7	−0.5	0.3
Caryophyllaceae	3.1	0.0	−0.4	0.9	−0.2	0.6
Rubiaceae	2.8	0.1	−0.4	0.5	−0.1	0.4
Caprifoliaceae	2.8	−0.0	−0.4	0.7	−0.3	0.4
<i>Aconitum</i> -type	2.7	−0.2	−0.4	0.6	−0.5	0.4
<i>Ephedra</i>	3.0	0.2	−0.4	0.6	−0.2	0.3
Onagraceae	2.8	−0.1	−0.5	0.6	−0.3	0.3
<i>Berberis</i>	2.8	0.0	−0.5	0.6	−0.3	0.3
Geraniaceae	2.9	0.1	−0.5	0.6	−0.3	0.4
<i>Plantago</i>	1.6	−0.1	−0.6	0.4	−0.4	−0.4
Unknowns	3.0	−0.2	−0.9	0.6	−1.5	0.5
<i>Isoetes</i> spores	−14.0	41.0	−21.9	−11.9	26.1	11.6
<i>Nuphar</i> leaf hairs	−1.3	−2.7	24.3	−0.3	5.3	1.6
Liguliflorae	2.8	−0.2	−0.5	0.7	−0.3	0.4
Orchidaceae	2.8	−0.2	−0.5	0.9	−0.3	0.4
<i>Sequoiadendron</i>	2.7	0.0	−0.5	0.6	−0.3	0.4

¹ TCT includes pollen of the families Taxodiaceae, Cupressaceae, and Taxaceae.

deep. Factors 3 may be considered as some measure of lake conditions; positive loadings indicate eutrophic conditions and negative loadings, oligotrophic conditions. Factor 3 probably represents primarily events within the lake, whereas factor 2 seems to deal with the lake as part of a regional pattern.

Factor 4 illustrates a pattern in which sedge (14.9) and *Acer-Menyanthes* (5.3) contrast with pine (−13.0) and *Isoetes* (−11.9). The pollen here designated as *Acer-Menyanthes* was originally identified as *Acer* and is so designated on the original pollen diagram (Adam, 1967a, fig. 6), but subsequent experience has led me to suspect that it is more likely to be *Menyanthes* (buckbean) pollen. Factor 4 is probably another pattern involving the behavior of the lake, with oligotrophic conditions during early postglacial time, but giving way to high frequencies of sedge and *Acer-Menyanthes* pollen after a

period involving the samples with high loadings on factor 3 near a depth of 2 m.

These conditions indicate rather shallow water and a falling lake level during the summers. *Menyanthes* grew where shallow water persisted, and sedges grew on the exposed lake bottom.

The interpretation of factor 4 is similar to those of factors 2 and 3. However, high loadings on factor 4 occur on different samples than for factors 2 and 3 and indicate shallower water, suggesting that fluctuations in lake level produce complicated changes in the local vegetation that cannot be adequately described with a one-dimensional model.

Factor 5 shows *Isoetes* spores (26.1), *Artemisia* (13.4), and TCT (13.3) pollen in contrast with the pollen of pine (-19.8), fir (-17.0), and the *Ericaceae* (-12.6). The pollen record of fir and the *Ericaceae* was used to infer cool conditions (Adam, 1967a); and factor 5 thus appears to represent cool conditions with high factor loadings. When the high loadings are positive, the cool conditions follow a period of colder conditions (the early postglacial), whereas negative loadings represent cool conditions following warmer ones (0–50, 140–150 cm).

The final significant factor is 6, which describes by strong negative factor loadings the peak in alder pollen during early postglacial time.

An example of the usefulness of this technique for description of patterns concerns factors 4 and 5, which involve pollen zone 2b of Adam (1967a). Using the records of fir and *Ericaceae* pollen, zone 2b represents a cool interval, although P. J. Mehringer, Jr. (oral commun., 1965) used the sedge curve to suggest that the zone represented a drying out of the swamp. The present analysis provides support for both positions, for both factor 4 and 5 show peaks within pollen zone 2b.

This analysis of the Osgood Swamp data shows the advantages gained from the application of principal component analysis and varimax rotation as descriptive tools for the study of palynological data. By considering pollen samples as a set of points in a space of relatively few dimensions and observing patterns in their distribution, worthwhile insights into the nature of the data may be obtained.

A principal component analysis may also be performed by comparing pollen types, rather than samples; however, the results are more difficult to interpret than when the method described above is used. An alternative approach to be tried is an analysis of the principal components of the variance-covariance matrix between pollen types, rather than the correlation matrix.

COMBINING TECHNIQUES

The various methods applied here provide summaries of the information contained in pollen data from several points of view. Each of these viewpoints has its usefulness, and it is advisable to apply as many of these methods to a given set of data as possible. By combining the results of the different analyses, further insights into the structure of the data may be achieved.

The relations between the cluster and principal component analyses of the site may be studied by preparing a graph of the principal components plotted with the samples arranged in the order specified by the clustering tree (fig. 7). Comparing the factors plotted in this way against the same data plotted in stratigraphic order (fig. 6), the differences between the orderings produced by the natural stratigraphy of the site and the clustering method may be observed.

The groups of pollen samples defined by the labeled stems on the clustering tree have systematically high factor loadings on some factors. This information together with the table of factor amplitudes (table 4) illustrates which variables are present in abnormally high or low frequencies in specific groups.

The interactions between groups and factors may also be summarized by a table, such as table 4, listing those factors with systematically strong loadings within a particular group. Factor 1 (glacial versus postglacial samples) affects the most groups (four), which is appropriate for the most important factor. Group F is unusual in that it is characterized by systematically high loadings on five of the six factors, showing that it is affected by several patterns. Comparison with the data (Adam, 1970, appendix A) and the pollen diagram (fig. 1) shows that the samples in group F are from the early postglacial and are transitional between glacial and postglacial samples. Factor 1 indicates a similarity of the group F samples to the postglacial samples (fig. 7), and factors 2, 3, 5, and 6 show similarities with the samples from late glacial time.

Another graphic method that combines the results of principal component and cluster analyses is to plot sample points on principal component axes, using separate symbols for the different clustering groups (fig. 8) and thus displaying the dispersion of the sample points in various two-dimensional projections. The first two varimax components are used as axes in figure 8A and it is clear that all groups with the exception of D and E occupy separate regions of the graph. When the first and third axes are used (fig. 8B), groups D and E are separated, but A and C overlap. If the first three axes were combined in a three-dimensional model, none of the groups would overlap. Additional graphs using additional axes could be prepared using the data in tables 1 and 2.

The combination of results from cluster and factor analyses uses each method to augment the other. Cluster analysis provides a way to order the samples depending upon their similarities to each other, rather than on their stratigraphic positions. Plotting the factors in the same order as the clustered samples shows how the samples within clusters are similar, and comparison with the factor amplitudes (table 3) gives information on the pollen types characteristic of the various clusters.

For instance, each labeled stem of the clustering tree could be characterized by the pollen types present in unusually high frequencies in the samples attached to that stem (fig. 7). Stems A through F all have higher than average pine pollen frequencies. Stems A and B also have high frequencies of fir,

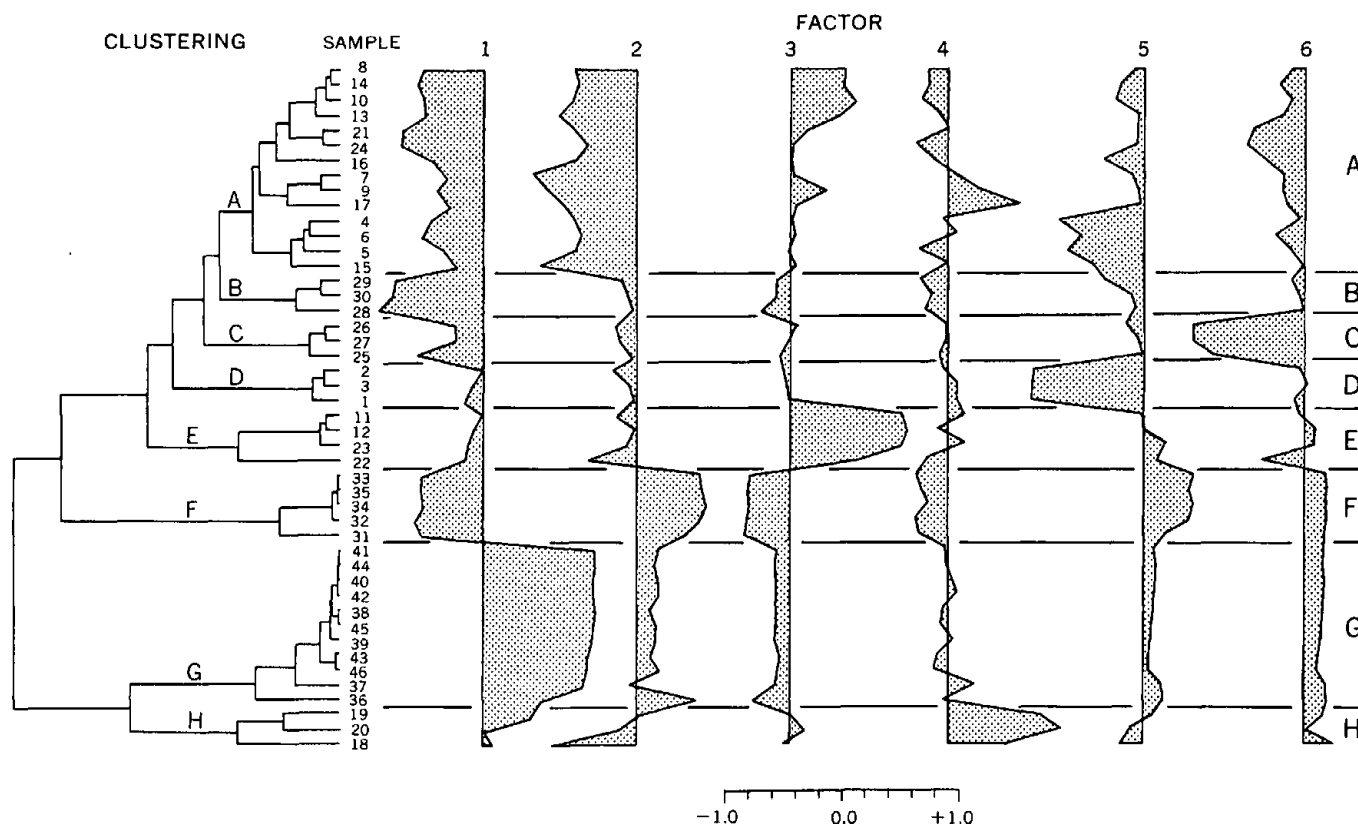


Figure 7.—Combined cluster and principal component analyses for Osgood Swamp. Note that samples are not in stratigraphic order.

Table 4.—Relations between factors and clustering groups in the Osgood Swamp data set

[When all the samples with a cluster show systematically high loadings on a factor, the sign of the loadings is entered in the relationship matrix. For example, all the samples in group E have high positive loadings on factor 3. Compare with fig. 6]

Clustering groups	Factors					
	1	2	3	4	5	6
A	—	—				
B	—					
C						—
D						
E			+		—	
F	—	+	—	—	+	
G	+					
H				+		

and A has more oak pollen than B. Stem C contains samples that have high frequencies of alder, while the samples of stem D have high frequencies of fir and Ericaceae pollen. *Nuphar* leaf hairs are relatively frequent in group E and stem F contains the samples that comprise the *Isoetes* peak.

Stems G and H contain those samples with lower than average frequencies of pine pollen. The two stems separate the late glacial samples with high frequencies of TCT and *Artemisia* pollen in stem G from the postglacial samples near the Mazama ash layer, which have high sedge pollen frequencies.

SUMMARY REMARKS AND CAUTIONS

Principal component and cluster analyses offer great promise for profitable application in the field of palynology. They have the ability to consider simultaneously all of the samples and all of the variables in a large data set, and they can do so in an objective, repeatable way. However, it is necessary never to forget the reason for using these methods: they are intended only as aids in the examination of the data, and the basic data should not be abandoned in favor of total reliance on the computer output. A computer may on occasion produce results that are ecologically equivocal or even ludicrous; all results must therefore be carefully evaluated to make sure that they are sound.

A particular hazard lies in the fact that these methods stress those pollen types with high variances at the expense of types that vary but little. A palynologist is well aware that this places undue emphasis on certain chronically overrepresented types, such as pine. We have learned to deal with over- and under-representation in the traditional interpretation of pollen diagrams, and we must do so with these new methods also.

If these methods are adopted, it will be desirable to develop methods of collecting pollen data in computer-compatible form. Many repetitive tasks can be automated if this is done; for example, the percentages and binomial confidence limits shown in figure 1. were calculated by a computer program, and

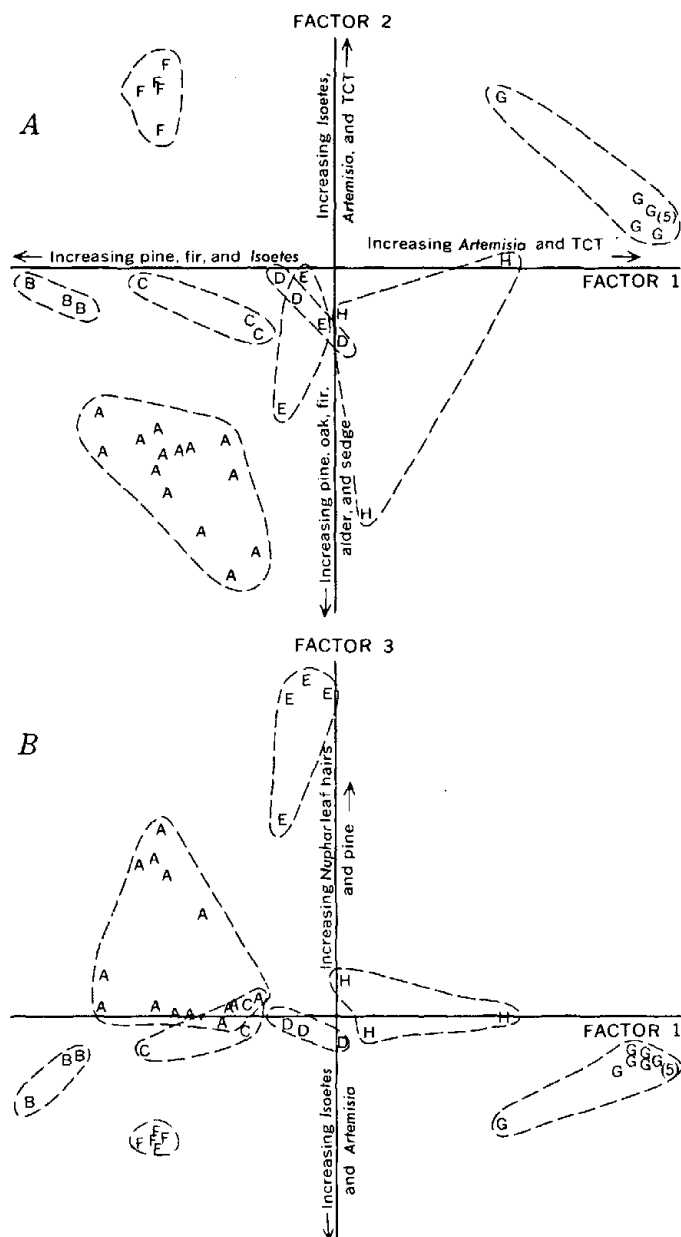


Figure 8.—Data points plotted along axes corresponding to varimax factors and labeled according to the clusters to which they belong. A, Canonical variates 1 versus 2. B, Canonical variates 1 versus 3.

the diagram itself was drafted by another program using a digital plotter.

Finally, the word "objectivity" has been used rather often in this report, and it is necessary to point out once more that the objectivity of these methods is limited solely to the description of the patterns in the data. Once these patterns have been described, the problem of interpretation must be handled with traditional scientific subjectivity.

ACKNOWLEDGMENTS

This work was supported by National Science Foundation Grants GB-1959 and GB-7794 to Paul S. Martin and by a National Science Foundation Graduate Fellowship to Adam.

Edward J. Cushing first suggested to me the application of computers to palynology and has offered much helpful criticism. Discussions with David Williams, Paul S. Martin, Harold C. Fritts, Charles Schweger, John Sims, Jack A. Wolfe, and Peter J. Mehringer, Jr., have been most helpful.

I thank the Numerical Analysis Laboratory (now the University Computer Center) at the The University of Arizona for extensive support of the computer time needed.

This paper represents part of a doctoral dissertation presented to the Geochronology Department of the University of Arizona.

REFERENCES CITED

- Adam, D. P., 1967a, Late-Pleistocene and recent palynology in the central Sierra Nevada, California, in Cushing, E. J. and Wright, H. E., Jr., eds., *Quaternary paleoecology*: New Haven, Yale Univ. Press, p. 275–301.
- 1967b, Nomogram for Mosimann's beta-compound multinomial correlation coefficient: *Am. Jour. Sci.*, v. 265, p. 907–908.
- 1970, Some palynological applications of multivariate statistics: Tucson, Arizona Univ., Ph. D. thesis, 132 p.
- Andersen, S. T., 1970, The relative pollen productivity and pollen representation of North European trees, and correction factors for tree pollen spectra: *Danmarks Geol. Undersögelse [Skr]*, ser. 2, no. 96, 99 p.
- Barkley, F. A., 1934, The statistical theory of pollen analysis: *Ecology*, v. 15, p. 283–289.
- Dale, M. B., and Walker, D., 1970, Information analysis of pollen diagrams I: *Pollen et Spores*, v. 12, p. 21–37.
- Davis, M. B., 1963, On the theory of pollen analysis: *Am. Jour. Sci.*, v. 261, p. 897–912.
- 1967, Pollen accumulation rates at Rogers Lake, Connecticut, during late- and post-glacial time: *Rev. Palaeobotany and Palynology*, v. 2, p. 219–230.
- 1969, Climatic changes in southern Connecticut recorded by pollen deposition at Rogers Lake: *Ecology*, v. 50, p. 409–422.
- Davis, M. B., and Deevey, E. S., Jr., 1964, Pollen accumulation rates—estimates from late-glacial sediments of Rogers Lake: *Science*, v. 145, p. 1293–1295.
- Davis, R. B., 1967, Pollen studies of near-surface sediments in Maine lakes, in Cushing, E. J., and Wright, H. E., Jr., eds., *Quaternary paleoecology*: New Haven, Yale Univ. Press, p. 143–173.
- Deevey, E. S., Jr., and Potzger, J. E., 1951, Peat samples for radiocarbon analysis—problems in pollen statistics: *Am. Jour. Sci.*, v. 249, p. 473–511.
- Dixon, W. J., ed., 1968, *BMD biomedical computer programs*: California Univ. Pubs. Automatic Computation, no. 2, 600 p.
- Fægri, Knut, and Iversen, Johs., 1964, *Textbook of pollen analysis* [2d ed.]: New York, Hafner Publishing Co., 237 p.
- Fægri, Knut, and Ottestad, Per, 1948, Statistical problems in pollen analysis: *Bergen Univ. Arb.* 1948, *Naturvitenskapelig Rekke*, 3, 29 p.
- Fagerlind, Folke, 1952, The real signification of pollen diagrams: *Botaniska Notiser*, v. 2, p. 185–224.
- Gnanadesikan, R. and Wilk, M. B., 1969, Data analytic methods in multivariate statistical analysis, in Krishnaiah, P. R., ed., *Multivariate analysis—II*: New York, Academic Press, p. 593–638.
- Gordon, A. D., and Birks, H. J. B., 1972, Numerical methods in Quaternary palaeoecology, I—Zonation of pollen diagrams: *New Phytologist*, v. 71, p. 961–979.
- Gray, H. H., and Guennel, G. K., 1961, Elementary statistics applied to palynologic identification of coal beds: *Micropalaeontology*, v. 7, p. 101–106.

- Greig-Smith, P., 1964, Quantitative plant ecology [2d ed.]: London, Butterworth & Co., Ltd., 256 p.
- Harman, H. H., 1967, Modern factor analysis [2d ed.]: Chicago, Univ. Chicago Press, 474 p.
- Imbrie, John, 1964, Factor analytic model in paleoecology, in Imbrie, John and Newell, N. D., eds., Approaches to paleoecology: New York, John Wiley & Sons, Inc., p. 407-422.
- Imbrie, John and Kipp, N. G., 1971, A new micropaleontological method for quantitative paleoclimatology—Application to a Late Pleistocene Caribbean core, in Turekian, K. K., ed., The Late Cenozoic glacial ages: New Haven, Yale Univ. Press, p. 71-181.
- Livingstone, D. A., 1969, Communities of the past, in Greenidge, H., ed., Essays in plant geography and ecology: Halifax, Nova Scotia Museum, p. 83-104.
- Maher, L. J., Jr., 1972, Nomograms for computing 0.95 confidence limits of pollen data: Rev. Palaeobotany and Palynology, v. 13, p. 85-93.
- Martin, P. S., and Mosimann, J. E., 1965, Geochronology of pluvial Lake Cochise, southern Arizona, III—pollen statistics and Pleistocene metastability: Am. Jour. Sci., v. 263, p. 313-358.
- Matalas, N. C., and Reiher, B. J., 1967, Some comments on the use of factor analyses: Water Resources Research, v. 3, no. 1, p. 213-223.
- McCammon, R. B., 1966, Principal component analysis and its application in large-scale correlation studies: Jour. Geology, v. 74, p. 721-733.
- 1970, Minimum entropy criterion for analytic rotation: Kansas Geol. Survey Computer Contr. no. 43, 24 p.
- Mehring, P. J., Jr., and Haynes, C. V., Jr., 1965, The pollen evidence for the environment of early man and extinct mammals at the Lehner Mammoth Site, southeastern Arizona: Am. Antiquity, v. 31, p. 17-23.
- Morrison, D. F., 1967, Multivariate statistical methods: New York, McGraw-Hill Inc., 338 p.
- Mosimann, J. E., 1962, On the compound multinomial distribution, the multivariate beta, and correlations among proportions: Biometrika, v. 49, p. 65-82.
- 1963, On the compound negative multinomial distribution and correlations among inversely sampled pollen counts: Biometrika, v. 50, p. 47-54.
- 1965, Statistical methods for the pollen analyst—multinomial and negative multinomial techniques, in Kummel, Bernhard, and Raup, David, eds., Handbook of paleontological techniques: San Francisco, W. H. Freeman, p. 636-673.
- Mosimann, J. E., and Greenstreet, R. L., 1971, Representation insensitive methods for paleoecological pollen studies, in Patil, G. P., Pielou, E. C., and Waters, W. E., eds., Statistical ecology, based on the proceedings of the International Symposium on Statistical Ecology, New Haven, Connecticut, August 1969: College, Pennsylvania State Univ. Press, p. 23-58.
- Ogden, J. C., III, 1969, Correlation of contemporary and late Pleistocene pollen records in the reconstruction of postglacial environments in northeastern North America: Mitt. Internat. Ver. Limnology, v. 17, p. 64-77.
- Orlaci, Laszlo, 1966, Geometric models in ecology, I—The theory and application of some ordination methods: Jour. Ecology, v. 54, p. 193-215.
- 1967, Data centering—A review and evaluation with regard to component analysis: Systematic Zoology, v. 16, p. 208-212.
- Parks, J. M., 1970, FORTRAN IV program for Q-mode cluster analysis on distance function with printed dendrogram: Kansas Geol. Survey Computer Contr. 46, 32 p.
- Pennington, Winifred, and Bonny, A. P., 1970, Absolute pollen diagrams from the British late-glacial: Nature, v. 226, p. 873-875.
- Pielou, E. C., 1969, An introduction to mathematical ecology: New York, John Wiley & Sons, Inc., 286 p.
- Rohlf, F. J., 1970, Adaptive hierarchical clustering schemes: Systematic Zoology, v. 19, p. 58-82.
- Seal, H. L., 1964, Multivariate statistical analysis for biologists: New York, John Wiley & Sons, Inc., 207 p.
- Sokal, R. R., and Sneath, P. H. A., 1963, Principles of numerical taxonomy: San Francisco, W. H. Freeman, 359 p.
- Tauber, Henrik, 1965, Differential pollen dispersal and the interpretation of pollen diagrams: Danmarks Geol. Undersøgelser [Skr.] ser. 2, no. 89, 69 p.
- 1967a, Differential pollen dispersal and filtration, in Cushing, E. J., and Wright, H. E., Jr., eds., Quaternary paleoecology: New Haven, Yale Univ. Press, p. 131-141.
- 1967b, Investigations of the mode of pollen transfer in forested areas: Rev. Palaeobotany and Palynology, v. 3, p. 277-286.
- Underwood, Robert, 1969, The classification of constrained data: Systematic Zoology, v. 18, p. 312-317.
- Waddington, J. C. B., 1969, A stratigraphic record of the pollen influx to a lake in the Big Woods of Minnesota: Geol. Soc. America Spec. Paper 123, p. 263-282.
- Webb, Thompson, III, and Bryson, R. A., 1972, Late- and postglacial climatic change in the northern Midwest, USA: Quantitative estimates derived from fossil pollen spectra by multivariate statistical analysis: Quaternary Research, v. 2, p. 70-115.

FLASHING FLOW IN HOT-WATER GEOTHERMAL WELLS

By MANUEL NATHENSON, Menlo Park, Calif.

Abstract.—The production characteristics of hot-water geothermal wells which flash to steam-water mixtures in the cased part of the hole were analyzed. The flashing flow is assumed to be isenthalpic and, for purposes of calculating pressure drop, a finely dispersed mixture of equal average velocity. Water flow in the aquifer is treated using steady, radial Darcy flow. Calculations for a typical geothermal well show the effects on production of varying the system parameters of aquifer permeability, depth to water table, and base temperature. Field data from Wairakei, New Zealand, demonstrate the reductions in flow caused by mineral deposits in the bore. Data from Imperial Valley, Calif., agree well with calculated results.

The flow characteristics of wells tapping hot-water geothermal systems are important to utilization of geothermal energy. The purpose of this work is to use an approximate formulation of the fluid mechanics of flashing steam-water mixtures to study the effects of various geothermal reservoir parameters on the production characteristics at the wellhead. The fluid mechanics and thermodynamics are formulated in the first section. Calculated results are presented and discussed in the second section. Some field data from Wairakei, New Zealand, and Imperial Valley, Calif., are analyzed in the third section.

PROBLEM FORMULATION

The physical situation is diagrammatically represented in figure 1. An aquifer of thickness L contains hot water at temperature T_3 with pressure p_3 at the datum level H (which corresponds to the well depth). The well either erupts spontaneously when the valve at the wellhead is opened or is induced to erupt (White, 1968). The steady state involves flow of water in the aquifer and up the well until a level Z^* is reached where the hydrostatic pressure has decreased sufficiently for boiling to commence (saturation pressure SVP_3 , corresponding to the temperature T_3). The pressure continues to decrease up the well in the two-phase regime, but the rate of change decreases upward as the proportion of vapor increases; and the density decreases. The driving force for the flow is the lower weight of the steam-water mixture from the level Z^* to the surface relative to that of the undisturbed

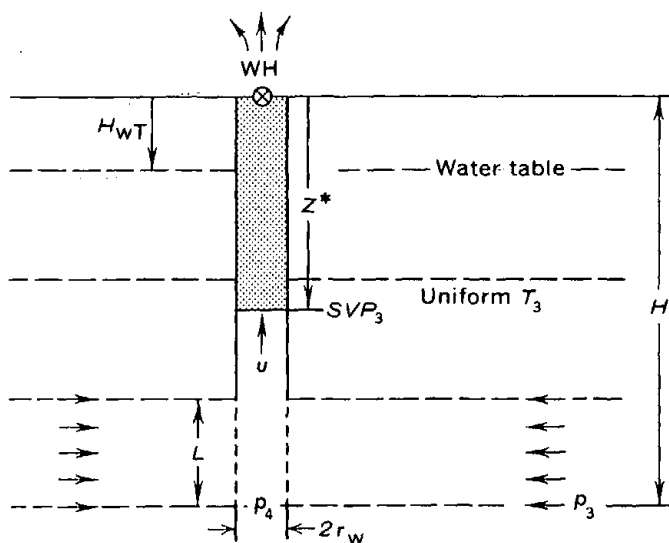


Figure 1.—Schematic diagram of flashing-flow system (exaggerated horizontally). H , well depth; p_3 , aquifer pressure; p_4 , well flowing pressure; SVP_3 , saturated vapor pressure; r_w , well radius; H_W , depth to water table; Z^* , level where boiling begins; WH, wellhead; u , flow speed of mixture; L , thickness of aquifer; T_3 , temperature of water in aquifer.

aquifer calculated at a datum equal to Z^* . The quantity of flow and the wellhead pressure can be controlled within certain limits by a throttling valve or orifice plate at the surface. The problems of two-phase flashing flow and bore-hole characteristics were discussed in a general way by Bodvarsson (1951). The formulation that follows is based on the work of Elder (1965).

Assuming that the waterflow in the aquifer is perfectly radial Darcy flow, the total mass flow M into the well is related to the pressure drop from the aquifer pressure p_3 (at the datum H) to the well pressure p_4 (at the same datum) by

$$M = \frac{2\pi LK}{V_{w3}\mu} \frac{(p_3 - p_4)}{\ln(r_e/r_w)}, \quad (1)$$

where K is the permeability, μ and V_{w3} are the viscosity and specific volume of water at the aquifer temperature, r_e is the

radius of drainage, and r_w is the well radius (Muskat, 1946). Equation 1 assumes that no flashing occurs in the aquifer. Because of the complications of adding several more parameters to the problem, flashing in the aquifer is not considered here. Note, however, that flashing flow in the porous medium significantly lowers the permeability as compared to that for all-liquid flow.

As water flows into and up the well, the hydrostatic pressure becomes low enough at the level Z^* for boiling to begin. The saturated vapor pressure SVP_3 at the level Z^* is related to the bottom-hole flowing pressure p_4 through hydrostatic equilibrium by

$$SVP_3 = p_4 - \frac{g}{V_{w3}}(H - Z^*), \quad (2)$$

where g is the acceleration of gravity. Neglected factors include the hydrodynamic resistance when there is only liquid water in the bore, conductive transfer of heat from the well to the surrounding rocks, and the partial pressures of dissolved gases.

Above the level Z^* , the flow of the flashing mixture is complicated. A reasonable approximation for flashing flow can be made by treating it as a finely divided mixture with equal average velocities of liquid and vapor when calculating the hydrodynamic resistance, including the changing proportions in the mass conservation and energy equations (Allen, 1951). This approximation neglects any slip of liquid relative to the vapor and is better at higher flow rates where the fluid is well mixed owing to turbulence. James (1968) has looked at the annular dispersed regime of two-phase flashing flow in a pipe and suggested certain modifications to the following formulation. If sufficiently detailed physical data on flashing discharges were available, it would be worthwhile to verify his suggestion; the published data for bore holes is too meager to warrant the additional complication.

Using the volume fraction of water X , conservation of mass at any section is

$$\frac{u}{V} = \left(\frac{X}{V_w} + \frac{(1-X)}{V_g} \right) u = \frac{u^*}{V_{w3}} = \frac{M}{\pi r_w^2}, \quad (3)$$

where u and V are the flow speed and specific volume of the mixture, V_w and V_g are the specific volume of liquid water and vapor at temperature T , u^* is the velocity of the water, and V_{w3} its specific volume below Z^* , where no flashing has taken place.

The energy equation is

$$\left[\frac{X}{V_w} h_w + \frac{(1-X)}{V_g} h_g \right] u = \frac{h_{w3}}{V_{w3}} u^*, \quad (4)$$

where h_w and h_g are the specific enthalpy of liquid and vapor, respectively (h_{w3} is the liquid enthalpy at T_3). The kinetic and potential energy of the flow has been neglected. Because of the large temperature change due to flashing, the transfer from internal energy to kinetic and potential energy has only a small effect on the overall temperature change and may be neglected (Elder, 1966).

The hydrodynamic losses may be treated by using a friction factor formulation for the momentum balance, and we can write

$$\frac{dp}{dz} = \frac{g}{V} + \lambda \frac{u^2}{4Vr_w}, \quad (5)$$

where we have neglected the momentum of the fluid but include the gravitation effect and friction. The friction factor for single-phase flow in circular pipes is tabulated as a function of Reynolds number and pipe surface roughness (for example, Katz and others, 1959). For geothermal bores, the Reynolds number is usually high ($\approx 10^6$) and the friction factor is then only a function of the surface roughness (Elder, 1966). (A tripling of surface roughness from that for gas-well tubing to that for wrought iron for a typical bore size leads to only a one-fourth increase in friction factor.) The neglect of the fluid momentum is consistent with the assumption of low Mach number flows. Although the Mach number can approach 1 in some high-output bores when backpressure is low, the large hydrodynamic resistance due to friction is more than adequate to limit the flow without need to appeal to sonic flow at the exit. Sonic flow at the exit is important for relating critical pressures to mass flows (James, 1962), but not for the quantities to be calculated here.

The method of calculation involves a computer program to numerically integrate the equations (Nathenson, 1974). Physically, the value of wellhead pressure and the physical parameters of the system determine the flow rate and distribution of temperature and pressure in the bore. Mathematically, it is much easier to pick a value for the bottom-hole flowing pressure. The flow rate can then be calculated from equation 1. The flashing depth is then calculated from equation 2. The distribution of pressure and temperature in the well can then be obtained by integrating (numerically) equation 5 up the bore in combination with equations 3 and 4. The integration has been done using Simpson's rule (Mathews and Walker, 1965, p. 332), and step sizes are chosen to give plotting accuracy. The thermodynamic properties of saturated water and steam are obtained from a look-up program using a four-point Lagrange interpolation routine (P. C. Doherty, written commun., 1973), and a stored set of steam tables (Keenan and others, 1969). The wellhead pressure is found when the integration has proceeded from $Z = Z^*$ to $Z = 0$. If the chosen value for bottom-hole flowing pressure is too low, the calculation terminates when the well pressure reaches 1 bar at some point below the surface. In the

process of debugging the program, I attempted to check the calculations for Elder's (1966) figure 25 and was unable to verify his results. In checking his calculations, I found that η -lines shown in his figure 24 are incorrect, and this is why his figure 25 was not reproducible.

GEOHERMAL BORE CHARACTERISTICS

Data for model reservoir and well

To investigate in a systematic manner how the reservoir parameters influence well performance, the variation of pressure with depth in the natural system must be established to specify the aquifer pressure. Since the density of liquid water is primarily a function of temperature, hydrostatic equilibrium combined with the temperature-depth relation recognized by Bodvarsson (1961) and White (1968, fig. 3) for high-temperature hot-water convection systems can be used to calculate the pressure-depth relation. Owing to natural convective overturn, the deep part of these systems has virtually a constant temperature (called the base temperature by Bodvarsson). In the near-surface part of an upflowing system, the hydrostatic pressure has decreased sufficiently to equal the saturated vapor pressure of the liquid water; vapor will then start to form. Above this point, decreasing hydrostatic pressure will cause increasing quantities of vapor to form with a corresponding decrease in temperature. This dependence of temperature on depth is approximated by the reference boiling-point curve (White, 1968, fig. 30; Hass, 1971) with the temperature at the water table fixed by atmospheric pressure at the altitude of the water table. The actual temperature distribution in a convecting hydrothermal systems differs in detail from the above, but this scheme is adequate for purposes of hydrostatic pressure calculations.

The water table is assumed to lie at some distance H_{WT} below the surface of the ground (negative values of H_{WT} would then correspond to overpressured systems such as the geyser basins of Yellowstone National Park described by White and others, 1968). Temperatures below this level are assumed to follow the reference boiling-point curve from 100°C at the water table to the base temperature of the system T_3 at a distance $H_{WT} + H_{BP}$ below ground level. Below this level, the temperature is assumed to be uniformly at T_3 and the pressure increases with depth at a slope depending on the density of water at T_3 . The pressure in the aquifer at datum H may then be written as

$$p_3 = SVP_3 + \frac{g}{V_{w3}} \left[H - (H_{WT} + H_{BP}) \right]. \quad (6)$$

Using equation 2 in equation 6, the driving force for flow in the porous medium is

$$p_3 - p_4 = \frac{g}{V_{w3}} \left[Z^* - (H_{WT} + H_{BP}) \right]. \quad (7)$$

Provided that the casing extends below Z^* (so that no flashing occurs in the porous medium), the driving force given by equation 7 is independent of the well depth.

The independent parameters for the problem formulated in this manner are aquifer temperature T_3 , permeability K , aquifer thickness L , well radius r_w , friction factor λ , and depth of water table H_{WT} . For geothermal bores, a reasonable radius of 12.7 cm and a surface roughness of 0.008 cm yield a friction factor of $\lambda = 0.015$. The ratio of drainage radius to well radius (r_e/r_w) will be taken as 500. The actual value matters little as long as it is large. A reasonable value for uncased length is 300 m, which will be used throughout.

Characteristics of a good geothermal bore

For a representative well in a good geothermal system, we assume an aquifer temperature of 250°C and a system permeability of 50 mD (millidarcys). Some of the details of pressure and temperature in this system for water table at the surface are shown in figure 2 and at depths of 100 m in figure 3 and 300 m in figure 4. Curves A of these figures are the initial system pressure and temperature. The initial temperature attains the base temperature at and below 463 m below the

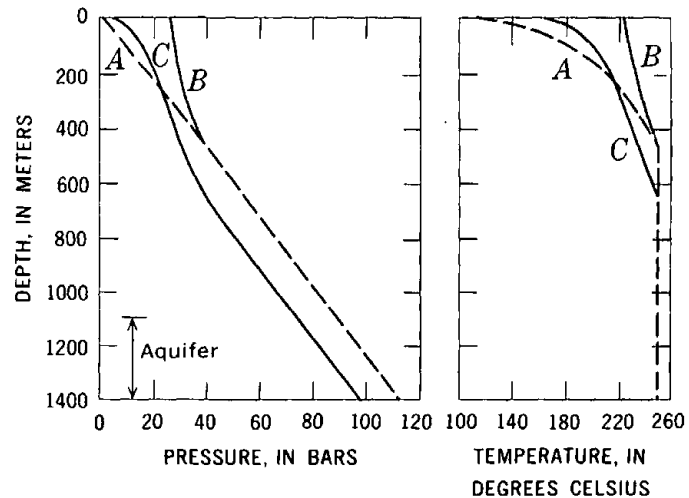


Figure 2.—Pressure and temperature profiles for water table at the surface. Curves A, system before discharge; curves B, zero-mass-flow limit; curves C, mass flow = 168 kg/s, wellhead pressure = 6.2 bars. Reservoir parameters: $T_3 = 250^\circ\text{C}$, $K = 50$ mD, $r_e/r_w = 500$. Well parameters: $L = 300$ m, $r_w = 12.7$ cm, $\lambda = 0.015$.

water table. Curves B show the pressure and temperature distributions obtained in the mathematical limit obtained by integrating equations 3, 4, and 5 with the mass flow equal to zero. The pressure and temperature distribution curves for a flowing bore neglecting friction can be obtained from curves B by shifting them down the amount needed to obtain the pressure drop in the porous medium for the flow under

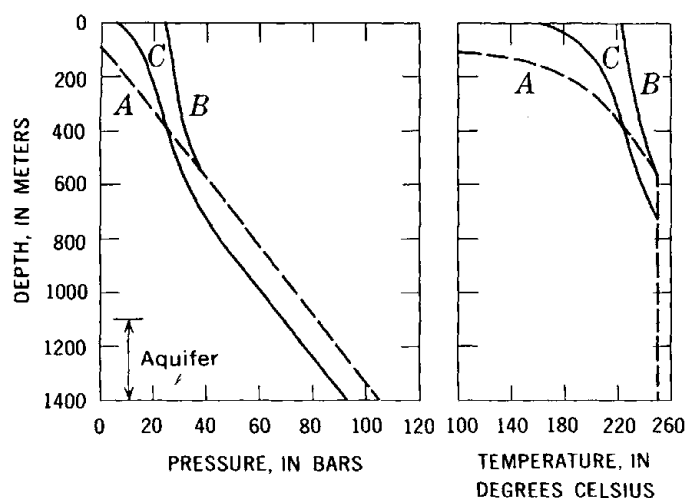


Figure 3.—Pressure and temperature profiles for water table at depth of 100 m. Curves *A*, system before discharge; curves *B*, zero-mass-flow limit; curves *C*, mass flow = 151 kg/s, wellhead pressure = 6.1 bars. Other parameters same as figure 2.

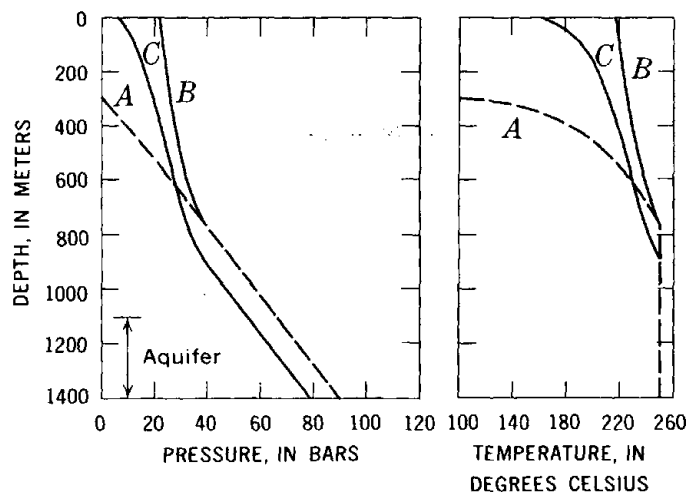


Figure 4.—Pressure and temperature profiles for water table at depth of 300 m. Curves *A*, system before discharge; curves *B*, zero-mass-flow limit; curves *C*, mass flow = 124 kg/s, wellhead pressure = 6.1 bars. Other parameters same as figure 2.

consideration (by using eqs 7 and 1). Although the conditions assumed to calculate curves *B* cannot occur (dispersed mixture of steam and water with no flow), the curves provide a useful mathematical limit. For flows at high wellhead pressure, the effects of friction should be small and the pressure distribution should be similar to curve *B* shifted downward. Curve *C* shows wellhead pressures of approximately production values (≈ 6 bar). In this example, the hydrodynamic resistance due to the two-phase mixture in the upper part of the bore is large, as shown by the bending over toward the origin of curve *C*

relative to curve *B* of these profiles, and further reductions in wellhead pressure do not bring corresponding gains in flow rate. Note also the movement of the flash point deeper in the hole with increased flow. A higher water table makes it possible to move the flashing surface deeper relative to its value for zero flow than for the lower water table, and this greater relative movement yields greater flows at the same value of wellhead pressure (compare curves *B* and *C* in figure 2 with *B* and *C* in 3 and 4).

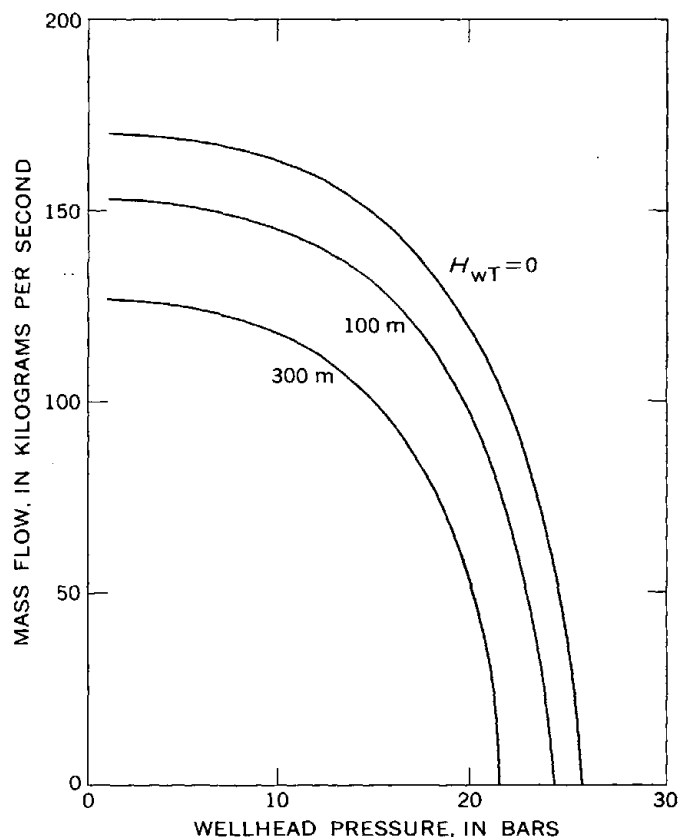


Figure 5.—Mass flow of steam-water mixture as a function of wellhead pressure for three depths to water table (H_{wT}). Reservoir and well parameters same as figure 2.

This behavior can be seen more easily in the wellhead curves for mass flow as a function of pressure shown in figure 5 for the three depths to water table, with other conditions held constant. Note that near the no-flow values of wellhead pressure, each decrease in wellhead pressure results in a large increase in mass flow. Near production pressures, however, the large resistance of the flashed mixture due to higher proportion of steam and greater velocity causes the wellhead pressure to have little effect on mass flow. This fact has important implications for finding the value of wellhead pressure that maximizes the flow of useful energy from a geothermal bore.

To calculate the flow of useful energy, we can apply the concept of availability (Jones and Hawkins, 1960, chap. 11;

Bodvarsson and Eggers, 1972). The availability of a system in a given state is defined by Jones and Hawkins as "the maximum amount of useful work which could be obtained from the system-atmosphere combination as the system goes from that state to the dead state while exchanging heat only with the atmosphere." To calculate the available energy as a function of wellhead pressure, we adopt the following scheme. Assume that, at the value of wellhead pressure under consideration, the steam and water of the mixture are separated, the steam is used to produce mechanical work, and the water is discarded. Neglecting the kinetic and potential energy, the specific availability of the steam (availability per unit mass of steam) is

$$y = (h_{g,wh} - T_0 s_{g,wh}) - (h_0 - T_0 s_0) \quad (8)$$

where T_0 is the absolute temperature of the cold reservoir, $h_{g,wh}$ and $s_{g,wh}$ are the enthalpy and entropy of saturated steam at the separation pressure, and h_0 and s_0 are the enthalpy and entropy of the dead state. The dead state will be taken as saturated liquid at pressures of 0.1 bar (45.8°C) and 1 bar (99.6°C). The ideal power (E) available from the bore may then be calculated from

$$E = \eta M y, \quad (9)$$

where η is the mass fraction of steam, M is the mass flow of the steam-water mixture, and y is the specific availability of the steam. For a unit mass of total fluid, the steam availability is ηy ; this quantity is plotted in figure 6 for water that was

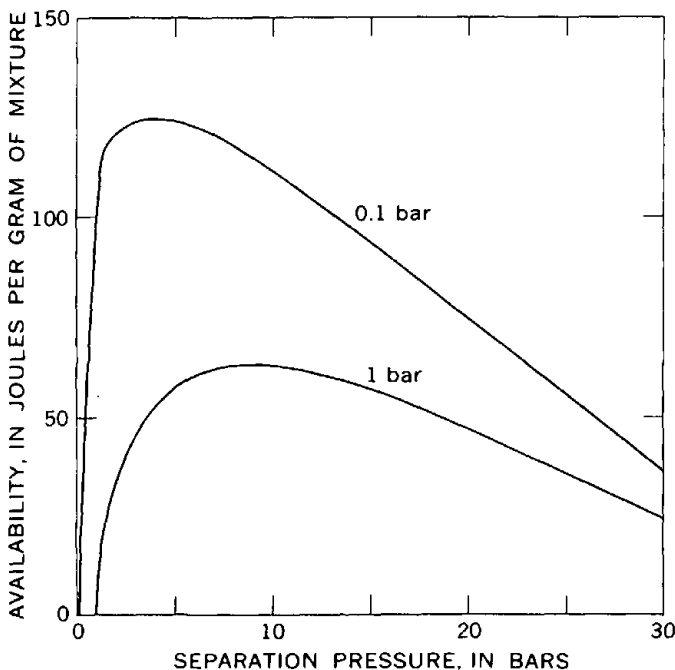


Figure 6.—Availability of steam phase per unit mass of mixture as a function of separation pressure for dead states of saturated liquid at 0.1 bar (45.8°C) and 1 bar (99.6°C) for water initially at 250°C.

liquid at 250°C. The calculation has been carried only to 30 bars because a 250°C bore will not normally be produced at wellhead pressures above this value. The plot shows the result of competition between two factors. Lower wellhead pressures result in higher steam fractions but bring the steam temperature closer to the cold reservoir temperature, thus lowering the availability per unit mass of steam. The competition results in a maximum of availability at a certain separation pressure, as shown. Note also that, with isenthalpic flow, once the aquifer temperature and dead state are fixed, the availability per unit mass of mixture is fixed by the separation pressure. Factors that tend to reduce the flow, such as deeper water table or lower permeability, affect only the quantity of fluids produced, not their specific availability (as long as there is enough flow that heat transfer is negligible).

Combining this thermodynamic calculation with output characteristic shown in figure 5 for a surface water table ($H_{WT} = 0$), we obtain the ideal power output shown in figure 7. Note that this calculation involves only the Carnot

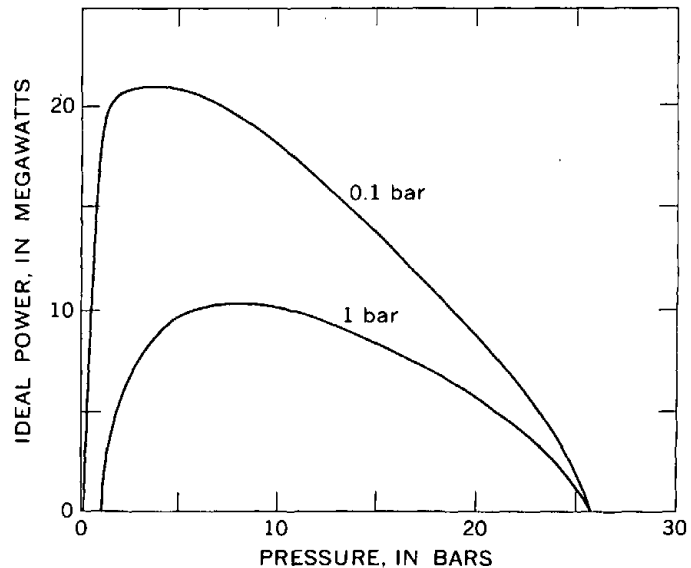


Figure 7.—Ideal output power as a function of separation (= wellhead) pressure for calculated flow shown in figure 5 for water table at surface.

efficiency and does not include any factors for losses in pipeline transmission, turbine losses, and other losses. The curves show the value of optimum wellhead (separation) pressure for maximum energy flow (James, 1967). As this optimum occurs in a flat part of the mass output curve, its location is basically governed by the thermodynamic considerations of figure 6 rather than the calculations of bore mass discharge.

Parametric investigation of geothermal bore characteristics

To study the effect of the reservoir parameters on well output, a number of wellhead characteristics such as the set

shown in figure 5 can be presented for different values of the parameters. These curves are all fairly similar in shape with the maximum flow and wellhead pressure for zero flow changing their size in response to changes in the reservoir properties. For comparison, a useful quantity is the mass flow for wellhead pressures of 6 bars, corresponding roughly to production conditions at Wairakei. Figure 8 shows the mass flow as a function of reservoir permeability for three depths of water table. For these values of flow the corresponding depth to first flashing is shown. The parameters L , D , λ and r_e/r_w have the same values as in previous calculations. For a system permeability of 100 mD and a surface water table, the flow at a wellhead pressure of 6 bars can then be read from figure 8 as 190 kg/s and the depth of initial flashing as 570 m. The dashed horizontal lines in the lower part of figure 8 show the depths at which the base temperature ($H_{WT} + H_{BP}$) of the system is first reached for each depth to water table. For high permeabilities, the depth to first flashing need only be a little below the reference value in order to obtain the large flows shown. The limiting resistance at these high flow rates is the

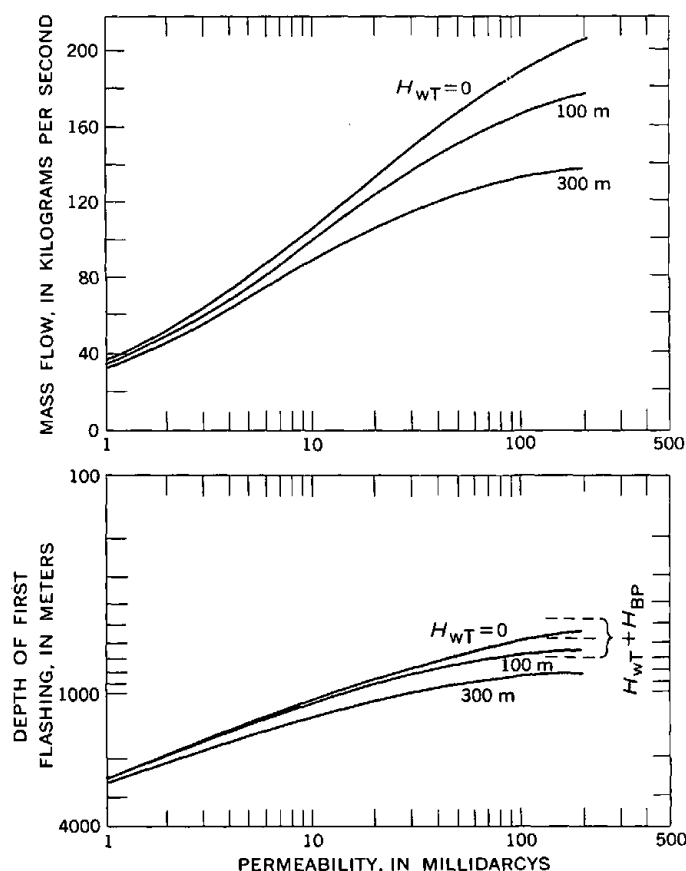


Figure 8.—Mass flow and depth of first flashing for wellhead pressure of 6 bars for range of permeabilities and several depths to water table (H_{WT}). Reservoir parameters: $T_3=250^\circ\text{C}$, $r_e/r_w=500$. Well parameters: $L=300$ m, $r_w=12.7$ cm, $\lambda=0.015$. The dashed horizontal lines show the depth at which the base temperature ($H_{WT} + H_{BP}$) of the system is first reached for each depth to water table.

hydrodynamic resistance in the bores owing to the flow of a two-phase mixture. For low permeabilities, large changes in the depth of first flashing are needed to obtain the flows shown. The lower flow rates force the flash point to move deep enough for the length and weight of the two-phase column to achieve low wellhead pressure before hydrodynamic resistance becomes the controlling mechanism. This can be seen clearly in figure 9, where the pressure distribution is shown for a well in a system where permeability is only 5 mD; curve C shows little bending over at low wellhead pressure as compared with curve C of figure 2. Decreasing the diameter of this well would cause hydrodynamic resistance in the bore to be the limiting factor and would decrease the maximum depth of first flashing, but would also lower the maximum flow rate.

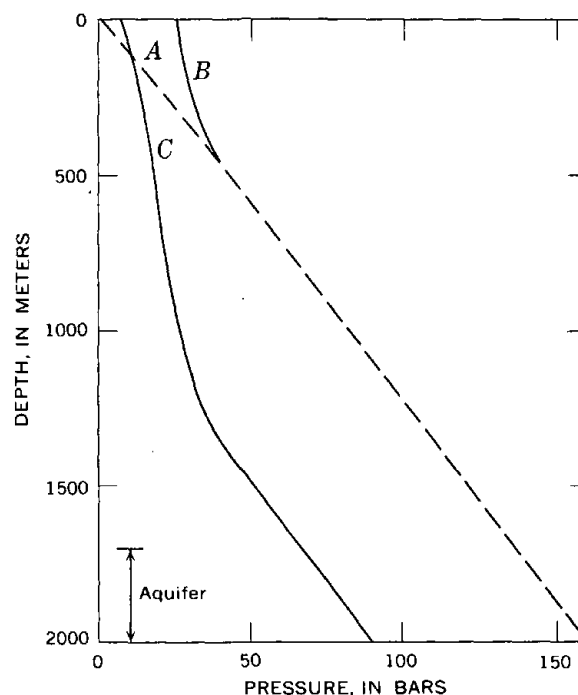


Figure 9.—Pressure profiles for water table at the surface. Low-permeability reservoir. Curve A, system before discharge; curve B, zero-mass-flow limit; curve C, mass flow = 78.3 kg/s, wellhead pressure = 7.3 bars. Reservoir parameters: $T_3 = 200^\circ\text{C}$, $K = 5$ mD, $r_e/r_w=500$. Well parameters: $L=300$ m, $r_w=12.7$ cm, $\lambda=0.015$.

To demonstrate the effect of system temperature on well deliverability, flow calculations for a 200°C aquifer are shown in figure 10. The wellhead pressure is still taken as 6 bars. As expected, this lower temperature produces consistently lower flows than were calculated for the 250°C water in figure 8. Note that the depth to water table has a significantly greater effect on the performance, owing to the lower saturated vapor pressure. For the same reason, the flash depths are consistently less than for the hotter water.

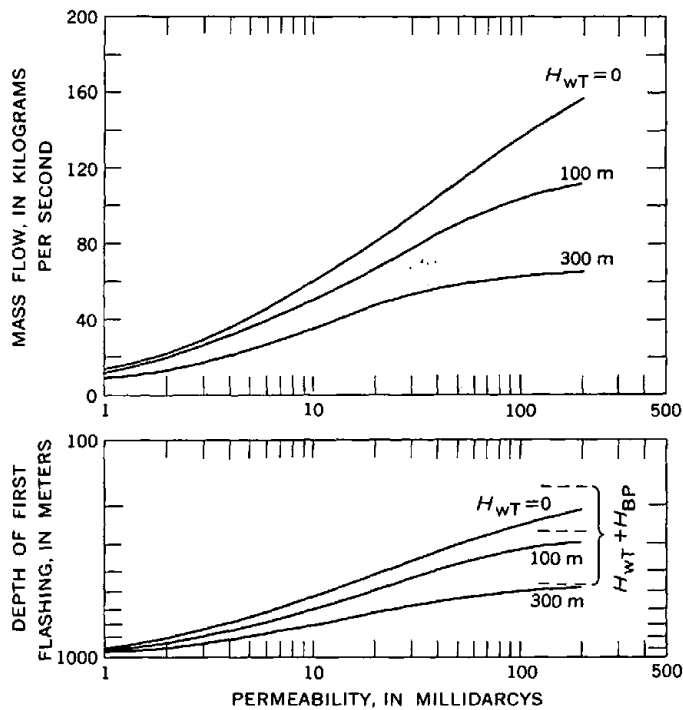


Figure 10.—Mass flow and depth of first flashing for wellhead pressure of 6 bars for range of permeabilities and several depths to water table (H_{wT}). Low-temperature aquifer. Reservoir parameters: $T_3=200^\circ\text{C}$, $r_e/r_w=500$. Well parameters: $L=300\text{ m}$, $r_w=12.7\text{ cm}$, $\lambda=0.015$.

FIELD DATA

Very few data are available on temperature and pressure distributions in flowing geothermal wells, and what is available must be interpreted with care. The first example is some field data obtained by Smith (1958) on the flowing-temperature distribution of Wairakei bore 27. This bore is 610 m deep and is thought to produce from a highly fractured zone about 1 m thick at a depth of 606 m. The bottom-hole shut-in and flowing pressures were measured by Smith, using a 5-cm-diameter tube that was supported at the surface and extended down to 605 m. The tube was supplied with pressurized nitrogen at the surface until the pressure in the tube at the wellhead remained constant. There was essentially no drawdown for this bore, and the gage pressure at 605 m was measured as 54 bars. The physical data used in the calculations are shown in table 1. Because the computer program uses the bottom-hole pressure to set the flow, a large but finite value of permeability was chosen such that drawdown would be very small—less than 1 bar out of the total bottom-hole pressure of 54.5 bars. The two radii shown are for calculations with and without the 5-cm tube in place. Calculating a Reynolds number of around 4×10^6 and a relative roughness of 8×10^{-5} , we obtain a friction factor of 0.012 (Katz and others, 1959). Using this value for

Table 1.—Data for bore 27, Wairakei, New Zealand

Parameter	Value
Aquifer:	
Temperature T_3	$^\circ\text{C}$.. 257
Pressure P_3	bar .. 54.5
Permeability K	D .. 120
Thickness L	m .. 1
Ratio, aquifer radius-well radius, r_e/r_w	500
Well:	
Depth H	m .. 609.6
Radius r_w :	
With tube	cm .. 9.8
Without tube	cm .. 10.2
Water viscosity μ	cP .. 0.104

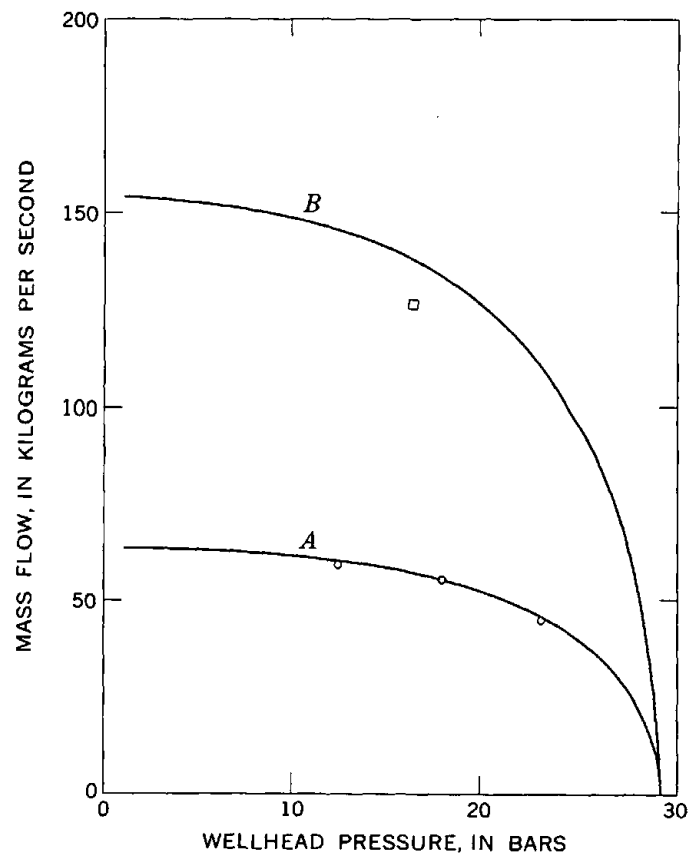


Figure 11.—Mass flows for bore 27, Wairakei, New Zealand. Curve A ($\lambda=0.062$) was calculated with friction factor chosen to match Smith's data (1958), shown as circles; curve B ($\lambda=0.012$) was calculated with friction factor chosen on the basis of estimated surface roughness. Square, data from Grindley (1965) for output in 1959 after bore had been cleaned of mineral deposits. See table 1 for other calculation parameters.

calculation, we obtain flows that are more than double those measured by Smith. Turning around and using the data to obtain a friction factor, a value of 0.062 was required to match the production data measured by Smith, shown in figure 11 as points on curve A. Smith obtained corresponding temperatures by lowering a thermocouple into the

5-cm-diameter tubing, and these are shown in figure 12 for the three mass flows and wellhead pressures for which measurements were made. Unfortunately, the validity of the comparison between the measured and calculated temperature data cannot be assessed for the following reasons: (1) The flow sampler used to measure bore outputs was calibrated between September 1957 and November 1958 for large output bores when a larger separator became available, and an output which had been previously been quoted as 75 kg/s became 102 kg/s (R. S. Bolton, written commun., 1973); the quoted outputs in Smith are probably lower than the real outputs, and (2) bore 27 was cleaned of mineral deposits in May 1958 (R. S. Bolton, written commun., 1973).

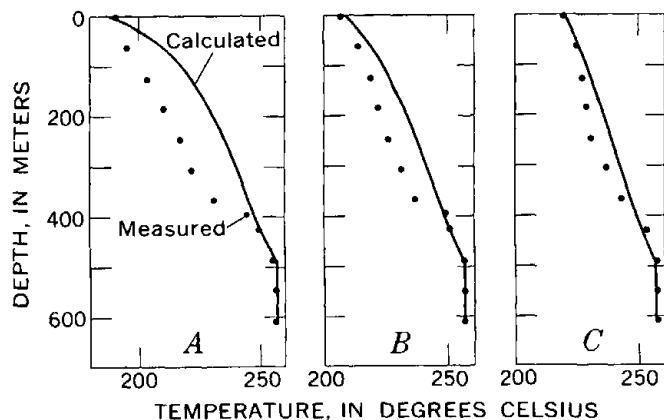


Figure 12.—Measured flowing-temperature profiles in bore 27(dots), Wairakei, New Zealand, compared to calculated values. A, Wellhead pressure = 12 bars, mass flow = 59 kg/s (61 kg/s calc). B, Wellhead pressure = 18 bars, mass flow = 55 kg/s (55 kg/s calc). C, Wellhead pressure = 23 bars, mass flow = 44 kg/s (45 kg/s calc). Parameters as given in table 1 with friction factor = 0.062.

The large effect of mineral deposition can be seen in the flow data for bore 27 reproduced here in table 2 (Grindley, 1965, tables 3 through 16). The cleaning in 1958 is a major cause of the jump in output from 73.4 kg/s in 1957 to 126 kg/s in 1959 with the calibration change causing a change almost as large (the 1957 value is probably closer to 100 kg/s than 75). The quoted flow for 1959 is plotted in figure 11, and the agreement with the predicted wellhead characteristic (curve B) is very good. The large difference in outputs from 1957 to 1959 and associated friction factors is due to an area

Table 2.—Mass flows and wellhead pressures for the years 1957, 1959–61, and 1963–65 for bore 27, Wairakei, New Zealand

[From Grindley, 1965]

	1957	1959	1960	1961	1963	1964	1965
Mass flow.....kg/s ..	73.4	126.0	69.2	45.2	70.3	84.2	73.2
Wellhead pressure ...bar abs ..	16.2	16.2	16.9	16.2	15.2	14.9	14.8

change from mineral deposition and possibly to a change in pipe surface roughness. Photographs in White (1968, figures 39 and 40) of mineral deposits in wells at Steamboat Springs, Nev., show that large quantities can be deposited and that the surface roughness of the deposits can be very large. Going back to the data in table 2, the jump between 1963 and 1964 also is due to a cleaning (R. S. Bolton, written commun., 1973). The inability of bore 27 to regain the 1959 output is probably due to the drop in aquifer pressure that started in 1958–59. By 1961, aquifer pressure at sea-level datum had decreased by approximately 8 bars (Grindley, 1965, figure 29B). The jump in output from 1961 to 1963 is part of a rise that started in November 1961 and peaked about 6 mo later, and for which there is no obvious physical reason (R. S. Bolton, written commun., 1973).

An example of a deep well in a lower temperature aquifer is the U.S. Bureau of Reclamation Mesa 6-1 well in Imperial Valley, Calif. (U.S. Bureau of Reclamation, 1973). The well is 2,443 m deep, has a producing section of 220.4 m (assumed to be equal to aquifer thickness) and an internal casing diameter of 22.05 cm. Steady water flow is given as approximately 250 gal/min (U.S. Bureau of Reclamation, 1973, p. 28). Using the density of water at 198°C, this is approximately 14 kg/s. These data, together with the flowing time of 49 d from figure 7 of the Bureau report and the head recovery data of their figure 17, can be used in Theis' recovery method (DeWiest, 1965, p. 269) to obtain a permeability estimate of 0.94 mD. The permeability can also be calculated from equation 1 with the drawdown obtained from their figure 8. Taking $r_e/r_w = 500$, we obtain 0.85 mD, in good agreement with the other calculation. The friction factor for Reynolds number of around 6×10^5 and relative roughness of 7×10^{-5} is 0.014 (Katz and others, 1959). These input data are summarized in table 3.

Calculations based on these data agree well with the measured quantities. The computed flow is 18 percent above the estimated value and the computed depth of first flashing for discharge at atmospheric pressure is within 22 percent of the actual depth. Because the correct friction factors are difficult to predict for these complicated flows, we can use the

Table 3.—Data for U.S. Bureau of Reclamation Mesa 6-1 well, Imperial Valley, Calif.

Parameter	Value
Aquifer:	
Temperature T_3	°C.. 198
Pressure p_3	bar.. 220.6
Permeability K	mD.. 0.85
Thickness L	m.. 220.4
Ratio, aquifer radius-well radius, r_e/r_w	500
Well:	
Depth H	m.. 2443.3
Radius r_w	cm.. 11
Friction factor λ	0.014
	0.03
Water viscosity μ	cP.. 0.134

data to calculate the friction factor. With two iterations, the depth of first flashing and mass flow are matched using a friction factor of 0.03. Note that the friction factor had to be doubled to change the depth of first flashing by 22 percent; this quantity, then, is not very sensitive to a chosen friction factor.

Calculated pressure and temperature distributions obtained by using a friction factor of 0.03 are compared with the measured data shown in figure 13. The predicted pressure decline near the depth of first flashing is too slow, whereas that higher in the hole is too rapid. The temperature curve should be a simple transformation of the pressure, but the saturation curve used in the calculations was for pure water, whereas the well fluid has 3 percent total dissolved solids. Although not a major factor, the dissolved solids would affect virtually every aspect of this analysis, including the flow equations and the fluid properties. Its overall effect is somewhat hard to predict and would be worth looking into as flow data on saline, steam-water mixtures becomes available. Another consideration in assessing the comparison in figure 13 is that the model was not designed to accommodate so low a flow rate. The assumption of a finely divided mixture of equal

average velocity should be less accurate here, and the relatively close agreement is reassuring.

ACKNOWLEDGMENTS

I would like to thank A. H. Truesdell and D. E. White, U.S. Geological Survey, for their helpful discussions and careful review of the manuscript.

REFERENCES CITED

- Allen, W. F., 1951, Flow of a flashing mixture of water and steam through pipes and valves: *Am. Soc. Mech. Engineers Trans.*, v. 73, p. 257-265.
- Bodvarsson, Gunnar, 1951, Report on the Hengill thermal area: *Engineers Assoc. Iceland Jour.*, v. 36, p. 1-48 (in Icelandic; abs. in English).
- 1961, Hot springs and the exploitation of natural heat resources in Iceland: Reykjavik, Iceland, State Electricity Authority, Geothermal Department, 20 p.
- Bodvarsson, Gunnar, and Eggers, D. E., 1972, The exergy of thermal water: *Geothermics*, v. 1, p. 93-95.
- DeWiest, R. J. M., 1965, *Geohydrology*: New York, John Wiley, 336 p.
- Elder, J. W., 1965, Physical processes in geothermal areas, in Lee, W. H. K., ed., *Terrestrial heat flow*: *Am. Geophys. Union*, p. 211-239.
- Elder, J. W., 1966, Heat and mass transfer in the earth-hydrothermal systems: *New Zealand Dept. Sci. and Indus. Research Bull.* 169, 115 p.
- Grindley, G. W., 1965, The geology, structure, and exploitation of the Wairakei geothermal field, Taupo, New Zealand: *New Zealand Geol. Survey Bull.* 75, 131 p.
- Hass, J. L., Jr., 1971, The effect of salinity on the maximum thermal gradient of a hydrothermal system at hydrostatic pressure: *Econ. Geology*, v. 66, p. 940-946.
- James, Russell, 1962, Steam-water critical flow through pipes: *Inst. Mech. Engineers Proc.*, v. 176, p. 741-748.
- 1967, Optimum wellhead pressure for geothermal power: *New Zealand Eng.*, v. 22, p. 221-228.
- 1968, Pipeline transmission of steam-water mixtures for geothermal power: *New Zealand Eng.*, v. 23, p. 55-61.
- Jones, J. B., and Hawkins, G. A., 1960, *Engineering thermodynamics*: New York, John Wiley, 724 p.
- Katz, D. L., Cornell, D., Kobayashi, R., Poettmann, F. H., Vary, J. H., Elenbaas, J. R., and Weinaug, C. F., 1959, *Handbook of natural gas engineering*: New York, McGraw Hill, 802 p.
- Keenan, J. H., Keyes, F. G., Hill, P. G., and Moore, J. G., 1969, *Steam tables. Thermodynamic properties of water including vapor, liquid, and solid phases*: New York, John Wiley, 162 p.
- Muskat, M., 1946, *The flow of homogeneous fluids through porous media*: Ann Arbor, J. W. Edwards, 763 p.
- Mathews, J., and Walker, R. L., 1965, *Mathematical methods of physics*: New York, W. A. Benjamin, 475 p.
- Nathenson, Manuel, 1974, Flashing flow in hot water geothermal wells: computer program: NTIS PB-233 123, 33 p.
- Smith, J. H., 1958, Production and utilization of geothermal steam: *New Zealand Engineering*, v. 13, p. 354-375.
- U.S. Bureau of Reclamation, 1973, Test well Mesa 6-1: Geothermal resources investigations, U.S. Dept. Interior Spec. Rept., 44 p.
- White, D. E., 1968, Hydrology, activity, and heat flow of the Steamboat Springs thermal system, Washoe County, Nevada: U.S. Geol. Survey Prof. Paper 458-C, 109 p.
- White, D. E., Muffler, L. J. P., Truesdell, A. H., and Fournier, R. O., 1968, Preliminary results of research drilling in Yellowstone thermal areas: *Am. Geophys. Union Trans.*, v. 49, p. 358.

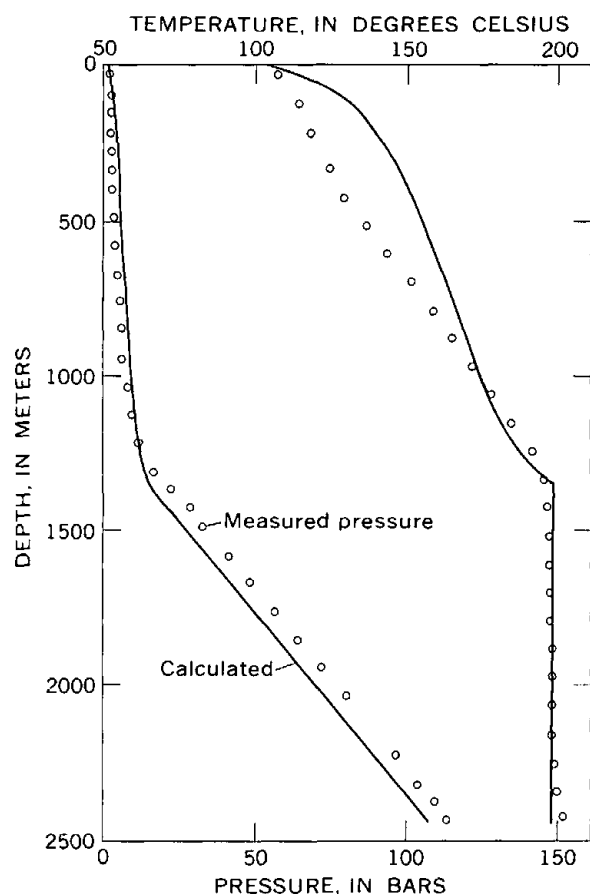


Figure 13.—Flowing-pressure and temperature profiles for U.S. Bureau of Reclamation Mesa 6-1 test well; curves calculated for wellhead pressure of 1 bar absolute and data in table 3 with $\lambda = 0.03$; points measured.

THE EFFECTS OF THE HURRICANE AGNES FLOOD ON CHANNEL GEOMETRY AND SEDIMENT DISCHARGE OF SELECTED STREAMS IN THE SUSQUEHANNA RIVER BASIN, PENNSYLVANIA

By JOHN R. RITTER, Harrisburg, Pa.

Abstract.—The Hurricane Agnes flood seems to have hardly changed the channel geometry of the Pennsylvania streams studied in this report. The 10 sites studied generally showed that the width of the stream channels had been changed little by the flood and that streambed altitudes had been lowered less than a foot (0.3 m). The velocity of the streams at a given discharge had decreased. In comparison, the sediment deposited by the December 1964 flood in northwestern California commonly raised the streambed altitudes several feet. The differences in the effects of the two floods may have been produced by the availability of sediment for transport, by the relative size of sediment carried in suspension or bedload, or by the relative magnitudes of the floods.

The Hurricane Agnes flood of June 20-24, 1972, was the largest historical flood ever to hit parts of Pennsylvania (fig. 1 and table 1) and adjoining States; flood damages totaled billions of dollars. During the flood, many Pennsylvania streams carried as much suspended sediment as they usually carry in 2-7 yr (table 2). Costa (1973) and Moss and Kochel (1973), however, noted surprisingly little deposition and erosion in two basins in the Piedmont physiographic province. Costa concluded that "the notion that these high magnitude, low frequency events account for a large portion of the topography of the Appalachians is not applicable to the Piedmont." This report analyzes the possible effects of the flood on sediment erosion and deposition in channels of Pennsylvania streams in the Valley and Ridge and the Appalachian Plateaus physiographic provinces as well as the Piedmont. The sedimentary effects of the flood on streams in the Susquehanna River basin are compared with the effects of a flood on streams in northwestern California.

METHODS

To detect changes in the channel geometry of a stream, its width, depth, and velocity were related to water discharge (Leopold and Maddock, 1953). If the hydraulic geometry of a stream was changed by the Hurricane Agnes flood, the post-flood relations of width, depth, and velocity to discharge would be different from the pre-flood relations. Data for the

relations were taken from discharge measurements made at gaging stations. The 10 stations (fig. 1, table 3) selected for analysis, two in the Delaware River basin and eight in the Susquehanna River basin, have drainage areas (table 1) ranging from 15 to 5,682 mi² (39 to 14,716 km²). The altitudes (table 3) of the stations range from 240 to 1,450 ft (73 to 442 m). Many other stations considered for study were rejected because available data were insufficient, because the channels had been bulldozed, or because the discharge measurements were made at sections too far apart, causing too great a variation in the data. Discharge measurements made within a year before the flood and within a few months after the flood were used.

The change in streambed altitude at each station was determined by Hickey's (1969) method of comparing altitudes at low flow. Hickey concluded that a 1-ft (0.3-m) difference was a valid indication of significant change in streambed altitude.

It must be stressed, however, that the above methods are not suitable for indicating deposition and scour on the flood plain or for determining the magnitude of lateral channel migration.

RESULTS

Figures 2-4 show the relations of width, depth, and velocity to discharge at the 10 Pennsylvania gaging stations selected for study of channel geometry before and after the Hurricane Agnes flood. From this analysis, very little channel change is indicated at Pohopoco Creek at Kresgeville (fig. 2A) and Tulpehocken Creek at Blue Marsh damsite near Reading (fig. 2B), which are in the Delaware River basin. Although the flood peak at Pohopoco Creek was about half the highest recorded peak, the peak at Tulpehocken Creek was about twice the previous highest recorded peak (table 1).

In the Susquehanna River basin little channel change was noted at West Branch Susquehanna River at Williamsport (fig. 2B) or at Conestoga Creek at Lancaster (fig. 4B). At the other stations, the average depth at a given discharge increased after the flood, whereas the average velocity decreased (figs.

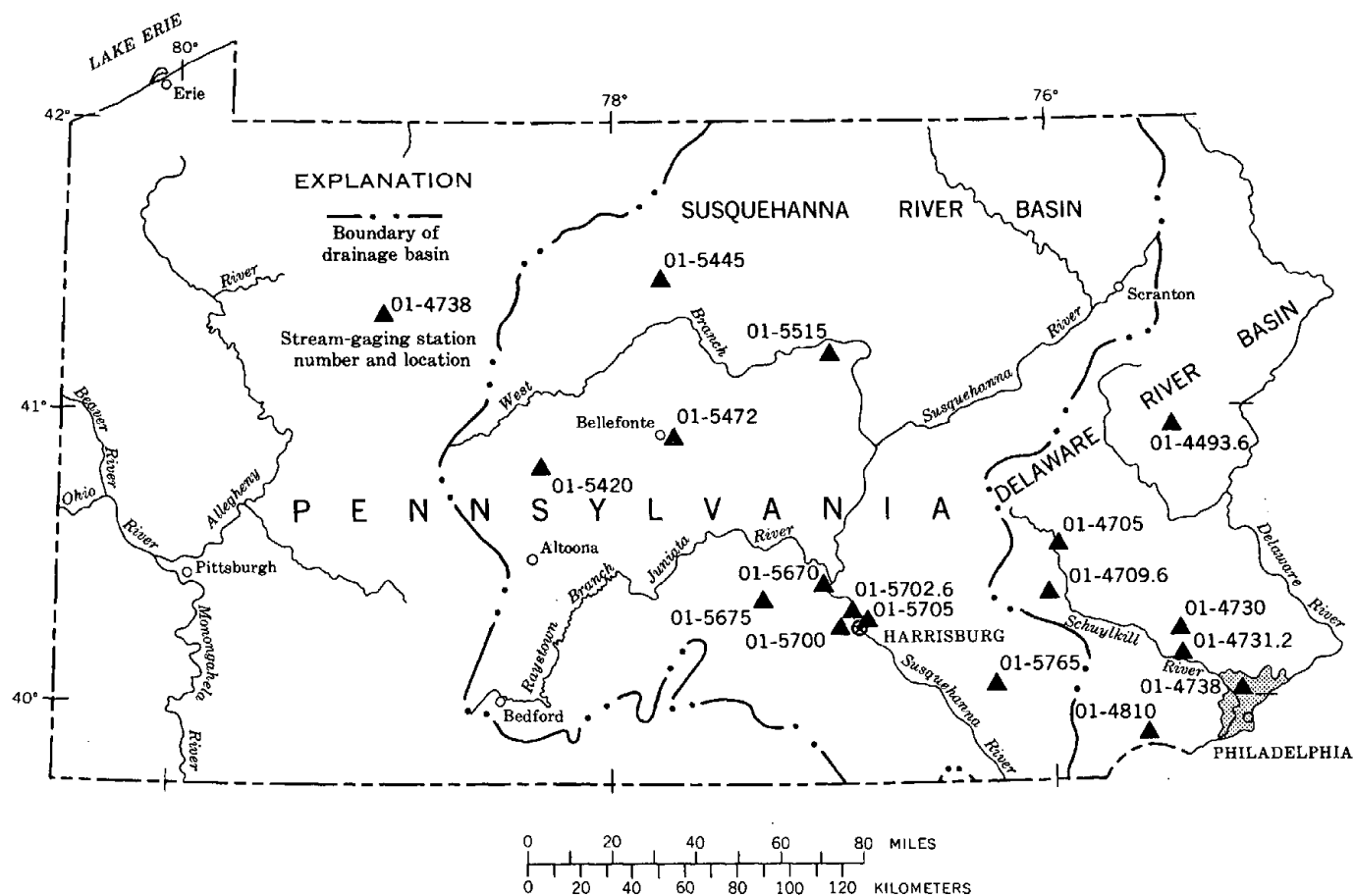


Figure 1—Locations of stream-gaging stations used in this report (see table 1).

Table 1.—Peak discharge during Hurricane Agnes flood at selected gaging stations in Pennsylvania

Station No.	Station name	Basin	Physiographic province	Drainage area (mi ²)	Period of water discharge record	Maximum peak discharge (ft ³ /s)		
						Previous	Hurricane Agnes ¹	Hurricane Agnes/ previous
01-4493.6 ²	Pohopoco Creek at Kresgeville.....	Delaware	Valley and Ridge	49.9	1966-72	2,080	1,020	0.49
4705	Schuylkill River at Bernedodo	355	1947-72	29,500	39,300	1.3
4709.6 ²	Tulpehocken Creek at Blue Marsh Dam-site near Reading.....	..dodo	175	1965-72	11,000	23,000	2.1
4730	Perkiomen Creek at Graterforddo	Piedmont	³ 208	1914-72	39,900	38,600	.97
4731.2	Skipack Creek near Collegeville.....	..dodo	53.7	1966-72	40,400	6,720	.17
4738	Schuylkill River at Manayunk, Philadelphia.....	..dodo	1,893	1931-72	96,200	93,600	.97
4810	Brandywine Creek at Chadds Forddodo	287	1911-53, 1962-72	17,200	19,100	1.1
5420 ²	Moshannon Creek at Osceola Mills	Susquehanna	Appalachian Plateaus	68.8	1940-72	2,930	5,120	1.8
5445 ²	Kettle Creek at Cross Forkdodo	136	1940-72	12,400	14,300	1.2
5472 ²	Bald Eagle Creek below Spring Creek at Milesburg.....	..do	Valley and Ridge	265	1955-72	8,950	21,300	2.4
5515 ²	West Branch Susquehanna River at Williamsport.....	..dodo	5,682	1895-72	264,000	279,000	1.1
5670 ²	Juniata River at Newportdodo	3,354	1899-72	190,000	187,000	.98
5675 ²	Bixler Run near Loysvilledodo	15.0	1954-72	8,780	4,400	.50
5700 ²	Conodoguinet Creek near Hogestowndodo	470	1911-19, 1929-58, 1967-72	15,700	31,900	2.1
5702.6	Conodoguinet Creek tributary No. 2B near Enola.....	..dodo65	1969-72	528
5705	Susquehanna River at Harrisburg.....	..dodo	24,100	1890-72	740,000	1,021,000	1.4
5765 ²	Conestoga Creek at Lancasterdo	Piedmont	324	1928-72	22,800	88,300	3.8

¹ Provisional data. ² Stations where effects of flood on channel geometry were studied. ³ Excludes area above Green Lane Reservoir.

Table 2.—Provisional data on suspended sediment transported by the Hurricane Agnes flood at 10 sampling stations in Pennsylvania

Station No.	Station name	Period of sampling	Average annual			Number of days	Hurricane Agnes flood			Suspended sediment Flood/annual
			Water discharge (ft ³ /s)	Suspended-sediment Discharge (tons)	Yield (tons/mi ²)		Water discharge (ft ³ /s)	Suspended-sediment Discharge (tons)	Yield (tons/mi ²)	
01-4705 . . .	Schuylkill River at Berne	1948-72	239,000	35,300	100	6	73,000	74,900	211	2.1
4730 . . .	Perkiomen Creek at Graterford . . .	1948-53 1963-66 1970-72	135,000	51,100	183	2	23,100	35,200	169	.92
4731.2 . .	Skipack Creek near Collegeville . .	1971-72	24,600	24,100	448	2	2,390	5,590	104	.23
4738 . . .	Schuylkill River at Manayunk, Philadelphia.	1948-72	1,010,000	269,000	142	6	240,000	707,000	373	2.6
4810 . . .	Brandywine Creek at Chadds Ford .	1963-72	137,000	51,000	178	2	14,200	28,500	99	.56
5670 . . .	Juniata River at Newport	1951-72	1,530,000	322,000	96	7	566,000	601,000	179	1.9
5700 . . .	Conodoguinet Creek near Hogs-town.	¹ 1971-72	207,000	23,900	51	4	59,000	43,900	93	1.8
5702.6 . .	Conodoguinet Creek tributary No. 2B near Enola.	1969-72	325	97.5	150	2	185	299	460	3.1
5705 . . .	Susquehanna River at Harrisburg . .	1964-68 1970-72	12,300,000	2,550,000	106	10	4,270,000	7,520,000	312	2.9
5765 . . .	Conestoga Creek at Lancaster . . .	1961-69 ²	135,000	50,200	155	4	79,200	283,000	873	5.7

¹ A few samples also collected during 1962, 1965, 1967, and 1968. ² Data for Hurricane Agnes flood from Franklin and Marshall College.

2C,D; 3A, C, D; 4A). At Bixler Run near Loysville (fig. 3D), the relative change in the channel was greater than that of most streams even though, unlike peaks in most of the Susquehanna River basin, the peak at Bixler Run for the Hurricane Agnes flood was much less than the peak recorded previously. This channel has changed frequently in recent years, perhaps in response to manmade alterations of the channel upstream. Generally, the width of the channels at the 10 stations studied (table 3) remained about the same, perhaps because the measurements at some stations were made from bridges, where the channel is confined. The pre- and post-flood width, depth, and velocity at the average discharge for the 10 stations are compared in table 3. The table shows that after the flood the depth at the average discharge had increased as much as 1.1 ft (0.34 m), and the velocity had decreased as much as 0.8 ft/s (0.2 m/s).

The noted change in streambed altitude after the flood was as much as -0.8 ft (-0.2 m), which is still below Hickey's (1969) criterion that 1-ft (0.3 m) is a valid indication of change. However, the data obtained by Hickey's method seem to substantiate the conclusion that the altitude of the streambed after the flood was lower at most of the 10 stations.

On the other hand, the data presented in figures 2-4 and table 3 do not necessarily reflect changes in the channel that may have occurred during the Hurricane Agnes flood. For example, figure 3B and table 3 indicate little, if any, change in the geometry of the channel of the West Branch Susquehanna River at Williamsport. However, cross sections of the channel (fig. 5) show that several points on the channel on June 25 (2 days after the flood peak) were 1-2 ft (0.3-0.6 m) deeper than they were on April 6 (about 11 weeks before the flood) or on August 29 (about 10 weeks after the flood). In fact, the

cross sections of April 6 and August 29 are not greatly dissimilar, an indication that the channel may be returning to its pre-flood cross section.

The deepening of the channels indicates that bed material was removed by the flood and moved downstream. Deposition of this scoured sediment was not noted in this study, suggesting that it was deposited in stretches of the streams not covered by this study or that it was carried out of the system. The decrease of velocity in the streams implies that the streams might not have carried as much suspended sediment as they did prior to the flood. Because the size of the transportable sediment is related to velocity, the suspended sediment may have been finer after the flood than before.

As shown in table 2, during the flood period, many streams in eastern and central Pennsylvania carried a quantity of suspended sediment equal to that generally carried in more than a year. This was particularly true of the streams in the Susquehanna River basin, which was, for the most part, hit harder by Hurricane Agnes than the Delaware River basin. Parts of the Delaware River basin, such as Skipack Creek near Collegeville, had a peak flow in 1971 that was several times higher than the peak during Hurricane Agnes (table 1). Therefore, in those areas the quantity of suspended sediment transported by the peak flow in 1971 was much greater than that transported during Hurricane Agnes and consequently the quantity of suspended sediment discharged during Hurricane Agnes may have been less than the average quantity discharged annually.

In the Susquehanna River basin, Conodoguinet tributary No. 2B (the smallest basin studied) discharged as much suspended sediment in 2 days during the flood as it normally would in 3.1 yr (table 2). However, the average annual

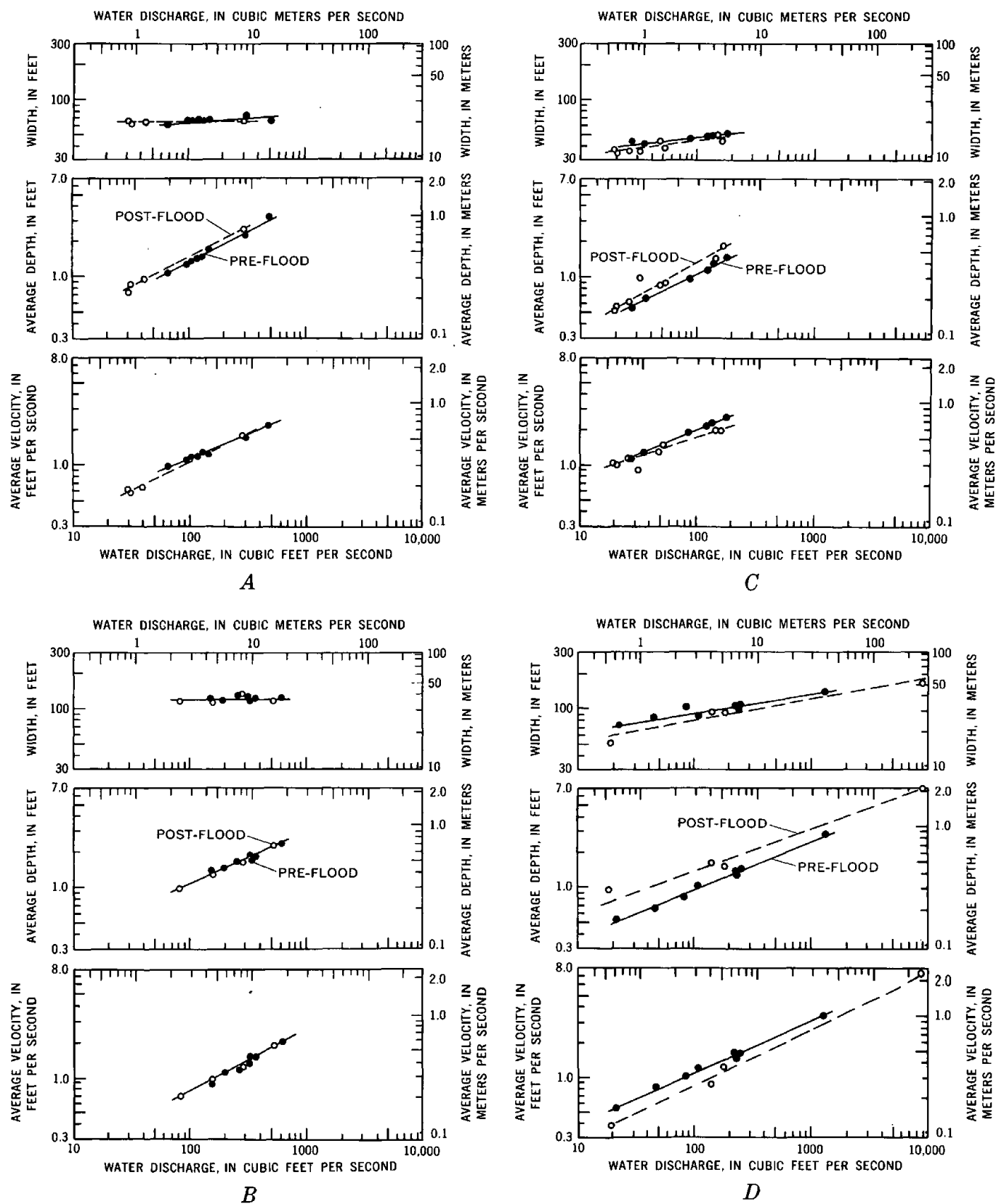


Figure 2.—Relation of width, average depth, and average velocity to water discharge (1971-73). A, Station 01-4493.6, Pohopoco Creek at Kresgeville, Pa. B, Station 01-4709.6, Tulpehocken Creek at Blue Marsh damsite near Reading, Pa. C, Station 01-5420, Moshannon Creek at Osceola Mills, Pa. D, Station 01-5445, Kettle Creek at Cross Fork, Pa.

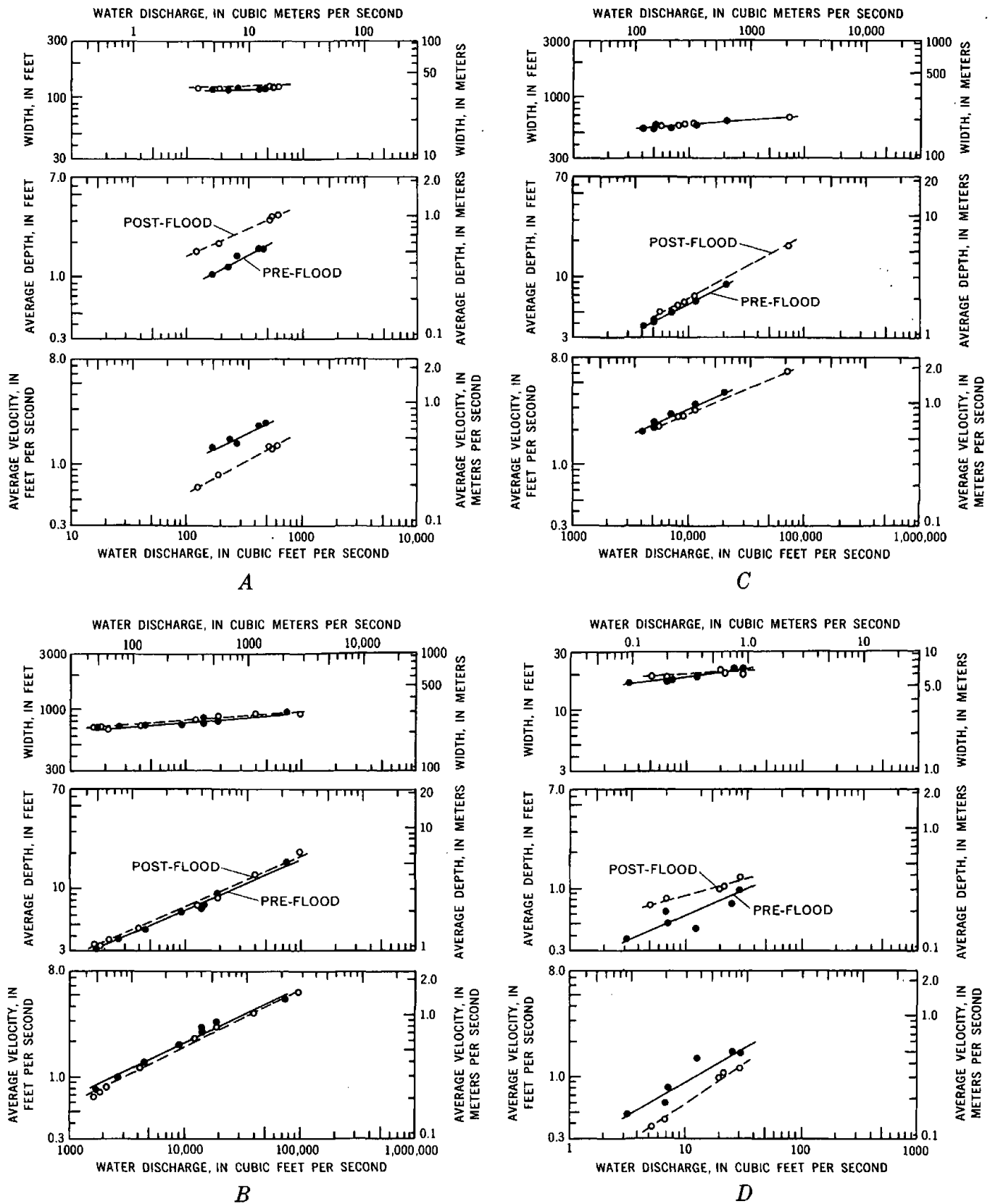


Figure 3.—Relation of width, average depth, and average velocity to water discharge (1971-73). A, Station 01-5472, Bald Eagle Creek below Spring Creek at Milesburg, Pa. B, Station 01-5515, West Branch Susquehanna River at Williamsport, Pa. C, Station 01-5670, Juniata River at Newport, Pa. D, Station 01-5675, Bixler Run near Loysville, Pa.

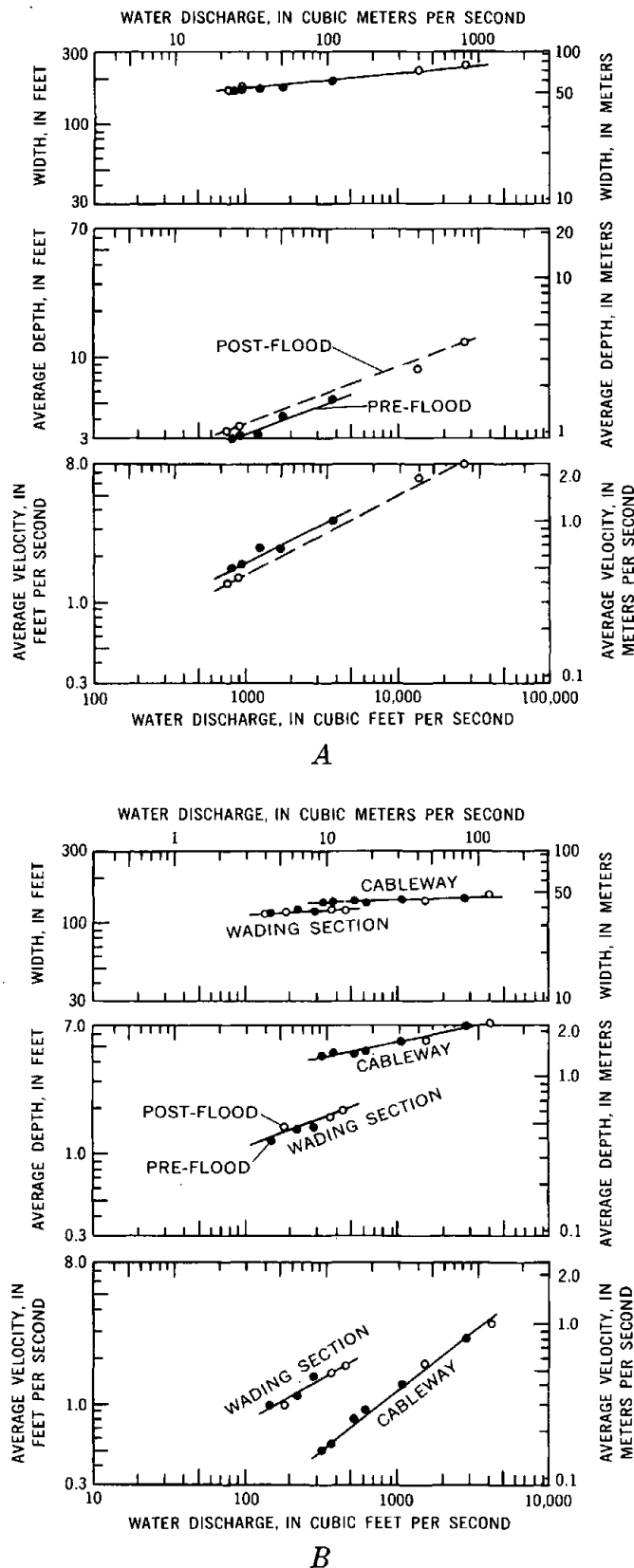


Figure 4.—Relation of width, average depth, and average velocity to water discharge (1971-73). A, Station 01-5700, Conodoguinet Creek near Hogestown, Pa. B, Station 01-5765, Conestoga Creek at Lancaster, Pa.

discharge is based on only a short-term record. On the other hand, Conestoga Creek at Lancaster, which has a record of several years, discharged a quantity of suspended sediment during the flood equivalent to the quantity normally discharged in 5.7 yr. The channel of this stream at this site, surprisingly, showed no evidence of being changed by the flood. In addition, lack of deposition or erosion on the flood plain of the creek was noted by Moss and Kochel (1973).

THE EFFECTS OF A HISTORIC FLOOD ON A BASIN IN PENNSYLVANIA COMPARED WITH THOSE ON A BASIN IN NORTH COASTAL CALIFORNIA

To place the channel changes produced by the Hurricane Agnes flood in Pennsylvania in perspective, the changes in the Susquehanna River basin were compared with those produced by the December 1964 flood in the Eel River basin in northwestern California (fig. 6). The California flood is estimated to have a recurrence interval of about 180 yr; the Hurricane Agnes flood one of more than 200 yr. The two basins, although both flow to an ocean, are quite dissimilar. The Eel River basin is narrow and steep; in contrast, the Susquehanna River basin is broad and gentle. Other comparisons of the two basins are given in table 4. Of particular interest to this report is that the Eel River basin has one of the highest suspended-sediment yields in the United States, an average of about 10,000 tons/mi² (3,500 metric tons/km²) per year (Brown and Ritter, 1971). The yield of the Susquehanna River basin is about 110 tons/mi² (39 metric tons/km²) per year, and yields within the basin range from 40 to 440 tons/mi² (14 to 150 metric tons/km²) per year (Williams and Reed, 1972, p. F7-F9). Sand represented about 35 percent of the suspended sediment transported by the Eel River at Scotia from 1958 to 1970 (Ritter, 1972, p. 6). Sand represents about 10 percent of the suspended sediment discharged in the Susquehanna River basin (Williams and Reed, 1972, p. F15).

The December 1964 flood in northwestern California drastically altered the stream channels and significantly increased the quantity of sediment discharged by streams (Stewart and LaMarche, 1967; Ritter, 1968; Hickey, 1969; Anderson, 1970a and 1970b; Brown and Ritter, 1971; Knott, 1971; and Ritter, 1972). The streambed altitude had changed more than a foot after the flood at 14 of 21 gaging stations in the Eel River basin, and the streambed altitudes at 17 stations had been raised (Hickey, 1969, p. E5). In the Eel River basin, the measured fill was as much as 7.8 ft (2.4 m) within a year after the flood, and in nearby basins the measured streambed fill was as much as 13.0 ft (4 m). In parts of the Eel River the filling continued for at least 2 yr after the flood (Knott, 1971, p. 41). Table 5 shows the changes in the channel geometry at two stations in the Middle Fork Eel River basin after the flood. At both stations the channel had widened, the depth of flow had decreased, and the current velocity had increased after the flood.

Table 3.—Comparisons of pre-flood and post-flood channel width, depth, and velocity at average discharge and change in streambed altitude at 10 Pennsylvania gaging stations

Station No.	Station name	Altitude (feet)	Average discharge (ft ³ /s)	Width (feet)		Average depth (feet)		Average velocity (ft/s)		Difference in pre- and post- flood streambed altitude (feet)
				Pre- flood	Post- flood	Pre- flood	Post- flood	Pre- flood	Post- flood	
01-4493.6	Pohopoco Creek at Kresgeville	670	87.9	65	65	1.2	1.4	1.1	1.0	+0.1
4709.6	Tulpehocken Creek at Blue Marsh dam- site near Reading.	240	207	120	120	1.5	1.5	1.2	1.2	+ .1
5420	Moshannon Creek at Osceola Mills	1,450	107	48	46	1.1	1.4	2.1	1.8	- .1
5445	Kettle Creek at Cross Fork	1,030	216	100	92	1.3	1.8	1.5	1.2	- .6
5472	Bald Eagle Creek below Spring Creek at Milesburg.	680	349	120	124	1.5	2.6	1.9	1.1	- .8
5515	West Branch Susquehanna River at Williamsport.	490	8,692	800	780	6.2	6.6	1.8	1.7	- .3
5670	Juniata River at Newport	360	4,183	550	550	3.7	4.0	2.1	1.9	- .4
5675	Bixler Run near Loysville	600	15.4	20	20	.72	1.0	1.2	.8	- .6
5700	Conodoguinet Creek near Hogestown	350	566	160	160	2.6	3.0	1.4	1.2	- .2
5765	Conestoga Creek at Lancaster	250	371	¹ 120	¹ 120	¹ 1.8	¹ 1.8	¹ 1.6	¹ 1.6	¹ - .2

¹Measured 400 ft downstream from station.

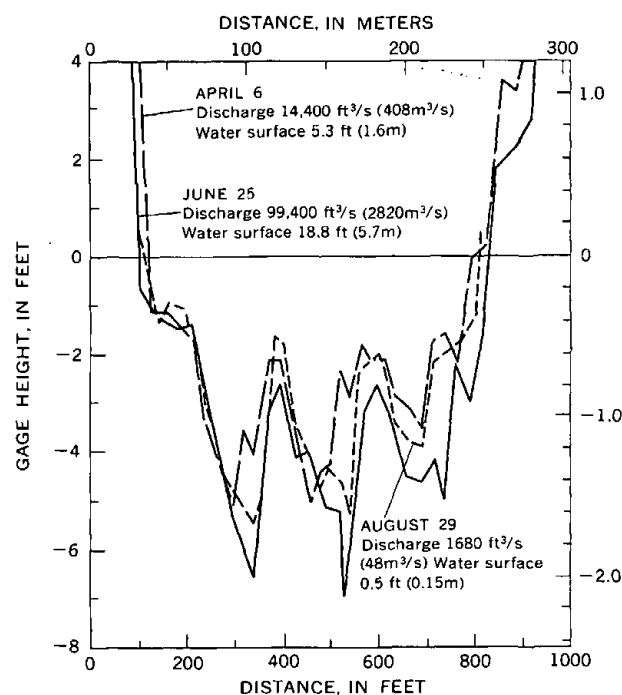


Figure 5.—Cross sections of West Branch Susquehanna River at Williamsport, Pa., April 6, June 25, and August 29, 1972. Stream-gaging station 01-5515.

A comparison of the effects of the major historical flood on the channels of streams in the Susquehanna and Eel River basins is given in table 6. The major flood of record evidently affected the Eel River basin much more than the Susquehanna River basin. The streambed altitudes in the Eel River basin

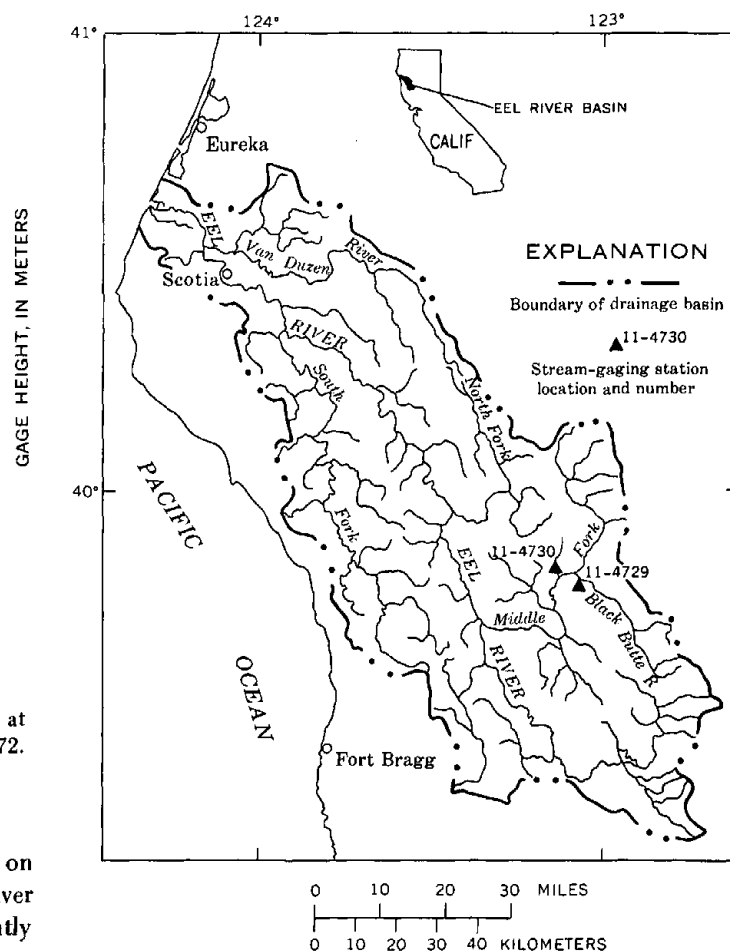


Figure 6.—Eel River basin, California.

Table 4.—Comparisons of the Susquehanna and Eel River basins

	Drainage area (mi ²)	Highest altitude (feet)	Climate	Average annual precipitation (inches)	Average annual runoff (inches)	Average discharge (ft ³ /s)	Principal land use	Population density	Chief bed material	Suspended-sediment yield (tons/mi ²)	
										Average annual	Flood
Susquehanna River. . .	27,500	3,100	Humid continental. .	40	19	¹ 33,700	Farming. . .	Fairly dense. . .	Gravel (>2mm).	^{1,2} 106	¹ 312
Eel River.	3,625	7,000	Mediterranean.	80	31	³ 7,200	Logging. . .	Sparse.	do. . .	³ 10,000	³ 47,000

¹ At Harrisburg, Pa.² Williams and Reed, 1972.³ At Scotia, Calif.

Table 5.—Comparisons of pre-flood and post-flood channel width, depth, and velocity at average discharge and change in streambed altitude at two gaging stations in the Eel River basin

Station name	Station No.	Drainage area (mi ²)	Period of record	Average discharge (ft ³ /s)	Physiographic section	Average discharge ¹						Difference in pre- and post-flood streambed altitude ² (feet)
						Width (feet)		Average depth (feet)		Average velocity (ft/s)		
						Pre-flood	Post-flood	Pre-flood	Post-flood	Pre-flood	Post-flood	
Black Butte River near Covelo, Calif.	11-4729	162	1959-70	317	California Coast Ranges. . .	90	150	1.3	0.5	2.7	4.2	+7.8
Middle Fork Eel River below Black Butte River near Covelo, Calif.	11-4730	367	1952-67	1,048	...do.	160	200	1.8	1.1	3.5	4.8	+6.7

¹ Knott (1971, figs. 26-27, p. 42-43).² Hickey (1969).

Table 6.—Effects of the major historical flood on the channels of streams in the Susquehanna and Eel River basins

Basin	Dates of flood storm	Estimated recurrence interval (years)	Maximum recorded precipitation for flood storm (inches)	Water yield peak discharge (ft ³ s ⁻¹ mi ⁻²)	Post-flood				
					Change in channel at average discharge			Streambed altitude	Quantity of suspended-sediment transported at a given discharge
					Width	Depth	Velocity		
Susquehanna River. . .	June 20-24, 1973	>200	17	¹ 42	Same. . .	Deeper. . .	Decrease. . .	Generally lower (<1.0 ft).	Probably same. . .
Eel River.	Dec. 19-23, 1964	180	23	² 242	Wider. . .	Shallower. . .	Increase. . .	Generally higher ³ (as much as 7.8 ft).	Increase (2X-5X). . .

¹ At Harrisburg, Pa.² At Scotia, Calif.³ Hickey (1969).

were generally several feet higher after the flood; they were less than a foot lower in the Susquehanna River basin. The Eel River and its tributaries were generally wider, shallower, and swifter after the December 1964 flood; the Susquehanna and its tributaries were generally deeper and slower. Differences in climate, land use, altitude, geology, and sediment yield probably partly explain why the Eel River basin had greater channel changes. Also, the water yield and precipitation were greater for the California flood than for the Pennsylvania flood.

In 1955, a flood occurred on the Eel River that was the second highest on record in most parts of the basin and the highest in some parts. Yet the 1955 flood apparently affected channels much less than the 1964 flood. For example, Hickey

(1969) showed no obvious changes in streambed altitudes after the 1955 flood. Perhaps the 1972 flood in Pennsylvania, even though it is estimated to have a longer recurrence interval than the 1964 flood in California, still did not reach a magnitude large enough to produce large-scale changes in channel geometry. The Susquehanna River basin, which is much less erodible than the Eel River basin, probably did not have as much sediment readily available for movement by an extreme flood, whereas the Eel River basin had more than enough available. Thus, the Susquehanna River probably did not reach its capacity for transporting sediment, but the Eel River, in places, was probably choked with sediment. This effect is suggested by the degradation of channels of streams in the Susquehanna River basin and the aggradation of the channels in the Eel River basin.

CONCLUSIONS

Preliminary data on 10 streams (table 3) in the Susquehanna River and Delaware River basins in the Valley and Ridge, Appalachian Plateaus, and Piedmont physiographic provinces suggest that the Hurricane Agnes flood generally produced little change in the stream channels. In many streams the bed was scoured after the flood by less than a foot and the velocity decreased, but the channel width was not changed appreciably. Although the likelihood of a Hurricane Agnes flood is less than once in 200 yr, its effects on stream channels were much less than those of the December 1964 flood in basins in northwestern California.

The differences of the effects of floods on stream channels in the Susquehanna River and Eel River basins indicate that a study comparing the effects of floods on sediment transport and on the channel geometry of streams in different areas of the country would be in order.

REFERENCES CITED

- Anderson, H. W., 1970a, Principal components analysis of watershed variables affecting suspended sediment discharge after a major flood: *Internat. Assoc. Sci. Hydrology Pub.* 96, p. 404-416.
- , 1970b, Relative contributions of sediment from source areas and transport processes: *Symposium Forest Land Uses and Stream Environment, Proc.*, p. 55-63.
- Brown, W. M., III, and Ritter, J. R., 1971, Sediment transport and turbidity in the Eel River basin, California: *U.S. Geol. Survey Water-Supply Paper* 1986, 70 p.
- Costa, J. E., 1973, Response of a Piedmont watershed to Hurricane Agnes, June 1972 [abs.]: *Geol. Soc. America Abs. with Programs*, p. 151.
- Hickey, J. J., 1969, Variations in low-water streambed elevations at selected stream-gaging stations in northwestern California: *U.S. Geol. Survey Water-Supply Paper* 1879-E, 33 p.
- Knott, J. M., 1971, Sedimentation in the Middle Fork Eel River basin, California: *U.S. Geol. Survey open-file rept.*, 60 p.
- Leopold, L. B., and Maddock, Thomas, 1953, The hydraulic geometry of stream channels and some physiographic implications: *U.S. Geol. Survey Prof. Paper* 252, 56 p.
- Moss, J. H., and Kochel, Craig, 1973, Unusual aspects of the Hurricane Agnes flood, Conestoga River drainage basin, southeastern Pennsylvania [abs.]: *Geol. Soc. America Abs. with Programs*, p. 199.
- Ritter, J. R., 1968, Changes in the channel morphology of Trinity River and eight tributaries, California, 1961-65: *U.S. Geol. Survey open-file rept.*, 60 p.
- , 1972, Sand transport by the Eel River and its effect on nearby beaches: *U.S. Geol. Survey open-file rept.*, 17 p.
- Stewart, J. H., and LaMarche, V. C., 1967, Erosion and deposition produced by the flood of December 1964 on Coffee Creek, Trinity County, California: *U.S. Geol. Survey Prof. Paper* 422-K, 22 p.
- Williams, F. K., and Reed, L. A., 1972, Appraisal of stream sedimentation in the Susquehanna River basin: *U.S. Geol. Survey Water-Supply Paper* 1532-F, 24 p.

UNIQUE CARTOGRAPHIC CHARACTERISTICS OF ERTS

By ALDEN P. COLVOCORESSES, Reston, Va.

Abstract.—The ERTS television sensing system has unique cartographic advantages over aircraft and satellite film systems. These are longer life combined with greater coverage, transmission of data in near real time, orthogonality, excellent geometric precision for planimetric mapping, suitability for automation (because of the basically continuous image on a mathematically definable map projection), radiometric fidelity, and the extension of sensing capability to near-infrared wavelengths.

Aerial cameras and the photographs they produce have been increasingly applied to mapping and related studies for more than 50 yr. The manned spaceflights demonstrated what film cameras can do in space, and cartographic cameras at orbital heights could provide a data source from which maps would be one of the principal products. ERTS was not defined with mapping as one of its principal objectives, but with ERTS-1 in orbit since July 1972 certain unique characteristics or advantages of the electronic transmission (television) Earth-sensing system become apparent to the mapmaker. Electronic transmission from geosynchronous orbit has characteristics completely different from either ERTS or film systems. This paper does not include any comparisons with geosynchronous Earth sensing.

This paper is an updated and elaborated version of "Unique Characteristics of ERTS" presented at the NASA "Symposium on Significant Results Obtained From ERTS-1," New Carrollton, Md., March 6, 1973.

Seven of the more obvious advantages of ERTS-type sensing systems over aircraft and satellite film systems are as follows:

1. *Long life and coverage.*—Apparently a full year is needed to provide complete suitable domestic coverage even though the ERTS sensor is turned on for every pass over the United States. That a single film-return satellite could be efficiently flown for such a long period, or come anywhere near complete U.S. coverage, is doubtful in the extreme. ERTS-1 promises to survive for 2 yr or more and thus provides significant repetitive as well as complete coverage, making the most of only one launch, spacecraft, and instrument package.

2. *Near real time.*—The advantage of electronic transmission in near real time is obvious even though the capability of realizing the advantage has not been fully developed. For

example, a cartographic product was prepared within 2 weeks after scene acquisition by ERTS. Electronic transmission of imagery has, in the past, included sizable internal geometric distortions. ERTS is proving that imagery can be electronically transmitted without serious distortion.

3. *Orthogonality.*—The field of view of the MSS (Multispectral Scanner) of ERTS extends only 5.78° from the nominal vertical. The near orthogonality of ERTS imagery plus a lack of complete overlap effectively prevents compilation of topographic (contour) maps but simplifies small-scale planimetric mapping and revision. Since topography changes little, maintaining up-to-date planimetry is the major mapping problem once an area has been topographically mapped. An image map, consisting of little more than an image precisely referenced to the figure of the Earth, is probably the most effective method of portraying up-to-date planimetry. ERTS imagery is ideal for small-scale image mapping for two reasons. First, external errors such as relief displacement are so small that the image can be used directly, except in areas of extreme relief, without undergoing the complex transformation provided by an analytical plotter or an orthophotoprinter. Second, the narrow field of view means that the entire scene is imaged from a nearly constant vertical aspect and thus provides uniform spectral response from objects of similar type throughout the scene.

4. *Suitability for planimetric mapping.*—It is hard to believe that an optical-mechanical scanner can generate imagery that has the geometric fidelity of a frame photograph. However, the MSS on ERTS is indeed generating data that, as corrected by NASA, are printed out in a form with spatial errors on the order of 50 m (rms). Since the scanner spot size (instantaneous field of view = pixel = picture element) is about 80 m, the surprisingly small rms error indicates a system of high internal geometric fidelity. The 50 m (rms) error equals about $1.5 \mu\text{m}$ at the original MSS imagery scale of 1:3,369,000, which approaches the expected accuracy of a calibrated mapping camera. Even though the internal geometric accuracy of the MSS may not be quite up to that of a good mapping camera, the accuracy it does have, when coupled with the external advantage of the near-orthographic continuous view, results in two-dimensional (planimetric) mapping of geometric precision which may well exceed that obtainable from comparable camera systems under like conditions.

5. *Suitability for automation.*—Frame cameras and vidicon imagers record discrete scenes. Each photograph or image frame has its own geometric characteristics, and unless extensive analytical adjustments are made, images in adjacent photographs will not fit together. A scanner such as the MSS produces a basically continuous image on a mathematically definable map projection of negligible distortion. Thus a means is established for relating the pixels of the image to the figure of the Earth in a continuous and (within the limitations of the corrections) rigorous manner. These characteristics provide the potential for development of an automated image mapping system by either analog or digital techniques, with a significant decrease in requirements for ground control.

6. *Radiometric fidelity.*—The ERTS signals, particularly those of the MSS, are in effect those of a focusing radiometer, recording radiated energy with a range and precision well beyond the capability of any current film system. Therefore, either on tape or as later recorded on film, the spectral image of a given scene is more meaningful from ERTS than from a film camera. Since ERTS records four wavebands, the images can be combined to provide a response optimized for particular scenes or for objects of sufficient size. Film cameras can record up to three bands on one film (color or color infrared), but altering the combination for a particular scene or object is complex and imprecise. The separate-band characteristic of ERTS is particularly important for mapping objects or areas that have unusual radiometric responses or that are imaged under unusual conditions of illumination, such as the polar regions.

7. *Extension into the near-infrared wavelengths.*—Available aerial films cut off between 0.8 and 0.9 μm , which is about the same limit as for band 6 of the MSS. MSS band 7, at 0.8 to 1.1 μm , has opened a window for remote sensing that operational film systems do not have. The band is enormously powerful and has demonstrated the following unique capabilities:

- (a) Effective penetration of thin clouds and contrails under certain conditions (fig. 1).
- (b) Definition of the water-land interface with high precision, enabling detection and identification of circular water bodies as small as 200-m diameter and linear water bodies of something less than 100-m width. Under suitable conditions, in gently sloping areas of known elevation, water stage can be determined to a fraction of a meter. The capability is particularly significant when one considers that the instantaneous field of view of the MSS (spot size or pixel) is 80 m.
- (c) Superior definition of vegetation patterns, largely due to the differential sensitivity of band 7 to vegetation types.
- (d) Superior definition of natural features. Geologists and others are selecting MSS 7 as the best single band for depicting the Earth's physiography.

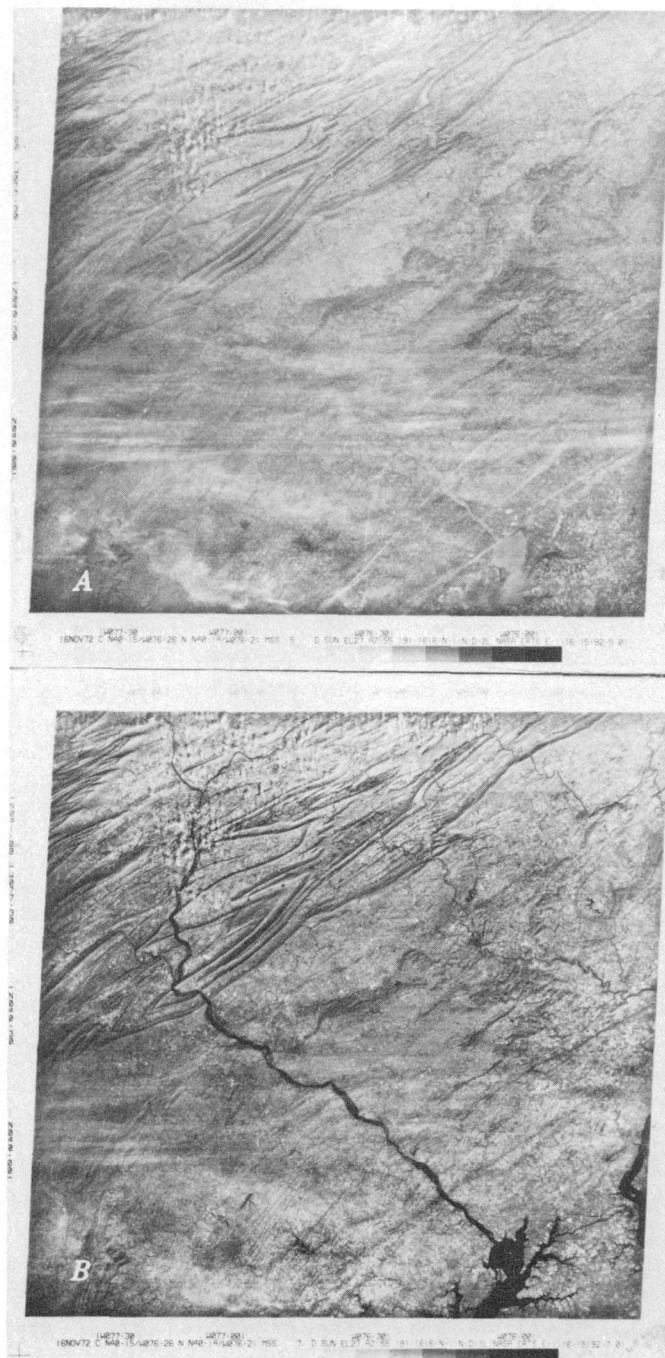


Figure 1.—Thin-cloud penetration capability of ERTS infrared sensor, southeastern Pennsylvania, Nov. 16, 1972. A, Visible spectrum, MSS band 5 (0.6–0.7 μm). B, Near infrared, MSS band 7 (0.8–1.1 μm).

- (e) Some cultural features are best defined on band 7, for example, the major road patterns in western U.S. cities as so far recorded by ERTS.

Today television is an accepted means of visual communication, and electronic-transmission Earth-sensing systems such as ERTS and its successors promise to take their place beside the film camera as essential tools for cartography.

ANNUAL INDEX TO VOLUME 2

Journal of Research of the U.S. Geological Survey

[Issue number precedes colon; page number follows colon]

SUBJECT INDEX

A	Page		Page		Page
Acanthite, Cripple Creek district, first report	3:339	Analyses—Continued		Base runoff, recession curve, upper Potomac River basin . .	1:125
Activity-product constants, aragonite	4:447	Spectrophotometric, Thermal conductimetric, X-ray, X-ray fluorescence.		Biological aspects, pools and riffles	3:379
calcite and aragonite	2:175	Analytical methods. See Methods and techniques.		Biostratigraphy, Utah, north-central part	1:97
Africa. See Liberia.		Andesite, vanadium determination	6:701	Biotite, copper content.	2:195
Age determinations, hornblende and trondhjemite, New Mexico	6:705	Antarctica, cartographic application of ERTS-1 imagery . .	4:385	Birnessite, in obsidian spherulite, Colorado	4:467
Kroenke Granodiorite, Colorado	6:705	Pensacola Mountains, tillite . .	6:711	Bolsa Quartzite, Arizona, stratigraphy	2:143
pantellerite, Oregon	1:25	Antimony sulfide, equilibria studies	4:457	Border Ranges fault, south-central Alaska	3:323
pyroclastic-flow deposits, California	1:49	Apollo lunar samples, carbon and hydrogen isotopic composition.	1:7	Brazil, chromitite, Campo Formoso, Bahia	5:551
Roberts Mountains thrust, Nevada	4:411	nonvolcanic implications	1:1	Brüggerite, Chile, new saline mineral	4:471
Aerial observations, suspended-sediment plumes, San Francisco Bay	5:519	Aquifer chemistry, geothermal systems	3:271	Buddingtonite, ammonium feldspar, in Phosphoria Formation, Idaho	6:693
Alabama, paleontology, eastern part	1:81	Aragonite, activity-product constants	4:447		
Alaska, petrology, St. Lawrence Island	1:41	stability in aqueous solution . .	2:175	C	
structural geology, south-central part.	3:323	Arctic region, cartographic application of ERTS-1 imagery	4:385	Calcite, analysis for isotope abundances	6:711
ultramafic rocks, Eagle quadrangle	6:657	Arizona, fluid-inclusion study of porphyry copper deposit.	1:31	stability in aqueous solution . .	2:175
Alaska-Aleutian Range batholith, chemical analyses	3:343	general geology	3:311	Calderas, Colorado, mineralization	4:405
Algae, blue-green, relation to bacteria under laboratory conditions	5:533	petrology, southern part	2:195	Nevada, Lunar Lake	5:599
Amaranth, selective staining of feldspar	1:73	stratigraphy, Vekol Mountains	2:143	California, age determination, pyroclastic-flow deposits . .	1:49
Ammonium feldspar, budding-tonite, in Phosphoria Formation, Idaho	6:693	structural geology	3:311	fault-zone studies	5:593
Ammonoids, Cretaceous, southeastern United States . .	1:81	Astrogeology, carbon and hydrogen isotopes in lunar samples	1:7	garrelsite, new data.	2:213
Analcime, relation to diagenetic dawsonite in oil shale and tuff.	1:35	nonvolcanic implications from lunar samples	1:1	geochronology, pyroclastic-flow deposits.	1:49
Analyses. See specific types: Chemical, Microprobe, Spectrochemical, Spectrofluorimetric, Spectrographic, Spectrometric,		Automation, potential mapping system from ERTS data	6:763	geophysical profile, continental slope	5:563
		B		geothermal studies	6:743
		Bacteria, relation to phytoplankton, Oneida Lake, N.Y.	5:533	landslides, fault related	5:593
		Barium, in hybrid granitoid rocks	6:671	petrology, Coast Range ophiolite	6:637
		Basalt, Oregon, volcanic rock sequence	4:395	Lassen Volcanic National Park	1:49
		vanadium determination	6:701	Cambrian, Nevada	5:609
				paleontology	6:717
				Carbon, isotopes, in gold deposit . .	1:13
				in lunar samples	1:7

	Page
Ground water—Continued	
Pennsylvania and Maryland . .	2:249
role in development of den-	
dritic dry valleys in	
karst areas	2:159
See also Quality of water.	
Gulf of Mexico basin, hydrologic	
aspects of structural de-	
formation	5:511
H	
Hawaiian Ridge—Emperor Sea-	
mounts chain, calcula-	
tion of shield volcano	
volumes	5:545
<i>Helena bella</i> Walcott, redescription	
as hyolithid appendage	
determination	6:717
Hornblende, New Mexico, age	
determination	6:705
Hot springs. See Geothermal	
studies.	
Hydrocarbons, in stream-bottom	
materials	5:541
Hydrogen, isotopes, in gold deposit	
in lunar samples	1:7
Hydrogeology, Antietam Creek	
basin	2:249
Hydrologic techniques, estimation	
of stream traveltime and	
solute dispersion	4:495
Hydrology, Ohio, western part . .	5:527
Hurricane Agnes, effect on Susque-	
hanna River basin	6:753
Hyolithid appendage, <i>Helena bella</i>	
Walcott	6:717
I	
Idaho, mineralogy, Hall Mountain	
southeastern part	6:693
stratigraphy, Blaine County . .	1:89
Iowa, economic geology, north-	
eastern part	2:219
Irrigation canal, dye dosage, time of	
travel	4:489
Isotope studies, gold deposit, Nevada	
indicators of continental de-	
position of tillite,	
Antarctica	6:711
lunar samples	1:7
pantellerite, Oregon	1:25
J	
Jarosite, Cripple Creek district, first	
report	3:339
Jurassic, Nevada, structural geology	
.	4:417
K	
Karst areas, development of dry	
valleys, Puerto Rico . .	2:159

	Page
Karst topography, Mississippian,	
Wyoming	2:133
Kroenke Granodiorite, Colorado,	
age determination	6:705
L	
Lacustrine deposits, chert derived	
from magadiite	5:625
Landslides, California, fault related	
.	5:593
Lassen Volcanic National Park,	
Calif., petrology	1:49
Lead, isotopes, in gold deposit . .	1:13
Liberia, monazite, economic po-	
tential	6:689
Louisiana, structural deformation,	
coastal plain sediments	
.	5:511
Luna 20 nonvolcanic implications	
from sample studies . .	1:1
Lunar analogs, morphometric prop-	
erties of experimentally	
cratered surfaces	3:279
Lunar highlands, implications from	
Luna 20 and Apollo 16	
samples	1:1
Lunar samples, carbon and hydro-	
gen isotopic composi-	
tion	1:7
M	
Madison Limestone, Wyoming,	
ancient karst features . .	2:133
Wyoming and Montana, strati-	
graphy	5:619
Magadiite, precursor of chert, lacus-	
trine deposit	5:625
Magnetic studies, continental slope,	
California-Oregon	5:563
Maine, economic geology, Catheart	
Mountain	2:189
Manganese mineral, birnessite, in	
obsidian spherulite . .	4:467
Mapping, suitability of ERTS	
imagery for automation	
.	6:763
Maquoketa Shale, Iowa, economic	
geology	2:219
Marine geology, silicoflagellates . .	3:303
Maryland, hydrologic studies, An-	
tietam Creek basin	2:249
upper Potomac River basin	
.	1:125
Massachusetts, retention of chlo-	
rides along highways . .	1:119
Mercury sulfide, equilibria studies	
.	4:457
Mesozoic. See Jurassic, Cretaceous.	
Metamorphism, Alaska, Eagle quad-	
range	6:657
Methods and techniques, determi-	
nation of dye dosage for	
time of travel in irriga-	
tion canals	4:489
determination of selenium in	
geologic materials	4:483

	Page
Methods and techniques—Continued	
determination of total water in	
silicate and carbonate	
minerals	2:185
determination of vanadium in	
rutile and mafic igneous	
rocks	6:701
selective staining, feldspar	1:73
spectrochemical computer	
analysis program	
description	1:61
spectrofluorimetric determina-	
tion of selenium in rocks	
.	5:631
spectrometry, ancillary system	
on electron microprobe	
.	4:441
Microprobe analyses, copper in bio-	
tite and chlorite	2:195
orpiment, Nevada	3:341
Mineral equilibrium studies, ara-	
gonite	4:447
calcite and aragonite	2:175
cinnabar and stibnite	4:457
Mineral separation, Clerici solution	
.	4:479
Mineralization, calderas, Colorado	
.	4:405
Mineralogy, birnessite, Colorado . .	4:467
brüggenite, Chile	4:471
buddingtonite, southeastern	
Idaho	6:693
Carlin gold deposit, Nevada . .	3:341
chert from magadiite, Oregon	
coloradoite, acanthite, and jaro-	
site, Colorado	3:339
garrelsite	2:213
Hall Mountain, Idaho	6:677
strontioginorites	6:699
Miocene, silicoflagellates	3:303
Mississippi, paleontology, north-	
eastern part	1:81
Mississippian, Wyoming, karst topo-	
graphy	2:133
Wyoming and Montana, strati-	
graphy	5:619
Molybdenum-copper deposit,	
Maine, economic geo-	
logy	2:189
Monazite, Liberia, analyses	6:689
Montana, stratigraphy, south-	
central part	5:619
Moon. See Lunar analogs.	
Morphometric analysis, lunar ana-	
log craters	3:279
N	
Nepheline syenite, Alaska, St.	
Lawrence Island	1:41
Nevada, age determination, Roberts	
Mountain thrust	4:411
barium, Snake Range	6:671
Cretaceous tectonics	4:417
geophysics, Nye County	1:105

	Page
Nevada—Continued	
isotope studies, north-central part	1:13
Jurassic tectonics	4:417
mineralogy, Carlin gold deposit	3:341
orogenic movement rate, Roberts Mountain thrust	4:411
Paleozoic tectonics	3:331
stratigraphy, Nye County	1:105; 5:599
Precambrian strata	5:609
structural geology	4:417
Nye County	1:105; 5:599
tectonic studies	3:331; 4:417
New Mexico, age determinations, hornblende and trondhjemite	6:705
New York, bacterial and phytoplankton populations compared, Oneida Lake	5:533
palynology, Long Island	4:431
New Zealand, aquifer chemistry	3:271
Niobium, spectrophotometric determination in rocks	3:353
Nitrate deposits, Chile, bruggenite	4:471

O

Ohio, ground water, western part	5:527
Oil shale, Colorado, relation of analcime to diagenetic dawsonite	1:35
Oman, remote sensing	2:147
Onesquethaw Stage, New York, paleontology	2:165
Open-channel flows, diffusion, dispersion, and turbulence studies	4:501
Ophiolite, chemical characteristics, California Coast Range	6:637
Oquirrh Group, Utah, paleontology and stratigraphy	1:97
Ore deposits, cinnabar and stibnite, equilibria studies	4:457
Colorado, association of geochemical-gravity anomalies	5:581
southwestern part	4:405
Ore reserves, chromitite, Bahia, Brazil	5:551
Oregon, age determination, pantellerite	1:25
geophysical profile, continental slope	5:563
isotope studies, Hart Mountain area	1:25
mineralogy, Malheur County	5:625
volcanic rock sequence, Coast Range	4:395
Organic carbon, dissolved, in ground water	3:361
Orogenic movements, age determination	4:411

Orpiment, thallium-bearing, Nevada	3:341
Ostracodes, Paleozoic, inconclusive evidence for heart	6:723
Overthrusts, Nevada	4:417
Oxygen, isotopes, in gold deposit	1:13

P

Pacific Ocean, Hawaiian Ridge—Emperor Seamounts chain, calculation of shield volumes	5:545
Paleontology, coral classification, New York	2:165
<i>Helenia bella</i> Walcott, redescription	6:717
Madison Limestone, Wyoming and Montana	5:619
ostracodes, inconclusive evidence for heart in Paleozoic forms	6:723
silicoflagellates	3:303
Utah, north-central part	1:97
See also Palynology.	
Paleozoic, ostracodes, inconclusive evidence for heart	6:723
tectonics, Nevada	3:331
See also Cambrian, Mississippian, Pennsylvanian.	
Palynology, application of statistical methods	6:727
Cretaceous, Long Island, N.Y., Block Island, R.I.	4:431
Pantellerite, isotope studies, Oregon	1:25
Pennsylvania, hydrologic studies, Antietam Creek basin	2:249
upper Potomac River basin	1:125
Hurricane Agnes effect, Susquehanna River basin	6:753
Pennsylvanian, Idaho, stratigraphy	1:89
Utah, paleontology and stratigraphy	1:97
Permian Basin, salt beds, rate of salt solution	2:253
Petrology, Alaska, Eagle quadrangle mapping of nepheline syenite	1:41
California Coast Range, ophiolite	6:637
Maine, molybdenum-copper deposit	2:189
Nevada, Carlin gold deposit	3:341
Phosphatic rock, Iowa, economic geology	2:219
Phosphoria Formation, budding-tonite, analyses	6:693
Phosphonite, Iowa, economic geology	2:219
Phytoplankton, relation to bacteria, Oneida Lake, N.Y.	5:533
Piedmont province, geophysical data	5:569
rock types	5:569

Plate tectonics. See Tectonic studies.	
Pleistocene-Pliocene, Puerto Rico, geomorphology	2:159
Polar regions, cartographic application of ERTS-1 imagery	4:385
Pollen. See Palynology.	
Pools and riffles, biological aspects	3:379
Porcelanite, conversion to spongy chert	6:685
Porphyry copper deposit, Arizona, fluid-inclusion study	1:31
Potassium-argon age, San Juan volcanic field, Colorado	4:405
Precambrian strata, Nevada	5:609
Principal component analysis, use in palynology	6:727
Puerto Rico, geomorphology, Ciales area	2:159
Pyroclastic-flow deposits, California, age determinations	1:49

Q

Quality of water, chloride retention in unsaturated zone	1:119
chlorinated hydrocarbons	5:541
estimation of contaminant traveltime in streams	4:495
Ohio, regional ground-water system	5:527
organic carbon in ground water	3:361
San Francisco Bay estuary system	5:519

R

Radiocarbon ages, recent pyroclastic-flow deposits, California	1:49
Radiometric studies, pantellerite, Oregon	1:25
Rare earths in monazite, Liberia	6:689
in thorium veins, Idaho	6:677
Recession curve, base runoff, upper Potomac River basin	1:125
Remote sensing, cartographic characteristics of ERTS	6:763
discrimination of geologic units by thermal inertia mapping from satellite data	2:147
polar regions, cartographic application of ERTS-1 imagery	4:385
Resistivity studies, Colorado	4:421
Rhodamine dyes, dosage, time of travel in irrigation canal	4:489
Rhode Island, palynology, Block Island	4:431
Ripley Formation, southeastern United States, paleontology	1:81

	Page
Roberts Mountain thrust, Nevada, age determination	4:411
Rockfall-avalanches, dacitic rock, California	1:49
Rubidium-strontium age, hornblende, New Mexico	6:705
Kroenke Grandiorite, Colorado	6:705
trondhjemite, New Mexico	6:705
Rutile, vanadium determination . .	6:701

S

Salt, retention in unsaturated zone	1:119
Salt beds, Permian Basin, rate of solution	2:253
San Andreas fault, relation to Sargent-Berrocal fault zone	5:593
San Francisco Bay estuary, suspended-sediment plumes	5:519
San Juan volcanic field, Colorado, mineralization in calderas	4:405
Seamounts, calculation of volumes	5:545
Sediments, deep sea, silicoflagellates	3:303
discharge, effect of Hurricane Agnes in Susquehanna River basin	6:753
hydrologic structural deformation, Gulf of Mexico basin	5:511
plumes, San Francisco Bay	5:519
Seismic refraction studies, Colorado	4:421
Seismic surveys, continental slope, California-Oregon	5:563
northeastern Caribbean	3:289
Selenium, determination of trace amounts in geologic materials	4:483
spectrofluorimetric determination	5:631
Shields, volcanic, calculation of volumes	5:545
Silica, spectrophotometric determination, high concentrations	3:357
Silicoflagellates, Cretaceous to Miocene	3:303
Silver-bearing mineral, Cripple Creek district	3:339
Sink-float mineral separation, Clerici solution	4:479
Sodium chloride, retention in unsaturated zone	1:119
Soil creep, unrelated to curved trees	3:371
Solubility studies, cinnabar and stibnite, relative to ore genesis	4:457
South America. <i>See</i> Brazil, Chile.	
Spectrochemical analysis, computer program description . .	1:61

Spectrofluorimetric analysis, selenium in rocks	5:631
Spectrographic analysis, budding-tonite, Phosphoria Formation	6:693
orpiment, Nevada	3:341
Spectrometric analysis, energy dispersive, ancillary system on electron microprobe	4:441
Spectrophotometric analysis, niobium in rocks	3:353
silica at high concentrations . .	3:357
vanadium in rutile and mafic igneous rocks	6:701
Spores. <i>See</i> Palynology.	
Staining, amaranth method for feldspar	1:73
Statistical methods, application to palynological analyses	6:727
Stibnite, equilibria studies	4:457
Stratigraphy, Arizona, Bolsa Quartzite	2:143
Idaho, Blaine County	1:89
Long Island, N.Y., Block Island, R.I.	4:431
Nevada	5:609
Nevada, Lunar Lake caldera . .	5:599
Roberts Mountains thrust	4:411
New York and Rhode Island . .	4:431
Utah, north-central part	1:97
Wyoming	2:133
Wyoming and Montana, Madison Limestone	5:619
Stream-bottom materials, hydrocarbons	5:541
Streamflow, traveltime, method for estimating	4:495
Strontioginorites, compositional data	6:699
Structural geology, Alaska, Eagle quadrangle	6:657
south-central part	3:323
Arizona	3:311
California, San Francisco Bay	5:593
Santa Clara Valley	5:593
Nevada	4:417
Lunar Lake caldera	5:599
Roberts Mountains thrust	4:411
northern Gulf of Mexico basin	5:511
ore deposits in faults and fractures	4:405
Sulfide ore deposits, equilibria studies relative to genesis	4:457
Sulfur, isotopes, in gold deposit . .	1:13
Surface water, Maryland and Pennsylvania	2:249
<i>See also</i> Quality of water, Streamflow.	
Suspended-sediment plumes, San Francisco Bay	5:519

T

Tectonic studies, Alaska, Eagle quadrangle	6:657
Caribbean, northeastern part . .	3:289
Nevada, Edna Mountain quadrangle	3:331
Temperature studies. <i>See</i> Geothermal studies	
Tertiary, Nevada, geologic history	1:105
<i>See also</i> Eocene, Miocene, Pliocene.	
Texas, coastal plain sediments, hydrologic aspects of structural deformation	5:511
Thallium, in orpiment	3:341
Thermal conductimetric determination, total water in silicate and carbonate minerals	2:185
Thermal inertia mapping, discrimination of geologic units from satellites	2:147
Thorium veins, rare-earth content, Idaho	6:677
Tillite, Antarctica, continental deposition	6:711
Time-of-travel study, irrigation canal	4:489
Transmissivity, upper Potomac River basin	1:125
Traveltime, streams, method for estimating	4:495
Tree-trunk curvature, unrelated to soil creep	3:371
Trondhjemite, New Mexico, age determination	6:705
Turbulence, open-channel flows . .	4:501

U

Ultramafic rocks, Alaska, Eagle quadrangle	6:657
USGS standard rocks, determination of niobium content	3:353
Utah dye dosage, time of travel in irrigation canal	4:489
garrelsite, new data	2:213
paleontology and stratigraphy, north-central part	1:97

V

Valleys, dry, development in karst areas	2:159
Vanadium, in rutile, spectrophotometric determination . .	6:701

	Page
Virginia, base runoff, upper Potomac River basin . .	1:125
geophysical data	5:569
rock types	5:569
Volcanic rock sequence, Yachats Basalt, Oregon	4:395
Volcanism, Nevada, Lunar Lake caldera	5:599
Volcanology, Hawaiian Ridge— Emperor Seamounts chain, calculation of shield volumes	5:545
W	
Washington, volcanic rock se- quence, Eocene	4:395

	Page
WATEQ, computer program for cal- culating chemical equili- bria of natural waters . .	2:233
Water content, analysis in silicate and carbonate minerals	2:185
Water, hot-springs, geochemical indicators of subsurface temperature	3:259, 263
Wells, geothermal, production analysis	6:743
West Virginia, base runoff, upper Potomac River basin . .	1:125
Wood River Formation, Idaho, stratigraphy	1:89
Wyoming, ancient karst topog- raphy, north-central part	2:133

	Page
Wyoming—Continued	
geothermal studies	3:263
stratigraphy, north-central part	5:619
X	
X-ray analysis, Phosphoria Forma- tion, buddingtonite . .	6:693
X-ray fluorescence analysis, mona- zite, Liberia	6:689
Y	
Yachats Basalt, Oregon, Eocene vol- canic sequence	4:395
Yellowstone National Park, geo- thermal studies	3:263

AUTHOR INDEX

A	
Ackermann, H. D.	4:421
Adam, D. P.	6:727
Adams, D. B.	4:489
B	
Bailey, E. H.	6:637
Banks, N. G.	2:195
Bargar, K. E.	5:545
Barker, Fred	6:705
Batchelder, John	1:89
Bates, R. G.	5:569
Bath, G. D.	1:105
Blake, M. C., Jr.	6:637
Boning, C. W.	4:495
Brobst, D. A.	1:35
Brown, C. E.	2:219
Bukry, David	3:303
C	
Campbell, E. Y.	3:353
Carlson, P. R.	5:519
Chaffee, M. A.	2:143
Christ, C. L.	2:175; 4:447
Christian, R. P.	6:699
Cobban, W. A.	1:81
Colvocoresses, A. P.	6:763
Cooper, A. K.	3:289
Crandell, D. R.	1:49
Crenshaw, G. L.	4:483

Csejtey, Béla, Jr.	1:41
Cunningham, C. G., Jr.	1:31
Curtin, G. C.	5:581
D	
Daniels, D. L.	5:569
Desborough, G. A.	4:441
Dickson, F. W.	3:341; 4:457
Dixon, G. L.	1:105
Doe, B. R.	1:13
Doering, W. P.	6:671
Douglass, R. C.	1:89; 1:97
E	
Eberlein, G. D.	6:699
Eccles, L. A.	3:361
Ehlke, T. A.	5:533
Ekren, E. B.	1:105; 5:599
Ericksen, G. E.	4:471
Erickson, R. L.	3:331
F	
Fernandes de Couto Moreira, J. . .	5:551
Ferraz Pinto, A. C.	5:551
Foster, H. L.	6:657
Foster, J. H.	3:303
Fournier, R. O.	3:259, 263
Friedman, Irving	1:7; 6:711

G	
Garrison, L. E.	3:289
Gleason, J. D.	1:7
Goerlitz, D. F.	5:541
Gonçalves da Silva, J. C.	5:551
Gott, G. B.	3:339
Greenland, L. P.	3:353
Gude, A. J., 3d	5:625
Gulbrandsen, R. A.	6:693
H	
Hall, W. E.	1:89
Harcastle, K. G.	1:7
Healey, D. L.	1:105
Hedlund, D. C.	5:551
Heidel, R. H.	4:441
Henderson, W. T.	6:705
Heropoulos, Chris	3:341
Hildebrand, F. A.	3:339; 4:467
Hildreth, R. E.	6:705
Hostetler, P. B.	2:175; 4:447
Howard, K. A.	1:1
Huddle, J. W.	1:97
J	
Jackson, E. D.	5:545
Jones, B. F.	2:233
Jones, P. H.	5:511

	Page
K	
Keefer, T. N.	4:501
Keith, T. E. C.	6:657
Ketner, K. B.	4:417
King, H. D.	5:581
Kleinhampl, F. J.	5:599
Konnert, J. A.	6:699
Krieger, M. H.	3:311

L	
Lakin, H. W.	4:483
Lanphere, M. A.	3:343
Law, L. M.	5:541
Learned, R. E.	4:457
Lee, D. E.	6:671
Lecnheer, J. A.	3:361
Lipman, P. W.	4:405
Lium, B. W.	3:379
Luedke, R. G.	4:405
Lugn, R. V.	3:279

M	
McCulloch, D. S.	5:519
MacDonald, W. R.	4:385
McKee, E. H.	1:25
MacKevett, E. M., Jr.	3:323
McKinley, P. W.	3:361
McLaughlin, R. J.	5:593
MacLeod, N. S.	4:395
McQuivey, R. S.	4:501
Madsen, B. M.	6:685
Malcolm, R. L.	3:361
Mamet, B. L.	5:619
Marinenko, J. W.	2:185; 4:471; 6:701
Marlow, M. S.	3:289
Marsh, S. P.	3:331
Martin, R. G.	3:289
Mei, Leung	6:701
Milton, Charles	2:213
Monroe, W. H.	2:159
Moore, H. J.	3:279
Moore, W. J.	1:97
Mrose, M. E.	4:471
Mullineaux, D. R.	1:49

N	
Nash, J. T.	1:31

O	
Nathenson, Manuel	6:743
Newman, E. B.	3:279
Noble, D. C.	1:25
Nolan, T. B.	4:411
Norman, M. B., II	1:73
Norris, S. E.	5:527
Nutter, L. J.	2:249

O	
Offield, T. W.	2:147
Oliver, W. A., Jr.	2:165

P	
Pabst, Adolf	2:213
Patton, W. W., Jr.	1:41
Pavrides, Louis	5:569
Peterman, Z. E.	6:705
Phipps, R. L.	3:371
Plafker, George	3:323
Pohn, H. A.	2:147
Pollock, S. J.	1:119

Q	
Quinlivan, W. D.	1:105; 5:599

R	
Radtke, A. S.	3:341
Reed, B. L.	3:343
Ritter, J. R.	6:753
Rosenblum, Sam	4:479; 6:689
Rubin, Meyer	1:49
Rye, R. O.	1:13

S	
Sando, W. J.	2:133; 5:619
Schmidt, D. L.	6:711
Schmidt, R. G.	2:189
Schnepe, M. M.	5:631
Shapiro, Leonard	3:357
Shaw, V. E.	6:677
Sheppard, R. A.	5:625
Siebert, R. M.	2:175; 4:447

S	
Sigafoos, R. S.	1:49
Silver, E. A.	5:563
Singers, Wendy	3:271
Sirkin, L. A.	4:431
Smith, J. F., Jr.	4:417
Snavey, P. D., Jr.	4:395
Snyder, R. P.	5:599
Sohn, I. G.	6:723
Southard, R. B.	4:385
Staatz, M. H.	6:677
Stephen, T. A.	4:405
Stewart, J. H.	5:609
Swenson, F. A.	2:253
Sylvester, K. A.	5:569

T	
Taylor, C. M.	3:341
Toler, L. G.	1:119
Trainer, F. W.	1:125
Truesdell, A. H.	2:233; 3:259; 263, 271
Trumbull, J. V. A.	3:289
Tucker, J. D.	1:35
Tunell, George	4:457

V	
Vianney V. Souza, G.	5:551

W	
Wahlberg, J. S.	6:677
Walker, G. W.	1:25
Wallace, R. H., Jr.	5:511
Walthall, F. G.	1:61
Watkins, F. A., Jr.	1:125
Watson, Kenneth	2:147
Wells, J. D.	1:13
White, D. E.	3:259
Wilhelms, D. E.	1:1
Wilshire, H. G.	1:1

Y	
Yochelson, E. L.	6:717

RECENT PUBLICATIONS OF THE U.S. GEOLOGICAL SURVEY

(The following books may be ordered from the Superintendent of Documents, Government Printing Office, Washington, DC 20402, to whom remittances should be sent by check or money order. Give series number, title, stock number shown in parentheses in this list, and catalog number shown in brackets. Prices of Government publications are subject to change. Increases in costs make it necessary for the Superintendent of Documents to increase the selling prices of many publications offered. As it is not feasible for the Superintendent of Documents to correct the prices manually in all the publications stocked, the prices charged on your order may differ from the prices printed in the publications and in this list)

Professional Papers

- 486-G. Geohydrology of the Parker-Blythe-Cibola area, Arizona and California, by D. G. Metzger, O. J. Loeltz, and Burdge Irelan. 1973 (1974). p. G1-G130; plates in pocket. \$5. (2401-00223) [I 19:16:486-G]
- 486-H. Geohydrology of the Yuma area, Arizona and California, by F. H. Olmsted, O. J. Loeltz, and Burdge Irelan. 1973 (1974). p. H1-H227; plates in separate case. \$11.60. (2401-02391) [I 19:16:486-H]
- 655-H. Quantitative and historical evidence of vegetation changes along the upper Gila River, Ariz., by R. M. Turner. 1974. p. H1-H20; plate in pocket. \$2. (2401-02491) [I 19:16:655-H]
- 686-B. Late-glacial-postglacial vegetational history of the Pretty Lake region, northeastern Indiana, by A. S. Williams. 1974. p. B1-B23; plates in pocket. \$2. (2401-02453) [I 19:16:686-B]
723. Geology and ore deposits of the Rico district, Colorado, by E. T. McKnight. 1974. 100 p.; plates in pocket. \$3.35. (2401-02467) [I 19:16:723]
772. Gold-bearing gravel of the ancestral Yuba River, Sierra Nevada, Calif., by W. E. Yeend. 1974. 44 p.; plates in pocket. \$2.70. (2401-02430) [I 19:16:772]
778. Embudo, N. Mex., birthplace of systematic stream gaging, by A. H. Frazier and Wilbur Heckler, 1972. 23 p. 90¢. (Reprinted 1974.) (2410-2049) [I 19:16:778]
815. Engineering geologic, geophysical, hydrologic and rock-mechanics investigations of the Straight Creek Tunnel site and pilot bore, Colorado, by C. S. Robinson, F. T. Lee, J. H. Scott, R. D. Carroll, R. T. Hurr, D. B. Richards, F. A. Mattei, B. E. Hartmann, and J. F. Abel, Jr. 1974. 134 p.; plates in pocket. \$5.55. (2401-02477) [I 19:16:815]
819. Geology of the southern Salinas Valley area, California, by D. L. Durham. 1974. 111 p.; plates in pocket. \$4.55. (2401-02471) [I 19:16:819]
829. Geology and mineral deposits of the Poncha Springs SE quadrangle, Chaffee County, Colo., by R. E. Van Alstine. 1974. 19 p.; plate in pocket. \$1.95. (2401-02444) [I 19:16:829]
832. Geology of the Skagway B-3 and B-4 quadrangles, southeastern Alaska, by E. M. MacKevett, Jr., E. C. Robertson, and G. R. Winkler. 1974. 33 p.; plate in pocket. \$2.05. (2401-02472) [I 19:16:832]
833. Computer model for determining bank storage at Hungry Horse Reservoir, northwestern Montana, by T. H. Thompson. 1974. 16 p. 65¢. (2401-02485) [I 19:16:833]

834. Systematics, environment, and biogeography of some Late Cambrian and Early Ordovician trilobites from eastern New York State, by M. E. Taylor and R. B. Halley. 1974. 38 p.; 4 plates showing fossils. \$1.35. (2401-02459) [I 19:16:834]
839. Palynological studies of the coals of the Princess Reserve district in northeastern Kentucky, by R. M. Kosanke. 1973 (1974). 22 p.; 1 plate showing fossils. \$1. (2401-02460) [I 19:16:839]
844. Geophysical investigations of the Pensacola Mountains and adjacent glacierized areas of Antarctica, by J. C. Behrendt, J. R. Henderson, Laurent Meister, and W. L. Rambo. 1974. 28 p.; plates in pocket. \$2.05. (2401-02499) [I 19:16:844]
885. Summary of 1972 oil and gas statistics for onshore and offshore areas of 151 countries, by S. E. Frezon. 1974. 163 p. \$2.70. (2401-02518) [I 19:16:885]

Bulletins

1307. Synopsis of the mineral resources and geology of Alaska, by E. H. Cobb. 1974. 53 p. 70¢. (2401-02478) [I 19:3:1307]
1338. Geology of Moorhead coal field Powder River, Big Horn, and Rosebud Counties, Mont., by R. P. Bryson and N. W. Bass. 1973 (1974). 116 p.; plates in pocket. \$3.40. (2401-00346) [I 19:3:1338]
- 1394-H. The Whitehorn Granodiorite of the Arkansas Valley in central Colorado, by C. T. Wrucke. 1974. 8 p. 25¢. (2401-02514) [I 19:3:1394-H]

Water-Supply Papers

- 1798-L. Effects of land use and retention practices on sediment yields in the Stony Brook basin, New Jersey, by L. J. Mansue and P. W. Anderson. 1974. p. L1-L33. 55¢. (2401-02465) [I 19:13:1798-L]
2022. Water availability in central Wisconsin—An area of near-surface crystalline rock, by E. A. Bell and M. G. Sherrill. 1974. 32 p.; plates in pocket. \$4.25. (2401-02446) [I 19:13:2022]
2033. Availability of ground water in the lower Pawcatuck River basin, Rhode Island, by J. B. Gonthier, H. E. Johnston, and G. T. Malmberg. 1974. 40 p.; plates in pocket. \$3.80. (2401-02468) [I 19:13:2033]

Techniques of Water-Resources Investigations

- TWI 5-A1. Methods for collection and analysis of water samples for dissolved minerals and gases, Chapter A1, by Eugene Brown, M. W. Skougstad, and M. J. Fishman. 1970. 160 p. \$2.40. (Reprinted 1974). (2401-1015) [I 19:15/5:BK 5/chap. A1]

U.S. GOVERNMENT
PRINTING OFFICE
PUBLIC DOCUMENTS DEPARTMENT
WASHINGTON, D.C. 20402
OFFICIAL BUSINESS
PENALTY FOR PRIVATE USE \$300

POSTAGE AND FEES PAID
U.S. GOVERNMENT
PRINTING OFFICE
375

